

AN ABSTRACT OF THE DISSERTATION OF

Martin Precek for the degree of Doctor of Philosophy in Chemistry presented on August 29, 2012.

Title: The Kinetic and Radiolytic Aspects of Control of the Redox Speciation of Neptunium in Solutions of Nitric Acid

Abstract approved: _____

Alena Paulenova

Neptunium, with its rich redox chemistry, has a special position in the chemistry of actinides. With a decades-long history of development of aqueous separation methods for used nuclear fuel (UNF), management of neptunium remains an unresolved issue because of its not clearly defined redox speciation. Neptunium is present in two, pentavalent (V) and hexavalent (VI) oxidation states, both in their dioxocation $\text{O}=\text{Np}=\text{O}$ neptunyl form, which differ greatly in their solvent extraction behavior. While the neptunium(VI) dioxocation is being very well extracted, the dioxocation of pentavalent neptunium is practically non-extractable by an organic solvent. As a result, neptunium is not well separated and remains distributed in both organic and aqueous extraction phases. The aim of this study was to develop or enhance the understanding of several key topics governing the redox behavior of neptunium in nitric acid medium, which are of vital importance for the engineering design of industrial-scale liquid-liquid separation systems.

In this work, reactions of neptunium(V) and (VI) with vanadium(V) and acetohydroxamic acid - two redox agents envisioned for adjusting the neptunium oxidation state in aqueous separations – were studied in order to determine their kinetic characteristics, rate laws and rate constants, as a function of temperature and nitric acid concentration. Further were analyzed the interactions of neptunium(V) and (VI) with nitrous acid, which is formed as a product of radiolytic degradation of nitric acid caused by high levels of radioactivity present in such systems. Once HNO_3 is distributed

between both the aqueous solutions and organic solvent, nitrous acid is also formed in both phases and has a key influence on redox speciation of neptunium; therefore, the effects of gamma-radiation on the redox speciation of neptunium were investigated. The work also includes the results of examination of scavenging of nitrous acid by hydrogen peroxide, which is generated along with nitrous acid during radiolysis of aqueous solutions of nitric acid, and also by chemical reactions with added scavenging agents (methylurea, acetohydroxamic acid).

©Copyright by Martin Precek

August 29, 2012

All Rights Reserved

The Kinetic and Radiolytic Aspects of Control of the Redox Speciation of Neptunium
in Solutions of Nitric Acid

by
Martin Precek

A DISSERTATION

submitted to

Oregon State University

in partial fulfillment of
the requirements for the
degree of

Doctor of Philosophy

Presented August 29, 2012

Commencement June 2013

Doctor of Philosophy dissertation of Martin Precek presented on August 29, 2012.

APPROVED:

Major Professor, representing Chemistry

Chair of the Department of Chemistry

Dean of the Graduate School

I understand that my dissertation will become part of the permanent collection of Oregon State University libraries. My signature below authorizes release of my dissertation to any reader upon request.

Martin Precek, Author

ACKNOWLEDGEMENTS

Firstly, I would like to express my deep appreciation to Dr. Alena Paulenova, who has more than fulfilled her duties of an academic advisor, who has never failed in arranging for my financial support, and who has always made herself available to provide academic and personal guidance through my doctoral studies.

I would also like to extend my appreciation to the past and present members of my doctoral committee at OSU: Dr. James D. Ingle, Dr. Walter D. Loveland, Dr. Philip R. Watson, Dr. Manish Gupta, Dr. Taifo Mahmud, and Dr. Abi T. Farsoni, who have found time in their busy schedules to supervise the progression of my degree.

My additional thanks are directed at my collaborators and co-advisors Dr. Bruce J. Mincher from the Idaho National Laboratory and Dr. Stephen Mezyk from the California State University, Long Beach, for creating a wonderful and exciting atmosphere of cooperation and for treating me as their equal.

I have been very lucky in getting to work in the wonderful collective of Dr. Paulenova's research group. I would like to especially acknowledge the support I had from the following colleagues: Dr. Peter Tkac (the group "postdoc"), graduate students M. Alex Brown, Vanessa E. Holfeltz, Joseph L. Lapka, and Brent S. Matteson, and also from undergraduate researchers Kyle C. Hartig, Nathan Knapp, and Corey R. Wright.

My work would not be possible without the support work of the personnel of the OSU Radiation Center, especially Scott A. Menn who facilitated my use of the Co-60 irradiator and provided necessary radiation protection oversight over my work.

I also address many thanks to the community of people of the town of Corvallis, Oregon, especially to the international students of the European Student Association of OSU, to Stephen Howell for the I.H.O.P., to Penelope Wollf and the Pro Musica Corvallis String Orchestra, and to the Rebhuhn family, all of whom have allowed me to develop a very fulfilling social life in what was initially a strange and foreign country to me.

Last, but not least, I need to express my thanks to the members of my family, especially to my mother Katalin, father Zdeněk and sister Tamara, who have remotely supported me during all the years while I left Europe in pursuit of my doctoral studies.

The Author

CONTRIBUTION OF AUTHORS

Dr. Peter Tkac and Nathan Knapp have undertaken the preliminary work on the effects of nitric acid radiolysis, production of nitrous acid and effectiveness of small doses of methylurea in scavenging nitrous acid.

Dr. Brent S Matteson has performed the initial kinetic experiments of Np(VI) reduction by acetohydroxamic acid in nitric acid environment.

Dr. Bruce J Mincher – has provided for use the scientific equipment and the irradiator at Idaho National Laboratory, and performed the irradiation of aqueous and organic nitric acid solutions – and, together with Dr. Stephen Mezyk, has helped with the interpretation of the data on kinetics of the reaction of H_2O_2 with HNO_2 .

TABLE OF CONTENTS

	<u>Page</u>
1 Introduction	1
1.1 General Background	1
1.2 Motivation.....	1
1.3 Expected Outcomes.....	2
1.4 Overview of the Dissertation	3
2 Review of Literature.....	5
2.1 Importance of Neptunium	5
2.1.1 Discovery	5
2.1.2 Neptunium in the nuclear fuel cycle.....	6
2.1.3 Long-term Radiotoxicity of Neptunium in SNF	7
2.1.4 Non-proliferation issues	8
2.1.5 Potential Uses of Neptunium.....	9
2.2 General chemical properties of neptunium among the actinide elements.....	11
2.3 Neptunium in Reprocessing of Used Nuclear Fuel.....	20
2.3.1 PUREX Process.....	20
2.3.2 Advanced PUREX processes	24
2.4 Control of the oxidation state of neptunium by redox reagents	27
2.4.1 Neptunium disproportionation and reaction with HNO ₃	27
2.4.2 Uranium(IV).....	33
2.4.3 Iron(II).....	34
2.4.4 Plutonium(III).....	35
2.4.5 Hydrazine	36
2.4.6 Hydrogen peroxide	38
2.4.7 Hydroxylamine.....	40
2.4.8 New prospective reducing agents.....	43
2.4.9 Vanadium(V) as a prospective oxidizing agent.....	50
2.5 Radiation chemistry of neptunium in nitric acid.....	54
2.5.1 Radiolysis of water.....	54
2.5.2 The radiation chemistry of actinides in nitric acid solutions.....	56
3 Materials and Methods	58
3.1 Materials.....	58
3.1.1 Neptunium	58
3.1.2 Solutions and their preparation.....	60
3.1.3 Volumetric titration	60
3.1.4 Nitric acid.....	61
3.1.5 Management of the instability of nitrous acid.....	62
3.2 Methods and Techniques	62

TABLE OF CONTENTS (Continued)

	<u>Page</u>
3.2.1	Electrochemistry..... 62
3.2.2	Spectrophotometry 68
3.2.3	Experimental techniques for analysis of reaction kinetics 77
3.2.4	Irradiation apparatus for radiolytic studies..... 82
4	Kinetics of Oxidation of Pentavalent Neptunium by Pentavalent Vanadium in Solutions of Nitric Acid 83
4.1	Abstract 84
4.2	Introduction..... 84
4.3	Experimental 86
4.3.1	Reagents 86
4.3.2	Measurement 86
4.4	Results and discussion 87
4.4.1	Analysis of kinetic data 87
4.4.2	Effect of concentration of Np(V) and V(V) 89
4.4.3	Effect of hydrogen ion concentration..... 89
4.4.4	Effect of temperature on the rate of oxidation of Np(V) by V(V) 92
4.5	Conclusion 93
5	Kinetics of reduction of hexavalent neptunium by nitrous acid in solutions of nitric acid 94
5.1	Abstract 95
5.2	Introduction..... 95
5.3	Experimental 97
5.3.1	Chemicals 97
5.3.2	Neptunium 97
5.3.3	Instrumentation..... 98
5.3.4	Observation of the kinetic progress..... 99
5.3.5	Nitrous acid instability 99
5.3.6	Data analysis 100
5.4	Results and discussion 100
5.4.1	Determination of reaction orders with respect to Np(VI) and HNO ₂ 100
5.4.2	Effect of H ⁺ concentration and ionic strength 101
5.4.3	Discussion on the form of the rate law 102
5.4.4	Effect of temperature..... 104
5.5	Conclusion 106
6	Kinetics of reduction of hexavalent neptunium by acetohydroxamic acid in solutions of nitric acid..... 107
6.1	Introduction..... 107
6.2	Experimental details..... 107

TABLE OF CONTENTS (Continued)

	<u>Page</u>
6.3 Stoichiometry of the reaction of Np(VI) with acetohydroxamic acid (AHA) in nitric acid	108
6.4 Analysis of the kinetics of the Np(VI) + AHA reaction in HNO ₃	110
6.5 Conclusion	114
7 Redox potential of the nitrous acid – nitric acid system.....	115
7.1 Introduction.....	115
7.2 Experimental	116
7.3 Results and discussion	117
7.4 Conclusion	120
8 Reaction of nitrous acid with acetohydroxamic acid in nitric acid solutions	121
8.1 Introduction.....	121
8.2 Stoichiometry of the reaction	121
8.3 Investigation of the kinetic system.....	122
8.4 Influence of acidity, nitrate concentration and temperature.....	124
8.5 Conclusion	127
9 Reaction of nitrous acid with hydrogen peroxide in nitric acid solutions	129
9.1 Introduction.....	129
9.2 Stoichiometry and reaction mechanism	129
9.3 Investigation of the kinetic system.....	130
9.4 Dependence of rate constants on acidity	133
9.5 Dependence of rate constants on nitric acid and on total nitrate concentration	133
9.6 Dependence of rate constants on temperature.....	136
9.7 Conclusion	137
10 Effect of Gamma Irradiation on the Oxidation State of Neptunium in Nitric Acid in the Presence of Selected Scavengers.....	138
10.1 Abstract	139
10.2 Introduction.....	139
10.2.1 Radiolysis of Nitric Acid.....	139
10.2.2 Importance of HNO ₂	140
10.2.3 Methylurea and Acetamide	140
10.2.4 Redox Reactions of Np with HNO ₂ and Vanadium(V).....	141
10.3 Experimental	142
10.3.1 Neptunium	142
10.3.2 Nitrous acid	143

TABLE OF CONTENTS (Continued)

	<u>Page</u>
10.3.3 Methylurea	143
10.4 Results and Discussion:	144
10.4.1 Nitrous Acid (HNO ₂) Radiolytic Production	144
10.4.2 Methylurea	145
10.4.3 Methylurea Degradation by Gamma Irradiation	146
10.4.4 Effect of Addition of Vanadium(V)	148
10.4.5 Effect of Low Concentrations of MU and V(V) on the Redox Speciation of Neptunium after Irradiation	148
10.4.6 Effect of High Concentrations of Methylurea on the Redox Speciation of Neptunium after Irradiation.....	149
10.5 Conclusion	151
11 Reduction of Np(VI) in irradiated solutions of nitric acid	152
11.1 Abstract	153
11.2 Introduction.....	153
11.3 Experimental	154
11.4 Results and Discussion.....	155
11.4.1 Effects of gamma radiation on neptunium(VI) in 4M HNO ₃	155
11.4.2 Influence of nitric acid concentration.....	157
11.5 Conclusion	160
12 Radiolytic production of nitrous acid in the HNO ₃ - TBP extraction system	162
12.1 Abstract	163
12.2 Introduction.....	163
12.3 Experimental	164
12.3.1 Chemicals	164
12.3.2 Nitrous acid instability, sample preparation and irradiation	165
12.3.3 Spectrophotometry	166
12.4 Results and Discussion.....	167
12.4.1 Extraction of HNO ₂ into 30% TBP/n-dodecane.....	167
12.4.2 Radiolytic production of HNO ₂ in aqueous and organic solutions	169
12.4.3 Combined organic and aqueous (biphasic system) system	171
12.4.4 Dependence of radiolytic yield of HNO ₂ on HNO ₃ concentration in aqueous and organic phases	172
12.5 Conclusion	173
13 General Conclusion	174
13.1 Impact of work and summary of results.....	174
13.2 Future work.....	176

TABLE OF CONTENTS (Continued)

	<u>Page</u>
Bibliography	177
APPENDIX A. Analysis of Kinetic Data using Numeric Integration	198
A.1 Background, rationale and significance	198
A.2 Chemical kinetics as a set of differential equations	201
A.3 Runge-Kutta 4 th order (RK4) method	202
A.4 Solution of rate equations by the RK4 numeric method	203
A.5 Implementation of the RK4 method in an Excel spreadsheet	204
APPENDIX B. Analysis Of Errors Of Pipetting Using Eppendorf Variable Volume Pipettes .	207
B.1 Introduction.....	207
B.2 Experimental	208
B.2.1 Dependence on the pipetting speed:	209
B.2.2 Effect of Pipette Tip Pre-rinsing	210
B.3 Results.....	211
B.3.1 1 mL digital pipettor.....	211
B.3.2 300 μ L digital pipettor	212
B.3.3 5mL digital pipettor.....	213
B.3.4 Dependence for the 10 μ L digital pipettor	214
B.3.5 Manual 100 μ L and 1000 μ L pipettors.....	215
B.4 Concluding Recommendations	216
APPENDIX C. Review of Redox Reactions of Vanadium Ions with Neptunium and Plutonium	218
C.1 Introduction.....	218
C.2 Review	220
C.3 Conclusion	227

LIST OF FIGURES

<u>Figure</u>	<u>Page</u>
Figure 1 – Diagrams of <i>formal</i> redox potentials $E^{\circ'}$ in 1M HClO ₄	15
Figure 2 – Simplified scheme of the PUREX separation method.....	20
Figure 3 - Distribution ratios of Np(IV), (V) and (VI)	22
Figure 4 – Overview of the steps of the UREX+3a separation scheme	25
Figure 5 - Effect of equilibrium HNO ₂ concentration on the redox speciation of neptunium	30
Figure 6 – Chemical structures of formohydroxamic (left) and acetohydroxamic (right) acid	46
Figure 7 – Design plan of the glass H-cell used for Np electrolysis.....	66
Figure 8 - Dependence of reducing electrolytic current	67
Figure 9 – Neptunium(III), (IV), (V) and (VI) absorption spectra in 4.0M aq. HNO ₃	73
Figure 10 – Aqueous UV absorption spectra of the nitrite anion in water and of the molecular nitrous acid and of the nitrate anions in HNO ₃ solution	76
Figure 11 - Effect of the initial concentration of V(V) on reaction rate and equilibrium.....	89
Figure 12 - Determination of reaction order with respect to concentration of Np(V) and V(V) ...	89
Figure 13 - Comparison of initial rates of oxidation of Np(V) by V(V) between reactions in solutions of 1M HNO ₃ + 3 M LiNO ₃ and in 4M HNO ₃ (t = 25 °C)	90
Figure 14 - Effect of the molar concentration of H ⁺ on the apparent rate constant k_1'' and the apparent equilibrium constant K'	91
Figure 15 - Determination of activation energy of oxidation of Np(V) by V(V)	92
Figure 16- Determination of reaction orders with respect to initial concentration of Np(VI) and HNO ₂	101
Figure 17 - Effect of the molar concentration of hydrogen ions H ⁺ and ionic strength μ on the initial reaction rate	102
Figure 18 - Determination of activation energy of reduction of Np(VI) by HNO ₂	105
Figure 19 - Determination of the stoichiometry of the Np(VI) + AHA reaction in conditions with excess AHA.	108
Figure 20 - Determination of the stoichiometry of the Np(VI) + AHA reaction in conditions of excess Np(VI).	109

LIST OF FIGURES (Continued)

<u>Figure</u>	<u>Page</u>
Figure 21 – Fitting of the kinetic data of the reactions of Np(VI) with AHA by a second-order rate law	110
Figure 22 – Identification of the role of H ⁺ and NO ₃ ⁻ ion in the effect of nitric acid on the reaction rate of Np(VI) by AHA.	112
Figure 23 – Determination of the activation energy of the reaction of Np(VI) with an excess of AHA.	113
Figure 24 - Nernstian plots for HNO ₂ /HNO ₃ couple at 25.0°C	117
Figure 25 - Dependence of the redox potential of 1mM HNO ₂ on the HNO ₃ /H ⁺ concentration.....	118
Figure 26 - Dependence of the cell potential with 1mM HNO ₂ on the total nitrate	119
Figure 27 – Temperature dependence of the redox potential.....	120
Figure 28 - Determination of the stoichiometry of the HNO ₂ + AHA reaction in conditions with excess AHA.	122
Figure 29 - Determination of the stoichiometry of the HNO ₂ + AHA reaction in conditions with excess HNO ₂	122
Figure 30 - Absorption spectra in 1M HNO ₃ of HNO ₂ and the long-lived reaction intermediate identified during the reaction of AHA with HNO ₂	123
Figure 31 - Reaction of 7.5mM HNO ₂ with 9.5 mM AHA in 1M HNO ₃ at 25°C.....	123
Figure 32 - Dependence of rate constants on acidity at constant nitrate concentration	125
Figure 33 - Dependence of rate constants on the total concentration of NO ₃ ⁻ in the solution	125
Figure 34 – Dependence of rate constants on reaction temperature	126
Figure 35 - Spectrophotometric titration of 10 mM H ₂ O ₂ by HNO ₂ (0.5M HClO ₄ , t = 25°C)....	130
Figure 36 - Spectrophotometric titration of 10 mM NaNO ₂ by H ₂ O ₂ (0.5M HClO ₄ , t =25°C)....	130
Figure 37 - Absorption spectra of nitrous acid (HNO ₂) and peroxonitrous acids (HOONO) used for fitting kinetic data	131
Figure 38 - Reaction of 5.0 mM HNO ₂ with 10 mM H ₂ O ₂ in 0.75 M HNO ₃ + 0.25 M LiNO ₃ at 2.5°C.	131
Figure 39 - Dependence of HOONO formation rate constant k _F on acidity - reaction of 5mM HNO ₂ , 10mM H ₂ O ₂ , t=2.5°C, 1M H/LiNO ₃	133

LIST OF FIGURES (Continued)

<u>Figure</u>	<u>Page</u>
Figure 40 -Dependence of HOONO decay rate constant k_D on acidity - reaction of 5mM HNO_2 , 10mM H_2O_2 , $t=2.5^\circ\text{C}$, 1M H/LiNO_3	133
Figure 41 - Determination of dependence of rate constants on HNO_3 concentration	134
Figure 42 -Dependence of rate constants on total concentration of nitrate - reaction of 5mM HNO_2 with 10mM H_2O_2 , $t=2.5^\circ\text{C}$, 0.25M HNO_3 + 0.75-3.75 M LiNO_3	135
Figure 43 -Dependence of rate constants on temperature - reaction of 5mM HNO_2 , 10mM H_2O_2 ,	136
Figure 44 - Proposed nitrous acid scavengers.....	140
Figure 45 - Methylurea nitrosation	141
Figure 46 - Increase of the final concentration of HNO_2 produced by radiolysis of aqueous solutions of HNO_3 as a function of the effect of radiation dose (irradiation time).	144
Figure 47 - Change of UV absorption spectrum of HNO_2 in HNO_3 by addition of methylurea (MU)	145
Figure 48 - Changes in absorbance spectrum of solutions of 4M HNO_3 with initial additions of 10mM NaNO_2 and variable concentrations of methylurea (MU) after irradiation by a dose of 40.5 kGy.	146
Figure 49 - Degradation of 50 and 100 mM solutions of MU in 4 M HNO_3 by radiolysis.	147
Figure 50 - Time dependent change of redox speciation of 1.3 mM Np in aq. 4 M HNO_3 containing 50 mM and 100mM methylurea of non-irradiated reference solutions.....	149
Figure 51 - Dose dependent change of redox speciation of 1.3 mM Np in aq. 4 M HNO_3 irradiated solutions containing 50 mM and 100 mM methylurea.	150
Figure 52 - The concentrations of Np(V), Np(VI) and HNO_2 versus absorbed dose	156
Figure 53 - Irradiation at the 0.38 kGy/h dose rate: Concentration profile of Np(V) versus absorbed dose in concentrations of HNO_3	158
Figure 54 - Irradiation at the 0.38 kGy/h dose rate: Concentration profile of Np(V) and HNO_2 versus dose in two Np samples in 4M HNO_3	158
Figure 55 – Normalized absorption spectrum of HNO_2 in organic (0.23 M HNO_3 in 30% TBP) and aqueous (1 M HNO_3) phase	166
Figure 56 – Distribution ratios of HNO_3 and HNO_2 for the non-irradiated and irradiated (61kGy) system of the 30% TBP/n-dodecane and aqueous solutions of nitric acid.....	168

LIST OF FIGURES (Continued)

<u>Figure</u>	<u>Page</u>
Figure 57 – Concentrations of nitrous acid (± 5 % system. error), produced by irradiation different initial concentrations of HNO_3 in aqueous solutions.	168
Figure 58 - Concentrations of nitrous acid in organic phase (± 15 % system. error), produced by irradiation of 30% TBP equilibrated with different initial aqueous concentrations of HNO_3 (concentrations of extracted HNO_3 are given in parentheses).	170
Figure 59 - Comparison of the aqueous (± 5 % system. error) and organic (± 15 % systematic error, error bars indicate random error) concentrations of HNO_2 produced by a 61 kGy dose in monophasic and biphasic experiments, plotted as a function of the nitric acid concentration in aqueous phase.	171
Figure 60 – Density of water (ref. [204]).....	210
Figure 61 – Example of dispersion data.....	210
Figure 62- Photography of pipette tips employed during this study.....	211
Figure 63 – Errors of the 1mL pipettor (fresh tips).....	212
Figure 64 – Errors of the 1mL pipettor (rinsed tips).....	212
Figure 65 – Errors of the 300 μL pipettor (fresh tips)	213
Figure 66 – Errors of the 300 μL pipettor (rinsed tips).....	213
Figure 67 – Errors of the 5 mL pipettor	214
Figure 68 – Errors of the 10 μL pipettor.....	215
Figure 69 – Errors of the 100 μL manual pipettor	216
Figure 70 – Errors of the 1 mL manual pipettor	216
Figure 71 – Diagrams of <i>formal</i> redox potentials $E^{\circ'}$ for redox couples of Np and Pu in 1M HClO_4	219

LIST OF TABLES

<u>Table</u>	<u>Page</u>
Table 1 – Overview of well-known oxidation states of lanthanide and actinides*	11
Table 2 – Differences (in volts) in potentials of oxidation and reduction of tetravalent and pentavalent uranides in 1M perchlorate system.....	17
Table 3 – Variation of the apparent equilibrium constants of Np(V) disproportionation in HNO ₃ and HClO ₄ (data from Escure et al., 1971 [44]).....	27
Table 4 – Equilibrium data reported on the oxidation of Np(V) by nitric acid.....	29
Table 5 – Results and experimental conditions of kinetic studies of oxidation of Np(V) by nitric acid	31
Table 6 – Rate constants, reaction orders for H ⁺ , and activation energies of Np(VI) and Pu(IV) reduction by selected hydrazine and hydroxylamine derivatives in nitric acid / nitrate solutions of 2 M ionic strength at the temperature of 25°C	45
Table 7 -Comparison of standard (25°C) thermodynamic values for thermal activation at of the reaction Np(V) + V(V) with published literary data	93
Table 8 - Rate constants of the HNO ₂ + AHA reaction system in 1.0 M HNO ₃	124
Table 9 - Parameters of thermal activation for the processes of the AHA + HNO ₂ reaction system	127
Table 10 – Determined values of rate constants in experiments with various H ₂ O ₂ concentration.....	132
Table 11 – Parameters of thermal activation according to the activated complex theory.	137
Table 12 - Overview of results of studies of radiolytic* yields of HNO ₂ from aqueous HNO ₃ ..	169
Table 13 - Comparison of radiolytic yields of HNO ₂ in aqueous and organic solutions of HNO ₃ in concentrations corresponding to extraction equilibrium.....	172
Table 14 – Summary of all experimental results	217
Table 15 – Standard electrochemical potentials for vanadium redox reactions [24]	219
Table 16 - Studied combinations of oxidation states of reactants in vanadium redox reactions with neptunium	220
Table 17 - Studied combinations of oxidation states of reactants in vanadium redox reactions with neptunium	225

LIST OF ACRONYMS

AHA	Acetohydroxamic Acid
An	Actinide element
ANL	Argonne National Laboratory
ATALANTE	ATelier Alpha et Laboratoires pour ANalyses, Transuraniens et Études de retraitement
BASi	Bioanalytical Systems, Inc.
CCD	Chlorinated Cobalt Dicarbollide
CMPO	Octyl(phenyl)-N,N-diisobutylcarboylmethyl-phosphine Oxide
DIAMEX	DIAMide EXtraction
DOE	Department of Energy
EDTA	EthyleneDiamine Tetraacetic Acid
FHA	Formohydroxamic Acid
FP	Fission Product
FPEX	Fission Product Extraction
H ₂ Q	Hydroquinone
HAN	HydroxylAminium Nitrate
HDEHP	Di-(2-ethylhexyl)phosphoric Acid
HPGe	High Purity Germanium Detector
I	Ionic Strength
INL	Idaho National Laboratory
Ln	Lanthanide element
LANL	Los Alamos National Laboratory
LSC	Liquid Scintillation Counting
MOX	Mixed Oxide
MU	Methylurea
NMU	N-nitroso-methylurea
NaI	Sodium Iodide Detector
NASA	National Aeronautics and Space Administration
NPEX	Neptunium Plutonium EXtraction
OLIS	On-Line Instrument Systems, Inc.
OSR	Off-site Source Recovery
PARC	PARtitioning Conundrum key process

LIST OF ACRONYMS (Continued)

PEG	Polyethylene Glycol
ppm	Parts-Per-Million
PUREX	Plutonium Uranium Reductional EXtraction
RK4	Runge-Kutta Fourth Order
RSM	Rapid-Scanning Monochromator
RTG	Radioisotope Thermoelectric Generator
SANEX	Selective ActiNide EXtraction
SHE	Standard Hydrogen Electrode
SIT	Specific Ion Interaction Theory
SRP	Standard Reduction Potential
SSC	Silver-Silver Chloride electrode
TALSPEAK	Trivalent Actinide Lanthanide Separations by Phosphorus-Reagent Extraction from Aqueous Komplexes
TBP	Tri- <i>n</i> -butyl Phosphate
THORP	Thermal Oxide Reprocessing Plant
TRU	Transuranic
TRUEX	Transuranium Extraction
TRUCLAB	TRansUranic Element LABoratory
UNF	Used Nuclear Fuel
UREX	Uranium Extraction
UREX+	Uranium Extraction (Suite of Extraction Processes)
US DOE	United States Department of Energy
UV-VIS-NIR	UltraViolet-VISible-Near Infra-Red

LIST OF SYMBOLS

A	Pre-Exponential Factor	α	Alpha Decay
a_i	Molar Activity of Species i	α	Order of Reaction
c_i	Molar Concentration of Species i	β	Beta Decay
D	Distribution Ratio	γ	Gamma Radiation
E	Half-Cell Potential (Specific Conditions)	γ_i	Activity Coefficient
E°	Standard Redox Potential	ε	Molar Absorption Coefficient
E'°	Formal Redox Potential	μ	Ionic Strength
E_a	Activation Energy		
ΔG	Gibbs Energy (Specific Conditions)		
ΔG°	Gibbs Energy (Standard Conditions)		
ΔH	Enthalpy of Reaction		
k	Rate Constant		
K_{mn}	Equilibrium Constant		
n	Number of Exchanged Electrons		
R	Gas Constant		
ΔS	Entropy of Reaction		
$T_{1/2}$	Half Life		
v/v	Volume Percentage		
z	Ionic Charge		

DEDICATION

For my grandmother

Milada Přečková

and my late grandfather

Jaromír Přeček

who showed me the path to the person I would like to be.

The Kinetic and Radiolytic Aspects of Control of the Redox Speciation of Neptunium in Solutions of Nitric Acid

1 INTRODUCTION

1.1 General Background

Chemistry of radioactive elements has been an essential part of the development of nuclear technology that began at the end of the 19th century by the discovery of radioactivity of uranium by Henri Becquerel in 1896 and of new chemical elements present in its radioactive decay chain by Marie and Pierre Curie in 1898. At present day, nuclear technology has many indispensable uses in research, medicine and general industry, but the most prominent use is generation of nuclear energy from the fission of heavy actinides. Prior to the March 2011 nuclear accident at the Fukushima Dai-ichi power plant in Japan that resulted in significant alteration of policies of a few important nuclear power producing countries (especially Germany), nuclear energy provided 5.8% of world total primary energy supply, primarily in the form electricity - its share was 13.4% of the 20 thousand terawatt-hours of electric power generated around the world per year . Despite a possible temporary setback, contemporary projections predict further increase in the use of nuclear energy, driven especially by many large countries in Asia (China, India, Korea). The activities of current world nuclear energy industry result in generation of approximately 10 000 metric tons per year [1] of used nuclear fuel (UNF)* – a complex mixture of chemical elements, each consisting of various isotopes. Approximately 0.05-0.1% of the mass of UNF is made of the chemical element neptunium (Np).

1.2 Motivation

Neptunium is an important actinide element from several different viewpoints (which will be discussed later) and its separation from used nuclear fuel is a desirable target,

* The author has decided to use in this document the more accurate and ideologically less burdened term “used nuclear fuel” (UNF) despite the widespread past and present usage of its synonym “spent nuclear fuel” (SNF).

because of the issue of its long-term radiotoxicity and because of its valuable potential application in production of the Pu-238 radionuclide, which has a recognized potential for reliably powering inaccessible equipment, particularly in applications in space technology.

At present, the technology of reprocessing of UNF employed by the nuclear fuel cycle industry is called PUREX. This method is based on the selective liquid-liquid extraction of uranium and plutonium from other elements in the nitric acid solutions of dissolved used fuel using 30% tri-n-butylphosphate in kerosene. The process starts with the dissolution of spent fuel rods in hot concentrated (8 M) nitric acid. The various nitrogen-oxide compounds produced during the dissolution process and the high radiolysis rate in the spent fuel solution result in neptunium existing in several different oxidation states – primarily as Np(V) and Np(VI), possibly as Np(IV). Consequently, neptunium can be distributed in both aqueous and organic product streams due to vastly different extractability of these oxidation states, complicating the purification of the uranium and plutonium products. Presently, neptunium is usually re-diverted into the highly active raffinate waste stream [2].

In the recent research work on an advanced PUREX process called UREX+ at Argonne National Laboratory in United States, original expectations about the behavior of neptunium failed in predicting its speciation and movement in the liquid-liquid separation process [3]. Despite significant adjustment of the feed solution (primarily by destroying organic reducing agents and by increasing the concentration of nitric acid), the redox speciation of neptunium did not reach the desired target. About a third of Np was not extracted when desired and was ultimately recovered only in a later process stream [3]. Therefore, a better understanding of the kinetic and radiolytic aspects of the redox chemistry of neptunium in nitric acid solutions is needed in order to effectively control the destination of Np.

1.3 Expected Outcomes

The aim of this study was to develop or enhance the understanding of several key topics governing the redox behavior of neptunium in nitric acid medium, all of which are of vital importance for the engineering design of industrial-scale liquid separation systems:

- the kinetics of reactions of neptunium(V) and (VI) with several redox-active compounds envisaged for use in the reprocessing and tested during UREX+ process development (vanadium-V, acetohydroxamic acid) – identification of their rate law and determination of rate constants as a function of nitric acid concentration and of temperature,
- interactions of neptunium(V) and (VI) with nitrous acid (HNO_2) as a key redox-active compound in the nitric acid chemistry of neptunium,
- effects of nitric acid radiolysis, which is perhaps the most important source of nitrous acid in the real reprocessing solutions,
- chemical reactions leading to scavenging of nitrous acid by artificially introduced agents (methylurea, acetohydroxamic acid) or compounds generated due to radiolysis of aqueous nitric solution (H_2O_2).

1.4 Overview of the Dissertation

The work presented in this dissertation was performed as part of the author's graduate studies at the Oregon State University and describes the scientific work performed in the Radiochemistry research group of Prof. Alena Paulenova. The dissertation is written in a manuscript format because most of its chapters will be published or have already been published in scholarly journals. The text is organized into 12 chapters followed by a bibliography and 3 appendices. The introduction sections of the manuscripts include information that is also discussed in the general review of the dissertation.

The twelve chapters of this dissertation can be thematically divided in four main parts:

Chapters 1, 2, and 3 briefly describe the general purpose, motivation and expected goals of the work, provide an argument about the importance of neptunium and describe its position among the actinide elements, give an extensive overview on practical issues in the control of neptunium redox state in extraction separation processes utilized for Used Nuclear Fuel reprocessing, and, lastly, deal about the theoretical and practical experimental details of the work described afterwards.

Chapters 4, 5, and 6 describe the research the author has undertaken to study the reactions of neptunium with two redox agents artificially administered (pentavalent vanadium and

acetohydroxamic acid) and one redox agent naturally present (nitrous acid) in the studied system of nitric acid solution.

Chapters 7, 8, and 9 focus on the chemistry of nitrous acid itself in the nitric acid solution and on the reactions leading to the scavenging of nitrous acid from the solution with acetohydroxamic acid and hydrogen peroxide.

Chapters 10, 11, and 12 summarize the studies performed to better understand the influence of radiation on the nitrous acid chemistry and especially on the redox chemistry of neptunium in real reprocessing conditions.

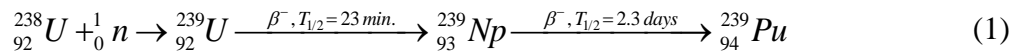
The list of bibliography that supports this dissertation is followed by three appendices, each related to a specific topic from the first three chapters of the dissertation, but in bigger breadth than would be appropriate as a subsection of one of these chapters.

2 REVIEW OF LITERATURE

2.1 Importance of Neptunium

2.1.1 Discovery

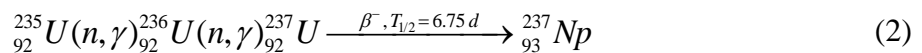
Neptunium, or element “93”, is a somewhat less well-known actinide chemical element, lying between uranium and plutonium. The discovery of neptunium and its introduction into the area of chemistry of transuranic elements has been made by Edwin M. McMillan and Philip H. Abelson in 1939 soon after the effect of nuclear fission was discovered [4]. Since element 93 is the first element after uranium, it was named after Neptune, the first planet to orbiting the Sun beyond Uranus. The neptunium isotope discovered was the short-lived Np-239 (half-life of 2.3 days), the precursor of the more famous plutonium-239, and the McMillan and Abelson have produced it using a neutron capture reaction:



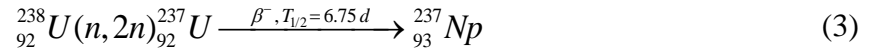
and proved its existence on the basis of Np-239 radioactive half-life.

Plutonium-239, which is an alpha-emitter, had a too long half-life of 24 110 years to be discovered in the small amounts produced; consequently, McMillan and Abelson were unsuccessful in detecting its radiation [5]. The discovery of the first plutonium isotope (Pu-238) then took place a year later as a result of experiments of continuation of transmutation experiments by Seaborg, Wahl and Kennedy [4, 6].

Even though Np-239 was the first isotope of neptunium to be discovered, due to its short half-life it had very little significance in the investigation of its chemical properties. These became of interest when Np-237 was discovered. It was first produced in weighable quantities in nuclear reactors during the US Manhattan Program[7]. The production of Np-237 happens by a thermal neutron capture on uranium-236, followed by a beta-decay; U-236 is itself a product of non-fissioning neutron capture on the isotope uranium-235, the fissile component of natural uranium. The process leading to Np-237 can be summarized in the following scheme:



In nuclear reactors featuring a fast neutron spectrum, which are so far relatively rare, another process also leads to the production of neptunium directly from the more abundant uranium isotope U-238 [8]:

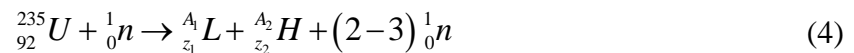


Neptunium-237 is a long-lived nuclide that decays with a half-life of 2.144 million years by an alpha-particle emission of several different energies between 4.5 - 4.9 MeV (most prevalent is the energy 4.788 MeV at 47.64% intensity [9]). The radioactive decay is accompanied by the emission of gamma-rays of various energies (29.4 keV and the 86.5 keV are of highest relevance with intensities of 15% and 12.4%, respectively [10]).

2.1.2 Neptunium in the nuclear fuel cycle

Since 1942, when the development of nuclear power started with Enrico Fermi's Chicago Pile 1 reactor experiment, hundreds of nuclear reactors have been operated around the world for the purposes of production of electric and heat power (including naval propulsion), plutonium for weapons, isotopes for medicine and industry, or just for general research and education purposes.

Most of these reactors utilize the only naturally available fissile nuclide U-235 for their fissile material. Presently, the primary reaction utilized for harvesting the energy contained in uranium is the nuclear fission of the excited U-236 nucleus created by a capture of a neutron on the nucleus of U-235. The reaction results in the production of several neutrons (2.4 on average), one of which carries the nuclear chain reaction, and a large variety of couples of two different-mass fragments L and H with atomic masses distributed around 94 and 140, respectively [2] :



A large amount of energy (187 MeV average) is released by this reaction, mostly in the form of kinetic energy of the fragments, neutrons and gamma rays. The fission fragments are in a highly unstable state which results in further radioactive transformation into more stable fission products that releases additional decay energy (~10-15 MeV).

However, some neutron captures do not lead to nuclear fission and as a result of the radiative neutron capture process (2), nuclear power reactors produce small, but

significant quantities of neptunium-237. At present day, the ~440 reactors in operation can be expected to create around 3000 kg of Np-237 annually [8]. Depending on the initial enrichment and length of power operation, the content of neptunium in the used nuclear fuel can reach up to nearly 1 kilogram per 1000 kg of initial uranium loading, while the content of plutonium is approximately ten times larger [2].

2.1.3 Long-term Radiotoxicity of Neptunium in SNF

Light water reactors are the most common type of commercial nuclear power reactors operated all over the world. Their fuel is initially made of uranium oxide, in which the initial uranium-235 content is enriched to 3-5 % compared to its natural abundance of 0.72%, while the rest is the uranium-238 isotope. The used fuel coming from these reactors consists of 94-96% uranium (with less than 1% U-235), 3-5% fission products (FP), approximately 1% plutonium (over 50% is Pu-239, the rest is primarily Pu-238, 240, 241 and 242), and around 0.1-0.2 % of the so called *minor actinide* (MA) elements that are comprised of neptunium-237 and various isotopes of americium and curium [2].

There are currently two main strategies of dealing with UNF – direct disposal without any kind of treatment (Open Fuel Cycle) and reprocessing the fuel with the aim of separating and recycling its uranium and plutonium content (Closed Fuel Cycle), while leaving both fission products and minor actinides in the waste stream. In both strategies neptunium ends up in a waste stream and is intended to be disposed of.

The 2.144 million year half-life of Np-237 represents an issue for the efforts of designing repositories for waste containing neptunium. The 10-fold of the half-life (approximately 20 million years), which is the time necessary to let radioactivity reduce the amount of neptunium 1000-fold, is too long for any engineered barriers to survive. Also, in certain repository environments featuring oxidizing chemistry (such as is the recently halted Yucca Mountain repository project [11]), neptunium favors the +V oxidation state, which has the highest mobility of all actinide elements, which can then render even the geological barrier of the repository much less effective [12].

2.1.4 Non-proliferation issues

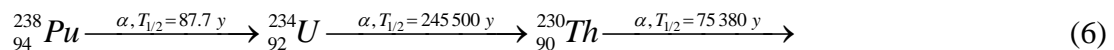
One of the more significant issues threatening the peaceful utilization of nuclear technologies is the potential of misuse of used nuclear fuel for the purpose of construction of nuclear explosive devices by non-recognized nuclear weapon states or interest groups (the so called *nuclear proliferation*). The attention has been focused on present-day industrial technologies for UNF reprocessing that lead to separation of fissile plutonium from other constituents in used uranium fuel. Even though the isotopic composition of plutonium from most kinds of civilian UNF is not entirely suitable for nuclear weapon applications [13], the technical knowledge and real capabilities associated with these separation technologies are under intensive international surveillance.

Neptunium-237 has also been found to be a possible material for construction of nuclear weapon (its bare sphere critical mass has been estimated to be around 60 kg, comparable to U-235 [14]). However, in contrast to separated plutonium which has isotopes that produce only weakly penetrating alpha and beta radiation and can thus be handled in glove boxes, neptunium-237 has an associated gamma-ray emission activity of its radioactive decay daughter product protactinium-233, which would significantly complicate the handling of this material compared to handling of plutonium.

Therefore, neptunium has been considered as a tool for enhancement of proliferation resistance of UNF reprocessing technologies by including both plutonium and neptunium into one product stream [13], as opposed to the current practice of separating plutonium from UNF in a pure form. Furthermore, plutonium is currently recycled in the form of so-called Mixed Oxide (MOX) fuel. If the MOX fuel would also include neptunium, further irradiation of Np-237 by thermal neutrons would lead to the production of Pu-238:



Plutonium-238 is a highly active alpha emitter due to its 87.7 years half-life and its decays into the long-lived uranium-234, which is a main member of the decay chain of natural uranium-238:



Increased concentration of Pu-238 in plutonium would contribute significantly to its specific heat generation (Pu-238 has an approximate power density of 0.5 W.g^{-1}). Concentration of Pu-238 reaching 20% would most likely preclude its possible use in preparation of a nuclear explosive device due to intensive heat generation (the critical mass of a plutonium sphere is approximately 5 kg [2], resulting in 500 W heat power generation – rendering the plutonium metal too hot to work with and possibly setting off the plastic explosive lens surrounding the device). Nevertheless, recent analysis of this particular application of neptunium has been considered rather impractical due to issues with nuclear fuel neutronics and insufficient supply of neptunium in general [15].

2.1.5 Potential Uses of Neptunium

Besides of the somewhat unrealistic idea of employing neptunium in an industrial-scale redox flow battery system investigated by Japanese scientists [16], the only practical use of isolated neptunium-237 is in the production of pure Pu-238 by neutron irradiation.

Plutonium-238 is a very valuable material outside of the classical nuclear power generation due to its high power density that is not accompanied by a significant gamma-ray hazard. In combination with thermoelectric conversion it is the most prominent material to be used in the so called Radioisotope Thermoelectric Generators (RTG), which have been employed for operation in situation where uninterrupted operation, maintenance and fuel replacement is too impractical or impossible – most notably as cardiac pacemakers (cardiostimulators) inside the human body and for powering deep-space probes [17].

In United States only, approximately 1600 pacemakers were implanted in 1970s, typically containing approximately 0.2 to 0.5 grams Pu-238 (130-310 GBq α -activity) as the heat source for the batteries. In terms of power reliability and longevity (only 11% power decrease in 10 years of operation) RTG source at that time outperformed any chemical battery sources; interestingly, most of these devices survived their users and are being collected by the Off-Site Source Recovery (OSR) Project at the Los Alamos National Laboratory (LANL) [18]. However, soon after the application of RTG pacemakers, long-lasting lithium batteries (>10 years) were developed in 1974 and the use of Pu-238 RTG-powered pacemakers has been discontinued [19].

Presently, production of Pu-238 for space power applications of is the most prominent practical application of neptunium. For a large space probe that ventures far from the availability of solar power, multiple-kilogram Pu-238 heat sources were installed (e.g. the famous Voyager 1, Voyager 2, and Cassini space probes had each over 10kg of Pu-238 [20])[†]. Recently, constraints in availability of Pu-238 for space programs of the National Aeronautics and Space Administration (NASA) have spurred the United States Department of Energy (DOE) into revitalizing the neptunium irradiation program in order to produce sufficient amounts (up to 2 kg per year) of Pu-238 for future expected applications [21]. Neptunium targets are planned to be irradiated in existing DOE research reactors, the High Flux Isotope Reactor in Oak Ridge National Laboratory and the Advanced Test Reactor at Idaho National Laboratory and then reprocessed using solvent extraction to extract Pu-238 [22, 23].

[†] The author has to also acknowledge the recent successful landing of the NASA Curiosity Mars rover that took place on August 6, 2012, in the last days of compiling of this work [214]. Curiosity was launched with a radioisotope thermoelectric generator containing 4.8kg of $^{238}\text{PuO}_2$ [215].

2.2 General chemical properties of neptunium among the actinide elements

2.2.1.1 Oxidation states of actinide elements

Neptunium is a member of the 5f electron series called the actinide elements, the discovery of which is primarily attributed to Glenn T. Seaborg. In contrast to the lanthanide elements which exhibit a very homogeneous redox behavior with increasing atomic number (with most stable oxidation state +III), the behavior of early actinides (Ac, Th, Pa, U) is more similar to transition metals. As is demonstrated in Table 1, actinide elements start to mimic lanthanide behavior only after curium.

Table 1 – Overview of well-known oxidation states of lanthanide and actinides*

Lanthanides	La	Ce	Pr	Nd	Pm	Sm	Eu	Gd	Tb	Dy	Ho	Er	Tm	Yb	Lu	
				(II)		II	II			(II)			(II)	II		
	<u>III</u>															
		IV	(IV)	(IV)					(IV)	(IV)						
Actinides	Ac	Th	Pa	U	Np	Pu	Am	Cm	Bk	Cf	Es	Fm	Md	No	Lr	
		(II)					(II)			(II)		(II)	II	<u>II</u>		
	<u>III</u>	(III)	(III)	III	III	III	<u>III</u>	III	<u>III</u>							
		<u>IV</u>	IV	IV	IV	<u>IV</u>	IV	IV	IV							
			<u>V</u>	V	<u>V</u>	V	V									
				<u>VI</u>	VI	VI	VI									
					VII	VII										

* most stable oxidation states are indicated by being underscored and bold, oxidation states in brackets are known from solids or non-aqueous solutions; table based on refs. [24, 25]

The elements of uranium, neptunium, plutonium and americium form a quite original chemical group – uranides – that is characterized by multiplicity of possible oxidation states in aqueous solutions. The properties of the corresponding oxidation states of these four actinides exhibit significant similarities. The possible and common oxidation states of uranides are +III, IV, V, and VI. In basic and strongly oxidizing solutions, stabilization of the +VII oxidation state has been achieved for Np and Pu [24].

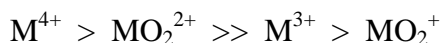
In acidic aqueous solution, the tri- and tetravalent cations are present in the form of M^{3+} and M^{4+} while penta- and hexavalent uranides form the nearly linear di-oxocations MO_2^+ and MO_2^{2+} . These *actinyl* molecular cations are remarkably stable, and “bare” M^{5+} and

M^{6+} ions have not been observed so far in aqueous environments (in non-aqueous environment the hexafluorides of U, Np and Pu have been well studied [26]). The structure of the actinyl ions is linear: $O=M=O$, the strength of the covalent bonds being only somewhat weaker (length of bonds longer) for the +V compared to the +VI oxidation state, without any significant change to the geometry.

All actinide ions are complexed by water or by other ligands present in aqueous solutions, and the coordination numbers of water molecules is between 8 and 10 for tri- and tetra-valent ions and between 5 and 6 for penta- and hexa-valent ions [27].

2.2.1.2 Basic principles of complexation chemistry of different redox states of actinides

The complexation chemistry of different redox states of actinides plays an enormously important role in their separation from other elements and from each other by many different separation processes, and especially so in liquid-liquid extraction or ion exchange. The degree of complexation by hard ligands (such as sulfate, chloride or nitrate anions) increases in the following order [27]:



The tendency of forming complexes increases in the series from uranium(IV) to americium(IV) and decreases from uranium(VI) to americium(VI). It is important to note that the degree of complexation of the pentavalent ions cannot be considered as entirely negligible since they form complexes with, e.g., NO_3^- , SCN^- and with anions of the ethylenediamine tetraacetic acid (EDTA) [27].

In general, the stability of the actinide complexes with important inorganic and organic anions increases in the order [27]:



The above-described rules are important for the understanding the differences in the stability of even-charged oxidation states of actinides, especially the tetravalent state, between non-complexing and complexing environment – one of the prime examples is the stabilization of tetravalent plutonium in 3M hydrochloric acid [28] or disproportionation of neptunium(V) into Np(IV) and Np(VI) in the medium of complexing 2M sulfuric acid [17].

Hydrolysis of actinide ions is a special case of complexation with hydroxide anions OH^- . The degree of hydrolysis depends on the actinide oxidation state in the same order, as described above for other complexants; therefore, it most strongly affects the tetravalent actinides. The effects of hydrolysis on actinide speciation are of paramount importance in neutral and alkalic solutions, but acidic solutions with $\text{pH} < 1$ are mostly free of the effects of hydrolysis [27].

2.2.1.3 Redox potentials of actinides in aqueous solutions

The explanation of stability and reactivity of different actinide oxidation state can be most quantitated by the comparison of the *standard reduction potentials* E° (also standard *redox* potential) of their redox couples. By definition, the E° is equal to the electric potential difference of an electrochemical cell reaction of the reduction of the actinide (or any other species) in higher oxidation state $\text{An}(\text{ox})$ to a lower oxidation state $\text{An}(\text{red})$ by the oxidation of molecular hydrogen to solvated protons (in standard conditions of ideal 1 mol/L concentration activities of all solute reactants and of 100 kPa of H_2 gas pressure at the temperature of $25\text{ }^\circ\text{C} = 298.15\text{ K}$) [25]:



The reaction is characterized by the change in the value of Gibbs free energy ΔG° (J/mol) and the standard reduction potential is related to this thermodynamic quantity by the relation:

$$E^\circ = -\frac{\Delta G^\circ}{nF} = \frac{RT}{nF} \ln K \quad (8)$$

where F is the Faraday constant of electric molar charge ($F = 96\,485\text{ C/mol}$), R is the ideal gas constant ($R = 8.314\text{ J/K/mol}$), T is the absolute temperature (in kelvins) and K is the equilibrium constant of reaction (7).

By international scientific agreement, the value of E° of reaction (7) is made equivalent with an ideal *half-cell* potential reaction that describes the reduction of the actinide (or any other species) in higher oxidation state $\text{An}(\text{ox})$ to a lower oxidation state $\text{An}(\text{red})$ by accepting a number of n electrons (e^-):



The Nernst Law describes the potential E of such a half-cell when the concentration activities $a_{An(red)}$ and $a_{An(Ox)}$ of the reduced and oxidized form of the actinide species are changing:

$$E = E^o - \frac{RT}{nF} \ln \frac{a_{An(red)}}{a_{An(Ox)}} = E^o - \frac{RT}{nF} \ln \frac{\gamma_{An(red)} \cdot [An(red)]}{\gamma_{An(Ox)} \cdot [An(Ox)]} \quad (10)$$

Due to complicated hydrolysis phenomena that take place in neutral solutions of very low ionic strength, where the activity coefficients γ would be equal to 1, the redox potentials of actinides have been tabulated as *formal reduction potentials* $E^{o'}$ that are defined by the relationship:

$$E = E^{o'} - \frac{RT}{nF} \ln \frac{[An(red)]}{[An(Ox)]} \quad (11)$$

The values of $E^{o'}$ are specific for a particular medium in which the activity coefficients of the actinides are independent of their own concentrations.

For acidic solutions of actinides, formal reduction potentials are usually determined at 1M H^+ concentration and therefore their values approximate the standard potentials – due to its weak complexation power, 1M perchloric acid medium is usually the most popular for accurate determination of actinide potentials.

Figure 1 shows the Latimer diagrams of the formal reduction potentials $E^{o'}(An^{ox}/An^{red})$ of the couples of different oxidation states of uranium in acidic aqueous solutions. The values are capable of explaining the tendency of progressive stabilization of lower oxidation states in the order from uranium to americium, previously denoted in Table 1, on the basis of comparison with the approximate half-cell potentials of reduction and oxidation of the primary matrix component of aqueous solutions – water[‡] [25]:



Redox couples with potentials lower than that of reduction of hydrogen ions should liberate hydrogen from aqueous solutions, which will oxidize the lower redox state of the couple $An(red) \rightarrow An(Ox)$, and, correspondingly, couples with redox potentials above the

[‡] H^+ ions in the reaction (12) are replenished by the autoionization of water: $H_2O \leftrightarrow H^+ + OH^-$

oxidation of water should liberate gaseous oxygen while the higher oxidation should get reduced $An(Ox) \rightarrow An(Red)$.

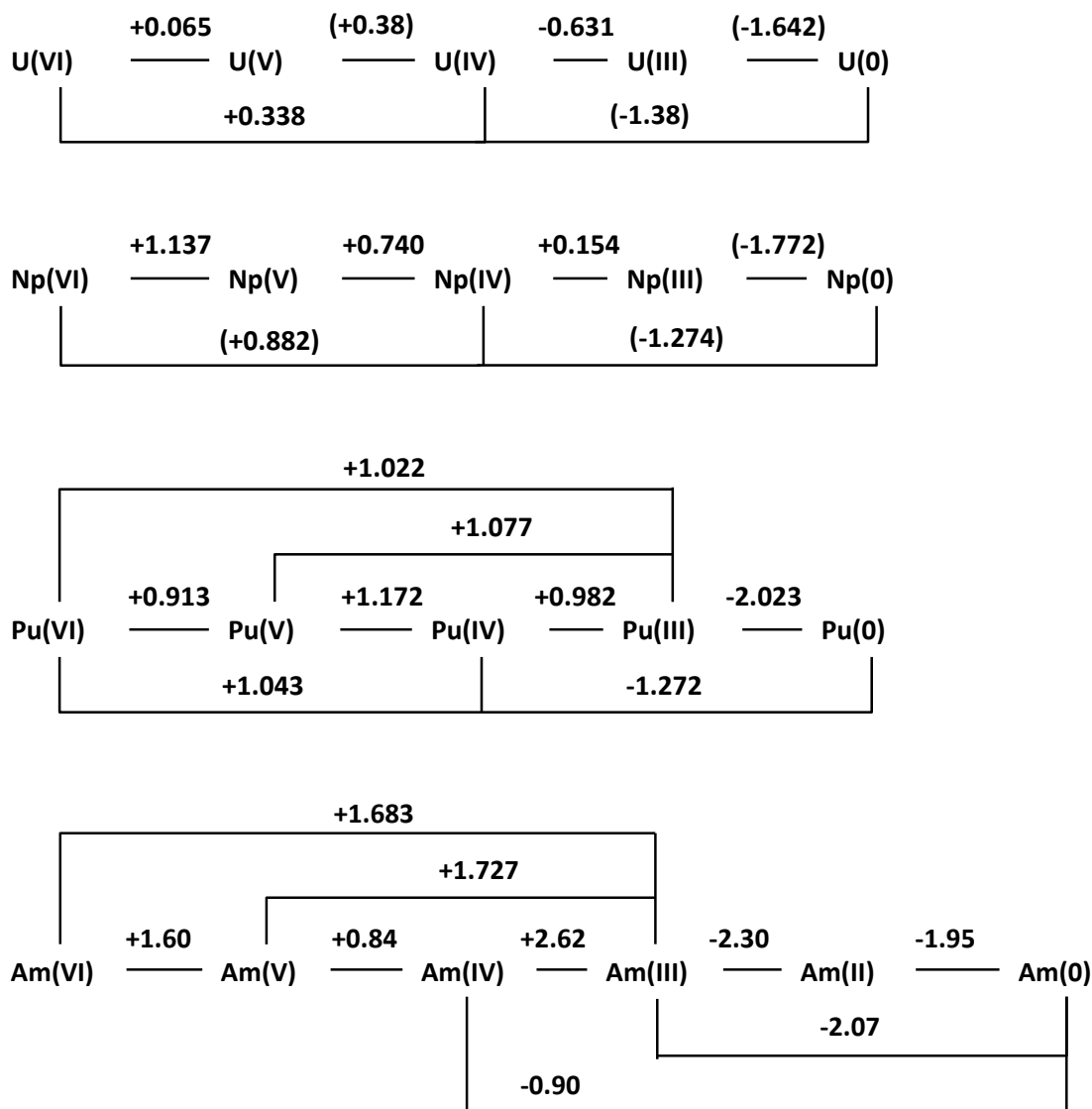


Figure 1 – Diagrams of formal redox potentials $E^{\circ'}$ in 1M HClO₄

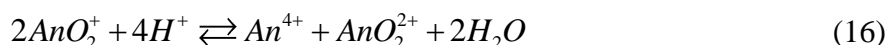
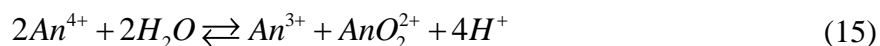
(in volts vs. normal hydrogen electrode at 25°C) for redox couples of U, Np, Pu and Am data adopted from: U and Np - ref. [29], Pu – ref. [28], Am – ref. [30] (data in brackets are standard potentials E° from ref. [25])

It is evident from Figure 1 that uranium(III), americium(II) and all uranides in their elemental form are strong reducing agents capable of reducing water to hydrogen, while americium(IV) and (VI) are powerful enough oxidizers to oxidize water to oxygen; therefore, these actinide redox species are not stable in aqueous solutions. In the case of

plutonium and neptunium, all oxidation states can be present in acidic aqueous solutions that have been de-aerated – since neptunium(III) is easily oxidized by oxygen in air.

2.2.1.4 Disproportionation reactions of actinides

Among the individual oxidation states of a particular uranium element, there are three possible types of reaction in acidic aqueous solutions:



These reactions can be observed with all uranium, but the equilibria depend on the nature of the element, acidity and especially the complexing power of the solution – complexing agents can significantly shift the equilibria by preferentially binding tetravalent and hexavalent actinides. The tendency of tetravalent and pentavalent oxidation state toward disproportionation can be assayed by calculating the differences in potentials of their oxidation to a higher oxidation state and reduction to a lower oxidation state, defined as:

$$\Delta E(\text{IV}) = E^\circ(\text{An}^{\text{V}}/\text{An}^{\text{IV}}) - E^\circ(\text{An}^{\text{IV}}/\text{An}^{\text{III}}) \quad (17)$$

$$\Delta E(\text{V}) = E^\circ(\text{An}^{\text{VI}}/\text{An}^{\text{V}}) - E^\circ(\text{An}^{\text{V}}/\text{An}^{\text{IV}}) \quad (18)$$

As can be derived from equation (8), variables $\Delta E(\text{IV})$ and $\Delta E(\text{V})$ are proportional to the negative values of the Gibbs free energy change ΔG° of reaction (15) and (16), which describe the disproportionation of An(IV) and An(V), respectively.

Since a positive value of $\Delta E(\text{IV})$ or $\Delta E(\text{V})$ would indicate a positive value of the Gibbs free energy change, the reaction (15) and (16) would not be spontaneous and the respective oxidation state would be most likely stable. However, when the difference $\Delta E(\text{IV})$ or $\Delta E(\text{V})$ is close to zero or negative, the particular ion An(IV) or An(V), respectively, is liable to a partial or complete spontaneous disproportionation [31]. The results based on calculations from data in Figure 1 are presented below in Table 2 and show that pentavalent U and Pu are unstable toward disproportionation, as is tetravalent Am. The value of $\Delta E(\text{IV})$ in case of tetravalent plutonium is also low enough to allow its disproportionation – so that solutions of initially pure Pu(IV) and Pu(V) in 1M HClO₄ system will over time disproportionate into solutions that will preserve the average

tetravalent or pentavalent oxidation state, respectively, but it will contain significant fractions of all four aqueous oxidation states of plutonium: +III,+IV, +V and +VI [28].

Table 2 – Differences (in volts) in potentials of oxidation and reduction of tetravalent and pentavalent uranides in 1M perchlorate system

	U	Np	Pu	Am
$\Delta E(\text{IV})$	1.01	0.59	0.19	-1.78
$\Delta E(\text{V})$	-0.32	0.40	-0.26	0.76

2.2.1.5 General characteristics of kinetics redox reactions of actinides

In the study of redox behavior of actinide elements in solutions, information about the kinetics of these processes (in combination with the knowledge of their thermodynamic aspects) is necessary to develop a sufficient level of understanding of these processes for their practical application in laboratory research and industrial use.

In a typical actinide reaction with redox agents, a 1:1 stoichiometry is observed - the actinide element An changes its oxidation state from (X) to (Y), while the redox agent R is converted to a product P or multiple different products:



The kinetics studies are usually interested in the temporal dependence of the *rate* of these reactions. Since sometimes the determination of stoichiometry is not possible, the rate in homogeneous solutions is typically defined as the negative value of the time derivative of the molar concentration of one of the reactants of interest, usually the actinide element in its starting oxidation state $An(X)$:

$$rate = -\frac{d[An(X)]}{dt} \quad (20)$$

The standard dimension of the rate is traditionally mol/L per second, $M.s^{-1}$.

In general, the rate of most of such reactions usually follows a mathematical expression called the *rate equation* or *rate law*, in which the rate at a particular point in reaction time is proportional to a certain power of each of the immediate concentrations of the reacting actinide $[A(X)]$ and the redox agent $[R]$:

$$-\frac{d[A(X)]}{dt} = k[An(X)]^\alpha [R]^\beta \quad (21)$$

The exponents α and β are called reaction orders with respect to the particular reactant and the overall order of the reaction is determined by their sum, while k is the *rate constant*, characteristic for each reaction. Actinide reactions usually follow some variation of the so called *overall second order* process, in which the rate is of 1st order with respect to both the actinide An(X) and the redox agent R:

$$-\frac{d[A(X)]}{dt} = k''[A(X)][R] \quad (22)$$

The quantity k'' is the *apparent 2nd order* rate constant of the reaction and has a standard dimension of $M^{-1}s^{-1}$. In the situation where one of the reactants (usually the redox agent) is in a significant excess, e.g. in conditions where $[A(X)]$ is much smaller than $[R]$ already at the beginning of the process, the reaction will follow an *apparent 1st order (pseudo-1st order)* rate equation:

$$-\frac{d[A(X)]}{dt} = k'[A(X)] \quad (23)$$

with k' being the apparent 1st order standard rate constant of the standard dimension of reciprocal time (s^{-1}).

The values of both apparent 1st and 2nd order constants usually depend on other parameters of the reacting system, primarily on the acidity, ionic strength, and temperature, which are usually assumed to be constant during a particular chemical reaction. The temperature dependence of most reactions follows the Arrhenius Law:

$$k = A \cdot e^{-\frac{E_a}{R \cdot T}} \quad (24)$$

in which T is the absolute temperature (in kelvins), R is the ideal gas constant ($8.314 \times 10^3 \text{ kJ} \cdot \text{K}^{-1} \cdot \text{mol}^{-1}$) and A is the so called *frequency factor* of the same dimension as the rate constant, and E_a (kJ/mol) is the activation energy [32].

equation (24) is usually employed in a logarithmic form to acquire the activation energy from the slope of a linear relationship:

$$\ln k_1'' = \frac{-E_A}{R \cdot T} + \ln A \quad (25)$$

In combination with the knowledge of stoichiometric coefficients, the exact form of the rate law (21), the value of the rate constant k and its dependence on the concentration of the major constituents of the solution (e.g., hydrogen ions) at the standard ambient

temperature of 25°C (298 K), and the activation energy E_a are the three characteristics that usually used to describe the kinetics of a chemical reaction.

Furthermore, data on thermal activation are frequently analyzed by the assumptions of Activated Complex Theory [32], where the rate constant is expected to be related to the thermodynamics of an activated state, which is an unstable intermediary between the reactants and the products. The activated state is usually characterized by several thermodynamic quantities - the free Gibbs energy, entropy and enthalpy of the activation process: ΔG^\ddagger , ΔS^\ddagger and ΔH^\ddagger , which can be calculated by a modified Eyring formula [32]:

$$k_1'' = \frac{k_B T}{h} \cdot e^{\frac{-\Delta G^\ddagger}{RT}} = \frac{k_B T}{h} \cdot e^{\frac{\Delta S^\ddagger}{R}} \cdot e^{\frac{-\Delta H^\ddagger}{RT}} = e \cdot \frac{k_B T}{h} \cdot e^{\frac{\Delta S^\ddagger}{R}} \cdot e^{\frac{-E_A}{RT}} \quad (26)$$

where $k_B = 1.38 \times 10^{-23} \text{ J K}^{-1}$ is the Boltzmann constant and $h = 6.63 \times 10^{-34} \text{ J s}$ is the Planck constant. The activation entropy may contain information about the structural relationships of the formation of the activated complex, negative entropy values indicating associative processes and positive values hinting on dissociative processes[32]. A more detailed description of the applied methodology for the study of reaction kinetics is provided in chapter 3.

2.3 Neptunium in Reprocessing of Used Nuclear Fuel

2.3.1 PUREX Process

The essential step of UNF reprocessing is the world-wide used PUREX process (Plutonium Uranium Reductonal EXtraction), which is based on solvent extraction of uranium and plutonium from fission products and minor actinides dissolved in aqueous nitric acid, their partitioning, and purification. The process employs a 30% solution of tri-n-butylphosphate (TBP) in an n-alkane diluent. The purpose of the diluent is to enhance phase separation kinetics (by reducing the density and viscosity of the organic phase) and also to fine-tune the extraction properties of TBP. The diluent is usually based on a mixture of paraffin hydrocarbons (alkanes) such as kerosene (for purposes of scientific research the most widely used standard is n-dodecane, $C_{12}H_{26}$) [33]. A significantly simplified scheme of the method is displayed in Figure 2.

Several elementary steps are to be performed prior to the extraction, such as removal or deterioration of fuel cladding, fuel dissolution in nitric acid, suction and purification of liberated gases, removal of fuel cladding and insoluble fission products from the dissolved UNF nitric acid solution, solution conditioning in preparation for liquid extraction.

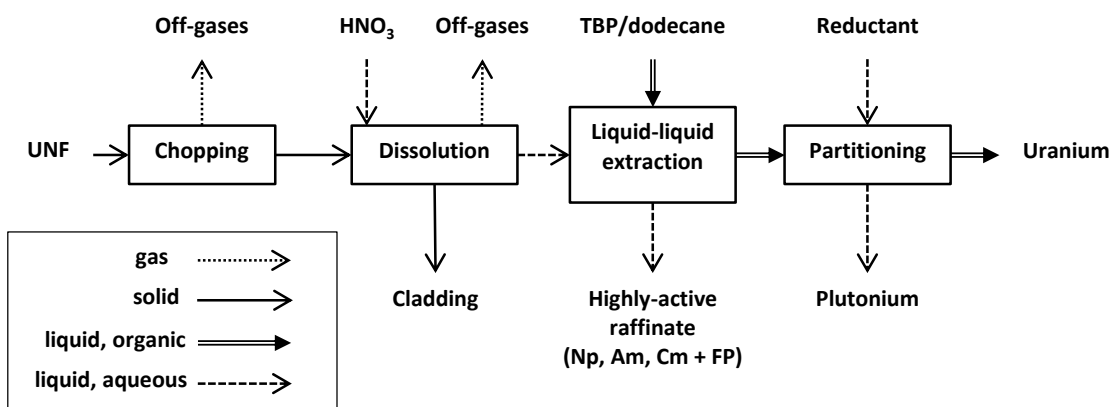
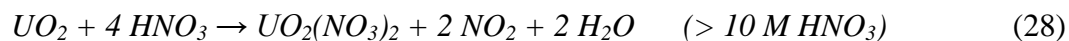


Figure 2 – Simplified scheme of the PUREX separation method

The most important chemical reactions for the most common nuclear fuel, which is based on uranium dioxide, are the dissolution reactions and uranium oxidation to the +VI state [2]:

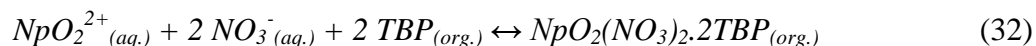
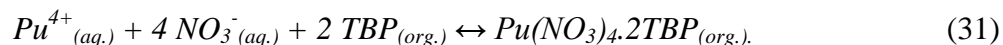
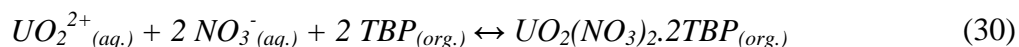


By feeding oxygen to the dissolving cell it is possible to reduce the amount of nitrogen oxide fumes [2]:



During dissolution the whole radioactive gaseous inventory of UNF is liberated. Explicitly they are radioactive gases like tritium, oxides of carbon-14, krypton-85, and iodine-129 and to some extent gaseous tetroxide of ruthenium-106. All these gases are directed (together with the created nitrogen oxides) to processes of nitric acid regeneration and purification systems.

The major advantage of the PUREX process is that it selectively extracts Pu(IV) and U(VI) from dissolved UNF solutions of moderate (multimolar) nitric acid concentrations. Tetravalent and hexavalent actinides such as U(VI), Pu(IV), Pu(VI), Np(IV) and Np(VI) are readily extracted whereas trivalent and pentavalent actinides like Pu(III) and Np(V) are almost inextractable – comparable to the extraction of the trivalent lanthanides that form a large part of the fission product elements. After UNF dissolution, neptunium is usually present as a mixture of inextractable Np(V) and extractable Np(VI) [2, 34]. A limited presence of small concentrations of the extractable Np(IV) is also possible, but unlikely due to the highly oxidizing effects of hot nitric acid used during the dissolution process. The extraction of actinides from the aqueous to the organic phase proceeds by the formation of neutral solvates – adducts of TBP and uncharged nitrate complexes of actinide ions molecules, which can then be transferred to the non-polar organic phase [35]. The most important extracting species are U(VI), Pu(IV) and Np(IV):



The affinity of a particular species present in the aqueous phase is described by its distribution ratio D , which is defined as the ratio of the equilibrium concentration of the particular species in the organic phase $c_{org.}$ against the concentration in the aqueous phase $c_{aq.}$:

$$D = \frac{c_{org.}}{c_{aq.}} \quad (33)$$

As is demonstrated in Figure 3 below the distribution ratios of the three neptunium redox species that can exist in the PUREX system – Np(IV), Np(V) and Np(VI), are dependent on the nitric acid concentration in the aqueous phase.

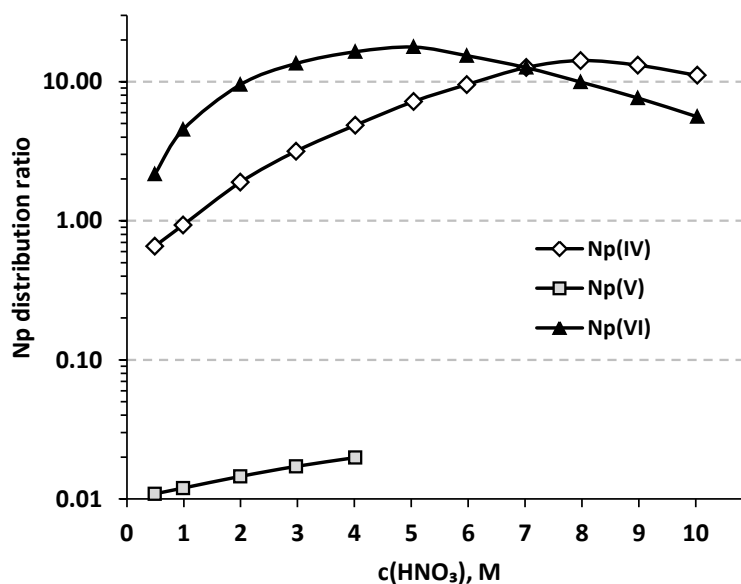
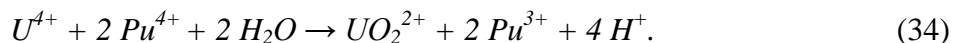


Figure 3 - Distribution ratios of Np(IV), (V) and (VI) between aqueous nitric acid and 30% TBP/n-alkane ($t= 20$ to 30°C); data from V.A. Drake, 1990 [17]

Besides the concentration of nitric acid, the distribution ratios are substantially influenced by the concentration of uranium and plutonium in the solution and by the concentration of TBP in organic phase. Decreased extraction of neptunium is a result of the tendency of uranium to replace neptunium in the organic phase, because the uranium-TBP complex is more stable than the neptunium-TBP complex [17]. As has been shown in equations (30)-(32), the result of the extraction are TBP adducts of UO_2^{2+} , NpO_2^{2+} , and Pu^{4+} nitrates in the organic phase and a mixture of fission products and minor actinides (which include Np-V) in the aqueous phase. The aqueous phase is called *highly active raffinate* and is the primary high level active waste produced in reprocessing [36].

The following step of the PUREX process is separation of plutonium from uranium and is traditionally called as *partitioning* [37]. It is performed by a reducing agent that converts plutonium into its poorly extracting trivalent state so that it is selectively stripped from the organic phase into the aqueous phase. There are multiple ways to reduce plutonium,

usually involving the use of a reducing agent. The historic use of salts of bivalent iron as a reducing agents has been discontinued to avoid the increasing of the weight and volume of the non-evaporable salt material content of the highly active waste, which is to be eventually be vitrified [36]. Presently, most facilities ended up utilizing reduced tetravalent uranium U^{4+} as a waste-free reducing agent for Pu^{4+} :



Preparation of U^{4+} is performed in a later step of the PUREX process where it is produced from pure uranium(VI) nitrate solution by electrolysis or by hydrogen reduction [36]. Alternatively, Pu^{4+} can be reduced by electrolysis directly [38], but despite its considerable advantages this method has been utilized in commercial reprocessing only in Russia [39]. Recently, stripping agents based on rapid selective complexation of tetravalent plutonium have been proposed, having the advantage of faster stripping kinetics compared to reducing agents [40].

The partitioned uranium and plutonium fractions are then several times purified with extraction and re-extraction (backwashing) steps in isolated uranium and plutonium purification cycles. The desired products of reprocessing – uranium and plutonium – are generated in the form of highly purified nitrate solutions which are thereafter subjected to several processes that result in solid U and Pu oxides [2]. Meanwhile, the contaminated nitric acid is recycled for repeated utilization in the process. Since neptunium is usually an undesirable contaminant in U or Pu product, it is routed along back to the waste processing of the highly active raffinate and ultimately ends up in a vitrified form.

The extraction of uranium and plutonium is performed either in a series of *mixer-settlers* or in several meters high continual *pulsed columns* [36]. In these devices the heavier aqueous phase of nitrate solution is contacted with the lighter organic phase containing TBP. A modern generation of contacting devices – *centrifugal contactors* – has various potential advantages (especially their compactness and throughput) and has been in research and development use for several decades [41], but has not met practical industrial application yet in the PUREX industry due to already previously established facilities. On the other hand, it is assumed that future reprocessing facilities will use centrifugal contactors for liquid-liquid extraction, due to much shorter residence times of

these contactors in comparison to mixer-settlers and pulsed columns, newer sufficiently fast redox reagents had to be identified [42].

2.3.2 *Advanced PUREX processes*

Since the 1990s there has been an increased international interest in advanced nuclear fuel cycles that would improve on the deficiencies of the current closed fuel cycle [43, 44]. Both partially closed cycles in which Pu is recycled as mixed-oxide fuel (MOX) and fully closed cycle which recycle all the transuranium (TRU) elements (Np, Pu, Am and Cm) have been suggested. It has been generally agreed that separation of neptunium alone is feasible with slight modifications of the PUREX process, because it is possible to maintain Np in a hexavalent state. Aside from neptunium, modification of the established PUREX process also enables the separation of iodine and technetium, important fission products with significantly long-lived radioactive isotopes (I-129 and Tc-99 have half-lives of 1.6×10^7 and 2.14×10^5 years, respectively). The case of separation of Am and Cm, which are most stable in their TBP-inextractable trivalent oxidation state, necessitates the employment of substantially different extraction systems (e.g. based on weak nitrogen donor extractants) [42].

Many advanced fuel cycle concepts were proposed and examined – e.g. DIAMEX/SANEX processes (CEA, France), “four-group process” (Japan) [42, 44]. In the United States a family of processes called under a generic name of UREX+ was in development by the US Department of Energy under the Advanced Fuel Cycle Initiative [3]. All of the UREX+ processes are distinguished by the fact that they do not separate pure plutonium, which is the main nonproliferation advantage of this UNF reprocessing concept [13].

The UREX+ process in general is a series of different solvent extraction processes and one ion exchange operation. Two of the solvent extraction steps are a modification from the PUREX process (based on extraction by TBP organic solution from aqueous nitric acid); the other solvent extraction processes utilize different organic extractants. The most recent demonstration of the process modification called UREX+3a, the scheme of which is summarized in Figure 4, was performed in 2007 in Argonne National Laboratory [45].

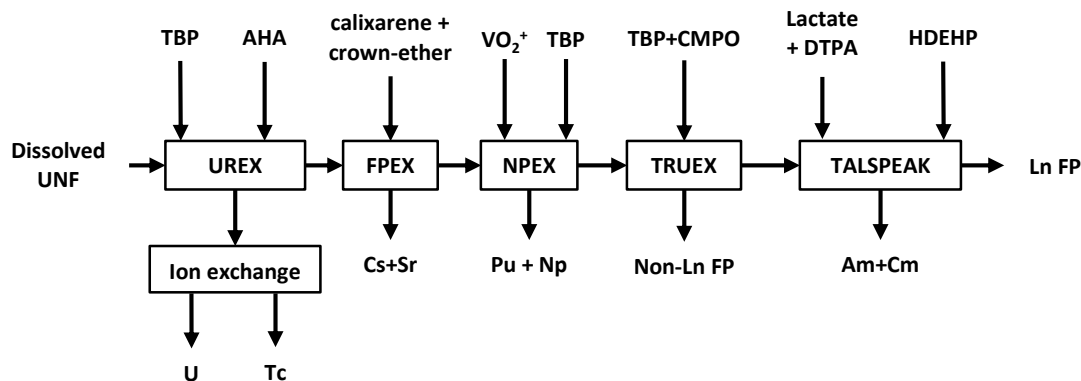


Figure 4 – Overview of the steps of the UREX+3a separation scheme

In the individual steps of the UREX+3a visible in Figure 4, the oxidation state of neptunium is conditioned by redox agents in the UREX and the NPEX steps.

The UREX step is a modified version of the first PUREX step involving the extraction of uranium and technetium by 30% TBP from a low-concentration (< 1 M) aqueous nitric acid solution of UNF. An aqueous complexing / reducing agent (acetohydroxamic acid, AHA) is employed to prevent extraction of plutonium (by formation of poorly extracted complexes of tetravalent Pu) and neptunium (by reduction of Np to the inextractable pentavalent oxidation state) from the aqueous phase.

In NPEX, which is based on another modification of the first PUREX step, the aqueous stream of the FPEX process is adjusted by heating and evaporation to increase the concentration of nitric acid in the solution and destroy the remaining acetohydroxamic acid complexant/reductant. An oxidizing agent like vanadium(V) as VO_2^+ is also added to ensure that most of neptunium is in the extractable hexavalent state [17] (a potential need of treating of the aqueous solution with a nitrous acid scavenger, such as is sulfamic acid, was also identified [46]); consequently, plutonium is extracted together with neptunium into the 30% TBP organic phase and separated from the rest of the fission products and minor actinides (Am, Cm).

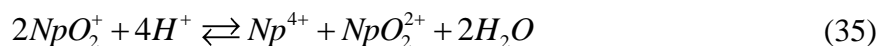
The increased proliferation resistance of the UREX+3a process is based on the fact the neptunium follows plutonium until the product phase, where mixed plutonium-neptunium oxides are expected to be made. As has been discussed before in chapter 2.1.4, an Np-237 impurity in plutonium would substantially increase the gamma-ray emission rate from the product material (somewhat discouraging its use as a weapons material) and lead to

Pu-238 production if used as MOX fuel in a nuclear reactor, further disqualifying the plutonium fraction from any consequent weapons material use, if the used MOX fuel were to be reprocessed. On the other hand, it is as yet an open question how hard it would be for a rogue agency to physically modify an industrial-scale UREX+ process to ensure the isolation of pure plutonium [13].

2.4 Control of the oxidation state of neptunium by redox reagents

2.4.1 Neptunium disproportionation and reaction with HNO_3

In strongly acidic solutions, such as is multimolar nitric acid used in most UNF reprocessing systems, Np(V) can partially disproportionate to Np(IV) and Np(VI). The reaction is dependent on the acid concentration, following the equilibrium reaction:



The apparent neptunium equilibrium concentration constant K_c and the fraction $R_{Np(V)}$ of pentavalent neptunium in total neptunium $[Np]_t$:

$$K_c = \frac{[Np^{4+}][NpO_2^{2+}]}{[NpO_2^+]^2} \quad (36) \quad R_{Np(V)} = \frac{[Np(V)]}{[Np]_t} = \frac{1}{1 + 2\sqrt{K_c}} \quad (37)$$

are dependent not only on the hydrogen ion concentration, but also on the complexing power of the anions of the particular acid. Examples of experimental values of the constant K_c and fraction of Np(V) in very weakly complexing perchloric acid and moderately complexing nitric acid environment are in Table 3.

Table 3 – Variation of the apparent equilibrium constants of Np(V) disproportionation in HNO_3 and $HClO_4$ (data from Escure et al., 1971 [47])

$K_c =$ concentration constant, $R_{Np(V)} =$ Np(V) fraction	Acid concentration (M)					
	5.5	6.0	6.5	7.0	7.5	8.0
$K_c(HNO_3)$	2.55	7.0	18.0	50	130	350
$K_c(HClO_4)$	0.02	0.09	0.4	0.8	8	35
$R_{Np(V)}(HNO_3)$	24%	16%	11%	7%	4%	3%
$R_{Np(V)}(HClO_4)$	78%	63%	44%	36%	15%	8%

These results would indicate that the complexing nature of nitric acid would lead to a progressive disproportionation of neptunium(V) and a significant portion of tetravalent neptunium should be present in multimolar nitric acid. This is, however, not the case due to the fact that the rate of the disproportionation reaction is very slow. The forward reaction (35) was found by Koltunov and Tikhonov [48] to obey the following rate law:

$$\frac{-d[Np(V)]}{dt} = 2k[H^+]^2[Np(V)]^2 \quad (38)$$

The value of the rate constant was determined in 2.1 - 4 M HNO₃ to be $k = 1.9 \times 10^{-3} \text{ M}^{-3} \text{ s}^{-1}$ at 90°C [48], along with the value of the activation energy of $E_a = 68.6 \text{ kJ/mol}$ [48]. The reasons for the low rate of the reaction is that the conversion of Np(V) to Np(IV) requires the breaking of the very stable oxygen bonds in the neptunyl molecular ion. This results in a relatively high activation barrier, so that the rate at temperature of 25°C in < 4M HNO₃ the rate of the disproportionation can therefore be considered negligible.

The redox chemistry of neptunium in nitric acid is therefore determined by an entirely different reaction, which is the oxidation of Np(V) by HNO₃ [47]:



which has been labeled as one of the most complicated and troublesome reactions in the PUREX process [17]. As is indicated above, this reaction is autocatalytic – i.e. the product of the reaction – nitrous acid – catalyzes the oxidation of Np(V) by nitric acid. Eventually an equilibrium is established when HNO₂ is produced in high enough concentration to shift the equilibrium back to the left. The thermodynamic equilibrium constant (in terms of activities) is given by the equation:

$$K = \frac{a_{\text{NpO}_2^{2+}}}{a_{\text{NpO}_2^+}} \sqrt{\frac{a_{\text{HNO}_2} \cdot a_{\text{H}_2\text{O}}}{a_{\text{H}^+}^3 \cdot a_{\text{NO}_3^-}}} \quad (40)$$

However, the authors who studied the equilibrium have generally arranged their findings in terms of the apparent concentration constant, which is calculated from the total analytical concentration of nitric acid $[\text{HNO}_3]_t$ as:

$$K_{app} = \frac{[\text{Np(VI)}] \sqrt{[\text{HNO}_2]}}{[\text{Np(V)}] [\text{HNO}_3]_t^2} \quad (41)$$

As can be seen in the summary of the results of past studies of the reaction in [17], there is not a very good agreement on the value of the apparent equilibrium constant K_{app} , which was also found to change with nitric acid concentrations in most studies. Most authors agree that the large variation in the values is caused by the significant changes of the values of activity coefficients with the increase of nitric acid concentration.

Table 4 – Equilibrium data reported on the oxidation of Np(V) by nitric acid

Reference	$K_{app}, 10^{-4} M^{-1.5}$	Experimental conditions*
Siddal & Dukes, 1959 [49]	5.2 ± 1.2	2.0 – 3.5 M HNO ₃ , 24.5°C, distr.
Swanson, 1969 [50]	9.7 ± 4.2	2.0 – 4.7 M HNO ₃ , 24°C, spec.
Gourisse, 1971 [51]	5.9 ± 2.7	1.0 – 3.9 M HNO ₃ , 24°C, distr.
Shilin & Nazarov, 1973 [52]	5.2 / 7.2	2 – 3 M HNO ₃ , 20 / 30°C, , spec.
Tochiyama et al., 1995 [53]	21.0 ± 11.0	3.0 – 6.0 M HNO ₃ , 25°C, distr.

* distr. – distribution, spec. – spectrophotometry

The last published study of the reaction by Tochiyama et al. [53] was probably the most thorough, going to great lengths to compensate for most of the effects of changing ionic strength μ and of the changing distribution coefficients of both nitric and nitrous acid. They summarized their data in a practical empirical expression of the dependence of K_{app} on nitric acid concentration:

$$\log K_{app} = -2.77 - 0.01121 [HNO_3]^2 + 0.4074 [HNO_3] - 0.7187 \sqrt{[HNO_3]} \quad (42)$$

Using known values of K_{app} and by modifying the equation (41), the fraction of pentavalent neptunium in total neptunium $R_{Np(V)}$ can be then calculated from known analytical concentrations of HNO₃ and HNO₂:

$$R_{Np(V)} = \frac{[Np(V)]}{[Np(V)] + [Np(VI)]} = \frac{1}{1 + \frac{[Np(VI)]}{[Np(V)]}} = \frac{1}{1 + K_{app} \frac{[HNO_3]_r^2}{\sqrt{[HNO_2]}}} \quad (43)$$

The results of these calculations reveal the paramount importance of nitrous acid on neptunium redox speciation in multimolar nitric acid. As is evident from Figure 5 below, where the values of the Np(V) fraction have been calculated, even minor equilibrium concentrations of approximately 1mM HNO₂ stabilize more than 50% of Np in its pentavalent form in 4 M and lower concentrations of nitric acid.

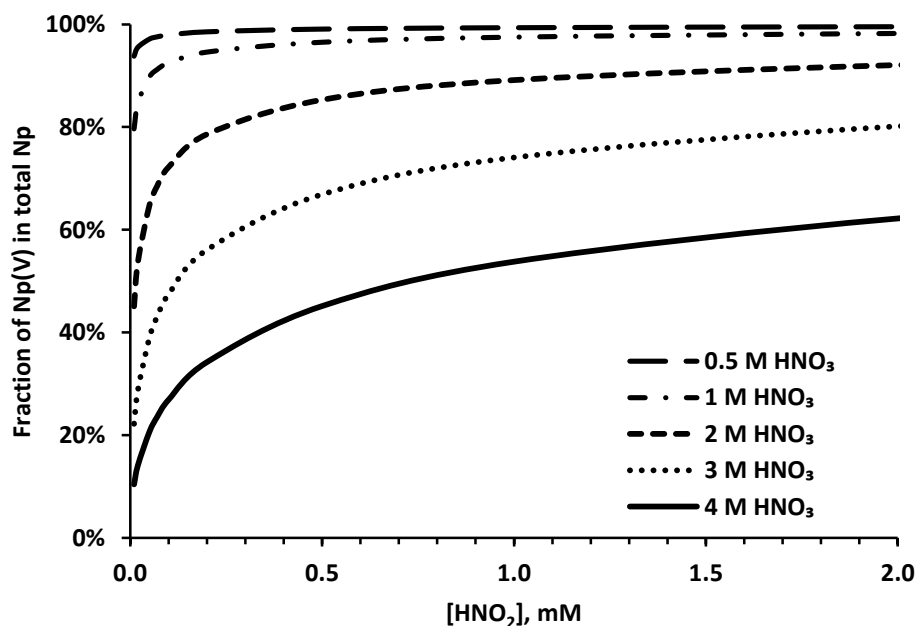


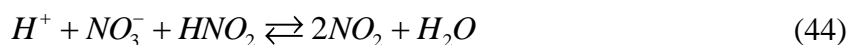
Figure 5 - Effect of equilibrium HNO₂ concentration on the redox speciation of neptunium in nitric acid at temperature of 25°C (based on data from Tochiyama et al., 1995 [53])

Maintaining the required oxidation states of neptunium (extractable Np-V or inextractable Np-VI) is not influenced only by the acidity and temperature of the solution, but also by the effects of the complicated mechanisms of generation and destruction of nitrous acid (e.g., radiolysis, redox reactions of nitric acid, venting of NO_x gases, etc.) in the extraction system and by its extractability into TBP solutions [17].

Since the rate of the oxidation of neptunium by nitric acid to its extractable hexavalent state was of great practical importance for the considerations of neptunium behavior in TBP-based extractions, many studies have also been dedicated to the analysis of the kinetics of reaction (39). The summary of these results presented in Table 5 demonstrates that analysis of the system has not yet provided a clear and consistent rate law description of the reaction. This is most likely due to the significant influence of rate accelerating materials generated by radiolysis of the organic phase (as suggested by Swanson [50]), and also due to the instability and interactions of nitrous acid in the HNO₃/TBP system.

Table 5 – Results and experimental conditions of kinetic studies of oxidation of Np(V) by nitric acid
<p>Siddal & Dukes, 1959 [49]:</p> $\frac{-d[Np(V)]}{dt} = \left\{ 2.1 \times 10^{-5} M^{-3.28} s^{-1} \right\} [HNO_3]^{3.28} \cdot [Np(V)] \quad \text{for } [HNO_2] \gg [Np(V)]$ <p>at $T = 25^\circ C$; $E_a = 50$ kJ/mol; radiotracer distribution method of analysis $\sim 10^{-12} M$ ^{239}Np, 0.006-0.02 mM ^{237}Np, 0.05 – 10mM HNO_2, 2.4 - 4 M HNO_3</p>
<p>Koltunov, Shilin & Nazarov, 1968 [54]:</p> $\frac{-d[Np(V)]}{dt} = \left(k_1 [HNO_2]^{0.5} [H^+]^{0.5} [NO_3^-]^{0.5} + k_2 [H^+] [HNO_2] \right) \cdot [Np(V)]$ <p>$k_1 = 8.5 \times 10^{-4} M^{-1.5} s^{-1}$, $k_2 = 1.17 \times 10^{-2} M^{-1} s^{-1}$ at $T = 20^\circ C$ and ionic strength $\mu = 4M$ $E_{a1} = 82.3$ kJ/mol, $E_{a2} = 83.2$ kJ/mol; spectroscopic method of analysis 0.27-0.66 mM Np, 0.56 – 1.9 mM HNO_2, 3 - 8 M HNO_3</p>
<p>Swanson, 1969 [50]</p> $\frac{-d[Np(V)]}{dt} = \left\{ 0.77 M^{-1} s^{-1} \right\} \cdot [HNO_2] \cdot \left([Np(V)] - [Np(V)]_{eq} \right) \quad \text{at } T = 24^\circ C *$ <p>$E_a = 63$ kJ/mol; spectroscopic method of analysis 0.5 mM Np, 0.25 - 50 mM HNO_2, 2 - 4.7 M HNO_3</p>
<p>Moulin, 1978 [31]:</p> $\frac{-d[Np(V)]}{dt} = \left(\left\{ 5 \times 10^{-6} M^{-1} s^{-1} \right\} + \left\{ 1.9 \times 10^{-4} M^{-3.3} s^{-1} \right\} [H^+]^{1.3} [HNO_2] \right) [NO_3^-] \cdot [Np(V)]$ <p>at $T = 25^\circ C$, $E_a = 63$ kJ/mol both radiometric distribution and spectroscopic methods of analysis using Np-237 0.06-2.2 mM Np, 0.07 – 1.3 mM HNO_2, 1 - 4 M HNO_3</p>
<p>Tochiyama et al., 1995 [55]:</p> $\frac{-d[Np(V)]}{dt} = \left\{ 1.81 \times 10^{-4} M^{-3.5} s^{-1} \right\} [HNO_3]^3 [HNO_2]^{0.5} \cdot [Np(V)] \quad \text{at } T = 25^\circ C$ <p>radiometric distribution methods of analysis using tracer concentrations of Np-239 0.16 – 8.1 mM HNO_2, 3.0 – 6.0 M HNO_3</p>
<p>*E_a – activation energy, $[Np(V)]_{eq}$ – neptunium(V) concentration at equilibrium</p>

In order to explain the mechanism of the reaction (39), which counter-intuitively accelerated in the presence of its reducing product – HNO_2 , Siddal and Dukes [49] initially proposed an activated state of Np(V) that can be oxidized by nitrous acid. What most authors do agree is that the catalytic effect of nitrous acid can be explained by an intermediary tetravalent nitrogen compound N^{IV} , formed by the synproportionation of trivalent nitrogen N^{III} in nitrous acid and pentavalent nitrogen N^{V} in the nitrate ion. The following mechanism has been proposed to explain reaction (39) by the latest study of Tochiyama et al.[55]:



In the presence of excess HNO_2 over Np(V) , reaction (44) is in a rapid equilibrium and the rate determining step becomes the slow reaction (45) of the NO_2 molecular radical with Np(V) . If only trace amounts of nitrous acid are present, the reaction becomes essentially 0th order with respect to the concentration of neptunium(V), which has been thoroughly investigated by Moulin [31]. In presence of significant amount of Np(VI) , the reverse direction of reaction (45) becomes significant, explaining the reversible nature of reaction (39).

The study of the reverse of reaction (39), i.e. the reduction of Np(VI) by nitrous acid, was undertaken as part of this dissertation work and will be discussed in greater detail in the discussion of Chapter 5.

Since reaction (39) is producing its own catalyzer - nitrous acid – it can be employed in enhancing the so a called *first-cycle* of the PUREX process for extraction of Np from the highly active raffinate into the TBP phase without the addition of any other reagent. The main principle behind the application is causing a shift in the equilibrium to the right by the extraction of hexavalent neptunium from the aqueous phase to the organic phase by reaction (32). With a slight increase of nitric acid concentration to from 3 to 4.5M and sufficiently long contact times of the organic phase with the aqueous phase, more than 99% extraction of Np was possible without the complementary introduction of nitrous

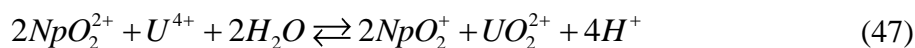
acid or any other agent in the experiments of Dinh et al. with real dissolved nuclear fuel in the French ATALANTE research facility [34].

2.4.2 Uranium(IV)

Besides its waste-free character, the choice for the selection of uranium(IV) as a reducing agent in the PUREX process was based on several other advantages – high rate of reduction of plutonium(IV) to the inextractable Pu(III) over wide working ranges of acidity and temperature, applicability to all types of extraction apparatus (mixer-settlers, pulsed column extractors, centrifugal contactors) and the possibility of electro-regenerating uranium(IV) inside the extractor itself [56]. Another feature of uranium(IV) is that it is well extracted by TBP – as opposed to many other agents – and can therefore reduce plutonium(IV) and (VI) present in the organic phase [57]. Unfortunately, the same feature is responsible for excessive consumption of uranium(IV) due to its oxidation by nitric acid in the organic phase catalyzed by HNO_2 [17, 58]. Hydrazine, the main agent used for the control of HNO_2 concentration, is not extracted into the organic phase. Thus, uranium(IV) that is extracted into the organic phase is then easily oxidized by the HNO_2 catalyzed reaction with HNO_3 , which markedly increases its consumption many times over the extent required by the reduction of Pu(IV) and Pu(VI) [56].

In the classical setup of the PUREX cycle, a major fraction of neptunium is in the hexavalent state and thus gets extracted in the first-cycle along with U and Pu (66% in the THORP plant in the United Kingdom, 82% at the UP-2 plant in France[59] and more than 99% at the TR-1 plant in Russia [56]) and is thus usually present in the partitioning step, where it comes in contact with uranium(IV).

Uranium(IV) rapidly reduces Np(VI) to Np(V) in both aqueous and organic solution according to the reaction:



Investigations were performed in both perchloric [60] and nitric acid [61]. The latter study found that in reaction follows the rate law:

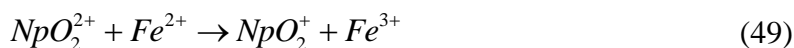
$$+\frac{d[\text{Np(V)}]}{dt} = \frac{\left(\{6.73s^{-1}\} + \{4.58M^{-1}s^{-1}\} \cdot [\text{H}^+]\right)}{\{0.009M\} + [\text{H}^+]} [\text{Np(VI)}][\text{U(IV)}] \quad \text{at } T=10^\circ\text{C} \quad (48)$$

with activation energy determined to be $E_a = 66.5 \pm 4.9$ kJ/mol in solutions of 2 M ionic strength.

The rate of Np(VI) reduction by U(IV) is comparable to the rate of the reduction of Pu(IV) by reaction (34) [62]; also, further reduction of Np(V) to Np(IV) is approximately 100-times slower [17], which is usual for all reactions involving the break-up of the actinyl dioxo-ion.

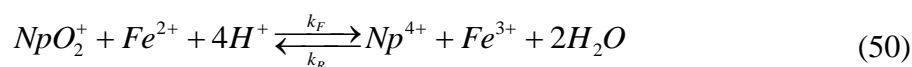
2.4.3 Iron(II)

Divalent iron Fe(II) is an inexpensive and fairly strong reducer for actinides of higher valence, which explains the popularity of its use in the early history of the PUREX process, before the utilization of salt-free approaches. It quantitatively reduces Np(VI) to Np(V) via the reaction:



The reaction is very rapid, which makes the study of its kinetics complicated, and as such, the value of its apparent 2nd order rate constant k'' has been only preliminary estimated to be approximately $3000 \text{ M}^{-1}\text{s}^{-1}$ in 1M HClO₄ at 1°C [62].

Due to its being a strong reducing agent, iron(II) is also capable of relatively fast reduction of Np(V) to the tetravalent state. However, the reaction is reversible:



The overall rate law for the Np(V)-Fe(II)-Np(IV)-Fe(IV) equilibrium reaction was studied by Bond et al.[63] can be expressed in terms of Np(V) disappearance as:

$$-\frac{d[Np(V)]}{dt} = k_F [Np(V)][Fe(II)][H^+]^{1.38} - k_R \frac{[Np(IV)][Fe(III)]}{[H^+]^3} \quad (51)$$

where the values of the rate constants for the forward and reverse reaction were determined at 25°C in 1M HNO₃ + 0.5M NaClO₄ as $k_F = 0.261 \text{ M}^{-2.38}\text{s}^{-1}$ and $k_R = 0.0285 \text{ M}^2\text{s}^{-1}$, respectively, while the values of the activation energies for the respective were $E_{aF} = 42$ kJ/mol and $E_{aR} = 146$ kJ/mol [63]. Increasing the nitrate ion concentration from 1-2M increased the forward rate by 25% and decreased the reverse rate by 50%, which has been explained by Bond et al. by the effect of formation of nitrate complexes [63].

In solutions of very high nitric acid concentration (~8 M HNO₃) where disproportionation of Np(V) by reaction (35) is shifted to the right due to strong complexation, application of iron(II) can convert all neptunium to the tetravalent state. This effect has been employed in laboratory and industrial anion exchange separations [17, 64].

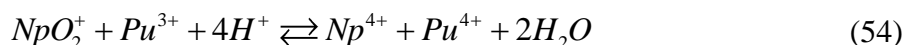
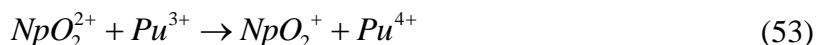
It is important to note that during the history of its application, iron(II) was also usually added in the form of ferrous sulfamate Fe(NH₂SO₃)₂ as a double-action reagent (recently it has still been used in the weapon-material related reprocessing plant at the Savannah River Site [65]). The sulfamate ion acts as a scavenger of nitrous acid:



However, sulfamate causes downstream problems as long term action of nitric acid degrades it to ammonium ion and sulfate. Production of ammonium is a problem if the waste is converted to an alkaline state, because volatile and flammable ammonia gas is then released. Large amounts of sulfate in the waste can cause problems in the formulation of glass waste forms [66]. Another issue identified with ferrous sulfamate was the possibility of long-term formation of iron(III) precipitates that could plug valves and tubing [65].

2.4.4 Plutonium(III)

During the partitioning step of PUREX, Pu(IV) is reduced to Pu(III) and Np(VI) to Np(V), usually by U(IV) as a reducing agent, as has been already described above. Pure Pu(III) can also act a reducing agent both on Np(VI) and on Np(V):



The reaction kinetics of reaction (53) – reduction of Np(VI) – was studied in perchlorate environment by Fulton and Newton [67] who have identified the following rate law:

$$-\frac{d[Np(VI)]}{dt} = \left(\left\{ 35.3 M^{-1} s^{-1} \right\} + \frac{\left\{ 3.1 s^{-1} \right\}}{[H^+]} \right) [Np(VI)][Pu(III)], \quad T = 25^\circ C. \quad (55)$$

The thermal activation enthalpy for the first and second term were 14.6±0.2 kJ/mol and 3.49±0.05 kJ/mol, respectively [62, 67].

Reduction of Np(V) to Np(IV) is reversible (plutonium-IV can reoxidize neptunium-IV to the pentavalent state) and also significantly slower, since it entails the breakup of the neptunyl ion structure. Kinetic investigations performed by Koltunov et al. [68, 69] were able to determine the rate of the forward reaction of (54) only at significantly elevated temperature. The overall rate law can be expressed as:

$$-\frac{d[\text{Np(V)}]}{dt} = k_F [\text{H}^+]^{1.3} \cdot [\text{Np(V)}][\text{Pu(III)}] - \frac{k_R}{[\text{H}^+]^4} \cdot [\text{Np(IV)}][\text{Pu(IV)}] \quad (56)$$

The forward reaction's rate constant was found to be $k_F = 0.086 \pm 0.005 \text{ M}^{-2.3} \text{ s}^{-1}$ at 69°C in 2M ionic strength [69]. The activation energy was estimated as $E_{aF} = 85 \pm 3 \text{ kJ/mol}$, so it is possible to extrapolate the value of the rate constant at 25°C would be $k_{F,25^\circ\text{C}} \approx 0.001 \text{ M}^{-2.3} \text{ s}^{-1}$, i.e. four orders of magnitude below the rate of reaction (53).

The reverse reaction rate constant is comparably higher; its value was determined to be $k_R = 1.2 \pm 0.1 \text{ M}^3 \text{ s}^{-1}$ at a lower temperature of 39°C . The reaction has a relatively high activation energy of $E_{aR} = 144.8 \pm 2.1 \text{ kJ/mol}$ [68], so the rate constant value extrapolated to 25°C would be $k_{R,25^\circ\text{C}} \approx 0.1 \text{ M}^3 \text{ s}^{-1}$; therefore, in aqueous solution of relatively low acidity the equilibrium (54) is virtually fully shifted toward the starting reactants.

Nevertheless, the reaction is of importance during the partitioning step of PUREX in the presence of the organic phase with TBP, because the equilibrium is shifted to the right by to the ongoing extraction of Np(IV) into the organic phase. This effect is magnified by the fact that in the presence of excess U(IV) any plutonium(IV) would be immediately re-reduced back into the trivalent state [56].

2.4.5 Hydrazine

At all PUREX radiochemical plants hydrazine (NH_2NH_2) is used in the reprocessing solutions as a stabilizer of U(IV) in the partitioning step. Due to the basicity of hydrazine ($\text{pK}_a = 8.1$ [70]), it is present in the solutions almost completely in the protonated form of the hydrazinium ion N_2H_5^+ and the compound used as the additive is its nitrate salt - hydrazine nitrate ($\text{N}_2\text{H}_5\text{NO}_3$).

The reason for using hydrazine is the high rate of its reaction with HNO_2 , which – among other of its effects – catalyzes the reoxidation of U(IV) in the partitioning step (see section 2.4.2 above).



The reaction proceeds very rapidly, its apparent 2nd order rate constant is proportional to acidity, and its value has been determined to be $k'' = 611[H^+] M^{-1}s^{-1}$ at 25°C and at 0.3M ionic strength (activation energy $E_a = 56.5$ kJ/mol) [71]. The resulting hydrazoic acid HN_3 is a volatile, potentially explosive compound, but it is extracted by the PUREX solvent and can be removed safely in the wash system [2]. Unfortunately, hydrazine is not well extracted by TBP while HNO_2 is extracted quite well (distribution ratio ≈ 10) [72].

Both neptunium(VI) and (V) are reduced with hydrazine, but only with the former does the reduction proceed at an appreciable rate. The reaction stoichiometry depends on which reactant is in the excess:



Under normal PUREX process conditions, excess hydrazine is usually present and the rate law of its reaction with neptunium(VI) has been described by Koltunov [73] as:

$$-\frac{d[Np(VI)]}{dt} = \{0.23s^{-1}\} \frac{[Np(VI)][N_2H_5^+]}{[H^+]^{1.24}} \quad \text{at } 25^\circ\text{C and } 2\text{M ionic strength} \quad (60)$$

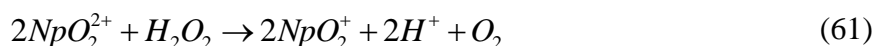
and an activation energy of 78.7 kJ/mol was identified.

The following reaction of hydrazine with neptunium(V) is predictably much slower, and is hardly observable at room temperature; in the investigations of Karraker et al.[74] no $Np(IV)$ was produced during an hour-long experiment in a solution of 0.10 M hydrazine nitrate in 1.5 M HNO_3 kept at 70°C. However, addition of 8mM iron(III) catalyst led to rapid acceleration of the reaction – all neptunium was reduced to the tetravalent form within 2 hours in the same solution kept at temperature of 50°C [74]. In the investigations of this catalytic effect by El-Naggar et al. [75], they found that then the reduction of $Np(V)$ proceeds through reaction (50) of $Np(V)$ with $Fe(II)$. Divalent iron is formed by reduction of $Fe(III)$ by hydrazine and this reaction then becomes the rate-determining step of the overall process [75].

2.4.6 Hydrogen peroxide

H_2O_2 is a possible salt-free reagent with a similarly ambiguous character like HNO_2 – it can be used for both reduction and oxidation of Pu and Np ions. Its major disadvantage is the possibility of highly undesirable precipitation of uranium and plutonium peroxides and of incomplete extractive recovery of Pu due to the formation of Pu(IV) peroxide complexes [56].

Neptunium(VI) can be rapidly reduced by H_2O_2 to Np(V) in solutions of low and medium acidity. In excess of hydrogen peroxide, the reaction follows a 2:1 stoichiometry:

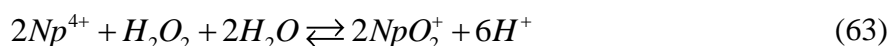


The kinetics of this reaction has been studied in perchlorate system by Zielen, Sullivan et al. [76] who have identified a rate law for the initial rate of the reaction:

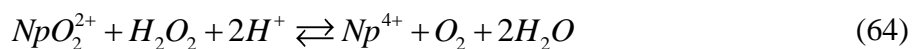
$$-\frac{d[Np(VI)]}{dt} = \frac{\{8.9s^{-1}\}}{[H^+] \left(1 + 1.9 \times \frac{[Np(V)]}{[Np(VI)]}\right)} [Np(VI)][H_2O_2] \quad \text{at } 25^\circ\text{C and } \mu = 3M \quad (62)$$

The activation energy for the primary process was found to be 51.8 kJ/mol. However, attempts to reliably predict the whole reaction progress based on this rate law have not been very successful. It was argued by the authors [76] that this is a result of complex interactions of intermediary product created by the single-electron reaction steps during the oxidation of the H_2O_2 molecule.

Already in the earliest investigations of neptunium redox chemistry during the Manhattan project by Magnusson et al. [77] it was found the further reduction of Np(V) to the tetravalent state does not proceed in solutions of 0.5 HNO_3 concentration. What is more, in $< 1 M HNO_3$ solutions, hydrogen peroxide would actually oxidize Np(IV) to the pentavalent state [56]:



Nonetheless, in high concentrations of nitric acid a direct reduction of neptunium(VI) to the tetravalent state is possible by the reversible reaction:



Krot et al. [78] have found that Np(V) is slowly and reversibly reduced to Np(IV) and rapidly and reversibly oxidized to Np(VI) in the presence of H_2O_2 in 6-8M HNO_3 at

20°C. As a result, an equilibrium between Np(VI) and Np(IV) is established in solutions containing initially Np(V) or Np(VI) ions. The apparent equilibrium constant, defined as:

$$K' = \frac{[Np(IV)][O_2]}{[Np(VI)][H_2O_2]} \quad (65)$$

had a mean value of 1.8 ± 0.4 in 7.5 N HNO₃.

The forward reaction of the equilibrium (64) was identified to be of first order with respect to both reactants, so that a rate law can be postulated:

$$+\frac{d[Np(IV)]}{dt} = k''[Np(VI)][H_2O_2] \quad \text{at } 20^\circ\text{C} \quad (66)$$

A very strong positive sensitivity to the HNO₃ concentration of the apparent 2nd order rate constant k'' was found, its value rising from 0.07 to 0.17 M⁻¹s⁻¹ when the HNO₃ concentration increased from 6.0 to 8.4 M. The effect of temperature on the rate was characterized by an activation energy of $E_a = 55 \pm 2$ kJ/mol [78].

2.4.6.1 Mutual reactivity of hydrogen peroxide and nitrous acid

In acidic environment, hydrogen peroxide acts as a rapid scavenger of nitrous acid by the means of its oxidation to nitric acid (as opposed to the reactions of many organic scavengers of nitrous acid that are usually leading to reduction of HN^{III}O₂ to nitrogen monoxide N^{II}O, nitrous oxide N^I₂O or nitrogen N⁰₂) by the summary reaction:



However, little is known about the kinetics of this reaction in multimolar nitric acid, because the reaction rate is strongly dependent on acidity of the solution and tends to proceed very rapidly below pH = 1, precluding the direct measurement of rates at multimolar acidities by classical approaches. In most studies the reaction of the oxidation of nitrous acid by hydrogen peroxide was studied in pH > 2 solutions and the rate law of the rate determining step has been identified in a form:

$$\frac{-d[HNO_2]}{dt} = k'''[H^+][H_2O_2][HNO_2] \quad (68)$$

with the 3rd order rate rate constant k''' having values between 1400 and 8000 M⁻²s⁻¹ at the temperature of 20-25°C [79, 80, 81, 82, 83].

A reactive intermediary called peroxonitrous acid (HOONO) was found in many of these investigations and has been studied in its more stable deprotonated anionic form ${}^{-}\text{OONO}$ ($\text{pK}_a=6.6$ [84]). Park et al. have also studied the effect of up to 0.1 M of various anions, including perchlorate and nitrate, [82] but his work has been done in weakly acidic conditions of $\text{pH} = 2 - 4$.

Only in one study of Benton and Moore [84] has the stopped-flow method been used for the investigation of higher acid concentrations (up to 1M perchloric acid) and the rate of reaction of the decomposition of peroxonitrous acid has been characterized by a decay constant consisting of a proton-dependent and a proton independent term.

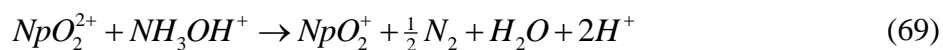
The lack of experimental observations about the rate of this reaction in multimolar nitric acid environment has led the author of this work to investigate the system by the stopped-flow method; therefore, further discussion about this topic and the results of this study are presented in Chapter 9 below.

2.4.7 Hydroxylamine

This reducing agent is used in most PUREX reprocessing facilities for Pu stripping in the multiple steps of its purification by repeated extraction and stripping and in the process of uranium decontamination from Pu and Np [56]. Hydroxylamine rapidly reduces Pu(IV) to Pu(III) [85] and Np(VI) to Np(V) [86].

In the acidic reprocessing solutions, similarly to hydrazine, hydroxylamine (NH_2OH) is completely protonated ($\text{pK}_a = 5.94$ [70]) into its hydroxylaminium ion (NH_3OH^+) and is usually added to the solutions in the form of its nitrate salt – hydroxylaminium nitrate (HAN). The foremost advantage of hydroxylamine is that it does not form salts in the process, because its reactions with nitric acid, nitrous acid, Pu and Np ions are gaseous nitrous oxide (N_2O) and nitrogen.

The final nitrogen-containing product and stoichiometry of the reaction with neptunium depends on which reactant is in excess. In excess of hydroxylamine the reaction with Np(VI) forms nitrogen gas:



In excess of neptunium(VI), the nitrogen in hydroxylamine (N^{-1}) is oxidized to a higher oxidation state in nitrous oxide (N^{+1}) than it would have in nitrogen (N^0), altering the reactant stoichiometry from 1:1 to 2:1, as is evident below:

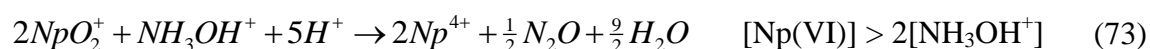


The kinetics of the reaction (69) in nitric acid in excess of hydroxylamine have been studied by Koltunov and Tikhonov [86]. They found that it is significantly faster than the reaction of Np with hydrazine. The identified rate law was:

$$-\frac{d[Np(VI)]}{dt} = \{1.53 \pm 0.17 s^{-1}\} \frac{[Np(VI)][NH_3OH^+]}{[H^+]} \quad \text{at } 15^\circ\text{C and } \mu = 2\text{M} \quad (71)$$

The activation energy had a value of $E_a = 82$ kJ/mol; therefore, the rate constant can be extrapolated to have an approximate value of $4.8 s^{-1}$ at 25°C . This can be compared with the rate constant value of $0.23 s^{-1}$ of the rate law of the same form identified for the reduction of Np(VI) with hydrazine [73].

Further reduction of Np(V) to the tetravalent state does not proceed appreciably at room temperature in nitric acid; hence, the study of the kinetics of this reaction was performed at elevated temperature and acidity [87]. Again, the reaction stoichiometry was found to differ between systems where the reactant in excess was Np(V) or hydroxylamine:



In very significant excess of hydroxylamine (up to 1M hydroxylamine nitrate concentrations were used, compared to $\sim 1\text{mM}$ Np concentrations) the kinetics of the reaction (72) in 1 - 3 M HNO_3 solutions kept between 61 and 92°C and was found to follow the rate law:

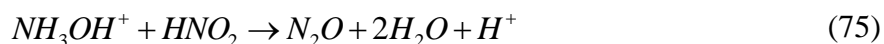
$$+\frac{d[Np(IV)]}{dt} = k'[H^+]^{1.65}[Np(V)][NH_3OH^+] \quad (74)$$

The rate constant had a value of $k' = (7.54 \pm 0.15) \times 10^{-4} M^{-2.65} s^{-1}$ at 92°C and the activation energy was determined as $E_a = (105 \pm 5)$ kJ/mol [87]. It has been also stated by the authors of [87] that in solutions of $\sim 100\text{mM}$ hydroxylamine the reduction of Np(V) (72) is much faster than the disproportionation of Np(V) (73) in the particular acidity region (see section 2.4.1 above).

2.4.7.1 Reaction of hydroxylamine with nitrous acid

The application of hydroxylamine in the nitric acid solutions used in nuclear fuel reprocessing is problematical due to its double-sided interaction with nitrous acid:

a) In low concentrations of nitric acid, a following reaction has been observed to scavenge nitrous acid from the solution:



The rate law of this reaction was examined in < 0.1 M perchloric acid solutions by Hughes and Stedman [88] in conditions of excess hydroxylamine shows a simple second order reaction with a 1st order of dependence on hydrogen ion concentration:

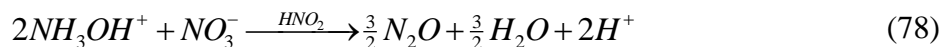
$$-\frac{d[HNO_2]}{dt} = k[H^+][HNO_2][NH_3OH^+] \quad (76)$$

Due to the relatively fast progress of the reaction, the rate law investigations were performed in perchlorate solutions cooled to 0°C and at this temperature the rate constant was found to have the value of $k = 0.24 \text{ M}^{-2}\text{s}^{-1}$ [88]. Evaluation of the effect of changing of the temperature revealed the value of the activation energy to be $E_a = 61.4 \text{ kJ/mol}$, so the rate constant can be extrapolated to have an approximately 10-times higher value of $2.3 \text{ M}^{-2}\text{s}^{-1}$ at the temperature of 25°C. Hence, the scavenging reaction is approximately 2 orders of magnitude slower than the rate of HNO_2 scavenging by hydrazine (see section 2.4.5 above).

b) In high concentrations of nitric acid (approximately above 2M HNO_3), it was discovered that another reaction might occur that has the inverse effect – i.e. net production of HNO_2 as a result of oxidation of hydroxylamine by nitric acid:



Stedman and Pembridge [89] found that the reaction is catalyzed by nitrous acid; therefore, oxidation of hydroxylamine by excess of nitric acid progresses as an autocatalytic process. At a sufficiently high concentration of nitric acid, hydroxylamine can appear to be stable in the absence of nitrous acid; however, if a small yet sufficient amount of nitrous acid is introduced into the system, all hydroxylamine can be suddenly oxidized by HNO_3 . The stoichiometry of the reaction (77) is not exact. A parallel reaction that leads to the production of gaseous nitrous oxide proceeds as well:



The combined stoichiometry of reactions (77) and (78), and, therefore, the composition of products from the oxidation of hydroxylamine by nitric acid depends on the initial concentrations of both reactants [89], favoring the maximum conversion to nitrous acid between 4 and 6 M HNO₃ at low initial concentrations of hydroxylamine (< 0.01M) .

The seeming conflict between reactions (75) and (77)+(78) of the reacting system of HNO₂, NH₂OH and HNO₃ has led Gowland and Stedman [90] to investigate the boundary conditions above which the system would prefer scavenging of HNO₂ over its production from oxidation of hydroxylamine. It was found that that net formation of nitrous acid was favored by increase in HNO₃ concentration, decrease in HNO₃ and increase in temperature – for instance, at the temperature of 21°C the boundary concentrations for nitric acid were approximately 2.0 and 3.3 M for 5 and 50mM NH₂OH, respectively [90]. The decomposition under definite conditions is accompanied by vigorous (“peak”) evolution of a large amount of gaseous products within a short time. This feature of hydroxylamine should be taken into account in its industrial use, e.g., in the course of uncontrollable storage of nitric acid solutions of hydroxylamine, which may be accompanied by their evaporation, or in adjustment of the acidity of hydroxylamine solutions with concentrated HNO₃. The instability of NH₂OH in HNO₃ has also a positive aspect, because the subsequent oxidation of Pu(III) to Pu(IV) can be performed by merely acidifying and/or heating the aqueous Pu strip without adding any oxidants.

2.4.8 *New prospective reducing agents*

Some of the most popular reducing agents for reduction of Pu and Np that are used in current PUREX reprocessing facilities suffer from a number of deficiencies such as the formation of non-evaporable Fe(III), Fe(II), and ammonium (hydrazine) nitrates and sulfates. This increases the amount of salts in the radioactive waste solutions, the instability of U(IV) in the organic phase, and the potential explosiveness owing to the formation of azides (from hydrazine – see reaction (57)) and other issues. Therefore, the search for new highly efficient reducing agents for Pu and Np that do not form salts has become an important area of research [91]. Hydrazine and hydroxylamine derivatives,

hydroxamic acids and butyraldehydes have shown the most promise and are described in greater detail in the sections below.

2.4.8.1 Derivatives of hydrazine and hydroxylamine

A large number of organic derivatives of hydrazine (R-NHNH₂) and hydroxylamine (R-NHOH) were analyzed by Koltunov et al. as part of this undertaking [73]. These compounds reduce Np(VI) to Np(V) and Pu(IV+VI) to Pu(III), they also stabilize the resulting Np(V) and Pu(III) in the aqueous phase by scavenging nitrous acid, even though kinetic data on these processes have not yet been completely evaluated. Further reduction of Np(V) to Np(IV) has been observed to be extremely slow for all of the compounds, so that they will be most likely of little - if any - significance in real reprocessing situation. The products of their reactions with Np and Pu and products of their decomposition in nitric acid are alcohols, aldehydes and also gaseous N₂O and N₂, which are all evaporable as opposed to the salts mentioned above [56]. The reaction kinetics of the reduction of Np(VI) and Pu(IV) with these compounds (indicated as *Red.*) was found to behave according to the following rate laws :

$$-\frac{d[Np(VI)]}{dt} = k' \frac{[Np(VI)][Red.]}{[H^+]^n} \quad (79) \quad -\frac{d[Pu(IV)]}{dt} = k' \frac{[Pu(IV)][Red.]}{[H^+]^n} \quad (80)$$

where n indicates an inverse n -th order of dependence on hydrogen ion concentration [73]. The most important results that of his work are summarized in Table 6 below (please note that most of the listed compounds would be present in their protonated forms in the acidic reprocessing solutions). A particularly fast reductant was phenyl-hydrazine (C₆H₅-N₂H₃). For the substituted hydrazines a significant difference by 2-3 orders of magnitude in the rates of reduction between Np(VI) and Pu(IV) was identified – reactions being usually slower for the latter. Utilization of this effect for selective reduction of Np(VI) in presence of Pu(IV) has been attempted with dimethylhydrazine, but satisfactory Np / Pu partitioning was not achieved [91].

The hydroxylamine derivatives have a weakness in common with the unsubstituted hydroxylamine in their liability toward oxidization into nitrous acid in high concentration of nitric acid and elevated temperature (as described in the section above). However, the values of critical concentrations and temperatures are different for each compound and

can provide a wider window of usage than is available for the unsubstituted hydroxylamine [56].

Table 6 – Rate constants, reaction orders for H⁺, and activation energies of Np(VI) and Pu(IV) reduction by selected hydrazine and hydroxylamine derivatives in nitric acid / nitrate solutions of 2 M ionic strength at the temperature of 25°C

Most data were adopted from Koltunov (1993), ref. [73]; see equations (79) and (80) for symbol explanation.

	Np(VI)			Pu(IV)		
	<i>n</i>	<i>k'</i> M ^{<i>n</i>-1} s ⁻¹	E _a kJ/mol	<i>n</i>	<i>k'</i> M ^{<i>n</i>-1} s ⁻¹	E _a kJ/mol
Hydrazine derivatives:						
N ₂ H ₄	1.24	0.23	78.7	1	1.42×10 ⁻⁴	120
CH ₃ -N ₂ H ₃	1.00	0.88	58.6	1	7.17×10 ⁻⁴	89.6
C ₂ H ₅ -N ₂ H ₃	1.00	0.50	61.5			
CH ₃ -N ₂ H ₂ -CH ₃	0.80	1.97	50.2	1	2.50×10 ⁻⁴	-
(CH ₃) ₂ CH-N ₂ H ₃	0.90	0.32	69.4			
(CH ₃) ₃ C-N ₂ H ₃	0.75	0.07	63.1			
H ₂ C=CHCH ₂ -N ₂ H ₃	1.00	0.77	63.6			
HC(O)-N ₂ H ₃	1.00	0.13	85.2			
CH ₃ C(O)-N ₂ H ₃	1.20	0.13	76.5			
HOC ₂ H ₄ -N ₂ H ₃	1.00	5.03	56.7	1	9.88×10 ⁻⁴	110
C ₂ H ₅ OC(O)-N ₂ H ₃	1.20	0.32	65.4			
C ₂ H ₅ OC(O)CH ₂ -N ₂ H ₃	1.10	1.63	70.1	1	5.83×10 ⁻⁴	-
C ₆ H ₅ CH ₂ -N ₂ H ₃	1.00	0.89	98.2			
C ₆ H ₅ -N ₂ H ₃	0.40	50.00	31.4			
Hydroxylamine derivatives:						
NH ₂ OH	1.0	0.48	82.1	2 ^{**}	2.05 ^{**}	96.2 ^{**}
CH ₃ -NHOH	0.4 [*]	0.58	63.6		fast	-
(CH ₃) ₂ CH-NHOH	0.8	0.66	58.2			
(CH ₃) ₂ -NOH	0.65	4.03	60.0	2	1.24	69.1
(C ₂ H ₅) ₂ -NOH	0.84	0.38	68.5	2	0.352 ^{***}	152

* methyl-hydroxylamine CH₃-NHOH exhibits a 0.7th reaction order, deviating from the rate law (79)

** data from Barney (1976), ref. [85], the rate constant *k'* was NO₃⁻ dependent: *k'* = 4.8/(0.34+[NO₃⁻]) M.s⁻¹

*** diethyl-hydroxylamine (C₂H₅)₂-NOH exhibits a 1.2nd reaction order, deviating from the rate law (80)

2.4.8.2 Hydroxamic acids

A special kind of hydroxylamine derivatives are hydroxamic acids, that have the general formula of R-CO-N(H)OH, where R represents a substituent. They are structurally

related to carboxylic acids with the hydroxyl group -OH substituted for a hydroxylaminyl group -NHOH. The most important representatives are formohydroxamic acid (FHA – HCO-NHOH) and acetohydroxamic acid (AHA, CH₃CO-NHOH) and their chemical structures are displayed in Figure 6 below.



Figure 6 – Chemical structures of formohydroxamic (left) and acetohydroxamic (right) acid

Hydroxamic acids have been intensively studied by R. J. Taylor and coworkers [92, 93] as useful stripping agents for Np and Pu in advanced versions the PUREX processes, because they can serve in a dual role as both reducing and complexing agents [42, 94]. Another positive aspect of their application is that they are salt-free agents, e.g. during evaporation of aqueous nitric acid reprocessing streams products of their decomposition and reactions will volatilize and not increase the mass and volume of solid waste [56].

As has been mentioned above, acetohydroxamic acid (AHA) is utilized in UREX, the first step of the UREX+ process suite. In UREX, both neptunium and plutonium are stripped back into the highly active raffinate after the successful extraction of uranium(VI) and technetium (see section 2.3.2 above)[43]. AHA rapidly reduces Np(VI) to non-extractable Np(V), while also reducing any potential Pu(VI) to Pu(IV), furthermore tetravalent actinides are strongly complexed by hydroxamates anions into non-extractable chelates, which leads to complete stripping of Pu(IV) (and potentially also tetravalent neptunium) to the aqueous phase. Hexavalent uranium U(VI) and technetium are not affected by AHA and stay in the 30% TBP organic phase at >1M nitric acid concentration [94].

The reaction of both FHA and AHA with Np(VI) and Pu(VI) proceeds extremely rapidly (within individual seconds) and can be studied in close-to-real conditions properly only by stopped-flow methods, so that only preliminary data on their reactions have been published so far [95, 96, 97], in contrast to more extensive literature relevant in their actual usage during quarter-scale industrial reprocessing tests [3, 42, 45, 46].

Colston, Choppin and Taylor [96] have determined that the reaction of *formo*-hydroxamic acid with Np(VI) is of first order with respect to each of the reactants:

$$-\frac{d[Np(VI)]}{dt} = k''[Np(VI)][FHA] \quad (81)$$

The value of the apparent 2nd order rate constant was determined to be $k'' = 1170 \text{ M}^{-1}\text{s}^{-1}$ in 2M HNO₃ at a temperature of 22°C [96]. No data on acidity dependence of the reaction were collected, but a rate-law similar of the reaction Np(VI) with hydroxylamine - described by equation (71) - was assumed, so that the apparent rate constant was assumed to be inversely proportional to hydrogen ion concentration $k'' = k' [\text{H}^+]^{-1}$ and the overall rate constant value would then be around $k' = (1170 \times 2) = 2340 \text{ s}^{-1}$. This value is 4 orders of magnitude higher than the rate constant for the reaction with simple hydroxylamine and higher than any other group of hydroxylamine derivatives.

Based on the reaction (69) of Np(VI) with excess of hydroxylamine, a 1:1 stoichiometry was proposed [96] for the reaction of Np(VI) in excess of FHA:



However, no experimental verification of the stoichiometry, as well as no thermal activation analysis of the reaction, was performed so far.

In the case of the apparently more important acetohydroxamic acid, the kinetics of its reaction with Np(VI) in nitric acid was studied by Chung and Lee [95]. They found for the rate law:

$$-\frac{d[Np(VI)]}{dt} = k''[Np(VI)][AHA] \quad (83)$$

a 2nd order rate constant of $k'' = (191.2 \pm 11.2) \text{ M}^{-1}\text{s}^{-1}$ in 1M HNO₃ at 25°C. This value is surprisingly low in comparison with the result for FHA. Chung and Lee used as magnetically stirred cuvette instead of an appropriate stopped-flow apparatus to determine the rate constant, possibly being a superposition of mixing and reaction kinetics. Later experiments of Matteson and the author of this dissertation [97] performed on a stopped-flow apparatus have confirmed this suspicion, providing a 2nd order reaction rate value of $k'' \approx 2500 \text{ M}^{-1}\text{s}^{-1}$ at 10°C in 1M perchloric acid; the topic will be therefore discussed in more detail in Chapter 6 below.

An important property of hydroxamic acid is their long-term instability in acidic environment due to hydrolysis that results in the parent carboxylic acid and hydroxylamine:



The reaction displays “classical” pseudo-first order kinetics, similar to many other hydrolysis reactions, and is catalyzed by hydrogen ion concentration:

$$-\frac{d[R-CONHOH]}{dt} = k''[H^+][R-CONHOH] \quad (85)$$

The values of the overall 2nd order constant for FHA and AHA were determined by Taylor et al. [93] to be $k''_{FHA} = 2.6 \times 10^{-4} \text{ M}^{-1}\text{s}^{-1}$ and $k''_{AHA} = 3.4 \times 10^{-5} \text{ M}^{-1}\text{s}^{-1}$ at 25°C, with activation energies of $E_{a,FHA} = 77 \text{ kJ/mol}$ and $E_{a,AHA} = 80 \text{ kJ/mol}$, respectively. The substantially lower acidic hydrolysis rate of acetohydroxamic acid has made it more attractive for application in a reprocessing facility.

Further analysis of the hydrolysis of AHA performed by Alyapyshev et al. [98] has identified that the hydrolysis rate increased 2-fold in presence of organic phase (30% TBP) and also increased 2-fold when lithium nitrate salt was added in amounts comparable to nitric acid; however, direct proportionality of the rate to the nitrate concentration was not found. The effect of ionizing radiation at a dose rate of 66 Gy/h increased the hydrolysis rate four-fold [98].

2.4.8.2.1 Reaction of acetohydroxamic acid with nitrous acid

Although scavenging abilities of hydroxylamine toward nitrous acid are well known (see section 0), it is surprising that almost no attention was paid toward the mutual reaction of acetohydroxamic acid and HNO_2 . The only study dedicated to the topic was performed by Zhang et al. [99] in both perchloric and nitric acid medium. Although the stoichiometry of the scavenging reaction was not investigated, the following rate laws were identified:

$$-\frac{d[\text{HNO}_2]}{dt} = k_{\text{HClO}_4} [\text{HNO}_2][\text{AHA}]^{0.75} [\text{HClO}_4]_t^{0.5} \quad (86)$$

$$-\frac{d[\text{HNO}_2]}{dt} = k_{\text{HNO}_3} [\text{HNO}_2][\text{AHA}]^{0.25} [\text{HNO}_3]_t \quad (87)$$

The rate constant values were $k_{HClO_4} = 2.37 \pm 0.21 \text{ M}^{-1.25} \text{ s}^{-1}$ at 5°C and $\mu = 0.5 \text{ mol/kg}$ in the perchlorate system and $k_{HNO_3} = 0.482 \pm 0.048 \text{ M}^{-1.25} \text{ s}^{-1}$ at 10°C and $\mu = 0.5 \text{ mol/kg}$ in the nitrate system, while the respective thermal activation energies were $E_{a,HClO_4} = 46.9 \text{ kJ/mol}$ and $E_{a,HNO_3} = 99.0 \text{ kJ/mol}$ [99].

The striking differences in the order of dependence with respect to the concentration of AHA with the change of reaction medium, which have not been observed by Stedmen and coworkers [88, 89, 90, 100, 101] for the reaction of either for hydroxylamine or for alkylhydroxylamines, cast serious suspicions as to the correct interpretation of the experiments by Zhang et al [99]. The reactions were quite rapid with most of the reaction has been over with several seconds. Since the authors have used a magnetically stirred cuvette system for the reaction, which has a multiple-second mixing time, it is most likely that they have observed a non-homogeneous kinetic process, resulting from the combination of mixing and chemical reaction. These suspicions were confirmed by stopped-flow method experiments performed by the dissertation author and are further discussed in Chapter 8 below.

2.4.8.3 Isomers of butyraldehydes

Another group of prospective agents for Np(VI) reduction during partitioning of U, Np and Pu was developed in Japan for the PARC process (“PARtitioning Conundrum key”), an advanced PUREX process [102]. The agents are the two isomers of butyraldehyde (commercial name for butyl-aldehyde or butanal, $\text{C}_3\text{H}_7\text{CHO}$): *n*-butanal $\text{CH}_3\text{-CH}_2\text{-CH}_2\text{-CHO}$, and *iso*-butanal $(\text{CH}_3)_2\text{CH-CHO}$. Although they are not particularly rapid reducing agents, they are relatively well extracted and can therefore react (albeit slower than in the aqueous phase [103]) with the actinides directly in the organic phase [56].

The kinetics of Np(VI) reduction by both butyraldehydes has been studied by Uchiyama et al. [104], but the reaction stoichiometry has not been studied properly and can only be inferred upon the studies with the kinetically similar reduction of vanadium from pentavalent ($\text{V}^{\text{V}}\text{O}_2^+$) to tetravalent ($\text{V}^{\text{IV}}\text{O}^{2+}$) oxidation state by Jones and Waters [105], where an 8:1 or 4:1 stoichiometric ratio of vanadium (V) to *n*-butanal or *iso*-butanal, respectively, were identified. Acetone, formic acid and even some small amount of insoluble polymer was found among the reaction product. The reactions of the two

aldehydes with neptunium(VI) then probably proceed according to the following equations:



The rate laws identified in 0.75-6 M nitric acid for the two reduction reactions at the temperature of 25°C are:

$$+\frac{d[\text{Np(IV)}]}{dt} = \{7.8 \times 10^{-3} \text{ M}^{-2} \text{ s}^{-1}\} [\text{H}^+] [\text{Np(VI)}] [n\text{-C}_3\text{H}_7\text{CHO}] \quad (90)$$

$$+\frac{d[\text{Np(IV)}]}{dt} = \{0.107 \text{ M}^{-2} \text{ s}^{-1}\} [\text{H}^+] [\text{Np(VI)}] [iso\text{-C}_3\text{H}_7\text{CHO}] \quad (91)$$

while the respective apparent activation energies were identified as $E_{a,n} = 28$ kJ/mol and $E_{a,iso} = 34$ kJ/mol. It can be seen that the rate constant for *iso*-butanal is significantly larger than for the *n*-butanal; however, even though *n*-butanal reduces Np(VI) to Np(V) at only a moderate rate, no parallel reduction of Pu(IV) can be observed, whereas *iso*-butanal reduces both appreciably. Reduction of uranium(VI) was not observed for neither of them. Therefore, application of *n*-butanal enables the selective reductive stripping of neptunium from 30% TBP-dodecane organic phase containing uranium, plutonium and neptunium, while *iso*-butanal can be used to reduce and strip both Np and Pu to the aqueous phase simultaneously.

Aside from reactivity toward actinides, it was also found that *iso*-butanal acts as a moderately fast scavenging agent for nitrous acid, within 5 minutes 0.069 M *iso*-C₃H₇CHO decomposed 99% of 1mM HNO₂ in 3M HNO₃. This would implicate that application of *iso*-butanal as a stripping reducing agent during partitioning of Pu and U would not necessitate the simultaneous usage of hydrazine or other nitrous acid scavenger, as opposed to the current situation with U(IV) or hydroxylamine [103].

2.4.9 Vanadium(V) as a prospective oxidizing agent

The relatively rapid oxidizing reaction of neptunium(V) by pentavalent vanadium (VO₂⁺) was first discovered in HNO₃ by Dukes and Sullivan in 1959 [106]; since then, it has been since proposed and applied as means to adjust and maintain the neptunium in the (+VI) oxidation state for the purpose of enforcing its extraction by TBP into the organic

phase [107, 108]. The parallel oxidization of Pu(IV) to the somewhat less extractable Pu(VI) by vanadium(V) is either very slow or it does not take place at all [106].

As has been discussed above (section 2.4.1), oxidation of Np(V) does occur also by the oxidizing effect of nitric acid in its very concentrated solutions, but its kinetics is much slower compared to the Np(V) + V(V) reaction; the same is also true for the kinetics of disproportionation of Np(V) into Np(IV) and Np(VI).

From a thermodynamic viewpoint, the relevant values of redox potential are very similar: 1.0 V for $\text{VO}_2^+/\text{VO}^{2+}$, 1.15 V for $\text{NpO}_2^{2+}/\text{NpO}_2^+$ and 1.1 V for $\text{PuO}_2^{2+}/\text{Pu}^{4+}$ [106]. Therefore, the differences in the oxidation kinetics of Np(V) and Pu(IV) are influenced by kinetic factors rather than by thermodynamic factors – i.e. the oxidation of Np(V) is much faster than the oxidation of Pu(IV) due to the necessity of the kinetically slow formation of oxygen double bonds in the plutonyl species $\text{O}=\text{Pu}=\text{O}$ of Pu(V) and Pu(VI). The reduction potentials indicate that the studied redox reaction is reversible and the generated Np(VI) is reduced back to Np(V) by tetravalent vanadium (VO^{2+}):



The kinetics of this reaction as, stated by equation (92), has been studied by Dukes [106] and Koltunov et al. [109, 110, 111] and has been found to behave almost ideally as a combination of two opposing 2nd order reactions[§]:

$$-\frac{d[\text{Np}^{\text{V}}]}{dt} = k_1'' \cdot [\text{Np}^{\text{V}}] \cdot [\text{V}^{\text{V}}] - k_2'' \cdot [\text{Np}^{\text{VI}}] \cdot [\text{V}^{\text{IV}}] \quad (93)$$

where k_1'' and k_2'' are the apparent rate 2nd order constants for the forward (oxidation of Np) and reverse (reduction of Np) reactions, respectively. The constants were found to be functions of the hydrogen ion concentration, ionic strength and the temperature of the solution.

Dukes [106] has studied the oxidation neptunium(V) in significant excess of vanadium(V) (10^{-12} to 10^{-5} M NpO_2^+ against 2×10^{-4} to 1.1×10^{-3} M VO_2^+) in solutions of HNO_3 using a solvent extraction technique based on the difference in the distribution

[§] Please note that for the sake of legibility, in this section the more classical notation for oxidation state in the superscript, e.g., Fe^{II} , in addition to the notation using parenthesis, e.g., Fe(II), the latter of which is in wider use by the radiochemical community for description of actinide redox chemistry and used throughout this document.

coefficients for Np(V) and Np(VI), with determination of Np concentration based on radiometric detection of alpha radiation from neptunium. The measurements were made in only HNO₃ solution environment, no treatment was made to keep the ionic strength at constant level (however, a side examination of the nitrate NO₃⁻ influence by addition of NaNO₃ at constant HNO₃ concentration was performed once without significant observational difference), therefore the second order rate constant measurements at 24°C and HNO₃ concentration range of 2.04 – 3.58 M yielded a value of relatively high error range:

$$k_1''(\text{HNO}_3) = \left(\{0.195 \pm 0.042\} \times [H^+]^2 \right) M^{-1}s^{-1} \quad (94)$$

Observation of the temperature measurement yielded an activation energy $E_a = 48.9 \pm 1.7$ kJ/mol [106]. Dukes has also made these experiments with plutonium and reached the conclusion that under the same oxidizing conditions Pu(IV) was not oxidized to an appreciable extent (only 3% have been oxidized by 5×10^{-4} M VO₂⁺ in 2.8 M HNO₃ to Pu(VI) as opposed to 96% conversion of Np(V) to the hexavalent form during the 30 minute oxidation time) [106].

Koltunov's research group [112] has started the studies of the Np^{VI}-Np^V-V^{IV}-V^V system in perchlorate solutions using spectrophotometric observation of Np(V) by determining its equilibrium. The value of the formal equilibrium constant, expressed for the inverse of reaction (92) as:

$$K' = \frac{[\text{Np}^{\text{V}}][\text{V}^{\text{V}}][\text{H}^+]^2}{[\text{Np}^{\text{VI}}][\text{V}^{\text{IV}}]} \quad (95)$$

was found to be equal to $K' = 7.65 \pm 1.31$ M² at 25.5°C at an ionic strength of $\mu = 4$ M. The enthalpy of the reaction was close to zero. Upon decreasing the ionic strength to $\mu = 2$ M the K' rose to ~ 36 M², slightly shifting the reaction (92) in the direction of reduction of Np(VI) to Np(V).

In additional kinetic study [113] the rate constant for the forward process (Np^V oxidation) was observed as being directly proportional to H⁺ concentration, and at $\mu = 4$ M and 25.5°C it was found equal to:

$$k_1''(\text{HClO}_4) = \left(\{1.97 \pm 0.17\} \times [H^+] \right) M^{-1}s^{-1} \quad (96)$$

The activation energy determined between 25.5 and 45.8°C had a value of $E_{a,1}(HClO_4) = 55 \pm 6$ kJ/mol.

The rate constant k_2'' for the reverse reaction at the same ionic strength of $\mu = 4$ M had an inverse power dependence of the rate constant on the H^+ concentration. At the temperature of 25°C the rate constant was observed to be:

$$k_2''(HClO_4) = \left(\frac{\{18.5 \pm 1.8\}}{[H^+]} \right) M^{-1}s^{-1} \quad (97)$$

From the rate constant temperature dependence between 25.5 and 45.8°C, it was found that the activation energy for the reverse reaction was $E_{a,2}(HClO_4) = 54 \pm 8$ kJ/mol, indistinguishable in value from the activation energy for the forward process.

As is clear, the value of the apparent second order rate constant k_1'' and its dependence on H^+ concentration reported by Dukes [106] for the oxidation of Np(V) in solutions of nitric acid is substantially different from the data on the oxidation of Np(V) in solutions of perchloric acid measured by VIS-NIR spectrophotometry by Koltunov and co-workers [113]. These discrepancies have led to further investigation of this reaction by the dissertation author and the topic is discussed further in Chapter 4.

Also, since vanadium has several oxidation states of different potential utility in its reactions with plutonium and neptunium, a review on the kinetics of these reactions has been compiled by the author and can be found at the end of this dissertation as Appendix C (chapter 0).

2.5 Radiation chemistry of neptunium in nitric acid

The nitric acid solutions resulting from the dissolution of used nuclear fuel are highly radioactive. The ionizing radiation emitted consists primarily (> 90% [2]) of β and γ radiation from the decay of short-lived fission products, whereas the dissolved actinide elements are responsible for the absolute majority of α radiation.

The energy deposited by the radiation is usually characterized by the physical quantity called *absorbed dose* D , which is the amount of radiation energy absorbed E_{abs} per unit of mass m [114]:

$$D = \frac{E_{abs}}{m} \quad (98)$$

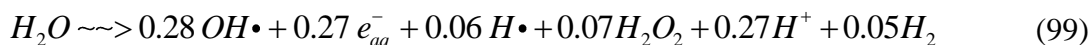
The unit of absorbed dose is the gray (Gy = J/kg). The *dose rate* D' is the absorbed dose per unit time and it is usually described in terms of Gy/s or, more commonly, kGy/h [114, 115]. The dose rate in typical solutions of dissolved used nuclear fuel is so high that it can be conveniently measured in terms of heat power and was calculated to reach levels of 6 watts per liter (W/L), which is approximately equivalent to 6 Gy/s or 21.6 kGy/h [2]. The dose absorbed from the ionizing radiation emitted by the decay of radioactive elements induces various radiolytic transformations in the dissolved components and significantly influences the redox chemistry of actinide ions, and, consequently, markedly influence their extractability into the organic phase. This has a clear impact on the performance and operation of the technological processes of UNF reprocessing [116].

2.5.1 Radiolysis of water

The radiation chemistry of aqueous solutions of actinides is based on the understanding of the fundamental mechanism of radiolysis of water, which absorbs the vast majority of the radiation dose.

The chemical transformation of water by radiation is called *radiolysis*. The primary products formed within 10^{-7} s [117] after in the process of conversion of the interaction of particles of ionizing radiation water molecules are: the hydrated electron e^-_{aq} , the hydrogen atom $H\bullet$, the $OH\bullet$ radical, molecular hydrogen H_2 , hydrogen peroxide H_2O_2 and H^+ and OH^- ions.

In the case of low LET (linear energy transfer) radiation, such as β (fast electron) and γ and X-ray (electromagnetic) radiation, the process of decomposition of an average molecule of water during radiolysis of pure water can be denoted as a chemical reaction of the following stoichiometry[117]:



The efficiency of conversion of radiation energy to chemical products is defined as the *radiation-chemical yield* G , characterized now in units of $\mu\text{mol}\cdot\text{J}^{-1}$, replacing an older unit of molecules per 100 eV absorbed ($1 \text{ molecule}/100\text{eV} = 0.1037 \mu\text{mol}/\text{J} \approx 0.1 \mu\text{mol}/\text{J}$). The yields of pure liquid water decomposition is equal to $G(-H_2O)_{\beta,\gamma} = 0.43 \mu\text{mol}/\text{J}$ for radiolysis by low-LET radiation and $G(-H_2O)_{\alpha} = 0.294 \mu\text{mol}/\text{J}$ for radiolysis by high-LET radiation, such as α -particles or accelerated ions [114].

Of the species produced by water radiolysis the $OH\cdot$ radical and H_2O_2 are strong oxidizing agents, while e_{aq}^- and $H\cdot$ are strong reducing agents. The radiation chemistry of solutes present in aqueous solutions during radiation processes is characterized by the complicated network of reactions with these highly reactive species.

In neutral water, the reducing and oxidizing species are produced in approximately equal amounts, but in a real solution the prevalent oxidizing or reducing character of radiolysis will depend on several characteristics of the solution - primarily its pH, concentration of dissolved oxygen, and the presence of *scavengers* – compounds that react with the primary species, usually resulting in a less reactive species.

For instance, in acidic solution with multimolar H^+ concentration, the aqueous electrons would be almost completely scavenged by the hydrogen ions and converted to hydrogen atoms:



This reaction is characterized by a diffusion-controlled kinetics with a very high second-order rate constant of $k = 2.3 \times 10^{10} \text{ M}^{-1}\text{s}^{-1}$ [117, 118]. Such very high magnitudes of reaction rates are typical for the reaction of primary products of radiolysis and can be primarily studied by the methods of pulsed-radiolysis.

Besides the reaction with primary products of radiolysis of water, the radiation-chemical reactions of actinide ions in solutions are significantly influenced by the presence of inorganic and organic free radicals resulting from the radiolysis of other compounds present in the aqueous solutions. Some of these reactions are very rapid, which limits the stationary concentrations of the reacting intermediates to very low levels.

The rate constants for these processes have been measured by various methods the method of pulse radiolysis with spectrophotometric recording of short-lived species has been used most often [119, 120, 121] and, in some cases, electrochemical methods have been employed [122]. Presently, many rate constants are being estimated by experiments combined with sophisticated computer modeling of radiolytic processes, based on reliably rate constant values established previously. Numerous studies have dealt with the kinetics of reactions of actinide ions with the primary products of water radiolysis [116].

2.5.2 *The radiation chemistry of actinides in nitric acid solutions*

After water, nitric acid is the compound with the highest concentration in the aqueous solutions relevant to nuclear reprocessing. Radiolysis of aqueous nitric acid and nitrate solutions has been investigated not only from the practical view point of nuclear technology, but also from a scientific interests in order to understand the radiolysis of water because the nitrate ion is an efficient scavenger of hydrated electrons and hydrogen atoms, significantly altering the overall effects of water radiolysis [123].

In general, radiolysis of aqueous nitrate solutions generates many highly reactive N-centered radicals [124]:



and the ultimate products of radiolysis of nitric acid solutions (after the end of irradiation) are O₂, H₂, H₂O₂ and HNO₂. The yields of these compounds are significantly dependent on the concentration of nitrate and acidity of the solution. Increasing the HNO₃ concentration decreases the yield of hydrogen and increases the yield of oxygen and nitrous acid. What is more, hydrogen peroxide and nitrous acid are mutually reactive (67) and cannot coexist in solution together, as has been already discussed in section 2.4.6.1 above.

Also, as has been mentioned multiple times above, specifically in section 2.4.1, the influence of HNO_2 on the redox speciation of neptunium and plutonium in nitric acid is of paramount importance. A high nitrous acid content in the aqueous phase acts as a stabilizer of the extractable tetravalent plutonium [125] but also leads to reduction of a significant portion of neptunium to its inextractable pentavalent state [53, 126] by the reverse of reaction (39):



It is important not to omit the fact that HNO_2 also influences the redox chemistry of actinides in the organic phase, but due to the complexity and magnitude of the topic will not be discussed here and the reader is referred to the comprehensive review on these reactions, which has been recently published by Marchenko et al. [57].

3 MATERIALS AND METHODS

As has been stated in the introduction to this work, the aim of this study was to develop or enhance the understanding of several key topics governing the redox behavior of neptunium in nitric acid environment. Of primary interest were the reactions of neptunium with several redox-active compounds, which were studied primarily by kinetic methods of analysis; furthermore, several issues in the topic of radiation chemistry of nitric acid were studied - especially the radiolytic production of HNO_2 and the rapid chemical reactions of nitrous acid with several compounds relevant to the reprocessing of used nuclear fuel.

The absolute majority of the work has been performed in the Laboratory of Transuranic Elements in the Radiation Center of the Oregon State University and utilized its available supply of materials, equipment and instrumentation, only some of these had to be acquired specifically for the purposes of this work. A part of the work on neptunium radiolysis and nitrous acid production from radiolysis of nitric acid solutions has been performed or utilized the equipment of the Actinide Separation Group in the Materials and Fuels Complex of the Idaho National Laboratory

3.1 Materials

3.1.1 *Neptunium*

Due to the very long half-life of neptunium-237 ($T_{1/2} = 2.144$ million years), neither the α - and γ -radiation of its own decay nor the β - and γ -radiation of its short-lived daughter product protactinium-233 ($T_{1/2} = 27$ days) represent a significant work hazard if worked in macroscopic (milligram) quantities. Therefore, utilization of classical methods of chemical analysis is quite feasible since "real" industrial concentrations of up to 20mM Np in milliliters of solution could have been utilized during the work. Moreover, due to the low activity, the effects of auto-radiolysis of its own α -radiation on the redox stability of neptunium in solutions are insignificant at these concentrations (compared to many short-lived transuranic nuclides, such as Pu-238 or Cm-244). This gives neptunium studies a significant advantage over the study of highly radioactive transuranic elements,

which are usually investigated using radiotracer methods at ultra-low concentrations, at which significant deviation of chemical behavior can occur.

Therefore, during the work, the detection of α -ray (of 4.5 - 4.9 MeV energy) and γ -ray emission of Np-237 (at 29.374 keV) and γ -ray emission Pa-233 (at 312.17 keV) [9, 125] has been used only in auxiliary activities, e.g., workplace decontamination and waste-processing activities. The instruments utilized for these were various Geiger-Müller counters (routine radiation surveillance), Perkin Elmer 3180 LSC (alpha/beta) liquid scintillation counter, and thalium-doped sodium iodide – NaI(Tl) or HPGe γ -ray spectrometers.

Neptunium for this study was received in the oxide form as $^{237}\text{NpO}_2$ from Argonne National Laboratory and then further processed and purified.** First, the solid oxide was dissolved in a slight molar excess of hydrogen peroxide and 8 mol·L⁻¹ nitric acid. Confirmation of the tetravalent oxidation state was determined using Vis-NIR spectroscopy. In order to remove any transuranic impurities, the Np solution was added to a prepared column of 1 cm wide *BioRad AG1×10* anion exchange. The column was rinsed with a solution of 8 M nitric acid, 0.3 M hydrazine monohydrate, and 20 mM hydroquinone. After washing the impurities, pure neptunium was then stripped from the column using 0.36 M hydrochloric acid and its isotopic purity was confirmed using thin-window High-Purity Germanium γ -ray spectroscopy (HPGe). Any organic impurities were destroyed by multiple re-evaporation with concentrated nitric acid and hydrogen peroxide. The clean solution was then evaporated to dryness and dissolved in a 4M nitric acid solution to create a Np stock solution (of mostly hexavalent, but generally mixed +5/+6 oxidation state). Further adjustment of the oxidation state was thereafter performed by the following ways:

- Np(VI): evaporation of the original stock nitric acid solution, fuming with perchloric acid until dryness and re-dissolution in desired concentration of nitric acid,

** The author would like to - specifically here - to express his appreciation and acknowledge the effort of his former colleague, Brent S. Matteson (OSU PhD graduate of 2010), who performed most of this tedious process.

- Np(V): dilution into dilute nitric acid (0.5M), followed by addition of a controlled amount of hydrogen peroxide followed by heating at 40°C to remove excess peroxide (to achieve pentavalency),
- Either oxidation state: controlled-potential electrolysis (see section below).

The final oxidation state was then always confirmed by Vis-NIR spectroscopy (see below), in one specific case, it was also confirmed by titration with hydroquinone. [127]

3.1.2 Solutions and their preparation

Most materials specifically not mentioned in this section have been acquired through standard vendors of chemicals and were of ACS reagent grade purity or greater.

Deionized water was first filtered by an on-site industrial-size reverse-osmotic unit installed at the OSU Radiation Center and then purified by a laboratory-size ultra-purifier unit (Barnstead Nanopure) to achieve 18 MΩ·cm resistivity.

Standard aqueous stock solutions of were prepared by dissolution of weighed samples or dilution of liquid samples of the desired chemical compound in class A Pyrex-glass volumetric flasks ($\pm 0.1\%$ tolerance).

All solid chemical were weighed using a Sartorius CP225D automatic digital analytical balance with 0.01mg accuracy for samples below 80 g and 0.1mg accuracy for samples below 220 g. Addition of liquid volumes was performed by pipetting with modern hand-held manual and digital pipettors with replaceable plastic pipette tips. For work where delivery of high systematic precision was necessary, digital electronic pipettors Eppendorf Research Pro and Eppendorf Xplorer were utilized.

Appendix B of this dissertation contains a detailed description of the procedure utilized for determination of systematic and random errors introduced by pipetting. The combined errors were found to be at worst on the order of $\pm 1\%$ of the value of desired delivery volume, and were therefore usually not calibrated for due to much higher relative errors introduced in the data from other parts of experimentation.

3.1.3 Volumetric titration

The concentration of all diluted stock solutions of strong acids was determined by a standard volumetric titration with a 0.1M NaOH (strongly basic) titrant to a pH = 7.00

endpoint. Most of these titrations were performed usually in a series of three to increase precision to within $\pm 0.2\%$ using a Mettler-Toledo DL-58 automatic titrator equipped with a Rondo-60 carousel with a capacity of 20 sample beakers. Before titration, the DG-115 glass combination pH-electrode, which was filled either with a 3M KCl or 3M NaCl solution, was calibrated by a series of three pH-buffers (pH = 4.00, 7.00, and 10.01).

The 0.1M sodium hydroxide titrant was prepared either from solid NaOH or from a standard commercial refill solution, and its exact titer was calibrated periodically (i.e., at least one week before every new titration set) to eliminate the effect of concentration change due to absorption of acidic carbon dioxide from air. Two calibration methods were utilized:

- 5 samples of solid potassium hydrogen phthalate (KHP), each of accurately weighed amount of 70-120 mg (± 0.01 mg), were titrated with the calibrated solution of NaOH until a steep increase of pH took place, evaluating the endpoint at the point of steepest pH change per volume addition (which took place usually around pH = 8.5),
- 5 samples of approximately 800 μ L ($\pm 0.1\mu$ L, calibrated pipette tip) of standardized hydrochloric acid of a guaranteed 1.0000 ± 0.0005 M concentration until a pH = 7.00 endpoint.

The calibrations usually resulted in a titer relative standard deviation below 0.15%.

3.1.4 Nitric acid

Nitric acid was procured as a 67-69 % HNO₃ solution (~15 mol/L) from different vendors (mostly EMD Chemicals and Mallinckrodt). In all cases, the manufacturer guaranteed ACS specifications for purity of nitric acid, especially for less than 0.2ppm iron impurity – this was an important concern to exclude potential catalytic effects on the studied redox reactions.

Aqueous stocks of 0.1-10 mol/L solutions of nitric acid and of other compounds were created by single-step or double-step dilution with deionized water. During experimentation, absence of significant amounts of nitrous acid in stock solutions of HNO₃ was checked by UV-spectrophotometry with a detection limit of 0.05mM HNO₂ (see section 3.2.2.4 below)

3.1.5 Management of the instability of nitrous acid

Nitrous acid, perhaps the most important chemical in this work, is a weak acid with a small dissociation constant ($pK_a = 3.3$ at 25°C , [128]), which makes it almost entirely protonated under conditions of >10 mM acid concentration. A special issue during most of the experimentation was the fact of mid-term instability of nitrous acid in acidic solutions opened to air (in the time scale of tens of minutes to hours).

Nitrous acid disproportionates into NO_x gases (including nitric oxide, NO) which are volatile, and thus HNO_2 decomposes with a half-life of single hours in both aqueous and organic solutions if kept in vessels opened to air (or gaseous headspace in general). The rate of decomposition is much increased if the contact with the gas phase is artificially promoted, e.g. by bubbling of inert gas through the solution [129, 130]. For this reason significant losses of HNO_2 have been observed in solvent extraction separation cascades, where vigorous mixing of the solutions under an inert gas blanket occurs [131].

As a result of its instability, where HNO_2 solutions had to be used as reagents, they were usually created *in-situ* by introduction of stable aqueous neutral sodium nitrite stock solutions into acid. Stock solutions of sodium nitrite (usually 100 - 200 mM) were prepared by dissolution of NaNO_2 (Mallinckrodt, analytical reagent, assay $\sim 97\%$) in neutral distilled water. Their standardization was performed to within 1% concentration accuracy by titration of standardized solution of potassium permanganate (KMnO_4) according to Lunge's method [132] (permanganate itself was standardized by oxalic acid).

Decomposition of HNO_2 can be prevented by using a hermetically sealed reaction vessel when nitric oxide (NO) vapors create a cover gas blanket; therefore, where possible closed screw-cap vials almost completely filled with liquid ($<5\%$ headspace) were used in experiments.

3.2 Methods and Techniques

3.2.1 Electrochemistry

Originally, the project was supposed to employ electrochemical approaches as its primary methods of analysis and investigation of redox reactions of neptunium. As a result,

a complete electrochemical workstation Epsilon E-2 from Bioanalytical Systems, Inc. (BASi) including a Faraday cage for cyclic-voltammetric analysis was acquired, along with many accessories, such as platinum working and auxiliary electrodes and Ag/AgCl reference electrodes.

However, the electrochemical approach has two major practical disadvantages compared to spectroscopic methods that were in the end most utilized instead.

Firstly, the electrodes need to be inserted directly into the liquid sample, which severely complicates working practices with radioactive samples. Manipulation of radioactive solutions require very stringent contamination prevention approaches – most surfaces that come into contact with a solution of radioactive neptunium become contaminated to a certain degree. Complete removal of radioactive contamination is not usually readily possible and almost always generates additional waste.

Secondly (and more importantly), interpretation of electrochemical data can be very complicated: while redox potentiometry offers only a 1-dimensional electric potential value at a particular time, which does not allow direct identification of speciation of a system of multiple redox-active components, voltammetric methods measuring current-voltage dependence (e.g., polarography, cyclic voltammetry) require a very well defined system with strong electro-kinetic response or a very sophisticated approach tailored to investigation of one particular system.

Therefore, with the exception of a limited number of potentiometric measurements, electrochemistry was primarily used in preparation of pure oxidation states of neptunium in different concentrations of nitric acid.

3.2.1.1 Redox potentiometry

When both the oxidized and the reduced forms of a redox couple are dissolved in a solution, an inert metal (such as platinum, Pt) can attain a potential, which only depends on the ratio of the activities of these two species. The inert electrode operates during the measurement as an electron source or drain [133].

As an example of a simple redox electrode with a homogeneous ionic equilibrium, in an aqueous solution containing neptunium(V) and (VI), the potential of an inert platinum electrode E_{Pt} depends on the standard redox potential the ratio of concentration activities

of the ions NpO_2^+ and NpO_2^{2+} . In a particular electrolyte solution (e.g. 1M HNO_3) with a known formal redox potential, the electrode potential can be calculated on the basis of the ratio of concentrations of NpO_2^+ and NpO_2^{2+} :

$$E_{Pt} = E^o(\text{NpO}_2^{2+} / \text{NpO}_2^+) - \frac{RT}{F} \ln \frac{a_{\text{NpO}_2^+}}{a_{\text{NpO}_2^{2+}}} = E^{o'}(\text{NpO}_2^{2+} / \text{NpO}_2^+) - \frac{RT}{F} \ln \frac{[\text{NpO}_2^+]}{[\text{NpO}_2^{2+}]} \quad (103)$$

In order to measure that potential, a reference electrode is usually used to complete the electrical circuit. A reference electrode is usually an electrode of second kind, where a simple metal electrode M^0 is coupled to the precipitation equilibrium of a highly insoluble salt of the same metal $\text{M}^{n+}\text{X}_n^-$ from a solution with controlled concentration of a different, highly soluble salt of the same anion X^- , e.g. NaX . The small concentration of dissolved M^{n+} cation is controlled by the solubility product of the highly insoluble salt MX_n and the concentration of the anion X^- . Since the activities of the metal and metal anion solid phases are constant, the reference electrode exhibits a potential controlled by the concentration activity of the anion X^- .

$$E_{ref.} = E^{o'}(\text{M} / \text{MX}_n) - \frac{RT}{nF} a_{\text{X}^-} \quad (104)$$

In a reference electrode the metal electrode, precipitate, and the electrolyte are separated from the rest of the electrochemical cell by a glass frit or a membrane, so that mixing of the electrochemical cell solution with the NaX solution inside the reference electrode is possible only by very slow diffusion processes and can thus be considered constant; hence, the potential of such electrode is also constant.

Electrically connecting the indicating inert metal electrode with a reference electrode across an apparently infinite resistance allows to measure the so called *open circuit potential* (or somewhat archaically, *electromotive force*) of the electrochemical cell, which is in an ideal case determined only by the potential of the indicating electrode (e.g. by the ratio of the concentrations of the redox couple):

$$E_{cell} = E_{Pt} - E_{ref.} \quad (105)$$

However, due to ion diffusion processes in the membrane, a small junction potential E_j (usually on the order of ± 1.0 mV) is introduced into the measurement of the difference

between the potential of the reference electrode and the potential of the working electrode.

$$E_{cell} = E_{Pt} - E(M / MX) - E_j \quad (106)$$

In the redox-potentiometric experiments performed in this work, a platinum wire redox-sensitive electrode was used against a small universal silver – silver chloride electrode (further-on abbreviated as SSC or Ag/AgCl) with 3M NaCl filling and a porous Vycor glass frit (RE-5B Bioanalytical Systems, Inc.) as a reference electrode. Alternatively a combination semi-micro redox electrode with a platinum ring and a built-in Ag/AgCl reference electrode with 3M KCl filling (InLab Redox Micro, Mettler Toledo) was used in certain applications. Depending on the temperature, both reference electrodes were assumed to have a potential of around 205-210 mV vs. standard hydrogen electrode (SHE) [133].

3.2.1.2 Controlled potential electrolysis and coulometry of neptunium

Preparation of pure oxidation states (+5) and (+6) of neptunium was performed in a custom-built electrolytic H-cell with a glass frit-separated compartments to separate anolyte from catolyte solution (Figure 7, three of these cells were generously donated by Argonne National Laboratory). A coiled platinum wire electrode as the primary working electrode was located in the smaller volume compartment along with a magnetic stirrer, whereas the auxiliary plain wire Pt electrode and an Ag/AgCl electrode as a reference electrode were located in the auxiliary compartment.

The complementary auxiliary compartment was filled with nitric acid of the same concentration as the acid used for the neptunium solution in the working compartment. Since the porosity of the frit had to be made relatively high to allow higher electrolytic currents, the level of liquid in the auxiliary compartment at the beginning of electrolysis was carefully adjusted, so that hydrostatic pressure would cause neither the neptunium solution to seep into the auxiliary compartment nor dilute the neptunium solution with pure solvent from the auxiliary compartment.

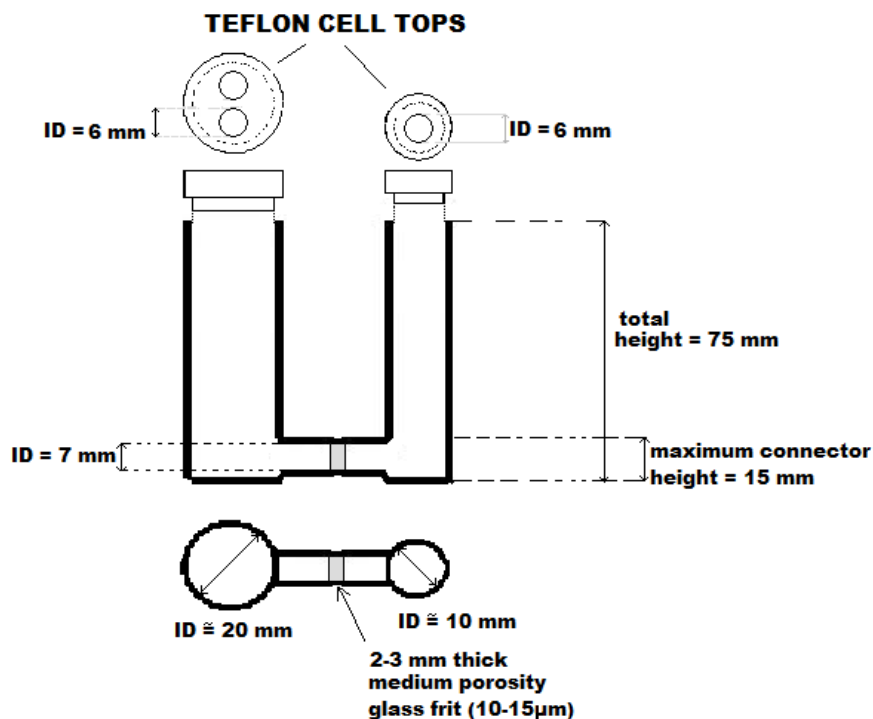


Figure 7 – Design plan of the glass H-cell used for Np electrolysis

The formal potential of Np(V)/Np(VI) couple in nitric acid is approximately +1.1 V vs. SHE (or around +900 mV vs. SSC). At 25°C (T=298.15 K), the equation (103) can be expressed as:

$$E = (+1100 \text{ mV}) - (59 \text{ mV}) \times \log_{10} \frac{[Np(V)]}{[Np(VI)]} \quad (107)$$

So, in theory, applying a potential of $3 \times 59 \text{ mV} \approx 180 \text{ mV}$ difference from the formal redox potential would ensure 99.9% conversion of neptunium to either pentavalent or hexavalent oxidation state. However, to achieve fast enough electrode kinetics, higher overpotentials had to be usually applied. Oxidation or reduction of neptunium solutions was performed by applying an appropriate oxidizing (+1250mV vs. SSC) or reducing potential (+700mV vs. SSC) on the working Pt coil electrode. Electrolysis of most samples was assumed to be complete after approx. 1-2 hours, with the majority of the electrochemical reaction:



taking place during the initial 30 minutes. During preparation of Np(VI) from solutions, shorter times were used, because the majority of neptunium was already mostly in the

hexavalent state as a result of enhanced multi-fold oxidation by hot nitric acid during the metathesis operations.

Current vs. time curve acquired by the Epsilon E-2 potentiostat followed approximately the ideal electrolysis exponential dependence (Figure 8). Using the assumption $I_t \sim c_{Np,t}$, i.e. that the actual current is proportional to the remaining concentration of neptunium in the oxidation state to be reduced / oxidized, the exponential dependence can be deduced from Faraday Laws of electrolysis:

$$I_t = I_0 \cdot e^{-const \cdot t} \quad (109) \quad const. = \frac{I_0}{F \cdot c_{Np,0} \cdot V} \quad (110)$$

where I_t and I_0 are the electric current at time t and the beginning of application of the particular electrolysis potential, $c_{Np,0}$ is the starting concentration of neptunium to be reduced/oxidized and V is the volume of the working compartment.

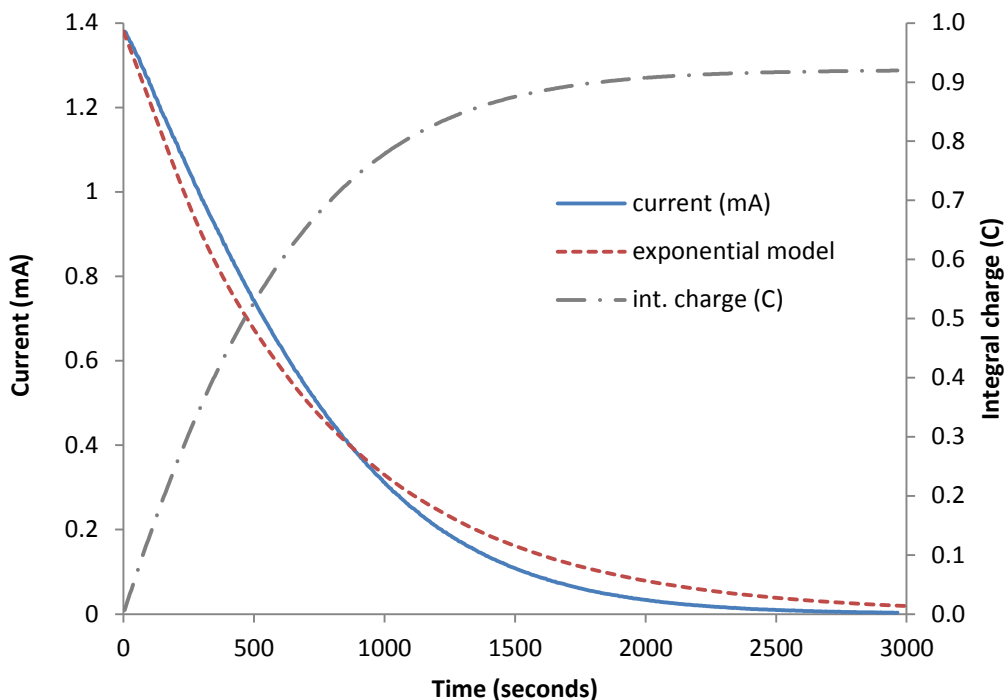


Figure 8 - Dependence of reducing electrolytic current of 2mL of initially 5mM Np(VI) solution in 1M HNO₃ with applied potential of +700mV vs. Ag/AgCl, 3M NaCl.

When the neptunium was initially in a pure (99.9%) oxidation state (usually created by an electrolysis in the opposing direction), the integral of the passed charge Q (Figure 8) was

used to calculate the coulometric concentration of neptunium c_{Np} in the solution, which was used to independently confirm concentrations determined by spectrophotometric or radiometric methods:

$$c_{\text{Np}} = \frac{Q}{F \cdot V} \quad (111)$$

3.2.2 Spectrophotometry

Since most of the experimental work performed was concerned with analysis of the redox speciation of neptunium or nitrous acid, the absolute majority of analytical data was collected using ultraviolet – visible – near-infrared (UV-Vis-NIR) molecular spectroscopy.

Molecular absorption spectroscopy or *spectrophotometry* is a method where the qualitative and quantitative information is obtained from the precise quantitation of absorption of electromagnetic radiation on each of its wavelengths that are generally between 200 and 1400 nm (corresponding photon energy range is 6.2 – 0.9 eV, nonetheless, the given range is given by spectral transparency window of water – other solvents allow of spectrophotometric observation of wider wavelength range). The method is based on the application of the Lambert-Beer-Bouguer's Law for an ideally absorbing compound homogeneously distributed in layer of material:

$$\frac{I(\lambda)}{I_o(\lambda)} = T = 10^{-\epsilon_{\lambda} \cdot b \cdot c} \quad (112)$$

The ratio of the exiting $I(\lambda)$ versus entering $I_o(\lambda)$ radiant intensity of a parallel beam of light at a particular wavelength, otherwise defined as *transmittance* T is an exponential function of the thickness b of the absorbing layer (usually expressed in centimeters, cm), concentration of the compound c (in mol/L), and a proportionality constant ϵ_{λ} ($\text{L} \cdot \text{mol}^{-1} \text{cm}^{-1} = \text{M}^{-1} \text{cm}^{-1}$) called the *molar absorption coefficient* (also molar absorptivity or molar *extinction* coefficient, hence the epsilon symbol) [134]. For practical purposes, a dimensionless^{††} linearized unit - *absorbance* A - is defined:

^{††} The *de-facto* internationally accepted unit of decibel (**dB**) or bel (**B**), in common use for quantifying dimensionless logarithmic ratios of intensities of sound or radio wave energy, is not being used in molecular spectroscopy. Usage of non-standard units, such as **Abs** or **AU** is occasionally encountered in chemical literature.

$$A_{\lambda} = -\log\left(\frac{I(\lambda)}{I_o(\lambda)}\right) = -\log T = \varepsilon_{\lambda} \cdot b \cdot c \quad (113)$$

Determination of absorbance of solutes in aqueous solutions is usually performed in transparent glass cells (cuvettes) with a standard 1.000 cm empty volume thickness, but other cell thicknesses are also utilized. The chief function of spectrophotometry is in the determination of a solute's concentration from the value of the absorbance at a particular wavelength, using a previously determined molar absorption coefficient:

$$c = \frac{A_{\lambda}}{\varepsilon_{\lambda} \cdot b} \quad (114)$$

The instruments used for observation and quantification of absorbance are called spectrophotometers. Several different designs exist, each with certain advantages and disadvantages, in the current work two types of spectrophotometers were used: a single-beam fiber-optic diode-array spectrophotometer (OceanOptics QE65000) and two double-beam monochromators (OLIS RSM 1000 and Agilent/Varian Cary 6000i).

3.2.2.1 Diode-array spectrophotometry

The OceanOptics QE65000 is a representative of a newer class of instruments that were made possible by significant advances in miniaturization of electronics. The whole instrumental setup of the device consist of a light source, connected by a light-guiding fiber optic cable to the sample cell holder, where the “white” light (i.e. polychromatic group of wavelengths) interacts with the sample, and then into the spectrometer itself, which consists of an optical grating that splits the individual wavelengths of the polychromatic spectrum onto a linear array of photodiodes. Each photodiode monitors only a small wavelength of the spectrum, the whole spectrum is therefore reconstructed from the parallel signal of all photodiodes in the array.

The advantage of this setup is the immediate broad spectrum information (QE65000 has a wavelength range of 200-1000nm) is obtained in one time-step, in principle in as low as 15 milliseconds. On the other hand, due to the high electronic noise of the photodiodes, averaging over a longer time-period (~1s) is usually required to acquire low-noise spectra – but this is still significantly shorter time than is characteristic for such a broad spectral acquisition in classical monochromators.

Another advantage is the flexibility and small size of the instrument, allowing for easy transport and utilization in various different applications. The use of fiber-optic cables makes it easy to accessorize the sample compartment (e.g. changing the 1 cm pathlength cell holder for and 10cm pathlength cell holder) and allows to separate the spectrometer instrument from the location of measurement (which is an important advantage for applications in work with highly radioactive compounds that need to be handled in glove boxes, etc.).

One of the main disadvantages of the instrument are partly in lower reliability of the universal grating (due to issues with multiple-order maxima wavelength sorting), which results in problems with resolution of absorption peaks of very narrow wavelength. But the primary issues with the instrument are its baseline stability due to mechanical sensitivity of the fiber-optic cable connections (e.g. during cuvette insertions into the non-rigid cell holder). Since the instrument has a single-beam design, simultaneous comparative quantification of the input and output light intensities is not possible. Absorbance is calculated as a ratio of output intensities I_S and I_B determined for a sample and a blank solution, respectively, corrected for the so called “dark-current” intensity of additive the photodiode thermal noise I_D , which is determined when the light source is temporarily obscured:

$$A = -\log\left(\frac{I_S - I_D}{I_B - I_D}\right) \quad (115)$$

Since the blank intensity is stored only in instrument memory, if the overall light output of the light-source and light-delivery (fiber-optics) system changes, the theoretical I_B value should change too, but its determination is not possible without reinserting the blank solution again. In certain applications (e.g. long-term chemical kinetics), this causes significant issues with long-term baseline stability and can entirely compromise data from such experiments (especially because the baseline intensity does not change proportionally in the same proportion for every wavelength).

Another issue of the OceanOptics QE65000 spectrometer system is the relatively high admittance of stray light, especially at UV-wavelengths, which fundamentally limited the applicability of the Lambert-Beer law for absorbance up to $A = 0.8$.

3.2.2.2 Double-beam monochromator spectrometry

The OLIS RSM1000 and Cary 6000i outclass the OceanOptics QE65000 diode-array spectrophotometer in almost every performance parameter besides portability and lack of simultaneous broad-band (UV-Vis-NIR) rapid spectral acquisition ability (the RSM1000 actually does have a competitive narrow-band rapid-scanning ability that will be discussed below).

In the double-beam monochromator spectrometers, the light coming from the light-source is first introduced through a system of slits and mirrors onto at least one optical grating (in the case of RSM1000 and Cary 6000i, there are 2 optical gratings to increase wavelength resolution and reduce the stray-light effect). Just as in the diode array spectrophotometer, the grating disperses the light into different angular directions, but here the grating is rotated in a way to direct only one wavelength onto an output slit, so that only a very thin band of wavelength (usually 0.2-1 nm) is exiting the monochromator. The resulting single-wavelength beam is then split by either a semi-permeable mirror (RSM 1000) or a high-frequency rotating mirror (Cary 6000i) into two beams. One of the beams travels through the sample and one through a stable reference optical system (usually just empty air). The intensity of each of the beams is analyzed independently by a “colorblind” detector. In the case of RSM1000 the light is captured by a pair of photo-multiplier tubes (for UV-Vis range) or a pair of large-surface InGaN diodes (for NIR), while in Cary 6000i the two light beams are impacting the same InGaN detector (Peltier-cooled) in separate time-periods with a high alternation frequency.

When the absorbance baseline is measured for the blank, the ratio of the intensities of first beam I_B and the second reference beam I_{RB} are recorded for the blank. Consequently, the sample intensity I_S is measured simultaneously with the sample references intensity I_{RS} . All four measurements are then used to calculate the absorbance from the ratio of relative intensities of the blank and the signal by the following formula:

$$A = -\log \left(\frac{I_S / I_{R,S}}{I_B / I_{R,B}} \right) \quad (116)$$

Since the reference intensity I_R is in constant proportion to the light intensity I_o entering the sample or the blank, stability of the baseline is significantly improved even when there are long-term changes in the light-source output.

Besides classical monochromator operation, the OLIS RSM 1000 is capable of a *rapid scanning mode* (RSM stands for Rapid Scanning Monochromator). In this mode a fixed slit used to isolate the critical wavelength is replaced by a moving slit on rotating disk. The very fast movement of the slit is synchronized with the data acquisition by the light detectors, which allows to scan a window of wavelengths (approximately 100-300 nm, depending on the central wavelength region) in one millisecond (frequency of 1000 s^{-1}). Due to the superior light-sensitivity of the photo-multiplier tubes over photodiodes in the visual range, the quality of the rapid spectra outperforms the capabilities of photo-diode arrays for such rapid spectrum acquisition. Very fast kinetic phenomena with characteristic reaction times around 10-100 ms can be therefore readily observed.

Since both instruments are based on a double-grating monochromator, interference with the stray light is not a significant issue, as mentioned above. The applicability of the Lambert-Beer law for most solutes is possible into multiple absorbance units; however, typical measurements were made up to $A \approx 2.0$.

3.2.2.3 Spectroscopy of neptunium in aqueous solutions of nitric acid

Molecular spectroscopy is probably the most useful method for the analysis of redox speciation of neptunium and of the actinides of the uranium group (U, Np, Pu, Am) in general due to rich f-electron spectroscopy. Each oxidation state of these actinides has a very characteristic color (and corresponding absorption spectrum); the spectra are not immutable and also depend on the type and number of ligands.

Already the first published information about the chemistry of neptunium made by Hindman, Magnusson and LaChapelle during the Manhattan project contained detailed UV-Vis-NIR spectra (350-1050 nm) of all of neptunium(III), (IV), (V) and (IV) ions in HCl, HClO₄ and H₂SO₄ [135].

The most recent published data on UV-Vis-NIR spectra neptunium oxidation states in 0.1 – 4M aqueous HNO₃ solutions were made by Friedman and Toth [136] (1981). Neptunium spectra feature several many important absorption bands and peaks in all the

350-1350 nm observable wavelength range in nitric acid solutions (nitric acid absorbs below 350 nm[137], while the absorption of water becomes significant above 1300-1400 nm [138]). Friedman's high-resolution spectra for Np(III) and Np(IV) and spectra determined for Np(V) and Np(VI) by Cary6000i in cooperation with Bruce Mincher at Idaho National Laboratory are displayed in Figure 9 below.

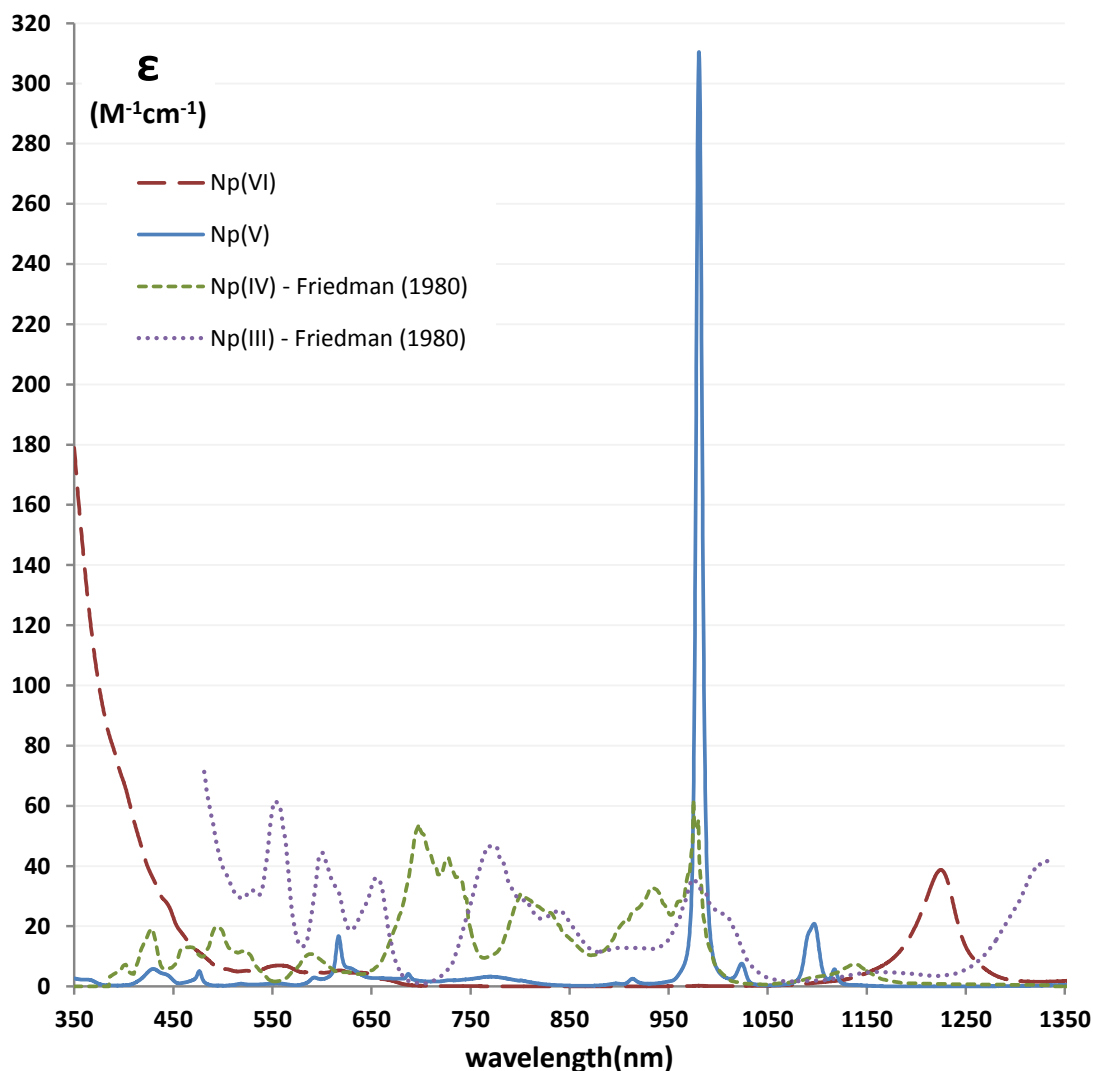


Figure 9 – Neptunium(III), (IV), (V) and (VI) absorption spectra in 4.0M aq. HNO₃ data for Np(V)+(VI) measured by Cary 6000i, data for Np(III)+(IV) from Friedman and Toth (1980) [136]

As can be seen, the spectra of the “naked” ions of Np³⁺ and Np⁴⁺ feature many different overlapping bands and peaks, primarily in the visual range, whereas the absorption of the neptunyl ions NpO₂⁺ and NpO₂²⁺ have rather isolated strong absorption peaks in the near-

infrared part of the spectrum and Np(VI) has an absorption shoulder in the UV, which is steadily increasing into shorter wavelengths. The neptunyl absorption peaks are primarily caused by excitation of molecular orbitals of the Np-O bonds with the neptunyl oxygens [139, 140]. However, exact assignment of these energy levels is complicated, because neptunium atoms have a large number of electrons and the electronic shell structure is heavily influenced by relativistic effects [141, 142, 143, 144].

The only absorption peak of practical utility for Np(V) is at 617nm and is responsible for the blue-green hue of Np(V) solutions; nonetheless, its most important absorption peak is at 980 nm and it is the most intensive in UV-Vis-NIR spectrum out of all neptunium oxidation states. The broadly accepted value of the peak molar absorption coefficient is $\epsilon(\text{Np}^{\text{V}}, 980 \text{ nm}) = 395 \pm 12 \text{ M}^{-1}\text{cm}^{-1}$ in solutions of nitric acid below approximately 2.0M [141, 145]. As can be seen from Figure 9, the value in 4M HNO₃ is close to $310 \text{ M}^{-1}\text{cm}^{-1}$, i.e. approximately by 1/4th lower. The effect of nitric acid on the absorption spectra of neptunium oxidation states has been observed by Friedman and Toth [136]. Changes of the absorption spectrum of Np⁴⁺ ions take place during the transition from 1M to 4M HNO₃ were explained on the basis of formation of nitrate complexes.; however, no explanation for Np(V) has been offered. Since the complexation of Np(V) by nitrate anions at this concentration of HNO₃ is expected to be very low, it can be hypothesized that the reason must be rather related to the change in in the water coordination environment as a result of decreasing water concentration in the 4M HNO₃ solution.

Neptunium (VI) has practical absorption features at the extremes of the available window of wavelengths in nitric acid solutions - the absorption shoulder in the UV, mentioned earlier, and a broad absorption peak with a relatively flat maximum at 1222-1225 nm. The molar absorption coefficient for this peak is $\epsilon(\text{Np}^{\text{VI}}, 1223 \text{ nm}) = 45 \text{ M}^{-1}\text{cm}^{-1}$ [146] in 1M HClO₄, spectra published in Friedman's data for the ϵ value in HNO₃, show a very similar value for 0.5M HNO₃ with a very small subsequent decrease with HNO₃ concentration increase toward 4 M, which corresponds well with the value $38 \pm 4 \text{ M}^{-1}\text{cm}^{-1}$ determined by Cary 6000i in 4M HNO₃ (see Figure 9).

In a 1974 study of Vasiliev et al. [147], the absorbance of the 1223 peak was constant and starting to only slightly decrease with the transition from 3 to 4M HNO₃, after which the consequent decrease is much more marked and the Np(VI) spectrum in near-IR is

undergoing a fundamental transformation. In 7-8M HNO₃ the 1223nm peak disappears and new absorption peak at 1140 nm emerges. These changes were satisfactorily described by NpO₂²⁺ complexation by nitrate anions [147].

Since the Np(V) 980nm peak and the Np(VI) 1223 nm peaks are not overlapping, it is easily possible to determine the concentration of the two redox species only from the single absorbance readouts at these two wavelengths. However, as an additional measure to eliminate baseline shifts, the absorbance readouts at 980 and 1223 nm were usually corrected by subtracting the absorbance at the wavelength of 1050nm, at which neither Np(V) nor Np(VI) absorb significantly (as can be seen at Figure 9).

3.2.2.4 Absorption spectra of nitrite, nitrous acid and nitric acid

Aqueous spectra of the nitrite anion and nitrous acid are well known [137]: the broad absorption band of the NO₂⁻ anion between 300 - 400 nm transforms into an overall more intensive distinct peak multiplet for molecular HNO₂. Figure 10 displays the prominent UV spectra of both nitrite and nitrous acid alongside the aqueous spectrum of the NO₃⁻ anions of the dissolved nitric acid solution. The peak molar absorptivity of the nitrate anion $\epsilon(\text{NO}_3^-, 302 \text{ nm}) = 7.4 \text{ M}^{-1}\text{s}^{-1}$ is almost ten-fold smaller than for the nitrous acid peak of $\epsilon(\text{HNO}_2, 370 \text{ nm}) = 58 \text{ M}^{-1}\text{s}^{-1}$. However, since nitric acid is usually present in relatively high concentration, the NO₃⁻ absorption in the UV-wavelengths shorter than 350 nm can easily overwhelm the available absorbance range of most spectrophotometers (already at concentrations of 0.2 - 0.4M).

The relatively high molar extinction coefficient of nitrous acid allows for the determination of fairly low concentrations of HNO₂ in solutions. At a concentration of approximately 0.05 mM the final absorbance is $A = 0.003$ that is still easily detectable in spectrophotometers of good baseline stability (such as RSM1000 and especially Cary 6000i), which can reliably quantify changes of $\Delta A = \pm 10^{-4}$. This effect has been used to check for the presence of nitrous acid in stock nitric acid solutions.

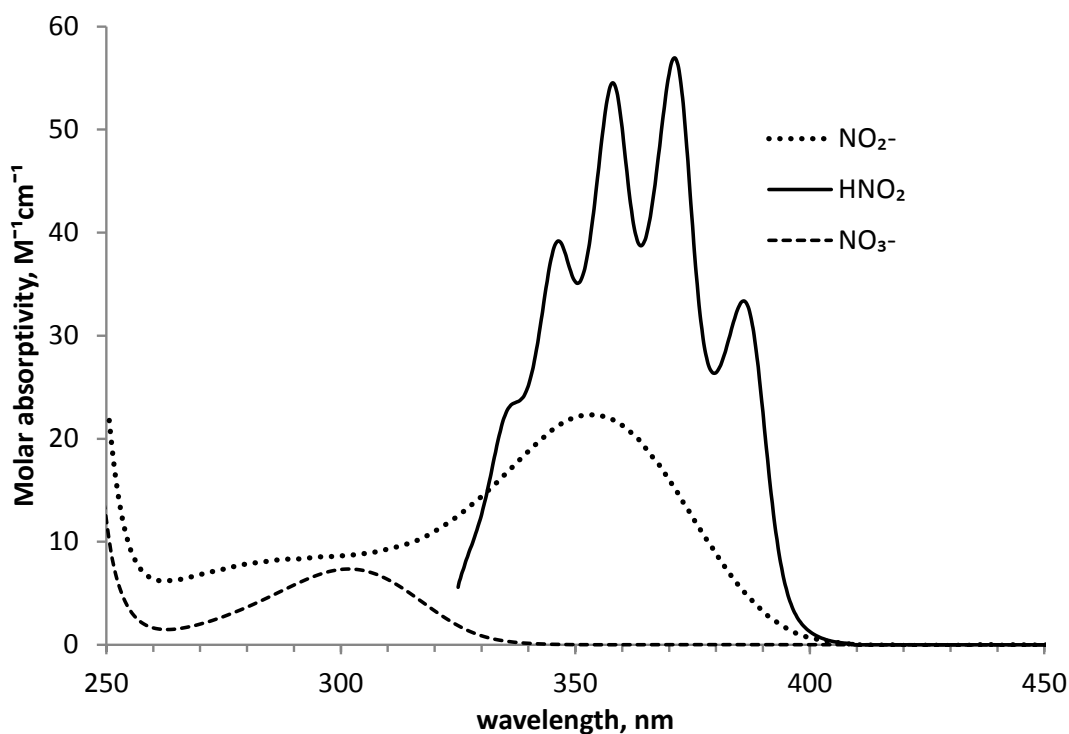


Figure 10 – Aqueous UV absorption spectra of the nitrite anion in water and of the molecular nitrous acid and of the nitrate anions in HNO₃ solution (data acquired at laboratory temperature of 21-22°C, accurate HNO₂ spectrum data below 325 nm could not be determined due to the overwhelming UV absorbance of the nitric acid solutions)

3.2.2.5 Deconvolution of overlapping spectra

When several absorbing species with overlapping spectra are present simultaneously in the solution, a simple evaluation of the particular absorption bands only at peak maxima or at several wavelengths can usually lead to erroneous results. This is especially true when the molar extinction coefficients of the absorbing species are of comparable magnitude.

Since the absorption spectra of the of HNO₂, Np^{IV}, Np^V and Np^{VI} in the UV-Vis range differ significantly (see Figure 9 and Figure 10), a better approach to simultaneously determine the concentrations of several absorbing species is a deconvolution of the spectra within a wide spectral range by applying known molar absorption coefficients ϵ_{λ} . Thus, for every spectrum analyzed, the concentrations of Np absorbing species in certain experiments were found by applying Lambert-Beer's law at 650 different wavelengths between 350 and 1000 nm. At one particular wavelength λ for cells of the thickness b the

final absorbance A_λ is a linear combination of the absorption spectra of the present compounds:

$$A_{(\lambda)} = [HNO_2] \cdot b \cdot \varepsilon_{HNO_2, \lambda} + [Np(IV)] \cdot b \cdot \varepsilon_{Np(IV), \lambda} + [Np(V)] \cdot b \cdot \varepsilon_{Np(V), \lambda} + [Np(VI)] \cdot b \cdot \varepsilon_{Np(VI), \lambda} \quad (117)$$

A generalization of equation (117) for a particular wavelength λ can be written for a system that has a number of $i = 1 \dots N$ different chemical species at concentration c_i :

$$A_\lambda = b \cdot \sum_{i=1}^N c_i \cdot \varepsilon_{i\lambda} \quad (118)$$

When the number of monitored wavelengths $\lambda = 1 \dots M$ (arbitrary scale) is much larger than N the number of species (which is quite usual), it is possible to deconvolute the absorption spectrum with known values of $\varepsilon_{i\lambda}$ by finding the N values of the concentrations c_i as parameters that will minimize the sum of squares of differences SS between the theoretical A_λ and experimental $A_{\lambda, \text{exp}}$ absorbance values, as defined by the following formula:

$$SS = \sum_{\lambda=1}^M (A_\lambda - A_{\lambda, \text{exp}})^2 = \sum_{\lambda=1}^M \left(b \cdot \sum_{i=1}^N c_i \cdot \varepsilon_{i\lambda} - A_{\lambda, \text{exp}} \right)^2 \quad (119)$$

In this work, the optimal values of c_i with a minimum of the squares of differences between the calculated and experimentally observed absorbances have been resolved using the Solver plug-in of the Microsoft Excel spreadsheet software (in versions of 2003, 2007 and 2010).

3.2.3 Experimental techniques for analysis of reaction kinetics

The study of reaction kinetics performed as part of this work has been in principle observed always by spectrophotometry, because it allowed simultaneous observation of one or multiple reacting species or their products in a non-destructive fashion. In this case always an optically transparent chemical reactor system had to be utilized. Depending on the type of the reactor and the introduction of species, the approaches can be divided into two types – approach with a classical optical cuvette for investigations of slow reactions with characteristic half-lives longer than 10 s, and an approach using a stopped-flow

apparatus for the study of reactions that were faster. Below, the two approaches are described in further detail.

3.2.3.1 Cuvette-based approach

The majority of spectrophotometric work was performed in cuvettes made of optically highly transparent materials - special optical glasses or quartz (it is important to note that for large-sample works these cells are too expensive and disposable UV-grade plastic cuvettes are available, but this was not the case in experiments performed under this work). The cuvettes were introduced into the cuvette holder of a spectrophotometer - for multi-hour reactions OLIS RSM1000 was used, for minute-long reactions OceanOptics QE65000 was utilized.

Both instruments had cuvettes holders equipped with temperature control and magnetic stirring:

- the RSM 1000 cuvette holder was part of the instrument bench and consisted of a hollowed out solid copper-alloy metal block cooled or heated by water circulating from a water bath (a Pt thermistor temperature sensor was used as a feedback control for the Julabo CF31 Cryo-Compact Circulator); magnetic stirring was performed by a small slide-in non-mechanic stirrer block based on variation of magnetic field, which was connected by a ribbon cable to an external independent controller,
- the cuvette holder for the QE65000 system was supplied Quantum Northwest and was connected to the spectrophotometer by a fiber-optic cables, temperature control was performed by Peltier-effect based cooling and resistive heating based elements in the enclosure of the holder (the Peltier cooling system necessitated the use of an unsophisticated heat exchange system based on an electric pump-circulated water from an ambient-cooled water reservoir); magnetic stirring was performed by an in-built mechanical electromagnet.

In a standard working procedure a mixing plan was calculated for the sequence of pipette-based filling of the cuvette with the desired matrix solvent (e.g. HNO₃ solution) and then additions of the reactants to achieve the desired starting concentrations. Since the volume change by the additions of the reactants was very little, baseline was usually

(but not always) acquired just prior to the last step - addition of the complementary reactant by a pipette, which would start the reaction.

With RSM1000 the progress of the kinetic experiment was observed as progressive accumulation of absorption spectra (the time necessary for taking one scan was approximately 1 minute for a 400 nm wavelength range), while on QE65000 the absorbance of few selected wavelengths was monitored.

Due to management of radioactive contamination in the case of work on kinetics of neptunium-237, special cuvettes were designated only for work with neptunium and all the liquid waste produced had to be processed and recycled in order to recover the neptunium. This complicated the work compared to studies performed with non-radioactive compounds where rinsing and procedures with the cuvettes were much simpler and faster.

3.2.3.2 Stopped-flow method

For reactions with characteristic half-lives under 10 seconds, the use of magnetically stirred cuvettes with pipetted addition of the reactant is insufficient, because the resulting reaction process will be rather controlled by the multiple second homogenization time than by the actual chemical kinetics of the reaction. A work-around for this problem was based on the utilization of the so called *stopped-flow* method, which was possible using the OLIS RSM 1000 (Rapid Scanning Monochromator) coupled with the OLIS U.S.A. Stopped-flow accessory.

In this method the reacting solutions are loaded into syringes that are connected via very thin tubing into a mixing jet. A precisely programmed piston suddenly pushes the liquid from the syringes into the mixing jet – where due to the high velocity intensive turbulent processes mix the two solutions into a homogeneous mixture. The outlet of the mixing jet is directed into a quartz flow-cell with a 2 cm pathlength to enable instantaneous observation by the 1000 Hz rapid scanning-mode of the OLIS RSM 1000. The dead-time reactant mixing in the jet and observation in the flow-cell was approximately 4 milliseconds, giving a 10 to 20 millisecond lower limit on the half-life of reactions (maximum value for a pseudo-1st order rate constant of approximately $k' = 35$ to 70 s^{-1}).

Due to the 1:1 volume mixing of the stopped-flow apparatus, the concentration of the reactants in the two syringes has to be two times of the desired reaction conditions. Before the reactions a reference spectrum solutions containing only the matrix solvent where collected and, when necessary, baseline corrections were determined.

For some experiments performed in temperatures below the 10°C experiments, a stable baseline was difficult to obtain due to water condensation formation on the exterior of the glass sample chamber. To alleviate this problem, the sample chamber enclosure was continuously purged with nitrogen gas during all experiments at 10°C.

When the reactants are loaded into the system, two empty stopped flow shots were necessary to remove any air bubbles in the tubing system that were introduced during the syring loading procedure. Subsequently, the rest of the samples in the syringes were used for the real experiment.

To give an example of experimental conditions – for rapid reactions of neptunium, where the intensive 980nm absorption peak of Np(V) was observed, the near-infrared wavelength range of the spectrophotometer was utilized by using optical gratings with 600 lines/mm and a blaze wavelength of 1000 nm, a wavelength range of approximately 140 nm was scanned with 1000 scans per second by a 0.7 nm wavelength resolution. Similar conditions were utilized for the rapid reactions of nitrous acid with H₂O₂ and AHA, apart from the region of scanning, which was between 310 and 450 nm.

Afterwards, the measured data had to be processed to reduce the collected information into a more manageable size (approximately 200 thousand absorbance data-points were acquired per second in the 1kHz scanning mode). Thereafter the information about the concentration of the species was extracted either by direct calculation of absorbance readout at an absorption peak by equation (114) or by spectral deconvolution by minimizing equation (119).

The resulting dependences of concentrations vs. reaction time were then evaluated using a kinetic model based using on numeric integration of differential rate equations, which is explained in the next section.

3.2.3.3 Analysis of kinetic data using numeric integration

Since integrated versions of differential rate laws are suitable for reaction analysis only of the simplest reactions, a part of the studies of reaction kinetic have been evaluated by a computer model, especially when the solution implied a complex set of chemical reactions.

For each analyzed species A_i a differential equation expressing the rate of the change of its concentration was used (120). The model was based upon a numeric integration of a general set of several of these differential equations using the Runge-Kutta 4th order method.

$$\frac{d[A_i]}{dt} = \sum_{m=1}^{m=M} \left(c_{im} \cdot k_m \cdot \prod_{j=1}^{j=N} [A_j]^{\alpha_{mj}} \right) \quad (120)$$

Generally, the rate of each of the M chemical reactions was modeled to be proportional to the rate constant k_m and to the product of N instantaneous concentrations of reacting species $[A_j]$ raised to a given power α_{mj} (reaction order with respect to the particular reactant A_i). The rate of change of their instantaneous concentration $[A_i]$ was then given by the sum of the effects of the m studied kinetic reactions weighed by a chemical stoichiometric coefficient c_{im} . This coefficient expressed the production (if $c_{im} > 0$), consumption (if $c_{im} < 0$) or no change ($c_{im} = 0$) of each reactant i by the reaction m .

The RK4 model then calculated the concentrations of reacting species as a function of time. For a given set of c_{im} and α_{im} (usually integers or half-integer numbers selected manually) the optimized variables were the rate constants k_m of each assumed reaction m . The predicted concentrations of the observed species were then compared to their experimentally established concentrations. Optimal values of the rate constants k_m were then acquired by using a fitting procedure by the least squares method performed by the MS Excel Solver plug-in.

A more extensive description of the utilized RK4-based kinetic model has been included in Appendix A.

3.2.4 Irradiation apparatus for radiolytic studies

Sample irradiation was performed in two almost identical Nordion GammaCell 220 irradiators^{‡‡} located in the Radiation Center of the Oregon State University and in the Materials and Fuels Complex of the Idaho National Laboratory, which utilize the cobalt-60 radionuclide ($T_{1/2} = 5.27$ years) for the source γ -rays of energy 1.332 and 1.173 MeV [148]. These irradiators are mobile (in principle, the total weight is around 4 metric tons) lead shield chambers, equipped with an elevator system for sample insertion without harmful radiation exposure to the irradiator operator. The irradiation/elevator chamber is a hollow cylinder 20.6 cm in height and 15.2 cm (in diameter [149]). The irradiation of samples is performed by lowering the elevator in the irradiation position by an automatic motor drive controlled by an integrated timer. While the OSU irradiator has a solid lead shield above the irradiation chamber, the irradiator at INL features a top access port for electrical cables or tubing. This feature has been, e.g., utilized in the attempts to measure the in-situ redox potential during radiolysis (due to several different reasons these unfortunately did not produce any data that would merit discussion in this work).

The nominal initial loading of the irradiators was around 20 000 curies (740 TBq) in initial Co-60 activity. However, due to the 5.27 year half-life, the corresponding dose rate is always dropping in time and has to be periodically re-calibrated due to non-ideal effects of the gamma-ray shielding. This calibration is usually performed using the Fricke dosimetry system [148], where an oxygenated solution of iron(II) in sulfuric acid is oxidized to iron(III) by the effect of radiation with a known radiolytic yield of $G(\text{Fe}^{3+}) = 1.56 \mu\text{mol/J}$ for this range of gamma-ray energies. The degree of oxidation of the original ferrous salt is then determined by classical chemical methods, e.g., by measuring the absorbance of Fe(III) at 303 nm ($\epsilon = 2200 \text{ M}^{-1}\text{cm}^{-1}$) [148] or by titration of the remaining Fe(II) by potassium permanganate .

During the experimentation for this work the dose rates of the Co-60 irradiator at OSU decreased from 0.45 to 0.36 kGy/h, while the dose rate variation for irradiations performed at the more recently refilled irradiator at INL were between 7.7 and 7.0 kGy/hr.

^{‡‡} The Nordion company has recently (2008) discontinued the production and refurbishing of the GammaCell 220 irradiators [216]

4 KINETICS OF OXIDATION OF PENTAVALENT NEPTUNIUM BY PENTAVALENT VANADIUM IN SOLUTIONS OF NITRIC ACID

Martin Precek and Alena Paulenova

IOP Conference Series: Materials Science and Engineering

IOP Publishing Ltd

Temple Circus

Temple Way

Bristol BS1 6HG

United Kingdom

Manuscript published on May 17, 2010 as part of the
Proceedings of 8th International Conference on Actinide Science ACTINIDES 2009,
July 12-17, 2009 in San Francisco, California, USA

IOP Conference Series: Materials Science and Engineering (2010) **9** (1) 012074

doi:10.1088/1757-899X/9/1/012074

ISSN 1757-8981 (Print)

ISSN 1757-899X (Online)

4.1 Abstract

Management of the oxidation state of neptunium in the reprocessing of spent nuclear fuel by solvent extraction is very important. The kinetics of the oxidation of neptunium(V) by vanadium(V) in solutions of nitrate acid was investigated at constant ionic strength 4M. The reaction rate is first order with respect to Np(V) and V(V). The effects of proton concentration on the apparent second order rate constant k_1'' was determined as $k_1'' = (0.99 \pm 0.03) \cdot [H^+]^{1.21} \text{ M}^{-1} \text{ s}^{-1}$ for temperature 25°C. Activation parameters associated with the overall reaction have been calculated; the standard reaction enthalpy and entropy were $52.6 \pm 0.9 \text{ kJ/mol}$ and $-55.8 \pm 0.9 \text{ J/K/mol}$ respectively.

4.2 Introduction

The PUREX separation technology for reprocessing of spent nuclear fuel based on extraction of hexavalent and tetravalent actinides with n-tributylphosphate (TBP) from their solutions in nitric acid is the most mature radiochemical process, established almost six decades ago. However, the extraction of neptunium is still of a special interest, since this actinide has rich redox chemistry among other f-elements. In order to optimize the balance of neptunium in separation processes the management of the oxidation state of neptunium is very important for the PUREX process and processes developed for PUREX raffinates (e.g. TRUEX) or group-extraction mixtures, such as the merged TRUEX-TALSPEAK.

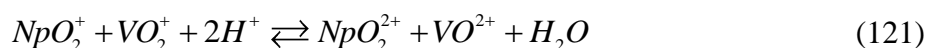
The pentavalent neptunium exists in aqueous solutions as a dioxocation neptunyl (NpO_2^+) that has an effective cationic charge only $z_{\text{eff}} = +2.2$ and is practically inextractable; whereas the extractability of tetravalent Np^{4+} ($z_{\text{eff}} = +4$) and hexavalent NpO_2^{2+} ($z_{\text{eff}} = +3.2$) species is quite good [27]. Since the extractability of Pu(VI) is lower than for Pu(IV), finding conditions for selective oxidation of Np(V) where Pu(IV) is not affected are important.

It was reported in the earlier literature that the pentavalent vanadium (VO_2^+) has been successfully utilized as an oxidizing agent for NpO_2^+ in extraction processes [106, 107, 108]. Pu(IV) oxidization by V(V) either occurs very slow or does not take place at all [106]. Oxidation of Np(V) does occur also by the oxidizing effect of nitric acid in its very concentrated solutions, but its kinetics is much slower compared to the $\text{Np(V)} + \text{V(V)}$

reaction; the same is also true for the kinetics of disproportionation of Np(V) into Np(IV) and Np(VI) [17].

This chapter presents the results of a deeper study on kinetics of the oxidation of Np(V) by V(V) in aqueous solutions of HNO₃. The values of approximate reduction potential considered for this reaction system are very similar: 1.0 V for VO₂⁺/VO²⁺, 1.15 V for NpO₂²⁺/NpO₂⁺ and 1.1 V for PuO₂²⁺/Pu⁴⁺ [106]. The differences in the oxidation kinetics of Np(V) and Pu(IV) are influenced by kinetic factors rather than by thermodynamic factors – i.e. the oxidation of Np(V) is much faster than the oxidation of Pu(IV) due to the necessity of the kinetically slow formation of oxygen double bonds in the plutonyl species O=Pu=O of Pu(V) and Pu(VI) [28].

The reduction potentials indicate that the studied redox reaction is reversible as the generated Np(VI) is reduced back to Np(V) by V(IV):



Therefore, the kinetics of the oxidation reaction stated by equation (121) can be described [106, 113] by the following two rate equations for the forward (79) and backward (80) reactions:

$$-\frac{d[Np(V)]}{dt} = k_1'' \cdot [Np(V)]^\alpha \cdot [V(V)]^\beta \quad (122) \quad + \frac{d[Np(V)]}{dt} = k_2'' \cdot [Np(VI)]^\gamma \cdot [V(IV)]^\delta \quad (123)$$

where the Greek symbols are the reaction orders, and k_1'' and k_2'' are the apparent rate constants for the forward and backward reactions, respectively. The values of the apparent rate constants are functions of the hydrogen ion concentration, ionic strength and the temperature of the solution.

The only data on kinetics of this oxidation reaction in nitric acid were estimated by Dukes [106] using an extraction method with TBP. Assuming that the hexavalent Np is the only extracted species and, hence, it can be isolated from Np(V), the reaction rate was measured using a method of periodical sampling of the aqueous phase, which was the reacting mixture of Np and V in nitric acid, and detection by radiometric counting. The decrease of neptunium concentration in the aqueous phase indicated the fraction of Np(V) oxidized to Np(VI). The individual reaction orders in equation (121) with respect to Np(V), V(V), Np(VI) and V(IV) were determined to be equal to one [106, 113]; hence, both the forward and backward reaction were found to obey second order kinetics.

However, the value of the apparent second order rate constant k_1'' and its dependence on acidity reported by Dukes [106] for the oxidation of Np(V) in solutions of nitric acid is substantially different from the data on the oxidation of Np(V) in solutions of perchloric acid measured by VIS-NIR spectrophotometry by Koltunov et al. [113]. In order to clarify the observed discrepancies between previously published data, the oxidation kinetics of the studied reaction was investigated experimentally using VIS-NIR spectrophotometry.

4.3 Experimental

4.3.1 Reagents

Ammonium Metavanadate (99.995%, Alfa Aesar), Lithium Nitrate (99%, anhydrous, Alfa Aesar), Nitric Acid (68%, J.T.Baker), nitric acid solution of ^{237}Np purified by solvent extraction and anion exchange were used (oxidation state checked by VIS-NIR spectrophotometry), distilled and deionized water (Barnstead, 18 M Ω ·cm resistivity) was used for all experiments.

4.3.2 Measurement

The current experiments were performed in a 1 cm cuvette thermostated to 25.0°C ($\pm 0.01^\circ\text{C}$) in a flow-through thermostat. OLISTM RSM-1000 monochromator was used for determination of concentration and speciation of redox states of neptunium by establishing the differences in absorbances at 980 nm (Np(V) absorption peak, $\epsilon = 395 \text{ M}^{-1}\text{cm}^{-1}$ [64]) and 1225 nm (Np(VI) absorption peak, $\epsilon = 45 \text{ M}^{-1}\text{cm}^{-1}$ [64]) in the stock solution of neptunium and kinetic measurements were performed using OceanOpticsTM QE65000 UV-VIS-NIR Spectrophotometer. The solution in the cuvette was continuously stirred with a small magnetic stir bar; therefore, the desired initial concentrations of the reactants in the cuvette were achieved in several seconds after injection of a calculated solution of V(V) to a prepared solution of Np(V) in the cuvette. The track of the reaction was monitored in 1 second intervals by recording the absorbance at 980 nm where the spectrum of NpO_2^+ has a maximum. The background noise and the influence of initial turbulences created by mixing during the first several seconds of the reaction were observed at a side wave-length of 950 nm, at which neither

of the involved reactants (Np(V), Np(VI), V(V), V(IV)) has a significant absorption coefficient. Subtracting the absorbance at 950 nm from absorbance at 980 nm allowed observing the reaction during the mixing period.

4.4 Results and discussion

4.4.1 Analysis of kinetic data

The decrease of Np(V) concentration over time was calculated from the experimental absorbance data, and the absolute value of the negative change of the NpO_2^+ concentration was investigated as a function of time, initial concentrations, acidity and temperature of the solutions. With the aim to verify the reaction orders versus the reactants and preliminary estimate the rate constant, the Np(V) oxidation rate data were evaluated by the method of initial rates. The method was applied by making a linear fit of the reaction curve on the points representing the first 10% of the total reaction extent toward equilibrium as it is shown in Figure 11 [32].

Because the method of initial rates uses a limited number of experimental points, it has a high error due to the relatively high signal noise compared to the absolute changes of absorption. Therefore, k_1 was determined also numerically, by fitting practically all experimental data collected while the redox system was moving toward the equilibrium. Once a proper form of the rate law is established, this approach is considered to be a more reliable approach for calculating the rate constant than using the method of initial rates.

The model employed is a solution of the differential equation resulting from the combined effect of both the forward (oxidation) and the backward (reduction) reactions on the change of concentration of Np(V). The selected reaction extent denoted as x is defined as:

$$\frac{dx}{dt} = -\frac{d[\text{Np(V)}]}{dt} \quad (124)$$

with boundary condition $x = 0$ at $t = 0$. The rate expression is formulated from the combination of the equations (79) and (80) using first order with respect to each of the immediate concentrations of reactants as in equation (125).

$$\frac{dx}{dt} = k_1'' \cdot [Np(V)] \cdot [V(V)] - k_2'' \cdot [Np(VI)] \cdot [V(IV)] \quad (125)$$

Substituting the known initial analytical concentrations $c_{Np(V)}$, $c_{V(V)}$, and $c_{Np(VI)}$ (in the same order) of Np(V), V(V) and Np(VI) at the beginning of the reaction and the observed reaction extent x for the immediate concentrations, the equation (5) can be rewritten as:

$$\frac{dx}{dt} = k_1'' \cdot (c_{Np(V)} - x) \cdot (c_{V(V)} - x) - k_2'' \cdot (c_{Np(VI)} + x) \cdot x \quad (126)$$

where the initial concentration of vanadium-IV is considered equal to zero, thus $[V(IV)] = x$. The backward reaction rate constant k_2'' is as a linear function of the fitting parameter k_1'' using the known negative change of concentration of Np(V) at the equilibrium (equilibrium reaction extent, x_E). At equilibrium the forward and backward reaction rates are both equal and the rate of the change is zero ($dx/dt = 0$). These conditions lead to:

$$k_2'' = k_1'' \cdot K' = k_1'' \cdot \frac{(c_{Np(V)} - x_E) \cdot (c_{V(V)} - x_E)}{(c_{Np(VI)} + x_E) \cdot x_E} \quad (127)$$

The symbol K' represents the apparent equilibrium constant of the redox reaction (8) going in the opposite direction than the reaction (121), i.e., the reduction of Np(VI) by V(IV):



The apparent equilibrium constant K' does not reflect the involvement of H^+ ions in the equilibrium described by equation (121) and is therefore obviously dependent on the proton concentration in the solution. K' is also dependent on ionic strength and temperature, but independent on the concentrations of the reactants and the products in the studied range.

The determination of the value of k_1'' is based on fitting of a numerical model of the reaction. The model was implemented as a numerical solution (integration) of the differential equation (126) by the Runge-Kutta fourth-order (RK4) method [150] in *Microsoft Office Excel 2003* software. The best fit was found using its *Solver* plug-in on the fitting parameter k_1'' .

4.4.2 Effect of concentration of Np(V) and V(V)

Both the observed reaction rate of the Np(V) oxidation and the equilibrium reaction extent increase with increased initial concentration of the oxidizer, pentavalent vanadium. Figure 11 displays this effect for three different initial concentrations of V(V) and a constant initial concentration of Np(V) in 4M HNO₃ at 25°C. The solid tangent line to the curve for 3.60 mM V(V) visualizes the initial rate of the reaction. The dashed curves in this figure were calculated by the least squares method fitting of the experimental points by the numerical model based on the rate expression formulated by equation (125) for the 2nd order reversible process. The individual reaction orders with respect to both Np(V) and V(V) were found from the log-log dependence of the initial oxidation rates in 4 M HNO₃ at 25°C against the variation of reactant concentrations; see Figure 12.

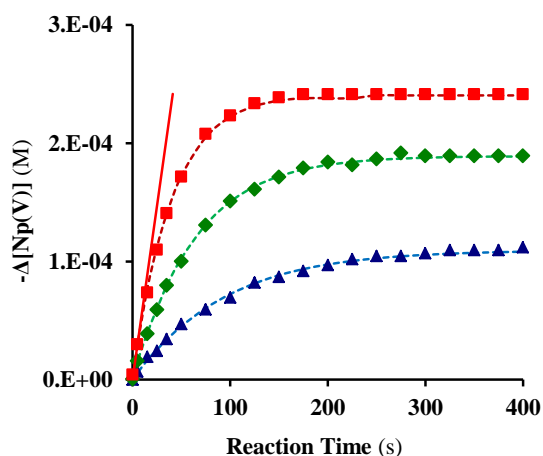


Figure 11 - Effect of the initial concentration of V(V) on reaction rate and equilibrium

$C_{V(V)}$: ▲ = 0.72 mM, ◆ = 1.80 mM, ■ = 3.60 mM

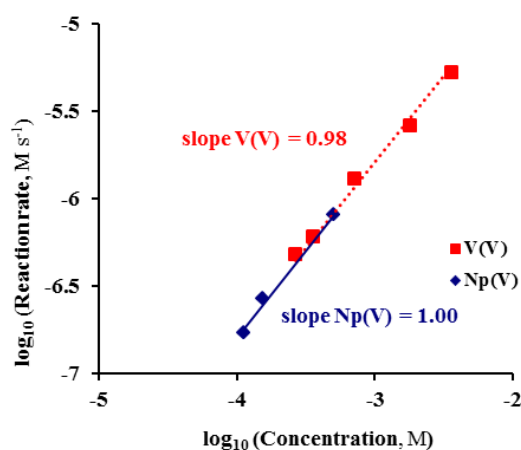


Figure 12 - Determination of reaction order with respect to concentration of Np(V) and V(V)

◆ : $C_{V(V)} = 0.375$ mM, $C_{Np(V)} = (0.113-0.504)$ mM
 ■ : $C_{Np(V)} = 0.360$ mM, $C_{V(V)} = (0.266-6.91)$ mM

4.4.3 Effect of hydrogen ion concentration

In order to observe the influence of the hydrogen ion concentration on the apparent rate constants k_1'' and k_2'' and the apparent equilibrium constant K' , the kinetic experiments were performed with a set of aqueous solution, where the concentration of nitric acid has been varied from 0.5 M to 4 M HNO₃, while maintaining the total ionic strength of solutions of 4M by addition of LiNO₃ as a background salt, see Figure 13 and Figure 14. The experimental points of initial oxidation rates were plotted against the numerical

product of the initial concentrations of the reactants $c_{\text{Np(V)}} \cdot c_{\text{V(V)}}$. A linear fit of the new data-points confirms the linearity of the reactions according to equation (79) in the conditions of lower acidity (see Figure 13). The slope of each linear fit represents an estimate of the value of the apparent rate constant of the forward reaction k_1'' . The effect of the hydrogen ion concentration on the apparent equilibrium constant K' is presented in Figure 14. All hydrogen ion concentrations were corrected for incomplete dissociation of the nitric acid by applying dissociation constant $\text{p}K_a = -1.44$ and ionic strength corrections ($\gamma_{\pm} = 1.15$) [151].

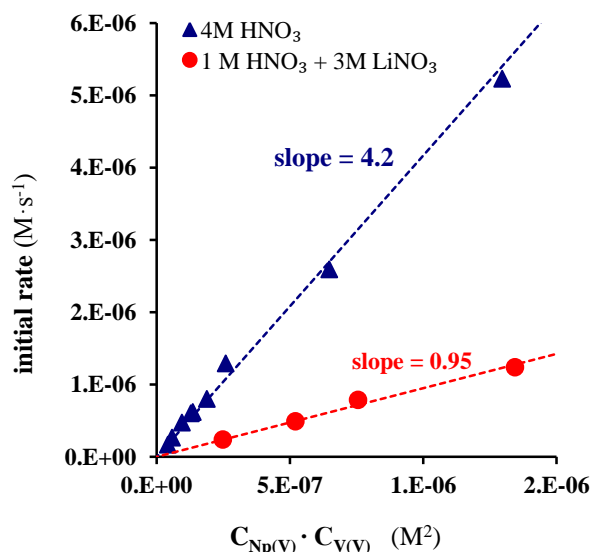


Figure 13 - Comparison of initial rates of oxidation of Np(V) by V(V) between reactions in solutions of 1M HNO₃ + 3 M LiNO₃ and in 4M HNO₃ (t = 25 °C)

The dependence of both the apparent rate constant k_1'' and the apparent equilibrium constant K' on the proton concentration are displayed in Figure 14. As can be seen, the linear slope of k'' determining the order of the apparent rate on the proton concentration, is to be of 1.21, i.e. close to first order. Then the apparent second order rate constant can be expressed in the form of $k_1'' = \{(0.99 \pm 0.03) \times [H^+]^{1.21}\} \text{ M}^{-1}\text{s}^{-1}$, where the uncertainty range is of one standard deviation. Because the reliability of the value of the nitric acid dissociation constant is limited, and so is the true hydrogen ion concentration, formulating this relation using the analytical concentration of nitric acid c_{HNO_3} is more practical: $k_1'' = \{(0.93 \pm 0.04) \times c_{\text{HNO}_3}^{1.14}\} \text{ M}^{-1}\text{s}^{-1}$.

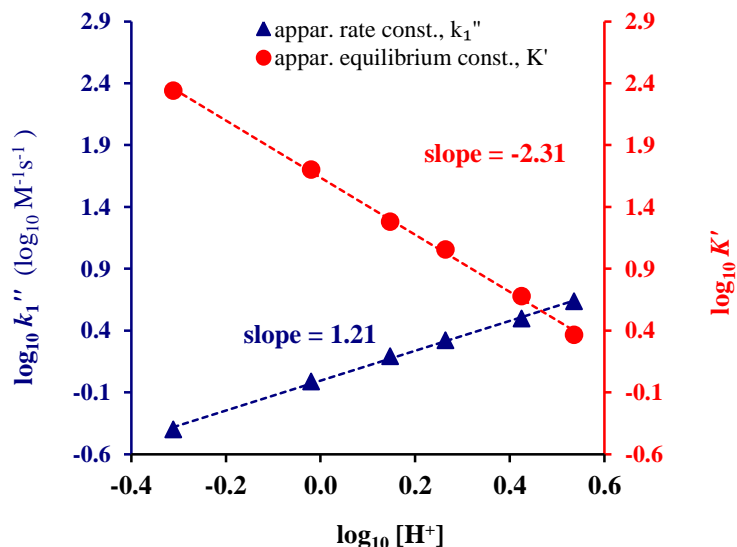


Figure 14 - Effect of the molar concentration of H⁺ on the apparent rate constant k_1'' and the apparent equilibrium constant K'

$t=25^\circ\text{C}$ and $\mu=4\text{M}$ (H/LiNO₃)

Values of the kinetic constant measured for the kinetics of Np(V) oxidation by V(V) by E.H. Dukes [106] and V.S. Koltunov [113] are considerably different, and they also differ in the dependence of the reaction on the concentration of hydrogen ions.

E.H. Dukes has measured the reaction rate in nitrate environment, which represents better the conditions of liquid-liquid extraction processes developed for treatment of nuclear fuel. His findings for the Np(V) oxidation rate constant by vanadium can be presented by the quadratic function $k_1'' = \{(0.195 \pm 0.042) \times [H^+]^2\} \text{ M}^{-1}\text{s}^{-1}$ [106], while Koltunov, who investigated this reaction in the non-complexing perchlorate media, reported the apparent second order constant as a linear function on hydrogen ion concentration: $k_1'' = \{(1.97 \pm 0.17) \times [H^+]\} \text{ M}^{-1}\text{s}^{-1}$ [113]. However, fitting Koltunov's published data with a power law gives $k_1'' = \{(1.89 \pm 0.08) \times [H^+]^{1.20}\} \text{ M}^{-1}\text{s}^{-1}$, which provides a value of the order of dependence on hydrogen ions that is very close to the order identified in the present study.

According to other authors [152, 153], pentavalent vanadium hydrolyzes in acidic solutions, forming species such as VO_2^+ , $\text{VO}(\text{OH})^{2+}$ and VO^{3+} that may form nitrate complexes. Further explanation of the quantitative dependence of the reaction rate on

acidity in nitrate environment is thus hindered by insufficient experimental data on vanadium complexation with nitrates at this moment.

4.4.4 Effect of temperature on the rate of oxidation of Np(V) by V(V)

Both forward and backward reaction rates are strongly dependent on temperature. Their thermal activation has been examined in 4M HNO₃ in temperature range 10-50°C in Figure 15.

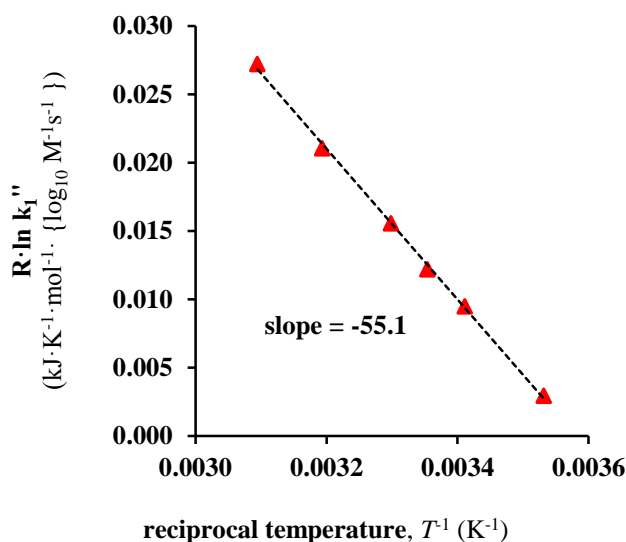


Figure 15 - Determination of activation energy of oxidation of Np(V) by V(V) (0.270 mM Np(V) and 2.375 mM V(V) in 4 M HNO₃)

The dependence of the apparent reaction rate constant k_1'' was evaluated according to the Arrhenius equation (78) in order to recover the activation energies E_A [32]:

$$\ln k_1'' = \frac{-E_A}{R \cdot T} + \ln A \quad (129)$$

$$k_1'' = \frac{k_B T}{h} \cdot e^{\frac{-\Delta G^\ddagger}{RT}} = \frac{k_B T}{h} \cdot e^{\frac{\Delta S^\ddagger}{R}} \cdot e^{\frac{-\Delta H^\ddagger}{RT}} = e \cdot \frac{k_B T}{h} \cdot e^{\frac{\Delta S^\ddagger}{R}} \cdot e^{\frac{-E_A}{RT}} \quad (130)$$

where A is the pre-exponential factor, $R=8.314 \text{ J} \cdot \text{K}^{-1} \cdot \text{mol}^{-1}$ is the universal gas constant and T is the absolute temperature in kelvins. Applying a modified Eyring equation (130) ($k_B = 1.38 \times 10^{-23} \text{ J K}^{-1}$ is the Boltzmann constant and $h = 6.63 \times 10^{-34} \text{ J s}$ is the Planck constant) for standard temperature $T = 298.15 \text{ K} = 25^\circ \text{C}$ provides the standard Gibbs energy, entropy and enthalpy of activation: ΔG^\ddagger , ΔS^\ddagger and ΔH^\ddagger [32].

The obtained results are summarized and compared to previous data on the reaction activation thermodynamics reported by Koltunov for Np in perchloric acid [113] and by

Dukes [106] for nitric acid in Table 7. Similarity between the measured parameters indicates that the activated complex of the reaction is probably the same in both the perchloric and nitrate media.

Table 7 -Comparison of standard (25°C) thermodynamic values for thermal activation at of the reaction Np(V) + V(V) with published literary data

<i>Data source</i>	E_A <i>kJ/mol</i>	ΔH^\ddagger <i>kJ/mol</i>	ΔS^\ddagger <i>J/K·mol</i>	ΔG^\ddagger <i>kJ/mol</i>
Present study, 10-50°C, 4M HNO ₃	55.1 ± 0.9 ^a	52.6 ± 0.9 ^a	-55.8 ± 0.9 ^a	69.3 ± 1.0 ^a
Koltunov, 25.5-45.8°C, 4M HClO ₄ [113]	55.7 ± 6.3	53.2 ± 6.3	-58.7 ± 21.0	71.4 ± 0.2 ^b
Dukes, 24-50°C, 2M HNO ₃ [106]	49.4 ± 12.3	N/A	N/A	N/A

^a The standard errors of ΔH^\ddagger and ΔS^\ddagger were calculated from the relative standard errors of the estimates of slope and intercept [154], respectively, of the linear regression of the Arrhenius plot in Figure 5. As the Gibbs energy of activation is calculated from both ΔH^\ddagger and ΔS^\ddagger , the relative standard error of ΔG^\ddagger was calculated on the basis of rules on error propagation.

^b The magnitude of the error of Koltunov's ΔG^\ddagger appears inconsistent with values and errors of ΔS^\ddagger and ΔH^\ddagger . The original published values and errors of free energy of activation, activation enthalpy and entropy were $\Delta F^\ddagger = 17.04 \pm 0.05$ kcal/mol, $\Delta H^\ddagger = 12.7 \pm 1.5$ kcal/mol and $\Delta S^\ddagger = -14 \pm 5$ e.u, respectively.

4.5 Conclusion

The utilization of pentavalent vanadium as a selective oxidizing agent for neptunium(V) in the treatment of spent nuclear fuel is of high interest. The apparent rate constant of the oxidation of Np(V) by V(V) was measured for a wide range (0.5-4M) of acidity in nitrate medium. The first reaction order with respect to both reactants neptunium(V) and vanadium(V) was confirmed. The dependence of the reaction rate on hydrogen ion concentration was quantified as being close to first order, which is similar to results reported for perchlorate medium. On the contrary, the previous results for nitric acid indicated a second order dependence on hydrogen ion concentration. The evaluation of thermal activation parameters also suggests that the reaction mechanism in nitric acid is identical to the reaction in perchloric acid.

5 KINETICS OF REDUCTION OF HEXAVALENT NEPTUNIUM BY NITROUS ACID IN SOLUTIONS OF NITRIC ACID

Martin Precek and Alena Paulenova

Journal of Radioanalytical and Nuclear Chemistry
Akadémiai Kiadó Zrt.
H-1519 Budapest, Pf. 245
Hungary

Manuscript published on 19 August 2010 as part of the Proceedings of the 16th Radiochemical Conference, April 18-13, 2010 in Mariánské Lázně, Czech Republic in:
Journal of Radioanalytical and Nuclear Chemistry (2010) vol. 286, no.3, p. 771–776
doi:10.1007/s10967-010-0724-0
ISSN: 0236-5731 (print version)
ISSN: 1588-2780 (electronic version)

5.1 Abstract

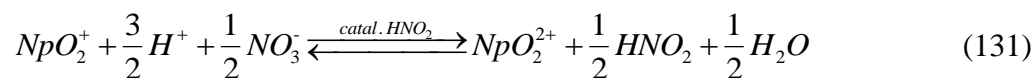
Nitrous acid is a key redox controlling factor, affecting the speciation of neptunium in the reprocessing of used nuclear fuel by solvent extraction. The kinetics of the reduction of neptunium(VI) by nitrous acid in solutions of nitric acid was investigated spectrophotometrically by the method of initial rates. The reaction is of first order with respect to Np(VI) while the order with respect to HNO_2 is 1.20 ± 0.04 . The reaction rate is almost inversely proportional to the hydrogen ion concentration (reaction order -0.92 ± 0.06), indicating that the reaction proceeds primarily through the reaction of neptunium(VI) with the nitrate anion. The experimental value of the rate constant k for the rate law $-\text{d}[\text{Np(VI)}]/\text{dt} = k \cdot [\text{Np(VI)}] \cdot [\text{HNO}_2]^{1.2}/[\text{H}^+]$ is of $(0.159 \pm 0.014) \text{ M}^{-0.2} \text{ s}^{-1}$ in $I = 4 \text{ M}$ and at 20°C . The activation energy is $(-57.3 \pm 1.6) \text{ kJ/mol}$, which is in agreement with previous data on this reaction in perchloric acid.

5.2 Introduction

Extraction of hexavalent and tetravalent actinides with tributyl phosphate (TBP) from nitric acid solutions is the most widely used industrial process for the reprocessing of used nuclear fuel (UNF) and is the basis for the development of advanced reprocessing schemes like UREX and TRUEX. An unresolved issue of UNF reprocessing is the management of neptunium in the extraction system because of its not clearly defined redox speciation. Neptunium is present in both pentavalent (V) and hexavalent (VI) oxidation states that differ greatly in their extractability to the organic phase (hexavalent state being very well extracted by TBP, whereas pentavalent neptunium is almost not extracted). As a result, neptunium is distributed in both organic and aqueous streams of the separation process.

Nitrous acid, the key redox controlling factor, is always present in these systems, as it forms during the dissolution of UNF and by the radiolysis of nitric acid. Low linear energy transfer radiation like β and γ have radiation yields of HNO_2 around 0.25 mM/kGy in 1 M HNO_3 , and the radiation yields of α particles are approximately two times lower [155]. Nitrous acid HNO_2 is relatively well extracted by TBP ($\log D \approx 1$) and is therefore distributed from the source raffinate solution into further stages of the separation system [72]. The influence of nitrous acid on the redox state of neptunium is

complex. If HNO_2 is present in a small concentration, it primarily acts as a catalyst of the oxidation of Np(V) by nitric acid. This reaction is an autocatalytic process, as additional HNO_2 is produced. However, if neptunium is initially present primarily in the hexavalent state, large concentrations of HNO_2 lead to reduction back to the pentavalent state. Both reactions are governed by an acidity-dependent equilibrium:



The reaction equilibrium can be characterized by an apparent equilibrium constant K_{app} from measured concentrations of Np(VI), Np(V), nitric acid and nitrous acid in equilibrium:

$$K_{app} = \frac{[\text{Np(VI)}][\text{HNO}_2]^{1/2}}{[\text{Np(V)}][\text{HNO}_3]^2} \quad (132)$$

The constant and its dependence on ionic strength, acidity and temperature has been measured by many authors [31, 49, 50, 51, 53] and its value varies between $K_{app} = 3 \times 10^{-4} - 2 \times 10^{-3}$. Some of the authors have also investigated the kinetics of oxidation of Np(V) by HNO_3 [31, 49, 50, 55]. Both spectrophotometry and solvent extraction methods have been employed. The analysis of the system proved to be quite complex and the reported forms of the rate law and its associated rate constants vary greatly among the authors.

The rapid reduction of Np(VI) to Np(V) by the addition of nitrite to solutions of 1M HNO_3 was observed already during the initial studies on the redox properties of neptunium performed during the Manhattan Project by Magnusson et al.[77] Since then, the kinetics of reduction of Np(VI) by HNO_2 has attracted just a little interest. To our best knowledge, only two in-depth studies about this issue have been undertaken [156, 157].

Shilin and Nazarov [156] studied the Np(VI) reduction kinetics in the nitric acid/nitrate system in an excess of HNO_2 as an apparent first order reaction with respect to the concentration of Np(VI). However, their original proceeding paper is not available, and all information about their results was adopted from a secondary reference, a review paper by Koltunov and Marchenko [54].

A comparative study between the rates of oxidation of HNO_2 by Np(VI) and Am(VI) in a non-complexing perchlorate system has been analyzed by a spectrophotometric stopped-flow method by Woods et al. [157]. These researchers have utilized both first and second order kinetic relations to describe the progress of the reaction. Differences between the activation energy values and dependencies of the reaction rate on the concentration of HNO_2 and hydrogen ion reported in these two studies are discussed below. In order to clarify these discrepancies, the kinetics of the studied oxidation reaction was investigated using UV-VIS-NIR spectrophotometry.

5.3 Experimental

5.3.1 Chemicals

Distilled deionized water (Barnstead Nanopure, 18 $\text{M}\Omega\cdot\text{cm}$ resistivity) was used in all experiments. 68% nitric acid (EMD Chemicals GR ACS grade) was used for preparation of HNO_3 stock solutions. The concentration of the nitric acid stock solution was determined to $\pm 0.3\%$ precision by titration using sodium hydroxide standardized by potassium hydrogen phthalate (Analytical Reagent, Mallinckrodt). Solutions of lithium nitrate (Alfa Aesar, anhydrous, 99.999% pure - metals basis) in distilled water were used in experiments to control ionic strength. Stock solutions of sodium nitrite NaNO_2 (Mallinckrodt, analytical reagent) were dissolved in neutral distilled water and used as a source of nitrite anions.

5.3.2 Neptunium

^{237}Np ($t_{1/2} = 2.1 \times 10^6$ y) was received as NpO_2 from Argonne National Laboratory and dissolved in a slight molar excess of H_2O_2 and 8 M HNO_3 . The tetravalent oxidation state was confirmed using Vis-NIR spectroscopy. In order to remove any transuranic impurities, the Np solution was added to a prepared BioRad AG-1 anion exchange column. The column was rinsed with a solution of 8 M HNO_3 , 0.3 M hydrazine monohydrate, and 2 g/L hydroquinone. Np was stripped from the column using 0.36 M HCl and its isotopic purity was confirmed using thin-window HPGe gamma spectrometry. Any organic impurities were destroyed by concentrated nitric acid and hydrogen peroxide. After re-evaporation with nitric acid, an approximate 15mM stock

solution of the purified neptunium was prepared in 4 M HNO₃. The solution had its oxidation state adjusted in a glass H-cell by electrolysis on a Pt wire electrode at potential +1.3V vs. reference Ag/AgCl electrode. The electrochemical process was controlled by a BASi Epsilon™ e2 potentiostat. Following the electrolysis, more than 95% of Np existed in the +VI oxidation state (the remainder was in the +V state).

5.3.3 Instrumentation

Absorption spectrophotometry in an open-air 1 cm path-length quartz cuvette was performed using two spectrophotometer instruments.

Near-infrared spectroscopy over a 900-1300 nm range was performed using an Olis® RSM 1000 Monochromator equipped with a double grating (600 lines/mm, 1 μm blaze wavelength), an 800 nm high-pass filter, two InGaAs (sample and reference) detectors and a 300W tungsten halogen light source. A full spectral scan was collected over a 1 minute period; however, in this mode the instrument was not appropriate for the subsequent kinetic experiments, whose timescale was only a few minutes.

A wide UV-VIS-NIR range of 200-1000 nm was monitored by an OceanOptics™ QE65000 spectrophotometer (fiber optic system) with combined deuterium/halogen light source DH-2000 BAL. As opposed to the RSM 1000, the diode-array detector of the QE65000 spectrophotometer permitted the recording of absorbance on all selected wavelength within the 200-1000 nm range simultaneously. To minimize noise, an integration interval of up to 5 seconds was employed for each absorbance measurement. The temperature of cuvette holder used during the kinetic experiments was controlled to ± 0.02°C (Quantum Northwest). To assure a homogenous solution during the reactions, a magnetic stirrer was used to mix the contents of the cuvette.

Full spectral scans recorded before and after each experimental run were taken by both instruments. The spectra were then fitted to a digitized reference spectra published for 0.1 – 4.0 M HNO₃ solutions by Friedman et al.[136] in order to determine the quantitative redox speciation of neptunium between Np(V) and Np(VI). The characteristic peaks at wavelengths 980nm for Np(V) and 1220 nm for Np(VI) were primarily observed. No absorption peaks characteristic of Np(IV) were observed during any experiments.

5.3.4 Observation of the kinetic progress

During kinetic experiments, the liquid content of the quartz cuvette was continuously stirred with a small magnetic stir bar; therefore, the desired initial concentrations of the reactants in the cuvette were achieved in several seconds after addition of a calculated volume of a NaNO_2 solution to the solution of Np(VI) prepared in the cuvette. The extent of the reaction was monitored in 1 or 5 second intervals by recording the absorbance at 980 nm where the spectrum of Np(V) has a maximum (the molar absorption coefficient value of Np(V) at 980nm is $\epsilon = 395 \text{ M}^{-1}\text{cm}^{-1}$ [64]).

The baseline noise and the influence of initial turbulences, created by mixing during the first several seconds of the reaction, were observed at a side wave-length of 950 nm, at which none of the involved species (Np(V) , Np(VI) , HNO_2) have a significant absorption coefficient. Subtracting the absorbance at 950 nm from absorbance at 980 nm allowed observing the reaction during the mixing period. The rate of the reaction can be calculated from the change in the absorbance A at 980 nm as follows:

$$\frac{d[\text{Np(V)}]}{dt} = -\frac{d[\text{Np(VI)}]}{dt} = \frac{1}{\epsilon} \cdot \frac{dA}{dt} \quad (133)$$

5.3.5 Nitrous acid instability

The setup of the experiments and their analysis was complicated by the instability of nitrous acid in solutions exposed to air. The solution of HNO_2 was prepared by a direct addition of a spike of concentrated stock aqueous solution of sodium nitrite in the nitric acid solutions. Because HNO_2 is a relatively weak acid, almost all nitrite was immediately protonated. A decrease of the HNO_2 concentration was observed by monitoring its absorption peaks in the 340-400 nm UV region in a stirred cuvette. A characteristic half-life of the HNO_2 in acidic solutions was quantified to be approximately 1 hour. The NaNO_2 stock solution in distilled water was stable, which was regularly checked by UV spectrophotometry. The decomposition rate of nitrite in acid decreased significantly when the top of solutions in cuvette was protected [129] with a thin layer of a pure n-dodecane; however, this practice wasn't eventually adopted as the regeneration of neptunium after the experiment became exceedingly complicated.

Due to the short time available for assuming a quasi-stable concentration of excess amounts of HNO_2 , the kinetic analysis was eventually performed through the method of initial reaction rates, as opposed to both studies by Shilin et al.[156] and Woods et al.[157] who assumed an apparent reversible first order kinetics for processing the data.

5.3.6 Data analysis

The initial rate of the Np(VI) reduction was calculated from the slope of a least squares linear regression through the first 10% of data points for the reaction extent. Replicate experiments were not performed due to limited amount of neptunium stock solution; however, the reaction rate uncertainties were estimated to account for a 10% uncertainty range which is indicated by the error bars in all figures. The influence of this uncertainty was taken in account in the estimation of uncertainty for slopes of dependencies on log-log plots. Rate constants have their uncertainty estimated by a single standard deviation.

5.4 Results and discussion

5.4.1 Determination of reaction orders with respect to Np(VI) and HNO_2

Both the observed reaction rate of the Np(VI) reduction and the equilibrium reaction extent increased with increasing initial concentration of the reducing agent, nitrous acid. The individual reaction orders with respect to both Np(VI) and HNO_2 were found from the slope of the log-log dependence of the initial reduction rates against the variation of reactant concentrations; see Figure 16.

The slope for the system with the varied initial concentration of Np(VI) was determined to be 1.04 ± 0.21 , which indicates that the order with respect to Np(VI) is most likely to be one (as expected). However, the order of reaction with respect to HNO_2 was 1.20 ± 0.04 , which is higher than 1.00 with a high degree of certainty.

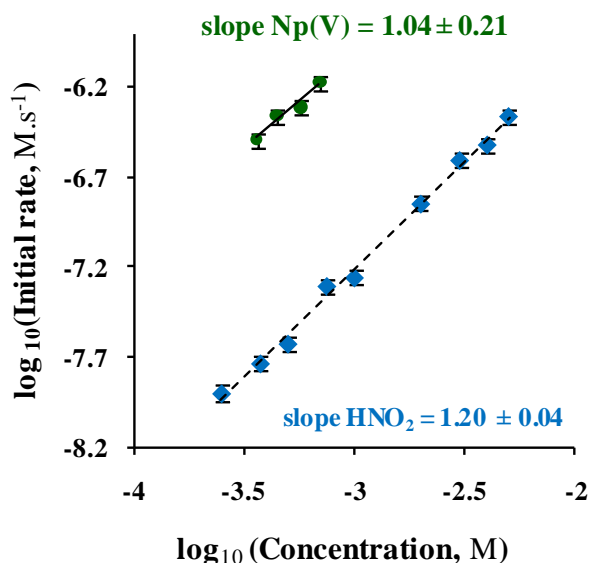


Figure 16- Determination of reaction orders with respect to initial concentration of Np(VI) and HNO₂

initial conditions: 4 M HNO₃, t = 20.0°C;

● C_{HNO₂} = 5.0 mM, C_{Np(VI)} = 0.36-0.70 mM; ◆ C_{Np(VI)} = 0.44 mM, C_{HNO₂} = 0.25 - 5.0 mM

5.4.2 Effect of H⁺ concentration and ionic strength

In order to observe the influence of the hydrogen ion concentration on the initial rate, the kinetic experiments were performed with a set of aqueous solutions, where the concentration of nitric acid varied from 0.75 M to 4 M HNO₃, while maintaining the total ionic strength of solutions of $\mu = 4$ M by the addition of LiNO₃ as a background salt, see Figure 17. The initial rate significantly decreases with increasing nitric acid concentration. The slope of the dependence of the initial rate on the analytical concentration of HNO₃ is equal to -0.92 ± 0.06 . Actual concentrations of hydrogen ions were calculated considering the incomplete dissociation of the nitric acid in its concentrated solutions. The value of the apparent dissociation constant $pK_a' = -1.41$ determined for 4 M nitric acid [158] was used in the calculations, assuming that it doesn't change significantly under the constant 4 M ionic strength conditions. The correction on incomplete dissociation led to H⁺ concentrations smaller by 12-13% than the analytical concentration of the nitric acid, but had no effect on the value of the slope (Figure 17).

Therefore, the rate was found to be approximately inversely proportional to the hydrogen ion concentration.

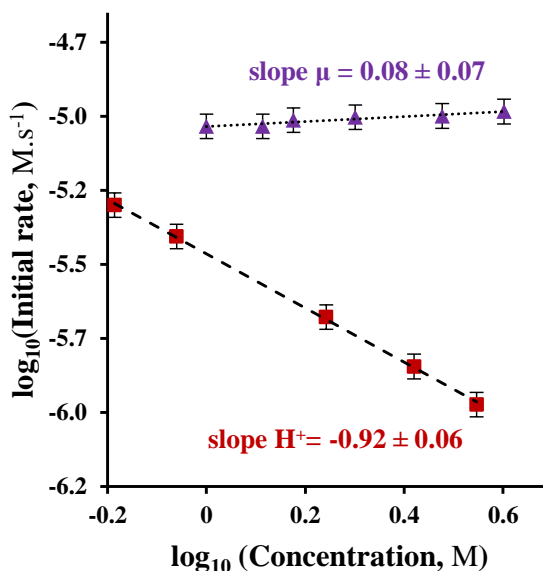


Figure 17 - Effect of the molar concentration of hydrogen ions H^+ and ionic strength μ on the initial reaction rate

initial conditions: $t = 25.0^\circ\text{C}$,

■ - effect of H^+ : $C_{\text{HNO}_2} = 5.0 \text{ mM}$, $C_{\text{Np(VI)}} = 0.90 \text{ mM}$, $\mu = 4 \text{ M (Li/H)NO}_3$

▲ - effect of μ : $C_{\text{HNO}_2} = 6.0 \text{ mM}$, $C_{\text{Np(VI)}} = 0.60 \text{ mM}$, $1 \text{ M HNO}_3 + 0.3 \text{ M LiNO}_3$

As opposed to the effect of H^+ concentration, no significant dependence of the initial rate was observed when the ionic strength μ (total nitrate concentration) was varied at a constant HNO_3 concentration of 1 M (Figure 17).

5.4.3 Discussion on the form of the rate law

The current investigation arrived at the following form of the apparent experimental form of the rate equation:

$$-\frac{d[\text{Np(VI)}]}{dt} = k^* \frac{[\text{Np(VI)}][\text{HNO}_2]^{1.2}}{[\text{H}^+]} \quad (134)$$

As calculated from the initial rate data for $T = 20^\circ\text{C}$ and $\mu = 4 \text{ M}$, the value of the apparent rate constant is $k^* = (0.159 \pm 0.014) \text{ M}^{-0.2}\text{s}^{-1}$. These findings are in approximate agreement with the previous results of Shilin and Nazarov [156] who have determined that the reaction orders with respect to Np(VI) were 1 and with respect to HNO_2 were

somewhere between 1.0 and 1.5. The reaction order with respect to the HNO_3 concentration was -0.85. This is in close proximity to the value determined presently.

Shilin and Nazarov proposed that the reverse reaction (39) proceeds via two pathways in which there are two direct species responsible for the reduction of Np(VI) [54]. The first is the nitrite ion NO_2^- produced by dissociation of nitrous acid (its concentration is therefore inversely proportional to the $[\text{H}^+]$ concentration). The second reductant is nitric oxide created by the disproportionation of HNO_2 :



The mechanism of the reaction can then be expressed by the following scheme:



Equations (136) and (137) are the rate limiting steps. The resulting form of the rate law then has two terms dependent on HNO_2 :

$$-\frac{d[\text{Np(VI)}]}{dt} = [\text{Np(VI)}] \left(k_1 \frac{[\text{HNO}_2]}{[\text{H}^+]} + k_2 \frac{[\text{HNO}_2]^{1.5}}{[\text{H}^+]^{0.5}[\text{NO}_3^-]^{0.5}} \right) \quad (139)$$

The values of the constants k_1 and k_2 were reported by Shilin and Nazarov as 0.97 s^{-1} and $15.5 \text{ M}^{-0.5} \text{ s}^{-1}$, respectively [54].

By modifying equation (139) for the case of the initial rate observation:

$$\frac{\left(-\frac{d[\text{Np(VI)}]}{dt} \right)_{\text{init}}}{[\text{Np(VI)}][\text{HNO}_2][\text{H}^+]^{-1}} = \left(k_1 + k_2 \frac{[\text{H}^+]^{0.5}}{[\text{NO}_3^-]^{0.5}} [\text{HNO}_2]^{0.5} \right) \quad (140)$$

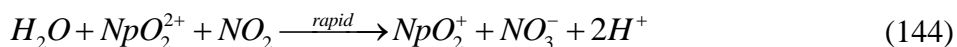
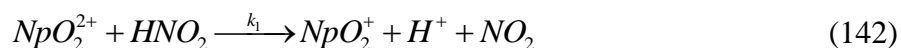
and plotting the left hand side against the variable initial concentration parameter $[\text{H}^+]^{0.5}[\text{NO}_3^-]^{-0.5}[\text{HNO}_2]^{0.5}$, the constants k_1 and k_2 can be obtained as an intercept and a slope of the resulting plot. In the case of the non-integer dependence of the reaction rate on the HNO_2 concentration, fitting our data by equation (140) yielded the values of constants $k_1 = (0.30 \pm 0.04) \text{ s}^{-1}$ and $k_2 = (5.60 \pm 0.81) \text{ M}^{-0.5} \text{ s}^{-1}$. This is in general agreement with the identified experimental rate law (134). However, plotting the data in the same manner for the dependence of the initial reaction rate on $[\text{H}^+]$ in a constant

nitrate concentration didn't provide constants with the same values. In the present investigation, no significant dependence on the nitrate concentration was identified (Figure 17); the particular form of the dependence of the second term on H^+ and NO_3^- is the most probable reason.

On the contrary, for Np(VI) reduction by nitrous acid in perchlorate medium of lower concentrations (0.1 - 1.0 M $HClO_4/NaClO_4$), Woods et al. [157] reported first order reaction with respect to both reactants. For the rate dependence on the H^+ concentration they have identified the rate law to be of a different form:

$$-\frac{d[Np(VI)]}{dt} = [Np(VI)][HNO_2] \left(k_1 + \frac{k_2}{[H^+]} \right) \quad (141)$$

The values of the second order constants were $k_1 = 2.01 \pm 0.45 \text{ M}^{-1}\text{s}^{-1}$ and $k_2 = 1.56 \pm 0.07 \text{ s}^{-1}$ for 25°C and 1 M ionic strength. The authors have proposed a mechanism plausible with this equation:



where reactions (142) and (143) are the rate limiting steps.

In the present study, the reaction order with respect to the concentration of HNO_2 has been found to be greater than 1. Also, no term independent on H^+ concentration has been identified in the rate equation (4). Therefore, it is most likely that in a nitrate environment, the direct reaction (12) of the HNO_2 molecule with Np(VI) is either not possible or very slow.

5.4.4 Effect of temperature

The initial reaction rates are strongly dependent on temperature. Their thermal activation has been examined in 4 M HNO_3 in a temperature range of $10-40^\circ\text{C}$. Under the same initial reactant concentrations the initial rate would be proportional only to the change of rate constant(s). Therefore, the dependence of the initial rate was evaluated by an

equation derived from the Arrhenius equation in order to determine the activation energy E_A :

$$R \cdot \ln \left(-\frac{d[Np(VI)]}{dt} \right)_{init.} = -\frac{E_A}{T} + const. \quad (145)$$

where $R = 8.314 \text{ J} \cdot \text{K}^{-1} \cdot \text{mol}^{-1}$ is the universal gas constant and T is the absolute temperature in kelvins. From the slope of the data points plotted in Figure 18 the activation energy was determined as $E_A = (57.3 \pm 1.6) \text{ kJ/mol}$. This is in slight disagreement with Shilin et al. [10] who reported that activation energy is $(62.0 \pm 1.3) \text{ kJ/mol}$.

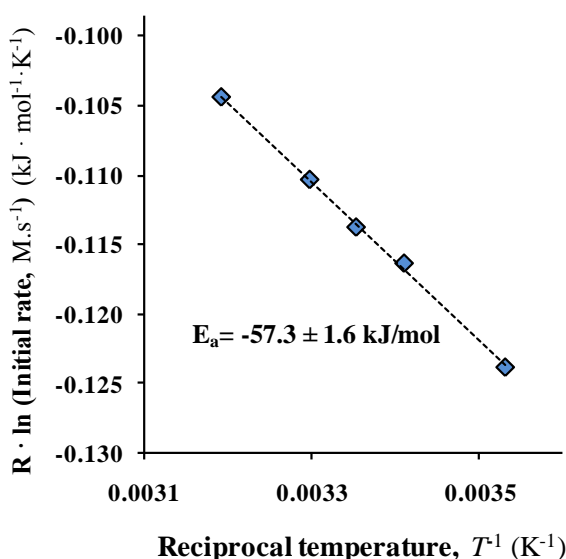


Figure 18 - Determination of activation energy of reduction of Np(VI) by HNO_2
initial conditions: $t = 10.0 - 40.0^\circ\text{C}$, $C_{\text{HNO}_2} = 6.0 \text{ mM}$, $C_{\text{Np(VI)}} = 0.60 \text{ mM}$, 4 M HNO_3 ,
errors of rate determination are smaller than the symbols

However, Woods et al. [157] have calculated activation energies of $(51.5 \pm 2.4) \text{ kJ/mol}$ and $(70.0 \pm 4.4) \text{ kJ/mol}$ for 1 M perchlorate system for the $[\text{H}^+]$ -independent and $[\text{H}^+]$ -inversely dependent rate constants k_1 and k_2 (141), respectively. Interestingly, using the data of Woods et al. with the assumption that $[\text{H}^+] = 1.0 \text{ M}$, the effective value of activation energy calculated from the temperature variation of an observed second order rate constant k_{obs} in the rate law:

$$-\frac{d[Np(VI)]}{dt} = k_{obs}[Np(VI)][\text{HNO}_2] \quad (146)$$

in perchlorate medium would be (57.9 ± 2.0) kJ/mol, which is in very good agreement with the value for nitrate medium reported in the present paper.

5.5 Conclusion

For the reduction of Np(VI) by nitrous acid in a nitrate medium, the results of the present investigations of the reaction orders with respect to concentrations of Np(VI), HNO_2 and H^+ agree reasonably well with the previous investigations in the nitrate environment [156]. However, a significant difference was determined in the exact form of the rate law. As opposed to previous findings, no notable dependence on the NO_3^- concentration was observed. The currently determined value of the activation energy is slightly different, but agrees well with the apparent value determined for the reaction in 1 M HClO_4 environment [157].

6 KINETICS OF REDUCTION OF HEXAVALENT NEPTUNIUM BY ACETOHYDROXAMIC ACID IN SOLUTIONS OF NITRIC ACID

6.1 Introduction

The kinetics of the reduction of Np(VI) by acetohydroxamic acid (AHA, formula $\text{CH}_3\text{CO-NHOH}$) has been already discussed in some detail in the literature review (section 2.4.8.2). The reaction was identified to closely follow an overall 2nd order process (1st order in both reactants), with rate constants in the perchloric acid (HClO_4) being significantly higher than kinetic analysis made by Chung et al. in the nitric acid (HNO_3) environment [95]. Also, differences were observed in stoichiometry when AHA is in lack and in excess, but the exact stoichiometry has not been quantified, and the effects of acidity, ionic strength and thermal activation were not investigated.

The rate law of the reaction has been previously investigated by Brent Matteson (with some help of the present author) in the perchloric acid system and the results have been published in 2010 [97], also some very early results were obtained at the time, confirming a similar rate law in nitric acid system have also been collected [159].

Since the past investigations did not cover the temperature and acidity dependence of the reaction, a deeper study of the reaction of Np(VI) (in the form of neptunyl NpO_2^{2+}) with AHA in the more process-like nitric acid system has been warranted.

6.2 Experimental details

The study has been performed using near-infrared (NIR) spectroscopy with the OLIS RSM 1000 double grating rapid scanning monochromator equipped with a stopped-flow accessory for on-line analysis of the fast reactions. For stoichiometry, well known absorption spectra of Np(V) (absorption peak at 980nm, $\epsilon = 395 \text{ M}^{-1}\text{cm}^{-1}$) and Np(VI) (peak at 1225nm, $\epsilon = 45 \text{ M}^{-1}\text{cm}^{-1}$) were utilized for determination of neptunium redox speciation. Coulometric electrolysis on a Pt-electrode and spectrophotometric titration with hydroquinone (this reaction has a well-defined stoichiometry $2\text{Np(VI)} : 1\text{H}_2\text{Q}$ [127]) were employed to prepare, quantify its concentration and confirm that the Np stock in the 2M HNO_3 solution matrix was in 99.5% hexavalent state.

6.3 Stoichiometry of the reaction of Np(VI) with acetohydroxamic acid (AHA) in nitric acid

The stoichiometry of the reaction was investigated by performing a spectrophotometric titration in a 1 cm cuvette with neptunium(VI) as titrant on a sample with an AHA aliquot and another titration with using AHA as titrant for a given Np(VI) aliquot. In the first case, small 10.0 μL droplets of 20mM Np(VI) in 2M HNO_3 were added to initially an excess of AHA (1mM AHA in water), followed by thorough mixing of the liquid sample using a plastic transfer pipette. The rise of neptunium(V) concentration was observed at its 980nm peak until the point of equivalence, after which the slope of the absorbance decreased, but did not level off. This is explained by a possible slow reduction of the increasing excess of Np(VI) with reactive products of AHA oxidation left in the solution after all AHA has quantitatively reacted [97].

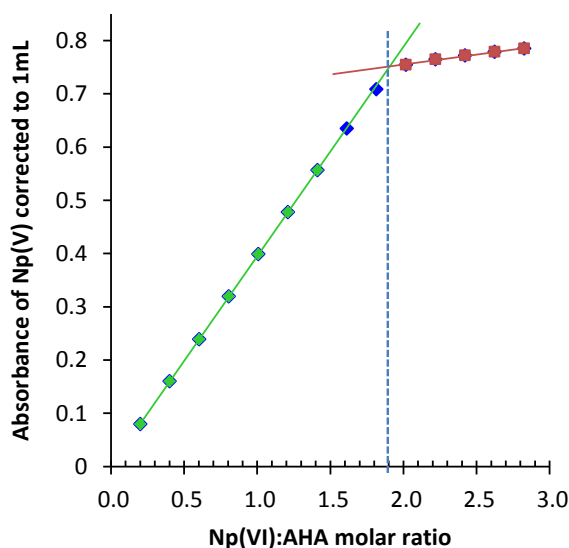
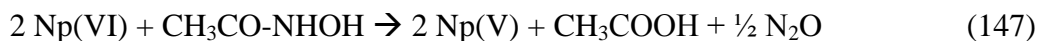


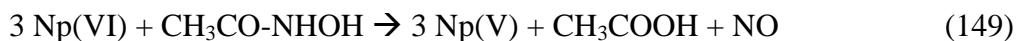
Figure 19 - Determination of the stoichiometry of the Np(VI) + AHA reaction in conditions with excess AHA.

Titration of initially 1mM AHA in 0.9mL of water by a solution of 20.4 mM Np(VI) in 2M HNO_3 ; temperature = 22°C

The stoichiometric ratio of Np(VI) : AHA in excess of AHA was 1.9 (see Figure 19), which is close to the expected 2 Np(VI) : 1 AHA stoichiometry. The dominant reaction likely leads to a product containing a nitrogen atom in an oxidation state of (+I), whereas the hydroxylamine group in AHA has a nitrogen in the (-I) oxidation state. Besides acetic acid, the likely products are therefore nitrous oxide or hyponitrous acid:



As has been mentioned earlier (section 2.2.1.3), the formal redox potential for the Np(VI)/Np(V) couple in acid is $E^{\circ} = +1.137 \text{ V}$ [29], which gives Np(VI) the role of a powerful oxidizer in most reactions. The much lower value of the standard potential for reduction of nitric oxide ($\text{N}^{\text{II}}\text{O}$) to hyponitrous acid in acidic environment $E^{\circ}(\text{N}^{\text{II}}\text{O}/\text{H}_2\text{N}_2\text{O}_2) = +0.71 \text{ V}$ vs. SHE [25] suggests that hyponitrous acid may still act as a reducing agent in conditions where significant fractions are still present in the hexavalent state. However, this reaction is much slower than the reaction of Np(VI) with AHA. This might explain the result of the second spectrophotometric titration, in which 1.1mM Np(VI) was titrated by small additions of 2.5mM AHA, as the equivalence point indicates (Figure 20) that the stoichiometry AHA : Np(VI) was equal to 0.30, i.e. Np(VI) : AHA = 3.3, which is slightly higher, but close to the 3 Np(VI) : 1 AHA stoichiometry. In that case the overall reaction might be expressed as:



The additional 10% reduction might be explained by further oxidation of NO to HNO_2 ($E^{\circ} = +0.99\text{V}$) [25], but that is less certain.

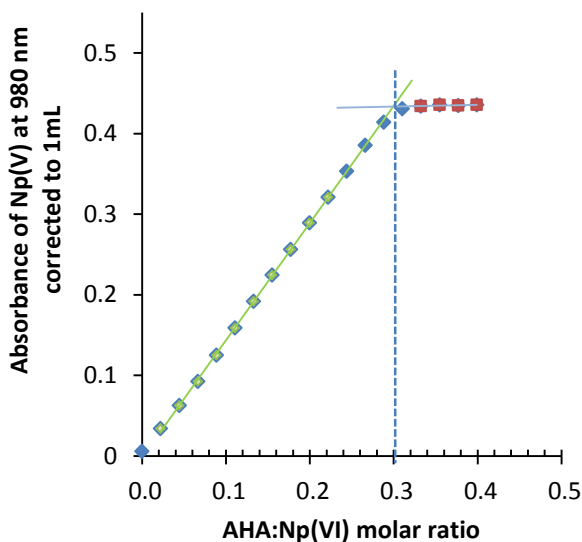


Figure 20 - Determination of the stoichiometry of the Np(VI) + AHA reaction in conditions of excess Np(VI).

Titration of initially 1.1 mM Np(VI) in 0.9mL of 0.2M HNO_3 by a solution of 2.5 mM AHA in water; temperature = 22°C

6.4 Analysis of the kinetics of the Np(VI) + AHA reaction in HNO₃

The primary purpose for utilization of AHA in process conditions is to reduce and complex plutonium [42], which is present in one order higher quantities than neptunium[2]; therefore, AHA is most likely to be present always in excess to Np(VI) and the investigation of the kinetics of the Np(VI) + AHA reaction was therefore performed in these systems. Previous investigation of the reactions with excess Np(VI) in perchloric acid show that the progress of the reaction was more complicated, consisting of a fast and a slow process [97].

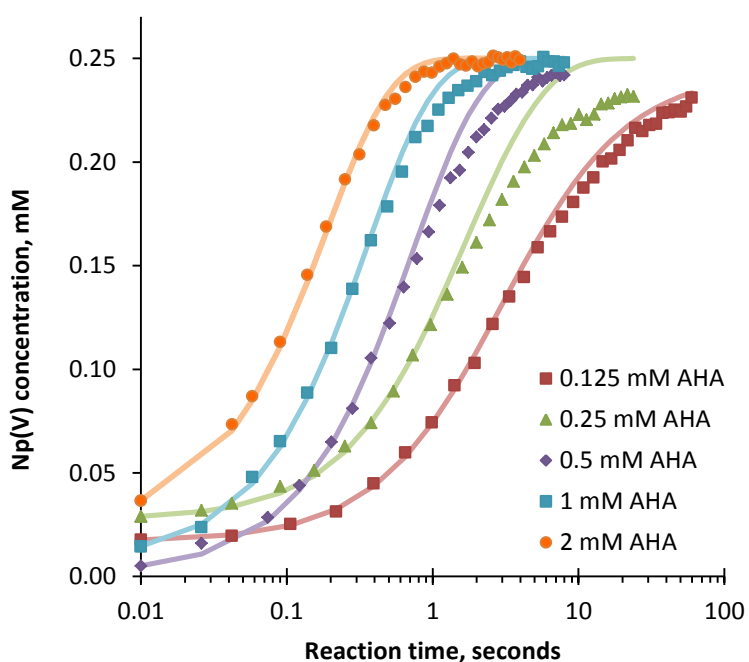


Figure 21 – Fitting of the kinetic data of the reactions of Np(VI) with AHA by a second-order rate law
initial conditions: 0.25mM Np(VI), 0.125 -2.0 mM AHA, 1.0 M HNO₃, t = 10°C;
symbols - experimental data, lines – RK4 kinetic model

Reactions with varying ratio of initial concentrations of AHA to Np(VI) were performed. In Figure 21, Curves of Np(V) concentration derived from recorded stopped-flow experimental data are plotted against reaction time and fitted through the first 50% of the reaction extent by a numeric integration of the assumed 2nd order reaction rate law (using the RK4 numeric method mentioned in previous reports):

$$-\frac{d[\text{Np(VI)}]}{dt} = 2 \times \left(-\frac{d[\text{AHA}]}{dt} \right) = +\frac{d[\text{Np(V)}]}{dt} = k'' [\text{Np(VI)}][\text{AHA}] \quad (150)$$

Although the proposed rate law qualitatively describes the reaction, quantitative data (rate constant values) agree only for the first major part of the reaction extent (>50%). Especially at low AHA:Np ratios, after the majority of Np(VI) has been reduced to Np(V), the rate of reaction significantly slows down. As yet, it is hard to deduce what kind of effect is responsible for this behavior. Multiple explanations including production of oxidizing intermediate products or catalytic inhibitors would need to be investigated to elucidate the observations. Nonetheless, fitting of the first half of the reaction data for the 10°C temperature in 1.0 M HNO₃ resulted in a very consistent 2nd order rate constant: $k'' = 2870 \pm 100 \text{ M}^{-1}\text{s}^{-1}$.

This results value is in significant disagreement with the value ($k'' = 191.2 \pm 11.2 \text{ M}^{-1}\cdot\text{s}^{-1}$) reported by Chung and Lee [95], for the same 1M HNO₃ system, but at an even warmer temperature of 22°C. However, the new value compares very well with the value of $k''_{\text{FHA}} = 1170 \text{ M}^{-1}\text{s}^{-1}$ determined by the stopped-flow method by Colston et al. in 2M HNO₃ for the similar reaction of Np(VI) with formohydroxamic acid (FHA) at the temperature of 22°C [96] The source of this discrepancy is most likely the inadequate mixing system utilized by Chung and Lee [95], consisting of a stirred 1cm cuvette. Since the characteristic reaction times are on the order of 1 second, the observed reaction rates must have been influenced by the multiple-second mixing time of their apparatus, in contrast to the 4 millisecond mixing time of the OLIS stopped-flow system.

Further investigation revealed that the reaction rate was decreasing with increasing nitric acid concentration in the reacting solution - an inverse first order dependence of the reaction rate on the concentration of nitric acid was found (Figure 22). In order to distinguish between the effects of hydrogen ion and nitrate ion (ionic strength) two experimental sets were prepared. In the first, the effect of increasing the nitrate concentration (as NaNO₃) was studied while keeping constant nitric acid concentration, the second the effect of H⁺ ion concentration in solution with constant nitrate concentration (maintained by nitric acid and sodium nitrate).

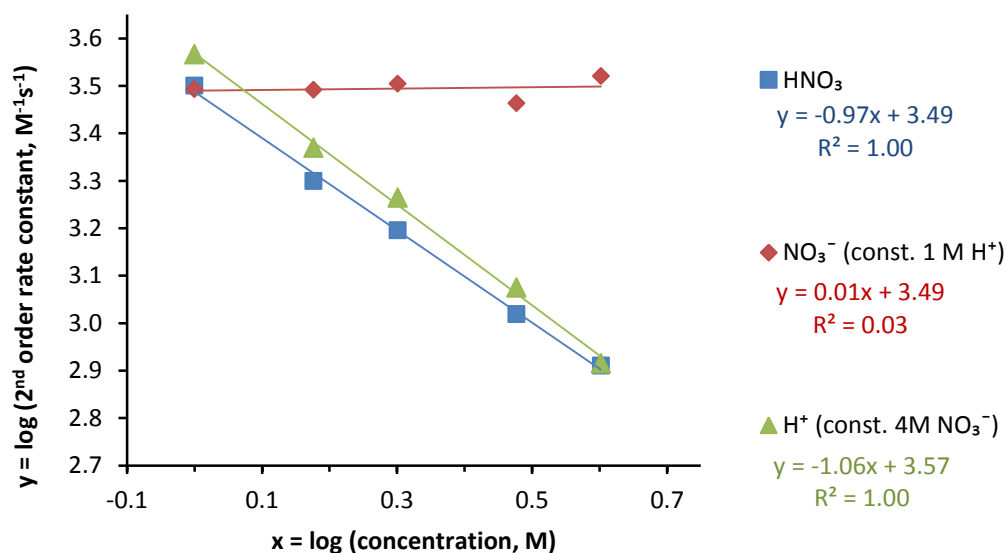


Figure 22 – Identification of the role of H⁺ and NO₃⁻ ion in the effect of nitric acid on the reaction rate of Np(VI) by AHA.

Rate constant dependence on the concentration of nitric acid (1-4 M HNO₃, blue squares), total nitrate (as 0-3 M NaNO₃ with 1M HNO₃, red diamonds) and hydrogen ion (1-4 M HNO₃, 4M (H+Na)NO₃, green triangles) was studied. Temperature was kept at 10°C

The findings and their comparison with the hydrogen ion dependence (presented in Figure 22) confirm that the primary responsible on the effect of HNO₃ on the reaction rate is the hydrogen ion. Slopes of dependence of logarithm of the rate constant on the logarithm of H⁺ and HNO₃ are both very close to 1, while the concentration of sodium nitrate did not have almost any effect on the rate of the reaction. These results confirm the expectations of both Chung et al. [95] and Colston et al. [96], based on the previous experience with the reaction of Np(VI) with hydroxylamine (NH₃OH⁺) [86] and its derivatives measured by Koltunov et al. [73]

The most likely explanation is that the reaction is primarily a result of the reaction of the dissociated acetohydroxamate anion CH₃CONHO⁻. The dissociation constant of acetohydroxamic acid (pK_a=9.31)[160] indicates that only a very small concentration of acetohydroxamate is present in solutions of multi-molar acidity and this concentration is approximately inversely proportional to the acidity in the 1-4 M HNO₃ solutions.

As a result of the studies, it is possible to summarize the final rate equation for the reaction of Np(VI) with AHA in nitric acid as:

$$-\frac{d[Np(VI)]}{dt} = k' \cdot \frac{[Np(VI)][AHA]}{[H^+]} \quad (151)$$

The value of the apparent first order rate constant k' is very sensitive to temperature and its value changes from approximately $(2870 \pm 100) \text{ s}^{-1}$ at 10°C to $(10500 \pm 400) \text{ s}^{-1}$ at 25°C in 1M HNO_3 . The dependence of the rate constant with changing temperature (Figure 23) between $5 - 45^\circ\text{C}$ has provided the thermal activation parameters of the reaction, summarized in Table 1.

Table 1 – Activation energy and parameters of thermal activation according to the activated complex theory for the Np(VI)+AHA reaction.

E_a (kJ/mol)	ΔH^\ddagger (kJ/mol)	ΔS^\ddagger (J/K/mol)	ΔG^\ddagger (kJ/mol)
59.5 ± 0.9	57.0 ± 0.9	23.2 ± 0.3	50.1 ± 0.9

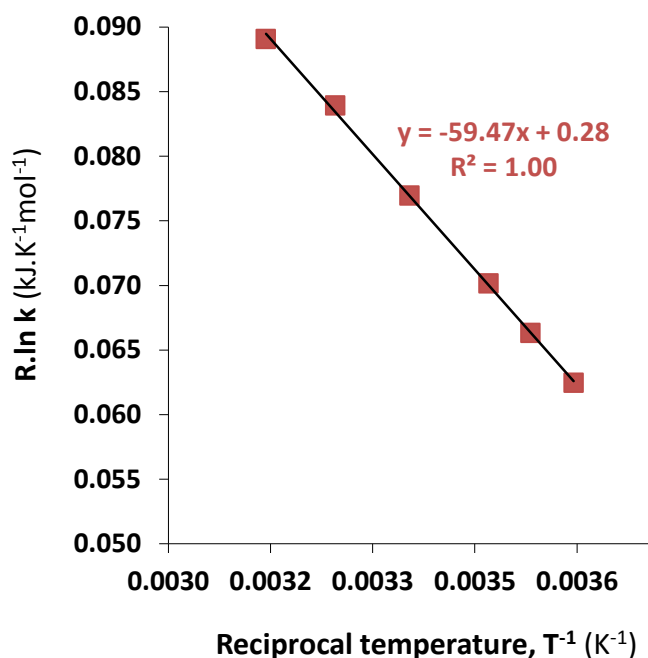


Figure 23 – Determination of the activation energy of the reaction of Np(VI) with an excess of AHA.

Initial reactant concentrations: 0.25mM Np(VI) and 4mM AHA in 1M HNO₃.

The positive activation entropy value indicates a dissociative rate determining process, which has a significantly lowered activation energy barrier compared to the reaction of Np(VI) with hydroxylamine ($E_{a,NH_2OH} = 82 \text{ kJ/mol}$ [86]), which contributes to the 4-orders of magnitude difference in reaction velocity between AHA and NH_2OH .

6.5 Conclusion

The investigation of the reaction of Np(VI) with AHA in nitric acid solutions revealed that the Np(VI):AHA stoichiometry changes from 2:1 to 3:1, depending on whether AHA or Np(VI) is in excess, respectively.

In conditions of excess of AHA, the reaction was studied using the stopped-flow method and it was found to follow an apparent overall second order rate law, while the reaction rates were found to be considerably faster than previously measured by Chung and Lee using a stirred-cuvette system [95]. The value of the apparent 2nd order rate constant for the reaction was determined in 1 M HNO₃ to be $k''_{\text{AHA}, 25^\circ\text{C}} = 1.05 \times 10^4 \text{ M}^{-1}\text{s}^{-1}$, which is approximately 4-times larger than the rate constant for the reaction of Np(VI) with formohydroxamic acid $k''_{\text{FHA}, 22^\circ\text{C}} = 2.4 \times 10^3 \text{ M}^{-1}\text{s}^{-1}$ determined by the stopped-flow method by Colston et al. [96].

An inverse first-order hydrogen ion dependence was found for the apparent rate constant k''_{AHA} , in agreement with results of kinetic studies performed by Koltunov et al. [73] with other hydroxylamine derivatives. The value of the activation energy of the reduction of Np(VI) by AHA ($E_{a,\text{AHA}} = 59.5 \pm 0.9 \text{ kJ/mol}$) is significantly smaller than for the analogous reaction of Np(VI) with hydroxylamine ($E_{a,\text{NH}_2\text{OH}} = 82 \text{ kJ/mol}$ [86]).

7 REDOX POTENTIAL OF THE NITROUS ACID – NITRIC ACID SYSTEM

7.1 Introduction

The nitrous acid – nitric acid redox equilibrium is an important determining factor for the speciation of neptunium between the inextractable pentavalent and the highly extractable hexavalent state. However, actual redox potential measurements using a redox sensitive Pt electrode of the $\text{HNO}_2/\text{HNO}_3$ system in the past have not been correlated to the redox speciation of neptunium. The general redox behavior of the $\text{HNO}_2/\text{HNO}_3$ system can be a significant tool for prediction of the balance of the $\text{Np(V)}/\text{Np(VI)}$ couple redox equilibrium.

The redox potential associated with the $\text{HNO}_2/\text{HNO}_3$ system is in acidic solutions determined by the following equation:



Since nitric acid is mostly dissociated in its aqueous solutions, the equilibrium is usually written as to be determined by the balance between nitrous acid and the nitrate anion according to the following chemical equation:



The form of the equation for the Nernst potential for the couple in dilute aqueous solutions is then determined by the following equivalence (E_{cell} is the open circuit potential, E'^o is the formal potential against the employed reference electrode):

$$E_{\text{cell}} = E'^o - \frac{RT}{2F} \ln \left(\frac{[\text{HNO}_2]}{[\text{NO}_3^-][\text{H}^+]^3} \right) \quad (154)$$

Replacing the natural logarithm with decadic and substituting for the ideal gas constant, the standard absolute temperature at 25°C and the Faraday charge constant (i.e., applying a factor of $\ln 10 = 2.303$, and substituting for $R = 8.314 \text{ J/K/mol}$, $T = 298.15 \text{ K}$, and $F = 96485 \text{ C/mol}$, respectively) the following practical relationship should be observed in close-to-ideal systems:

$$E_{\text{cell}} = E'^o - \left(\frac{59.2 \text{ mV}}{2} \right) \log \left(\frac{[\text{HNO}_2]}{[\text{NO}_3^-][\text{H}^+]^3} \right) \quad (155)$$

The general validity and practical applicability of expression (155) for potentiometric measurements in real nitric acid/nitrate systems of up to 4 mol/L concentrations was experimentally investigated.

7.2 Experimental

An Epsilon E-2 potentiostat from *Bioanalytical Systems Inc.* (BASi) was used to measure the cell potential between a Pt-wire electrode and an Ag/AgCl, 3M NaCl (SSC) reference electrode ($E_{\text{ref}} = +207$ mV vs. standard hydrogen electrode - SHE at 25°C [133]), immersed in the measured nitrous acid/nitric acid solutions. Nitrous acid was created by direct acidification of sodium nitrite ($\text{p}K_{\text{a}, \text{HNO}_2} = 3.3$ [128]) in the nitric acid solutions. The solutions were sealed in a threaded 2 mL extraction vial with a screw-cap, the top of which was penetrated by the two electrodes through two leak-tight openings. The leak-tightness of the system was necessary to ensure the stability of nitrous acid that is otherwise decomposing through disproportionation into volatile nitrogen oxides of NO and NO₂. The vial was kept at a constant temperature by a water bath controlled by a *Julabo* F-12ED temperature bath. The 1.8 mL solutions in the vial were stirred by a magnetic mini-stirbar. The kinetics of the redox equilibrium on the surface of the Pt electrode was very slow, determination of the stable open circuit potential for each liquid sample took up to 2 hours.

Daily drift of the reference Ag/AgCl electrode potential were compensated for using an external reference couple of potassium ferro- and ferri-cyanide made as a solution of 10mM K₄Fe^{II}(CN)₆ and 10mM K₃Fe^{III}(CN)₆ in 1M HCl, which has a well-poised and stable formal potential of $E^{\circ} = +710$ mV vs. SHE [161]. Measured values of the potential of this couple against the SSC reference electrode were between +500 and +510 mV during the multiple weeks of measurements (in good agreement with the assumed value of $E_{\text{ref}} = +207$ mV vs. SHE for the reference electrode) indicating an ± 5 mV uncertainty in the determined potential values.

7.3 Results and discussion

The slope of the redox potential with respect to the change in the concentration of the reduced species (HNO_2) at two different nitric acid concentrations (1 M and 4 M HNO_3) were in accordance with the Nernst equation (see Figure 24, for both acids the slopes are approaching $59.2/2 = 29.6$ mV per decade). Extrapolation of the slope in 1 M HNO_3 to the logarithm of the $\text{HNO}_2:\text{HNO}_3$ ratio equal to 0 result in a formal potential of $E^{\circ} = +721$ mV vs. SSC, which translates to a formal potential of $E^{\circ} = +928$ mV vs. SHE. Reference [25] gives the value of the standard potential at $E^{\circ} = +980$ mV vs. SHE. The difference between the formal and standard potential is therefore to be attributed especially to the highly non-ideal ionic strength effects and possibly also due to the junction potential of the Ag/AgCl, 3M NaCl reference electrode.

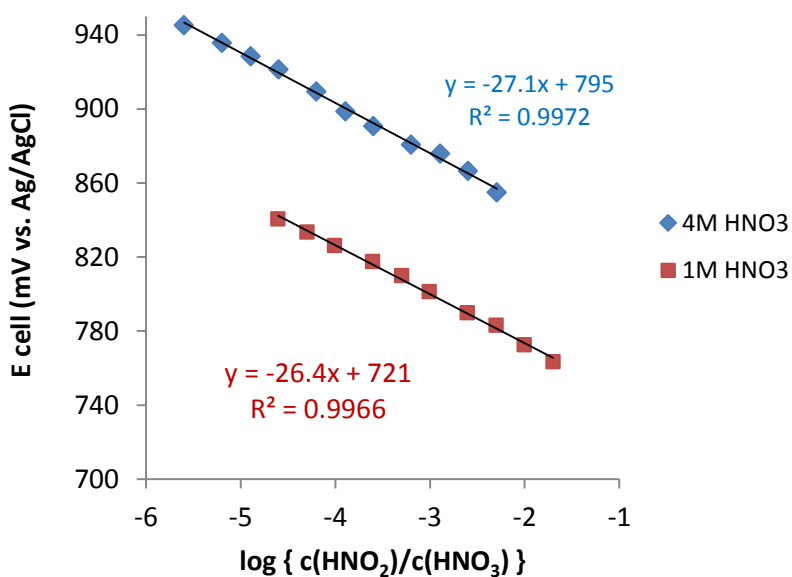


Figure 24 - Nernstian plots for $\text{HNO}_2/\text{HNO}_3$ couple at 25.0°C

Effect of changing HNO_2 concentration between 0.01 mM and 20 mM
at constant 1.0 and 4.0 M HNO_3 concentration

Nonetheless, the dependence of the potential of solutions with constant HNO_2 concentrations on the changing concentration of nitric acid (hydrogen ion concentration) is non-ideal and strongly depends on the magnitude and character of the ionic strength of the solution (Figure 25). The theoretical slope against H^+ concentration at a given total nitrate concentration should have been equal to $3/2 \times 59 = 88.8$ mV/decade according to

the Nernst equation; however, the dependence was observed to follow a slope of $\sim 100\text{mV/decade}$ at acid concentrations below 0.1M indicating an exchange of more than 3 protons during the reaction. At higher acidity the trend broke down and followed a nearly perfect 59mV/decade slope indicating an exchange of 2 protons per reaction.

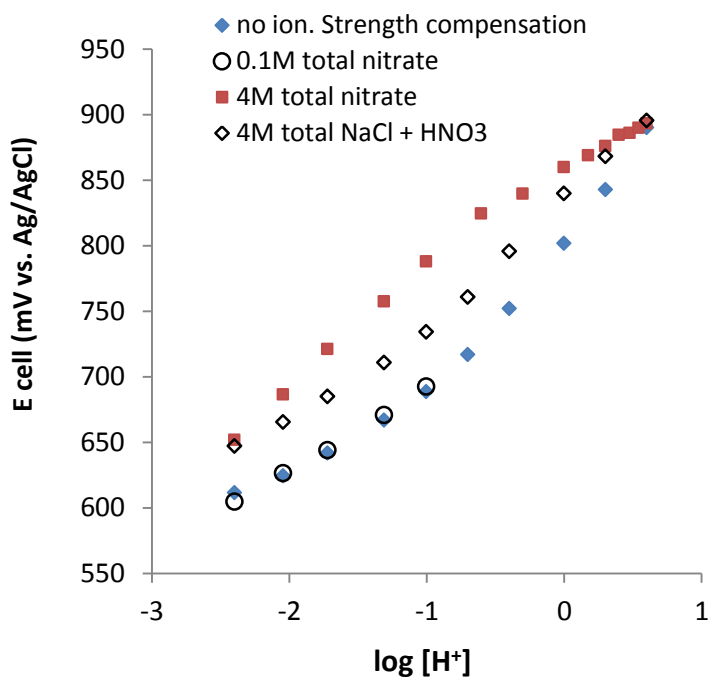


Figure 25 - Dependence of the redox potential of 1mM HNO_2 on the HNO_3/H^+ concentration

under different conditions (maintained by additions of LiNO_3 and/or NaCl), $t = 25^\circ\text{C}$

Results of potential dependence nitric acid concentration without ionic strength compensation revealed an inverse behavior – the 55mV slope in low concentrations which more than doubles its value in concentrations exceeding 0.1M HNO_3 . A very similar behavior was observed when the ionic strength was kept constant by NaCl instead of LiNO_3 and when the total nitrate concentration was kept at 0.1M . The difference in the behavior therefore needs to be attributed to the varying effect of the nitrate at different acidities.

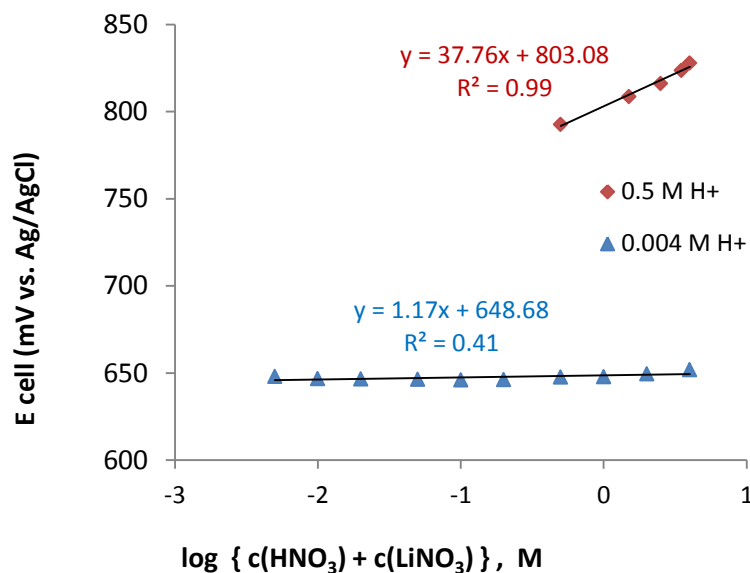


Figure 26 - Dependence of the cell potential with 1mM HNO₂ on the total nitrate concentration at two constant HNO₃ concentrations (4mM and 0.5M), t= 25.0°C

Dependence of the potential on the total nitrate concentration in the 4M LiNO₃ +NaCl ionic strength system with 1mM nitrous acid at two different constant nitric acid concentrations was investigated. It was discovered (Figure 26) that at low acid concentration of nitric acid (5mM HNO₃ →final H⁺ concentration of 4mM due to protonation of 1mM sodium nitrite to HNO₂) the effect of nitrate on the potential is almost unobservable. No significant increase of the potential was detected with the 5mM to 4M increase of total nitrate concentration. However, when the acid concentration was 0.5M the potential was following an increasing slope with the nitrate, somewhat higher than the theoretical 29.6mV/ decade. This also indicates a change in the mechanism of the electron exchange reactions.

Figure 27 shows the results of the investigation of the temperature dependence of the 1mM HNO₂ + 4M HNO₃ solution system. The measurements were generally less reliable due to lower predictability of the reference electrode potential E_{ref} , which was estimated on the basis of a literature reference [25] to change from +221 to +192 mV with the increase of temperature from 5°C to 45°C. The general trend is increasing and seems to contradict in its slope value the temperature dependence predicted by the Nernst equation for ideal solutions (156):

$$\frac{\Delta E_{cell}}{\Delta T} = \left(\frac{1}{298.15K} \right) \cdot \left(\frac{-59.2 mV}{2} \right) \log \left(\frac{[HNO_2]}{[NO_3^-][H^+]^3} \right) \quad (156)$$

The slope value of 1.75 mV/K in Figure 27 is approximately three times higher than the theoretically predicted value of 0.54 mV/K for 1mM HNO₂ and 4M HNO₃.

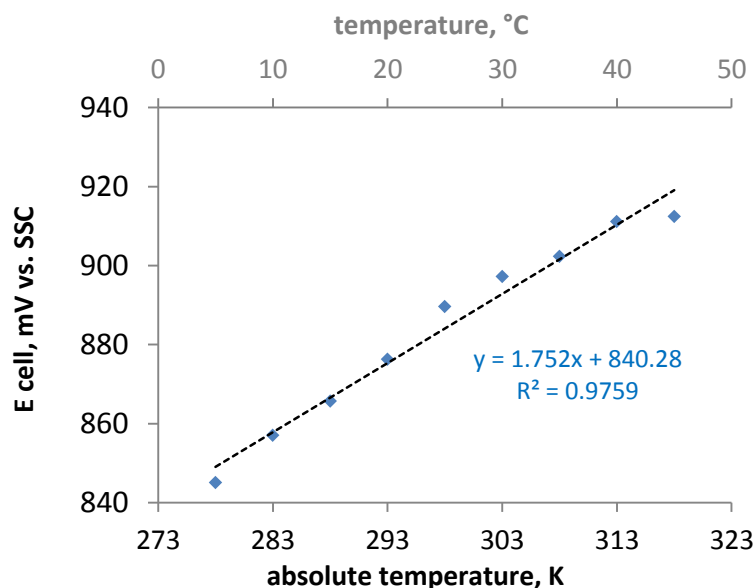


Figure 27 – Temperature dependence of the redox potential of the 1 mM HNO₂ + 4 M HNO₃ system between 5 and 45°C

7.4 Conclusion

The ideal solution form of the Nernst equation without accounting for activity coefficient effects (and possibly also for the association of HNO₃) is unfortunately a poor tool for prediction of the open circuit potential in the nitrous acid/nitric acid system. A good Nernstian behavior was observed only for the dependence of the potential on the nitrous acid concentration; however, the practical utilization of redox potentiometry for the determination of the nitrous acid concentration in nitric acid solutions is unfortunately significantly impacted by the very poor electro-kinetic behavior of the HNO₂/NO₃⁻ couple, making direct spectrophotometric methods significantly faster and thus more useful.

8 REACTION OF NITROUS ACID WITH ACETOHYDROXAMIC ACID IN NITRIC ACID SOLUTIONS

8.1 Introduction

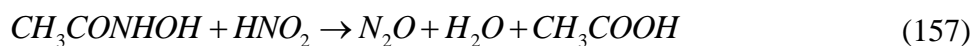
As has been mentioned above (section 2.4.8.2.1), nitrous acid was found by Zhang et al. [99] to rapidly react with acetohydroxamic acid, potentially depleting the concentration of AHA in a UREX-like separation process much more rapidly (within seconds) than due to the effect of its acidic hydrolysis (half-life of several hours). However, the work of Zhang et al. revealed serious discrepancies in the mechanism and rate law dependence compared to studies of reactions of nitrous acid with hydroxylamine and alkylhydroxylamines observed by Stedmen and coworkers [88, 89, 90, 100, 101].

A possible explanation of the inconsistencies was that the reactions were too rapid to be reliably observed by the stirred cuvette method utilized by Zhang et al. [99]. The multiple-second homogenization time of such a chemical reactor system might have resulted in obscuring the true kinetic relationship as resulting of the combination of both mixing and chemical kinetics. Therefore, a verification of the reported behavior by the more appropriate stopped-flow method has been undertaken.

8.2 Stoichiometry of the reaction

By spectrophotometric titration performed by systematic additions of small aliquots of HNO_2 to a solution of AHA, while monitoring the presence of HNO_2 at its absorption maximum at 370nm, it was determined that their reaction follows 1:1 stoichiometry in both excess of HNO_2 and excess of AHA (Figure 19). Also, a titration from excess of HNO_2 in 4M HNO_3 (Figure 29) has proven that a runaway autocatalytic oxidation of AHA by nitrate does not occur (at least at these concentrations of nitric acid), in contrast to such behavior of hydroxylamine, which has been discussed in section 2.4.7.1.

On the basis of the stoichiometry of the very similar reaction of HNO_2 with hydroxylamine [2], the overall reaction most probably produces nitrous oxide, water and acetic acid:



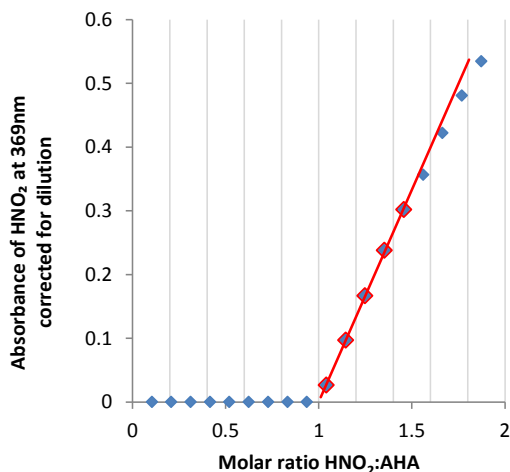


Figure 28 - Determination of the stoichiometry of the HNO₂ + AHA reaction in conditions with excess AHA.

Titration of 15mM AHA in 3mL of 1M HNO₃ by a solution of 96 mM NaNO₂ in water, temperature = 25°C

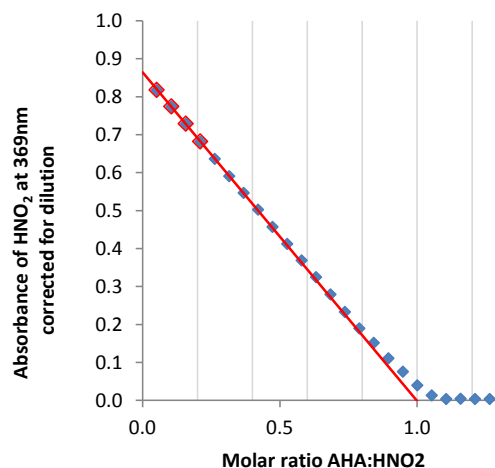


Figure 29 - Determination of the stoichiometry of the HNO₂ + AHA reaction in conditions with excess HNO₂.

Titration of 15mM HNO₂ in 2mL of 4M HNO₃ by a solution of 31 mM AHA in water, covered by a 3mm layer of dodecane to prevent HNO₂ decomposition, temperature = 25°C

8.3 Investigation of the kinetic system

Individual snapshots of the absorption spectra of the solution were taken using OLIS RSM 1000 stopped-flow spectrophotometer in the wavelength range of 330 - 475 nm at acquisition rate of up to 1000 spectra per second to conveniently observe the characteristic absorption multiplet of nitrous acid in the range of 330-400nm.

Analysis of the recorded spectra has led to identification of a reaction intermediate (Figure 30). The shape of the absorption spectrum of the intermediate has been determined from spectra recorded in later stages of reactions with excess AHA when all HNO₂ and the molar absorbances were received by subtraction of known HNO₂ spectrum from the earliest stage reaction spectra, where the concentrations of nitrous and the intermediate were assumed to be complementary. By deconvolution of all spectrum snapshots (discussed in further detail in section 3.2.2.5) recorded during one experiment, time-dependent values of concentrations of HNO₂ and of the intermediate were identified. At the beginning, the nitrous acid is rapidly converting into the intermediate until a maximum intermediate concentration is achieved (Figure 31). Thereafter, the

intermediate is somewhat slower decaying into the reaction products (most likely nitrous oxide and acetic acid), as is indicated in the following reaction scheme:

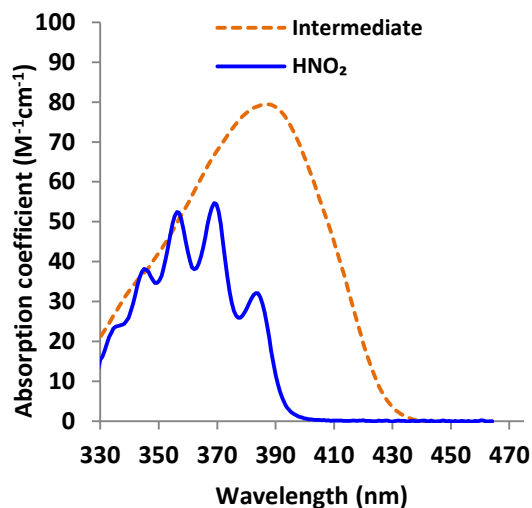
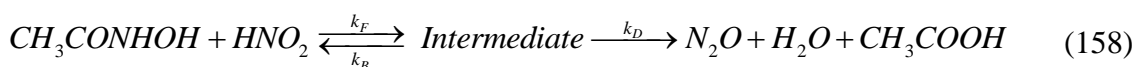


Figure 30 - Absorption spectra in 1M HNO_3 of HNO_2 and the long-lived reaction intermediate identified during the reaction of AHA with HNO_2 .

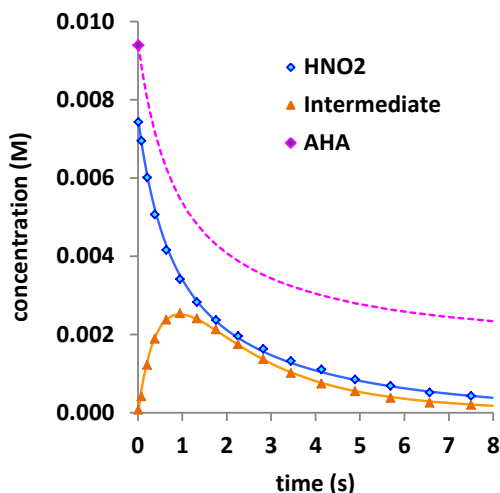


Figure 31 - Reaction of 7.5mM HNO_2 with 9.5 mM AHA in 1M HNO_3 at 25°C.

Symbols represent actual concentrations determined from deconvolution of spectra, lines are modeled by mechanism (158).

Utilizing a numeric integrator of chemical kinetics based on the Runge-Kutta method (see section 3.2.3.3), different reaction rate laws have been modeled to fit the acquired data. In the model with the most successful fit, the intermediate is produced by an overall second order reaction of AHA and HNO_2 with a rate constant k_F ; while the reverse of this reaction and the decay of the intermediate into the reaction products is governed by first-order processes with rate constants k_B and k_D , respectively. The rate equation system has the following appearance:

$$-\frac{d[HNO_2]}{dt} = -\frac{d[AHA]}{dt} = k_F[HNO_2][AHA] - k_B[Intermed.] \quad (159)$$

$$+\frac{d[Intermed.]}{dt} = k_F[HNO_2][AHA] - k_B[Intermed.] - k_D[Intermed.] \quad (160)$$

This proposed reaction mechanism has consistently explained the outcome of reactions of both HNO_2 and AHA in varying initial ratios. Rate constants determined by fitting of the numeric model of the mechanism (159)+(160) are summarized in the Table 8 below:

Table 8 - Rate constants of the HNO_2 + AHA reaction system in 1.0 M HNO_3

concentration ratio HNO_2 : AHA	k_F [$\text{M}^{-1}\text{s}^{-1}$]	k_B [s^{-1}]	k_D [s^{-1}]
0.3	114	0.099	0.89
0.6	112	0.099	0.87
0.8	121	0.100	0.83
1.0	118	0.099	0.92
1.5	116	0.098	0.91
Average \pm st.dev.	116 ± 5	0.099 ± 0.001	0.86 ± 0.03

Experimental conditions: $c(\text{AHA}) = 5.0\text{-}9.5$ mM, $c(\text{HNO}_2) = 2.7\text{-}9.5$ mM, $t = 25.0$ °C

8.4 Influence of acidity, nitrate concentration and temperature

Experiments in which the reactants were kept at a constant ratio of $\text{AHA}:\text{HNO}_2 = 0.66$ while the nitric acid concentration was varied (constant ionic strength of 1.0 mol/L was maintained by LiNO_3) showed that rate constants k_F and k_D are dependent and are increasing with the H^+ concentration with an approximately 1st order dependence. Rate constant k_B governing the partition of the intermediate into the original reactants is independent on the acidity.

As can be seen on Figure 32, for the forward reaction the order with respect to $[\text{H}^+]$ was 0.89, which is close to 1.0. For the decomposition reaction the order is somewhat lower – close to 3/4, but the possibility of a very good linear fit through the k_D dependence in the graph strongly suggests that the decomposition of the intermediate may proceed through two parallel reactions – a proton dependent and a proton-independent path.

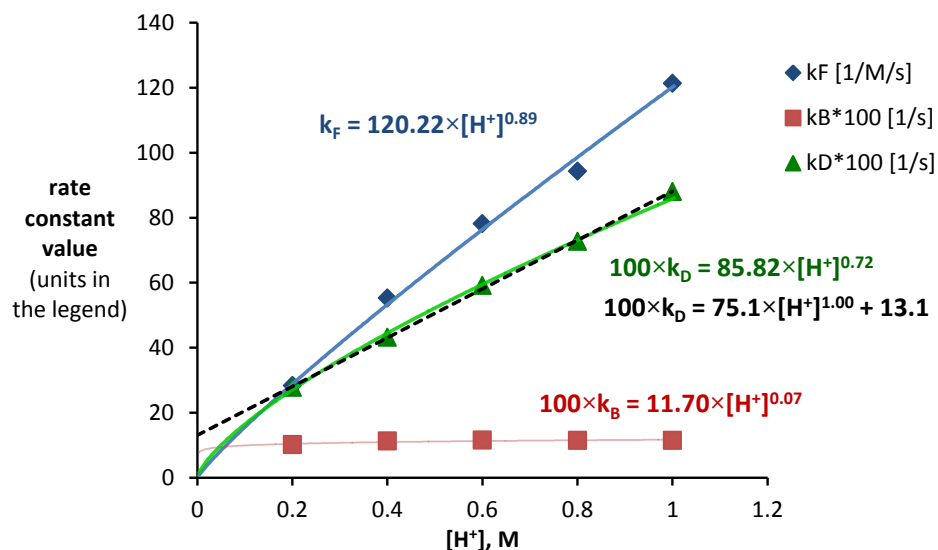


Figure 32 - Dependence of rate constants on acidity at constant nitrate concentration

Initial experimental conditions:

$c(\text{HNO}_3 + \text{LiNO}_3) = 1 \text{ M}$, $c(\text{AHA}) = 5.0 \text{ mM}$, $c(\text{HNO}_2) = 7.5 \text{ mM}$, $t = 25.0 \text{ }^\circ\text{C}$

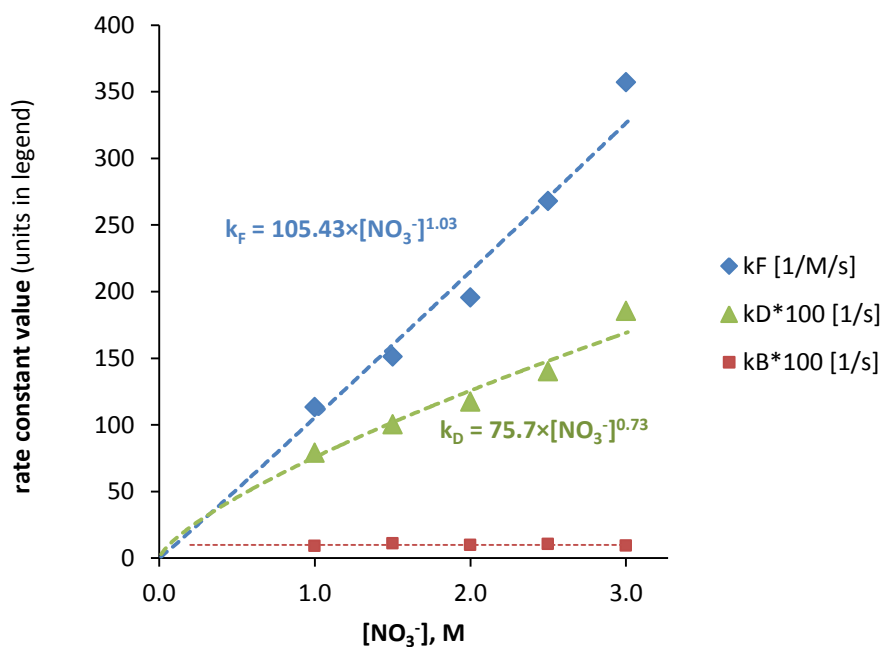


Figure 33 - Dependence of rate constants on the total concentration of NO_3^- in the solution

Initial experimental conditions:

$c(\text{HNO}_3) = 1 \text{ M}$, $c(\text{LiNO}_3) = 0 - 2 \text{ M}$, $c(\text{AHA}) = 5.0 \text{ mM}$, $c(\text{HNO}_2) = 7.5 \text{ mM}$, $t = 25.0 \text{ }^\circ\text{C}$

Experiments of the same reaction system under constant concentration of nitric acid and with changing concentration of LiNO_3 salt were undertaken to investigate the effect of the nitrate ion / ionic strength of the solution (Figure 33). The dependence of the rate constant k_F and k_D was very similar to the effect of hydrogen ion, i.e. promoting the rates of the forward reaction (k_F) and of intermediate decomposition (k_D) by 1st and 3/4th order of dependence versus total concentration NO_3^- , while the rate constant k_B of the reverse reaction remained unchanged.

This seems to indicate that the reaction rate constants k_F and k_D might be a function of the concentration of undissociated HNO_3 that is approximately proportional to the concentration of both H^+ and NO_3^- ions as a result of the protonation equilibrium of nitric acid ($\text{p}K_a \approx -1.44$ [158]):

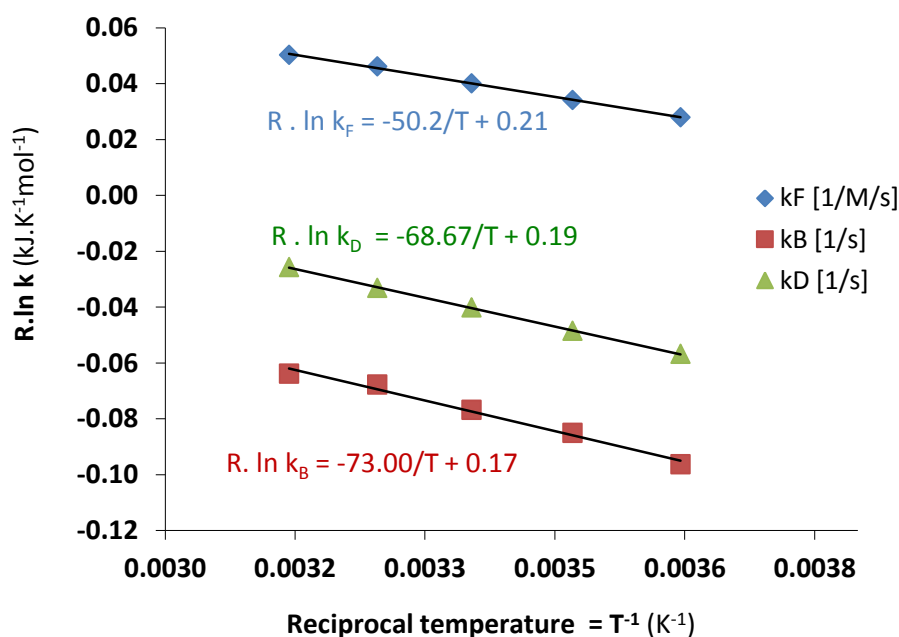


Figure 34 – Dependence of rate constants on reaction temperature

Initial experimental conditions:

$c(\text{HNO}_3) = 1 \text{ M}$, $c(\text{AHA}) = 5.0 \text{ mM}$, $c(\text{HNO}_2) = 7.5 \text{ mM}$, $t = 25.0 \text{ }^\circ\text{C}$

Further investigation of the sensitivity of the three reaction rate constants to thermal activation has revealed that both of the first-order processes have relatively high activation energy barriers, compared to the synthesis of the intermediate (Figure 34), also explaining the relatively higher rate of the forward reaction. However, the calculated entropy of the activated complex for each process (in Table 9) clearly shows that the activated complex for the forward reaction requires a much higher level of organization than the other two apparent 1st order processes of the intermediate.

Table 9 - Parameters of thermal activation for the processes of the AHA + HNO₂ reaction system

parameter	process-indicating rate constant		
	k_F	k_B	k_D
ΔH^\ddagger (kJ/mol, 25°C)	47.7 ± 1.1	70.5 ± 4.9	66.2 ± 0.6
ΔS^\ddagger (J/K/mol, 25°C)	-44.9 ± 0.8	-28.4 ± 2.1	-24.9 ± 0.2
ΔG^\ddagger (kJ/mol, 25°C)	61.1 ± 1.2	79.0 ± 5.0	73.6 ± 0.6

The nature of the intermediate cannot be identified with a sufficient degree of certainty, so far. Nonetheless, Stedman and coworkers [88, 101] have concluded that the very similar reactions of HNO₂ with hydroxylamine and alkyl-hydroxylamines follow through an N-nitrosylation step. For acetohydroxamic acid, the following scheme can be proposed:



The intermediate CH₃CON(OH)-NO in the proposed reactions (162) and (163) is N-nitroso-acetylhydroxylamine, which is structurally related to N-nitroso-methylurea (H₂NCON(CH₃)-NO), a compound with a very similar absorption spectrum that has been investigated in another part of this work (see Figure 47 in chapter 10).

8.5 Conclusion

The reaction of nitrous acid and acetohydroxamic acid was found to follow a complicated, yet credible, scheme with a central role of an UV-absorbing intermediate,

most likely a nitroso-derivative of acetohydroxamic acid. Zhang and coworkers [99] – who were the only ones to investigate the system so far – could unfortunately not discover this due to two principal limitations of their experimental system: Firstly, their instrument allowed the monitoring of only one wavelength at once (the major absorption peak of HNO_2 at 371nm [99] was used), and, secondly, they used a stirred-cell system for studying a reaction with a too rapid reaction rate to maintain the conditions of homogeneous reaction kinetics.

Based on the previous studies of Stedmen and co-workers [88, 101], for the next step in potential future investigations of the exact structure of the reaction intermediate, use of stable isotopic markers (e.g., nitrogen-15 and oxygen-18) can be suggested.

9 REACTION OF NITROUS ACID WITH HYDROGEN PEROXIDE IN NITRIC ACID SOLUTIONS

9.1 Introduction

Radiolysis of aqueous solutions of nitric acid mainly produces gaseous compounds such as H₂, O₂, and N₂ while producing significant amounts of HNO₂ and H₂O₂. The latter two are mutually reactive:



Hydrogen peroxide is not present in solutions after irradiation if the radiolytic production of HNO₂ was significantly higher. This happens in solutions with HNO₃ concentration greater than approximately 0.5 M (= 0.5 mol/dm³), because the production of HNO₂ is proportional to the concentration of nitrate anion [162].

As has been discussed above in section 2.4.6.1, the parameters of the kinetics of reaction (164) have been investigated mostly in pH > 2 solutions of low ionic strength. However, recent studies of the radiation chemistry of redox reactions of neptunium(VI) in 4M nitric acid performed by Bruce Mincher, Stephen Mezyk, Leigh Martin and the author of this work [163] have created a necessity to determine whether the rate laws and rate constants of this reaction determined in solutions of lower ionic strength and higher pH are applicable for the 1-4 M nitric acid solutions.

9.2 Stoichiometry and reaction mechanism

Following the absorption maximum of nitrous acid at 369 nm, spectrophotometric titrations were performed, starting from excess of nitrous acid (Figure 19) and hydrogen peroxide (Figure 29). Both experiments have proven that the reaction stoichiometry in both cases is 1 : 1, exactly following reaction (164).

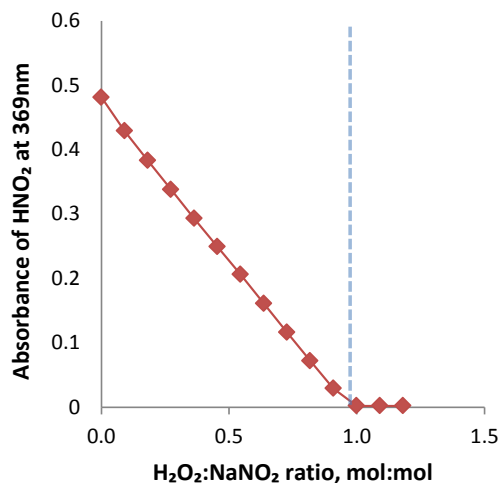


Figure 35 - Spectrophotometric titration of 10 mM H₂O₂ by HNO₂ (0.5M HClO₄, t = 25°C)

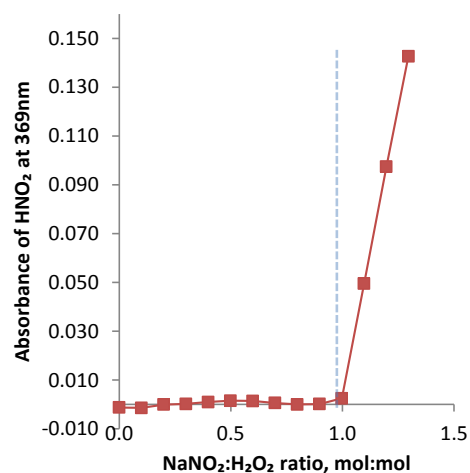
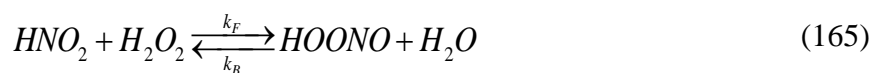


Figure 36 - Spectrophotometric titration of 10 mM NaNO₂ by H₂O₂ (0.5M HClO₄, t = 25°C)

9.3 Investigation of the kinetic system

Kinetic observations (recorded using stopped-flow absorption spectrophotometry OLISTM RSM 1000) have shown that the reaction proceeds through a very rapid formation of a UV-absorbing intermediate (characterized by 2nd order rate constant k_F), which has been previously identified as peroxonitrous acid HOONO [84]. In some of our experiments, evidence was found of the reverse of this reaction, i.e breakup of HOONO back into the original reactants (characterized with a 1st order rate constant k_B). The intermediate consequently undergoes a somewhat slower decay (quantified by a 1st order rate constant k_D) into the product HNO₃. The observed reactions behave according to the following simplified reaction scheme:



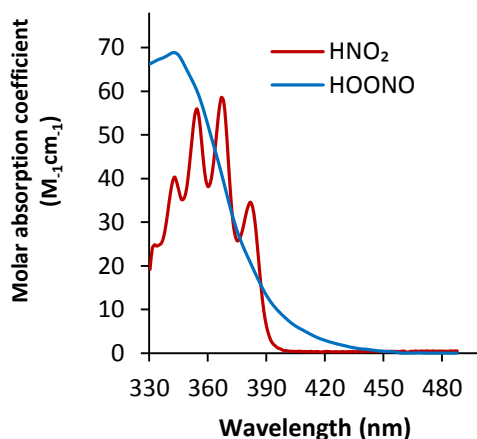


Figure 37 - Absorption spectra of nitrous acid (HNO_2) and peroxonitrous acids (HOONO) used for fitting kinetic data

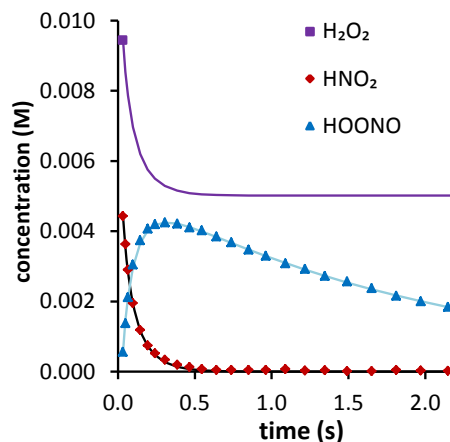


Figure 38 - Reaction of 5.0 mM HNO_2 with 10 mM H_2O_2 in 0.75 M HNO_3 + 0.25 M LiNO_3 at 2.5°C.

Symbols represent actual concentrations determined from deconvolution of stopped-flow spectra, lines represent the fit of the numeric model based on the two consecutive reactions (165) and (166).

The shape of the absorption spectrum of HOONO between 330 and 480 nm has been determined from spectra recorded in later stages of reactions with excess H_2O_2 when all HNO_2 has already reacted. Using previously obtained spectrum of HNO_2 , the values of molar absorption coefficients vs. wavelength were consequently quantified by parameterized subtraction from reaction spectra recorded at the beginning of the reaction where very little HOONO had time to decay. The shape of the resolved spectrum of the peroxonitrous acid is comparable in shape and intensity to the spectrum determined by Benton and Moore using a continuous flow-cell [84].

The final spectra of HOONO and HNO_2 presented in Figure 30 were used for deconvolution of all spectra recorded during a particular kinetic run in order to determine the time-dependent concentrations of reactants. As can be seen in Figure 31, the reaction curves were then successfully fitted by a numeric model consisting of differential equations (4) and (5), which were based on reactions (2) and (3). With rate constants for the forward, backward and decomposition processes (k_F , k_B and k_D , respectively) used as fitting parameters.

$$-\frac{d[\text{HNO}_2]}{dt} = -\frac{d[\text{H}_2\text{O}_2]}{dt} = k_F \cdot [\text{HNO}_2] \cdot [\text{H}_2\text{O}_2] - k_B \cdot [\text{HOONO}] \quad (167)$$

$$+\frac{d[HOONO]}{dt} = k_F \cdot [HNO_2] \cdot [H_2O_2] - (k_B + k_D) \cdot [HOONO] \quad (168)$$

The reaction of formation of peroxonitrous acid was therefore determined to be of first order with respect to both HNO_2 and H_2O_2 , confirming that the reaction in the nitrate system generally confirms the previous experimental findings of Benton and Moore performed in the perchlorate system [84]. The reaction model identified by equations (159) and (168) could successfully explain all runs in a series of experiments in which the ratio of initial concentrations of reactants (HNO_2 and H_2O_2) was varied by changing the initial hydrogen peroxide concentration. The resulting values of rate constants determined by fitting to the acquired data are displayed in Table 1.

Table 10 – Determined values of rate constants in experiments with various H_2O_2 concentration

$t = 2.5 \text{ }^\circ\text{C}, 0.25 \text{ M } HNO_3 + 0.75 \text{ M } LiNO_3$

Run no.	c(HNO_2), mM	c(H_2O_2), mM	$HNO_2 : H_2O_2$	$k_F, M^{-1}s^{-1}$	k_B, s^{-1}	k_D, s^{-1}
1	5.0	0.75	6.67	615	*	0.27
2	5.0	1.0	5.00	584	*	0.28
3	5.0	2.4	2.08	596	0.10	0.29
4	5.0	3.6	1.39	584	0.13	0.27
5	5.0	4.9	1.02	557	0.15	0.25
6	5.0	7.5	0.67	655	0.20	0.25
7	5.0	15.0	0.33	509	0.15	0.21
8	5.0	25.0	0.20	472	0.19	0.20
9	5.0	40.0	0.13	477	*	0.19
10	5.0	50.0	0.10	471	*	0.18
Average				552 ± 66	0.15 ± 0.04	0.24 ± 0.04

* due to the low effect of the backward reaction (2) on the progress of the reaction, values of k_B could be reliably determined only in experiments where $HNO_2 : H_2O_2$ ratio was close to 1

9.4 Dependence of rate constants on acidity

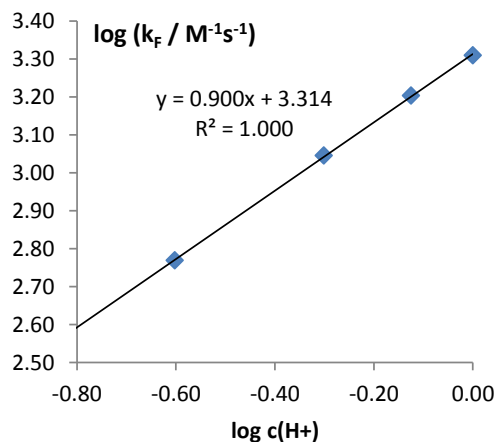


Figure 39 - Dependence of HOONO formation rate constant k_F on acidity - reaction of 5mM HNO_2 , 10mM H_2O_2 , $t=2.5^\circ\text{C}$, 1M H/LiNO_3

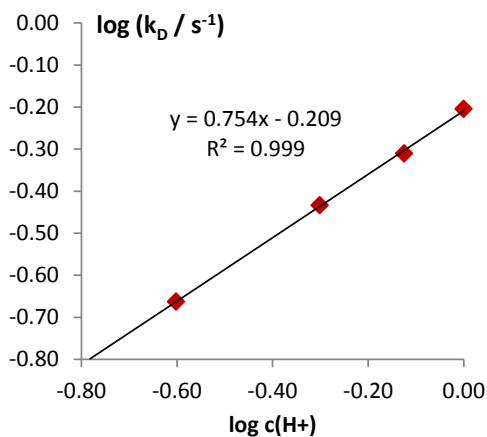


Figure 40 -Dependence of HOONO decay rate constant k_D on acidity - reaction of 5mM HNO_2 , 10mM H_2O_2 , $t=2.5^\circ\text{C}$, 1M H/LiNO_3

9.5 Dependence of rate constants on nitric acid and on total nitrate concentration

In Figure 41 the dependence of the reaction rate constants k_F and k_D on the total nitric acid concentration in the wide range from 0.1 to 4 M HNO_3 is presented. In the chosen experimental conditions, the contribution of the backward reaction of HOONO breakup was too small to reliably quantify the exact value and changes of the rate constant k_B . The increase in reaction rates of the forward HOONO formation and decomposition into products was much more significant than in experiments where constant nitrate concentration (and thus ionic strength) was maintained, especially in the higher end of nitric acid concentration. Below 1 M HNO_3 , the rate constant of HOONO formation (k_F) follows an approximately $1\frac{1}{2}$ order of dependence on HNO_3 until approximately 1M HNO_3 .

The half-order increase compared to the nitrate compensated area could be possibly explained by changes in the ionic strength of the solution; however, above 1 M HNO_3 the rate increases much more rapidly with a 3rd order of dependence on HNO_3 concentration.

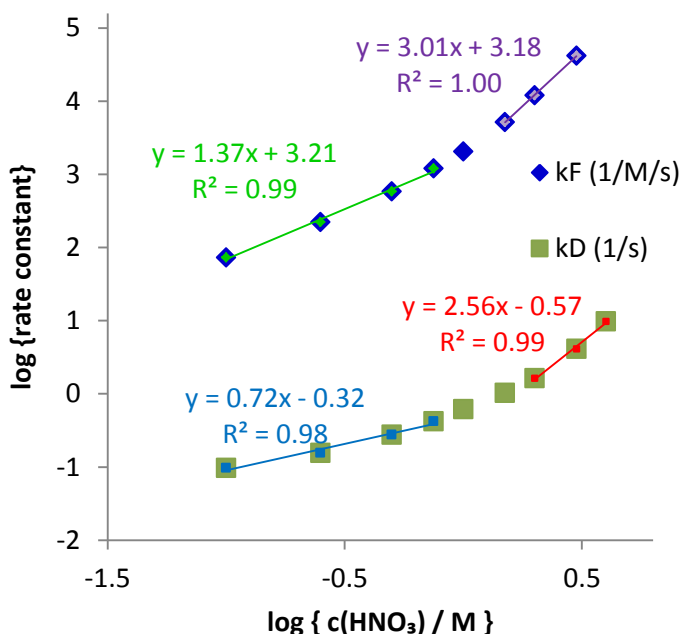


Figure 41 - Determination of dependence of rate constants on HNO_3 concentration

0.1 - 4 M HNO_3 , $t = 2.5^\circ\text{C}$; reaction of 5mM HNO_2 with 10mM H_2O_2 , no compensation for ionic strength and nitrate concentration was employed

In 4M HNO_3 , the rate of the forward reaction was so high that it was impossible to accurately determine the value of the rate constant k_F . Nitrous acid has reacted with hydrogen peroxide already in the mixing jet (within 4 milliseconds) of the stopped-flow apparatus and almost pure HOONO was entering the optical cell of the spectrophotometer. The rate constant of HOONO decomposition k_D exhibited a very similar behavior. In the lower end of HNO_3 concentration, its order of dependence on nitric acid was 0.7, which is very close to the reaction order versus hydrogen ion concentration. However, above 1 M HNO_3 , the decomposition rate was increasing more rapidly with HNO_3 concentration and the order increased to 2.6.

Since it was most plausible that the effect of increased rate HNO_3 dependence compared to the data on hydrogen ion sensitivity H^+ should be attributed to the effect of nitrate ion, additional experiments examining the dependence of the reaction rates on total nitrate concentration at constant acidity were also performed.

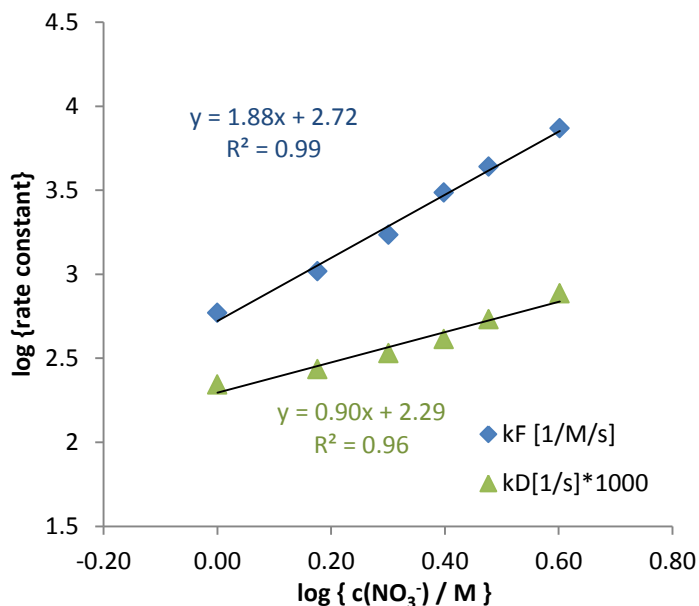


Figure 42 -Dependence of rate constants on total concentration of nitrate - reaction of 5mM HNO₂ with 10mM H₂O₂, t=2.5°C, 0.25M HNO₃ + 0.75-3.75 M LiNO₃

In Figure 42 the dependence of the reaction rate constants k_F and k_D on the total nitrate concentration is presented. Nitrate anion seems to have a very significant effect on the acceleration of the HOONO formation reaction step: the rate of HOONO formation increases with the square of the nitrate concentration. In the 1-4 M HNO₃ region, the combination of 1st order with respect to H⁺ ion and 2nd order with respect to NO₃⁻ fully explains the observed 3rd order with respect to HNO₃.

A less prominent, approximately 1st order effect of the total nitrate concentration on the HOONO decomposition rate was also observed in the high nitrate concentration range of 1 – 4 M NO₃⁻. In combination with the 3/4 order with respect to hydrogen ion concentration, the added effect of nitrate dependence is not entirely enough to explain the 2½ order with respect to HNO₃ concentration in Figure 41. It can be only speculated that the remaining increase in reaction rate sensitivity could be possibly caused by significant changes in ionic strength.

The discovery of significant effect of NO₃⁻ concentration is surprising since Park et al. [82] haven't observed any effect of added nitrate ion concentration up to 0.1 M on the rate of reactions performed at pH ≈ 2 and NO₃⁻ concentration. It is most likely that the

effect of NO_3^- ion catalysis becomes more prominent only in higher concentrations, as can be seen in the “breaking” of the curves of rate constant dependence on HNO_3 in Figure 41. It can be speculated that the real reason behind the change in behavior above 1M nitrate concentration is the formation of non-dissociated HNO_3 which exists only in very limited relative concentrations in solutions with low nitrate concentration[158]. A side-reaction catalyzed by HNO_3 could become more prominent only at higher nitrate concentrations.

9.6 Dependence of rate constants on temperature

Figure 7 displays the Arrhenius plots of dependence of the rate constants k_F , k_B and k_D on the reaction temperature. The absolute values of the slopes of the dependencies represent the values of activation energies E_A (kJ/mol) for each reaction step. Due to the high activation energy of the HOONO reverse break-up to the original reactants, the rate constant k_B is quantifiably increasing with temperature.

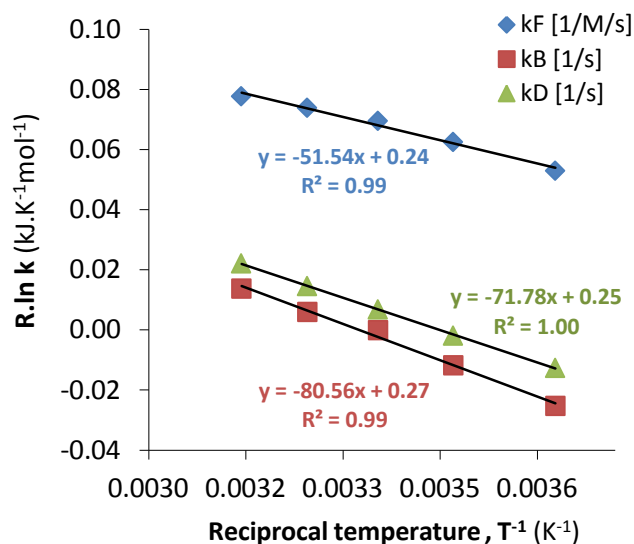


Figure 43 -Dependence of rate constants on temperature - reaction of 5mM HNO_2 , 10mM H_2O_2 , $t = 2.5 - 45$ °C, 0.25M HNO_3 + 0.75M LiNO_3

The parameters of thermal activation calculated on the basis of the activation complex theory are summarized in Table 11. It appears that the activated complex is the same species in the forward (k_F) and reverse (k_B) reactions of the reversible reaction (165),

because the activation entropies for these reactions have very similar opposing values. However, the activation energy barrier for the entropically favored dissociation of this complex is significantly higher than for its association.

Table 11 – Parameters of thermal activation according to the activated complex theory.

	ΔH^\ddagger (kJ/mol, 25°C)	ΔS^\ddagger (J/K/mol, 25°C)	ΔG^\ddagger (kJ/mol, 25°C)
Reaction (165) forw., k_F	49.1 ± 3.3	-12.2 ± 0.7	52.7 ± 3.3
Reaction (165) backw., k_B	78.1 ± 4.0	14.7 ± 0.9	73.7 ± 4.0
Reaction (166), decay, k_D	69.3 ± 0.7	-5.6 ± 0.1	71.0 ± 0.7

9.7 Conclusion

Through the utilization of the stopped-flow method, confirmation of previously reported reaction scheme for synthesis and decay of peroxonitrous acid from nitrous acid and hydrogen peroxide has been confirmed. However, the values of the rate constants, and especially the value of the forward 2nd order reaction rate k_F has been found to depend significantly on the concentration of nitric acid in the region 1-4M HNO₃ – an overall 3rd order of dependence was found as a result of the expected 1st order for hydrogen ions and an emerging 2nd order of dependence for NO₃⁻.

Extrapolating on the measured data, values of the forward rate constant k_F on the order of $10^5 - 10^6 \text{ M}^{-1}\text{s}^{-1}$ and values for the peroxonitrous acid 1st order decay rate constant $k_D = 10^2 \text{ s}^{-1}$ can be expected to arise in 4M HNO₃ at the temperature of 25°C.

**10 EFFECT OF GAMMA IRRADIATION ON THE OXIDATION STATE OF
NEPTUNIUM IN NITRIC ACID IN THE PRESENCE OF SELECTED
SCAVENGERS**

Martin Precek and Alena Paulenova

Separation Science and Technology
Taylor & Francis, Inc
7625 Empire Drive
Florence, Kentucky 41042-2919
United States of America

Manuscript published on 30th August 2010 as part of the Proceedings of the 16th Symposium on Separation Science and Technology for Energy Applications, October 18-22, 2009, held in Gatlinburg, Tennessee, in the journal:

Separation Science and Technology (2010) vol.45, no.12-13, p. 1699–1705

doi: 10.1080/01496395.2010.493833

ISSN: 0236-5731 (print version)

ISSN: 1588-2780 (electronic version)

10.1 Abstract

A series of experiments was performed with selected reagents that were added to inhibit the reduction of Np(VI) to Np(V) during irradiation of its solutions in HNO₃. Acetamide and methylurea as nitrous acid scavengers, and vanadium(V) as a neptunium(V) oxidizer, were examined in this effort. Solutions of these reagents in 4 M HNO₃ were irradiated in a Co-60 gamma irradiator. Additions of 1-10mM of methylurea and vanadium(V) essentially had no effect on the final oxidation state of Np after irradiation with a dose of 60 kGy, while addition of higher concentrations of methylurea (50 and 100mM) led to an almost complete reduction of Np to the tetravalent oxidation state.

10.2 Introduction

During the reprocessing of used nuclear fuel (UNF) solutions, Np(VI) is reduced to Np(V) by radiolytic degradation products. In particular, nitrous acid (HNO₂), which is produced by the radiolysis of nitric acid, causes significant reduction of Np(VI). Formation of Np(V) is undesirable, as it is poorly extracted by TBP. A series of experiments was performed in an attempt to inhibit this reduction. Vanadium(V) was used to reoxidize Np(V) back to Np(VI). Methylurea (MU) and acetamide (AcA) were used to prevent the formation of HNO₂.

10.2.1 Radiolysis of Nitric Acid

Radiolysis of aqueous solutions of nitric acid mainly produces gaseous compounds such as H₂, O₂, and N₂ while producing significant amounts of HNO₂ and H₂O₂. The latter two are mutually reactive:

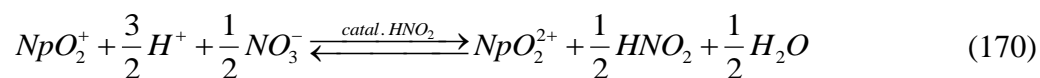


Hydrogen peroxide is not present in solutions after irradiation if the radiolytic production of HNO₂ was significantly higher. This happens in solutions with HNO₃ concentration greater than 0.5 M (= 0.5 mol/dm³). Production of HNO₂ is proportional to the concentration of nitrate anion; however, its radiation yield decreases with the acidity of the aqueous solution: the production of HNO₂ in solution of 0.1 M HNO₃ + 5.9 M NaNO₃ was almost 3 times higher than in 6 M HNO₃ [162]. Low linear energy transfer

(LET) radiation like β and γ has radiation yields around 0.25 mM/kGy in 1M HNO_3 . The radiation yields by α particles are approximately two times lower [155].

10.2.2 Importance of HNO_2

The significance of HNO_2 in the redox speciation of neptunium is based on its reducing behavior toward Np(VI) . The reduction of Np(VI) to Np(V) is not complete, as the reaction extent is controlled by an acidity-dependent equilibrium [53, 55] in which the nitrous acid acts as a catalyzer of oxidation of Np(V) by the effect of nitrate:



The traditional approach to eliminate HNO_2 from HNO_3 solutions uses sulfamic acid or ferrous sulfamate $\text{Fe}(\text{NH}_2\text{SO}_3)_2$, where the sulfamate anion reacts with HNO_2 and produces nitrogen gas and sulfate anion, which is another undesirable compound in the separation streams [2]. Therefore, the general effort toward reducing of amount of radioactive waste from the reprocessing of UNF necessitates the use of “salt-free” compounds that contain only of C, H, N and O elements, and as fully combustible, they will not add to the weight and volume of the high level wastes from UNF reprocessing.

10.2.3 Methylurea and Acetamide

Recently, primary and secondary amides such as acetamide (AcA) and methylurea (MU), respectively, were proposed as possible scavengers for nitrous acid (Figure 44).

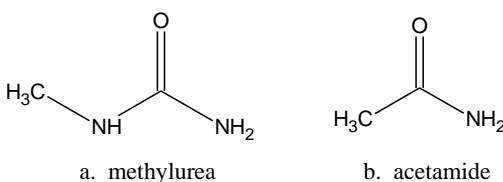


Figure 44 - Proposed nitrous acid scavengers

It is well known that these compounds are reactive toward HNO_2 [164, 165]. Methylurea reacts with HNO_2 through a nitrosation reaction (Figure 45) [165].

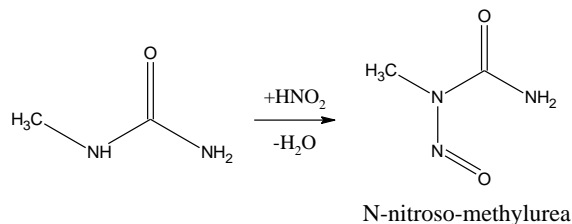
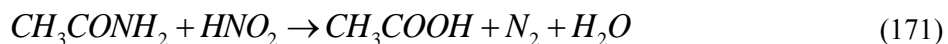


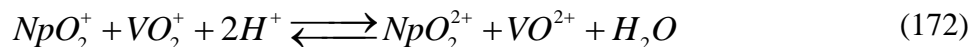
Figure 45 - Methylurea nitrosation

This forms N-nitrosomethylurea (NMU) by an attack of the NO^+ intermediate (produced by the protonation of HNO_2) on the carbonyl oxygen, which is followed by deprotonation and rearrangement of the NO group [166]. Since NMU is not reactive toward Np(VI) , methylurea functions as an efficient inhibitor of Np(VI) reduction by HNO_2 . The reaction of acetamide with HNO_2 is similar to the reaction of other primary amides, such as urea, which results in the production of gaseous nitrogen [167]. The rate of the reaction (2) that leads to the elimination of HNO_2 is considerably slower than in the case of methylurea [164].



10.2.4 Redox Reactions of *Np* with HNO_2 and Vanadium(V)

Pentavalent vanadium V(V) is a fast oxidizing agent toward Np(V) , as 90% of the reaction is complete within several minutes for mM concentrations of V and Np . V(V) can be used as a holding oxidant in an attempt to keep neptunium in its hexavalent oxidation state, as described by the following reaction:



The concentration equilibrium constant for this reaction in 4 M perchloric acid/perchlorate system was determined to be $0.13 \pm 0.02 \text{ M}^{-2}$ [112]. Raising the nitric acid concentration from 1 to 4 M leads to significant shift of the reaction (172) from left to right with the equilibrium ratio of $[\text{Np(VI)}]/[\text{Np(V)}]$ increasing 16 times for a given ratio of $[\text{V(IV)}]/[\text{V(V)}]$.

10.3 Experimental

UNF from light water reactors cooled for 150 days have a 20kW/t heat production [2], which assumes that a 1 M concentration of uranium after the fuel dissolution will have an estimated dose rate well below 100 kGy/hr; hence, integral doses of up to 61 kGy were applied. Aerated solutions with additions of MU, AcA, V(V), and Np in HNO₃ were irradiated in hermetically enclosed glass vials or screw-cap polypropylene extraction vials in a gamma irradiator (⁶⁰Co) with a dose rate of 445 Gy/hr. A relatively small dose rate did not significantly increase the temperature of the irradiated solutions above the ambient laboratory temperature (21-22°C).

10.3.1 Neptunium

²³⁷Np ($t_{1/2} = 2.1 \times 10^6$ y) was received as NpO₂ from Argonne National Laboratory and dissolved in a slight molar excess of H₂O₂ and 8 M HNO₃. Confirmation of the tetravalent oxidation state was determined using Vis-NIR spectroscopy. In order to remove any transuranic impurities, the Np solution was added to a prepared BioRad AG-1 anion exchange column. The column was rinsed with a solution of 8 M HNO₃, 0.3 M hydrazine monohydrate, and 2 g/L hydroquinone. Np was stripped from the column using 0.36 M HCl and its isotopic purity was confirmed using thin-window HPGe gamma spectroscopy. Any organic impurities were destroyed by concentrated nitric acid and hydrogen peroxide. The clean solution of Np in 4 M HNO₃ had its oxidation state adjusted to hexavalent in a custom-made electrolytic H-cell by electrolysis on a Pt wire electrode at potential +1.3V vs. reference Ag/AgCl electrode. The electrolysis was controlled by a BASi EpsilonTM e2 potentiostat.

UV-VIS-NIR spectroscopy of solutions in 1 cm path-length quartz cuvettes in spectral ranges of 200-1000 nm (OceanOpticsTM QE65000 spectrometer with DH-2000 BAL light source) and 900-1300 nm (Olis[®] RSM 1000 Monochromator, equipped with a 800 nm high-pass filter, InGaAs detectors and a tungsten halogen light source) was employed in order to determine the quantitative redox speciation of neptunium between Np(IV), Np(V) and Np(VI) by fitting to digitized published reference spectra [136]. The differences in speciation results of the fitting procedure between the spectra acquired by

QE65000 and RSM 1000 led to an estimate of $\pm 5\%$ error in the value of each species fraction of the total neptunium.

10.3.2 Nitrous acid

Preparation of HNO_2 for analysis of its absorption spectra was performed by mixing a spike consisting of a neutral solution of concentrated NaNO_2 in the nitric acid solutions. UV-VIS spectroscopy (RSM 1000 equipped with a Xe arc lamp or QE65000) was used for identification and quantification of HNO_2 and its interaction with methylurea and acetamide. The HNO_2 solutions have a distinctive absorption pattern between 350 and 400 nm. This pattern interferes somewhat with the broad and intensive absorption of HNO_3 in the shorter wavelength region. While NaNO_2 is stable in neutral solutions, the concentration of HNO_2 in strongly acidic solutions exposed to air significantly decreases over the course of 1-2 hours; therefore, the spectral analysis of both non-irradiated and irradiated solutions were performed within minutes after removal from the irradiator and opening the vial containing the solution. The estimate of the combined standard error due to HNO_2 instability in acidic solution and uncertainty of spectrophotometric determination was less than $\pm 5\%$.

10.3.3 Methylurea

Concentration of MU was quantified by spectrophotometric titration. Aliquots of irradiated or non-irradiated reference solutions were diluted 10- or 20-times in 1 M HNO_3 and then titrated by a 0.100 M aqueous solution of NaNO_2 . Absorbance of the newly formed NMU was observed in a magnetic stirred 1 cm path-length quartz cuvette by the QE65000 spectrometer at 415 nm where it was the only absorbing species. Repeated titrations of methylurea aliquots led to an estimate of a $\pm 5\%$ uncertainty in the MU concentration value determined. Two set of experiments were performed. It was presumed that the concentration of Np in dissolved UNF solutions is approximately 1 mM, so a range of 1-15 mM concentrations of reactants was chosen for the initial set of experiments. The second set of experiments was performed with 50-100 mM of methyl urea. Due to a small dose rate available, relatively long exposure times were needed; hence, for correct evaluation of the radiation changes only, the reference samples (the

non-irradiated portions of studied solutions) were stored at the ambient temperature (22°C) during the same time as the irradiation time, and were analyzed together with the irradiated solutions.

10.4 Results and Discussion:

10.4.1 Nitrous Acid (HNO_2) Radiolytic Production

Solutions containing 1 – 8 M HNO_3 concentrations were irradiated for several days and concentrations of HNO_2 were determined by absorption spectroscopy in the wavelength range of 350-390 nm. Production of HNO_2 increases with dose (Figure 46) and with the initial concentration of HNO_3 , and evidently, a significant amount (mM) of HNO_2 can be produced and affect the chemistry of Np in extraction systems. However, due to either the instability of HNO_2 in nitric acid or its interaction with radiolysis products, the rate of HNO_2 production at higher doses (>30 kGy) decreases.

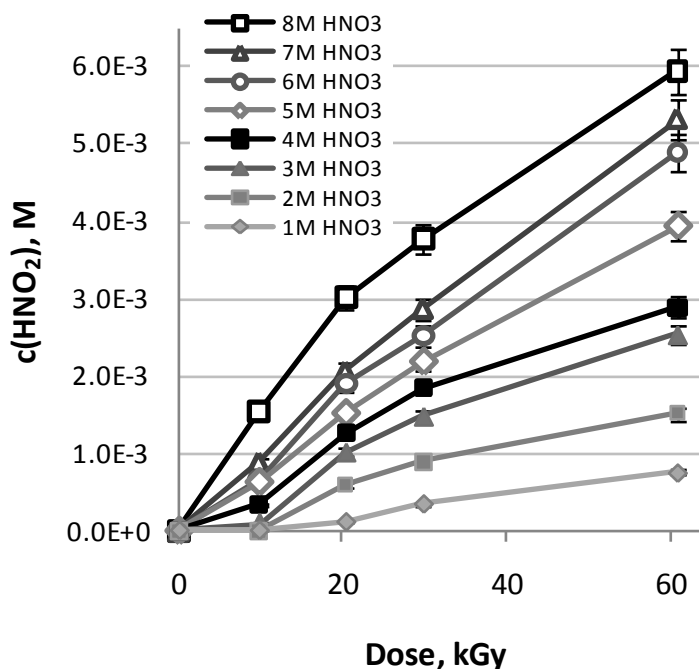


Figure 46 - Increase of the final concentration of HNO_2 produced by radiolysis of aqueous solutions of HNO_3 as a function of the effect of radiation dose (irradiation time).

For the non-replicate measurements, a $\pm 5\%$ error associated with the spectrophotometric measurements is indicated.

10.4.2 Methylurea

Experiments with NaNO_2 solutions in HNO_3 have shown that MU very rapidly combines with HNO_2 . MU itself has not been observed in the UV-VIS spectrum of its solution in HNO_3 , but it can be identified due to the formation of NMU. The absorption spectrum of the NO group is altered, as its amplified absorption band is widened with the resulting broad maximum shifting to longer wavelengths (Figure 47).

Additions of 1-10 mM MU in 4 M HNO_3 did not prevent the formation of significant quantities of HNO_2 during irradiation. Almost all MU/NMU was decomposed during the irradiation, as determined by the nearly unaltered spectra of HNO_2 that was produced during irradiation. Only the solutions with initial MU concentration 8 and 10 mM have slightly amplified spectra, indicating, that a small fraction of MU might have endured the effects of irradiation.

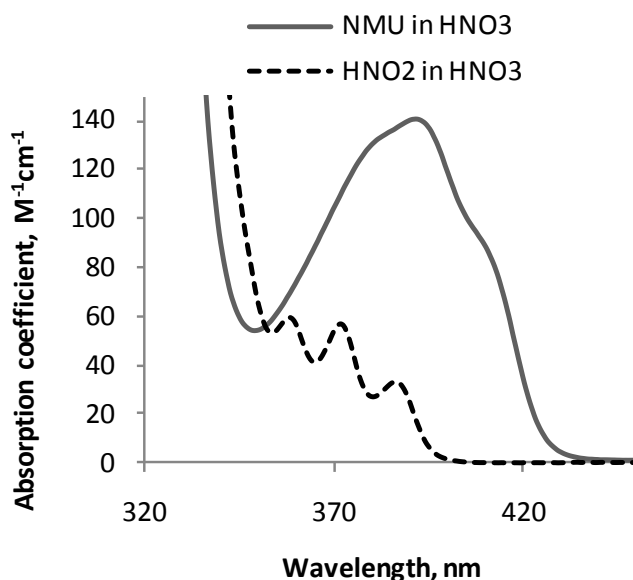


Figure 47 - Change of UV absorption spectrum of HNO_2 in HNO_3 by addition of methylurea (MU)

The new characteristic spectrum can be easily distinguished from the spectrum of HNO_2 in HNO_3 . The MU itself does not have any absorption spectrum in the UV-Vis region.

As a result of insufficient radiolytic stability of MU, experiments with larger concentrations of MU were also performed. Solutions of MU of varying concentration (5-500mM) in 4 M HNO_3 were prepared. In addition to previous experiments with low

concentrations of MU, 10mM NaNO₂ was added to the mixtures to simulate the presence of HNO₂ at the moment of utilization of the scavenger in a real separation process.

In Figure 48, the absorption spectra of post-irradiated solutions are compared. A decreasing trend in the final concentration of HNO₂ was observed for samples with MU concentrations of 5, 10, and 20mM, with no free HNO₂ detected in samples with the MU concentrations of 100 and 500mM. Concentration of HNO₂ bound with MU as nitroso-methylurea (Figure 47) was smaller than expected; a small increase in the post-irradiation concentration of NMU was observed for the initial concentrations of MU from 100 to 500 mM for which there is so far no conclusive explanation. Only a very small part of the NMU formed by either the reaction of MU with the initial 10mM HNO₂ or new HNO₂ formed by radiolysis of HNO₃ was observed. These results suggest that NMU is unstable in HNO₃ either by itself or degrades during irradiation.

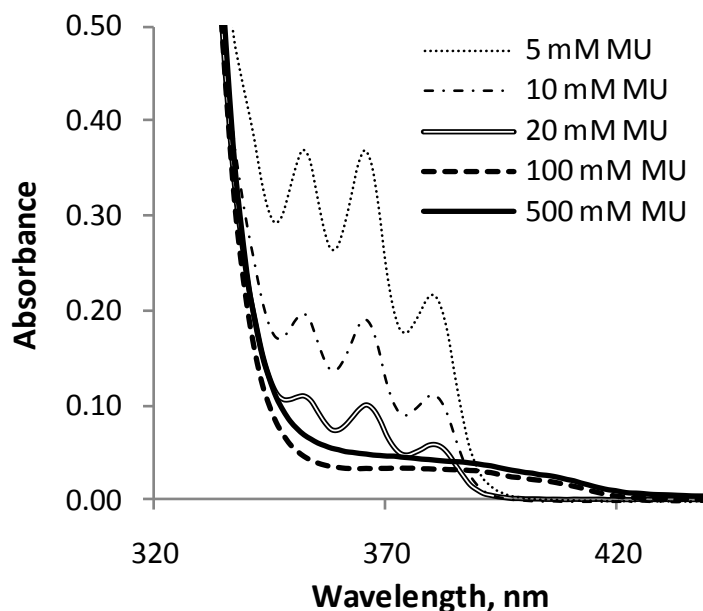


Figure 48 - Changes in absorbance spectrum of solutions of 4M HNO₃ with initial additions of 10mM NaNO₂ and variable concentrations of methylurea (MU) after irradiation by a dose of 40.5 kGy.

10.4.3 Methylurea Degradation by Gamma Irradiation

Solutions of 50 and 100 mM MU in 4 M HNO₃ were subjected to doses of 20, 40, and 60 kGy. Any remaining MU was determined by a spectrophotometric titration with

NaNO₂. Titration of the non-irradiated reference solutions of MU at the dose-equivalent time intervals showed no degradation of MU caused by a concentrated nitric acid.

The concentration of methylurea decreases linearly with dose (Figure 49). Only a small decrease in the radiolytic yields from 0.84 mM/kGy to 0.68 mM/kGy was observed for the solutions with 100 mM and 50 mM MU, respectively. This indicates that MU is being consumed by reactions with compounds or radicals that are produced by radiolysis at a constant rate.

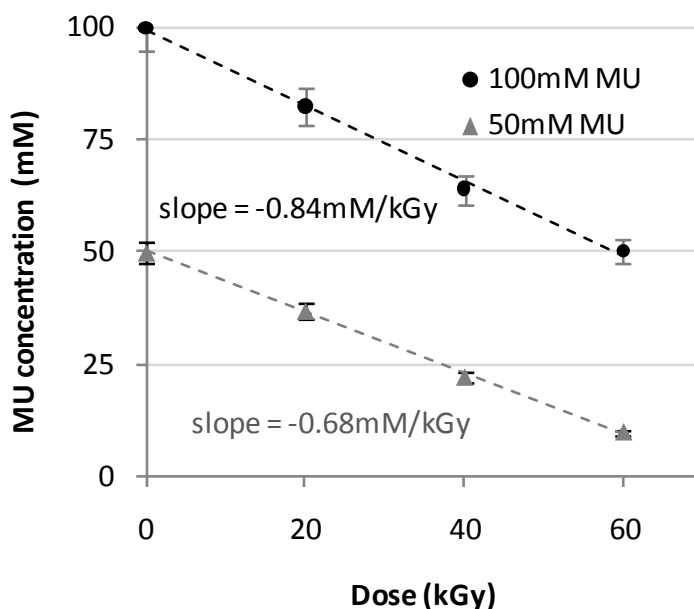


Figure 49 - Degradation of 50 and 100 mM solutions of MU in 4 M HNO₃ by radiolysis. Non-replicate measurements, error bars indicate a $\pm 5\%$ uncertainty range of the analytical method.

Acetamide

The addition of AcA had very little immediate effect on the spectrum of HNO₂. This is in agreement with the findings of Plimmer [164], who has observed significant evolution of N₂ gas caused by reaction (3) only the course of several hours. Therefore, only the post-irradiation effects are presented. The initial concentrations of 1-15mM AcA caused none or only a very small decrease of the final concentration of radiolytically produced HNO₂. Because of the long irradiation time, the AcA should have already extensively reacted with HNO₂, and, therefore, has been either completely consumed by the produced HNO₂ or degraded by the radiolysis.

10.4.4 Effect of Addition of Vanadium(V)

The addition of vanadium(V) did not seem to have any effect on the final redox speciation of neptunium after irradiation, despite a 5-fold excess of V(V), indicating that the oxidizing ability of vanadium has decreased during the irradiation. It was experimentally confirmed that V(V) is not directly reduced to V(IV) by HNO₂; therefore, it is likely reduced either by intermediate products of radiolysis or indirectly by Np(V) generated from reduction of Np(VI) by HNO₂.

10.4.5 Effect of Low Concentrations of MU and V(V) on the Redox Speciation of Neptunium after Irradiation

Solutions containing about 2 mM Np(VI) in 4 M HNO₃ and various concentrations of MU and vanadium(V) were irradiated with a dose of 0-61 kGy. The initial ratio of Np(VI):Np(V) was 95:5. A synergistic effect of the scavenging properties of MU toward HNO₂ and oxidizing properties of V(V) toward Np(V) were expected. It was assumed that if any HNO₂ was produced, it would be scavenged by MU. Moreover, if any Np(V) was produced by HNO₂, it would be re-oxidized back to Np(VI) by V(V).

However, it was found that neither the presence of 1-10mM MU or 1-10 mM V(V) nor the combination of 10mM MU and 10mM V(V) affected the reduction of Np(VI) to Np(V) with respect to the scenario of the absence of MU and addition of V(V). The ratio Np(VI):Np(V) decreased down to 50:50 in all cases.

The findings are a consequence of the fact that at a dose level of 61 kGy, all the 50 mM MU initially added has decomposed. More interestingly, the addition of vanadium(V) also did not alter the result, despite being in a 5-molar excess. Using higher concentrations (on the order of 50mM) of V(V) as a holding oxidant is of course possible and has been exploited in the past [108], but the consequential substantial increase in the weight of non-evaporable residues in the high level waste is not likely to be desired in a real separation process.

10.4.6 Effect of High Concentrations of Methylurea on the Redox Speciation of Neptunium after Irradiation

As the experiments with concentrations of MU below 10 mM were unsuccessful in preventing the reduction of Np(VI), new sets of irradiations with larger additions of MU were performed. Solutions of 1.3 mM neptunium (initial redox speciation was 5% Np(V) and 95% Np(VI)) in 4 M HNO₃, containing 50 and 100mM MU were subjected to integral doses of gamma radiation of 20, 40, and 60 kGy, and compared with their reference sample (a non-irradiated portion of the same solution, stored aside during the irradiation process). Analysis of the reference samples, presented in Figure 50, showed that a very slow reduction of Np(VI) into Np(V) in 4M HNO₃ occurs even without the influence of irradiation. After ~7 days, the initial ratio of Np(VI):Np(V) dropped from ~95:5 to ~75:25; however, the extent of Np(VI) reduction is clearly not significant enough to explain the changes taking place during irradiation (see below). This slow reaction is also not likely to be of importance in the shorter time-scales of real reprocessing conditions.

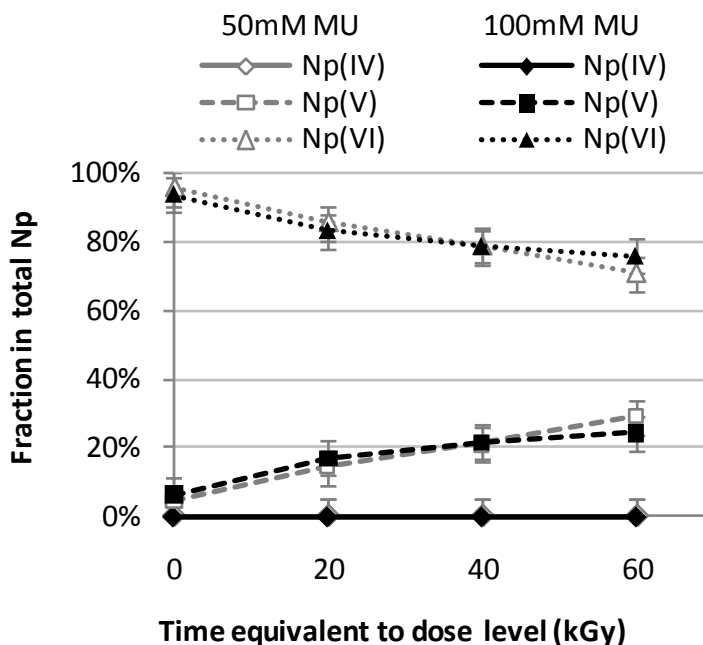


Figure 50 - Time dependent change of redox speciation of 1.3 mM Np in aq. 4 M HNO₃ containing 50 mM and 100mM methylurea of non-irradiated reference solutions.

For the non-replicate measurements, a $\pm 5\%$ error associated with the spectrophotometric measurements is indicated.

Redox speciation of irradiated samples was determined spectrophotometrically and is shown in Figure 51. Surprisingly, the reduction of Np(VI) was actually enhanced by the presence of higher concentrations of MU and progressed during the radiation exposure, resulting with Np(IV) as the dominant redox state of neptunium. The reduction reaction was faster for the samples with initial concentration of 100mM MU than with 50 mM MU; upon a dose of 40kGy, the ratio of Np(IV):Np(V) reached approximately 10:1, and additional 20kGy did not show any significant change.

As stated in the introduction above, the presence of hydrogen peroxide is negligible in solutions with higher HNO_3 concentrations, because it reacts with HNO_2 by reaction (1). However, since the nitrous acid is removed from the system by addition of MU, the concentration of H_2O_2 may grow and significantly affect Np speciation even in 4 M HNO_3 . As shown in Figure 51, all Np(VI) is first reduced to Np(V), which can be explained by the reaction with H_2O_2 [76, 168].

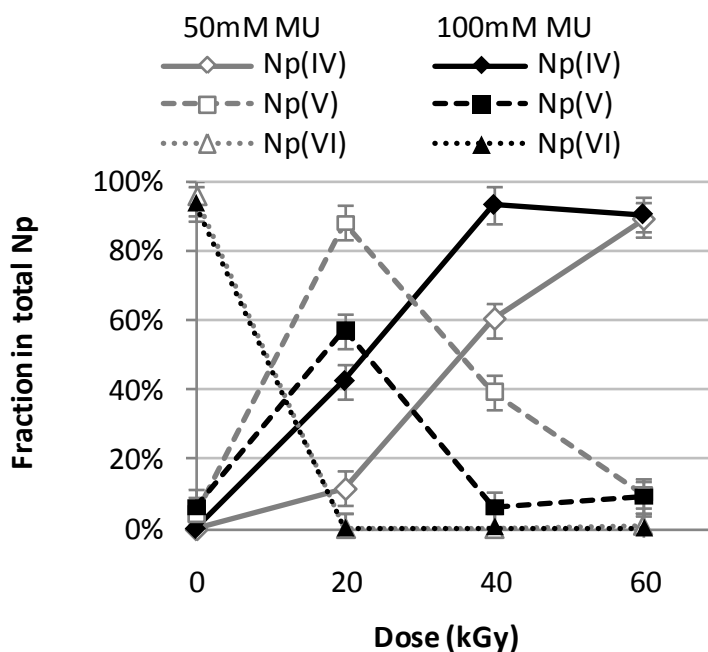


Figure 51 - Dose dependent change of redox speciation of 1.3 mM Np in aq. 4 M HNO_3 irradiated solutions containing 50 mM and 100 mM methyleurea.

For the non-replicate measurements, a $\pm 5\%$ error associated with the spectrophotometric measurements is indicated.

The reason for the next reduction step, from Np(V) to Np(IV), is less understood. The reduction more likely proceeds as a result of further reduction of Np(V) by accumulated

H_2O_2 , as the progress of the complete reduction of Np(V) to Np(IV) by H_2O_2 has been observed in solutions with HNO_3 concentrations greater than 4 M concentration [169]. Another possible mechanism for the reduction would be Np(V) disproportionation to Np(VI) and Np(IV), followed by reduction of Np(VI) by H_2O_2 [31]. During radiolysis of neptunium(IV) in 1-6 M HNO_3 , oxidation to Np(V) and Np(VI) was observed [170], and the primary oxidizing agent of Np(IV) was attributed to NO_3 radicals. Additional research is needed to explain why the effect of Np(IV) oxidation by $\text{NO}_3\cdot$ is overcome by reduction of Np(V) in the absence of HNO_2 and presence of H_2O_2 in concentrated nitric acid solutions.

10.5 Conclusion

In solutions of 4 M HNO_3 , acetamide (1-15mM) does not efficiently scavenge nitrous acid. Experiments performed with methylurea (1-500mM) indicate that doses of 40-60 kGy result in degradation of methylurea at concentrations lower than 50 mM, with radiation yield of 7-8 mM/kGy.

Attempts to prevent the radiolytic reduction of Np(VI) to Np(V) by additions of 1-10mM methylurea and 1-10mM vanadium(V) as a holding oxidant were unsuccessful. More than 50% of the Np(VI) was reduced to Np(V), which would be problematic for UNF reprocessing since Np(V) is poorly extracted by TBP. Unexpectedly, the radiolytic reduction of Np(VI) was promoted with additions of higher concentrations of methylurea (50 and 100 mM). With a dose of 60 kGy, about 90% of Np existed as the tetravalent oxidation state. This is likely caused by scavenging the nitrous acid by MU, which permits an increase of H_2O_2 concentration. Hence, high concentrations of MU did not prevent Np(VI) reduction; however, this could have a positive practical implication during the solvent separation process because Np(IV) is also well extracted by TBP. Nonetheless, application of MU has to be experimentally verified since the scavenging of HNO_2 by MU appears to significantly alter the redox processes during nitric acid radiolysis. In perchlorate media it was observed that Np(IV) may act as a reducing agent for Pu(IV) [171]. These effects may adversely affect the extractability of plutonium, since Pu(III) is very poorly extracted by TBP.

11 REDUCTION OF NP(VI) IN IRRADIATED SOLUTIONS OF NITRIC ACID

Martin Precek, Alena Paulenova, and Bruce J. Mincher

Procedia Chemistry

Elsevier B.V. (Corporate Office)

Radarweg 29

Amsterdam 1043 NX, Netherlands

This manuscript was submitted in June 2012 as a peer-reviewed proceeding paper for the conference: ATALANTE 2012 – Nuclear Chemistry for Sustainable Fuel Cycles, September 2-7, 2012, Montpellier, France.

If accepted, it will be published on-line in *Procedia Chemistry* in December 2012

URL: <http://www.elsevier.com/locate/procedia>

11.1 Abstract

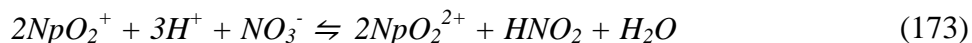
The reliable separation of neptunium from dissolved nuclear fuel assumes the ability to maintain a preferred oxidation state. However, regardless of its initial redox speciation, a series of reactions occurs in nitric acid to create a mixture of oxidation states including Np(V), Np(VI) and sometimes Np(IV). To further complicate the situation, irradiated solutions such as fuel dissolution contain both transient and long-lived radiolysis products which may be strongly oxidizing or reducing. Thus, irradiation may be expected to impact the equilibrium distributions of the various neptunium valences.

We have irradiated nitric acid solutions of neptunium with ^{60}Co gamma-rays, and measured radiolytically-induced changes in neptunium valences, as well as the nitrous acid concentration, by UV/Vis spectroscopy. It was found that in 4M HNO_3 at low absorbed doses, the oxidizing radicals oxidized Np(V) to Np(VI). However, as the irradiation proceeded the concentration of nitrous acid became sufficient to reduce Np(VI) to Np(V), and then continued irradiation favored this reduction until an equilibrium was achieved in balance with the oxidation of Np(V) by nitric acid itself. The starting abundances of the two neptunium valences did not affect the final equilibrium concentrations of Np(V) and Np(VI), and no Np(IV) was detected.

11.2 Introduction

In aqueous solutions of nitric acid, neptunium may exist as Np(V), Np(IV) and/or Np(VI). The cationic charge of Np(V) ($z = 2.2$ [172]) in its monovalent dioxocation is the lowest among actinides and causes the lowest separation yields in both liquid/liquid and solid/liquid separations, while higher cationic charges of both Np(VI) and Np(IV) provide satisfactory yields. The success of a selected separation method relies on the ability to maintain neptunium in an appropriate oxidation state.

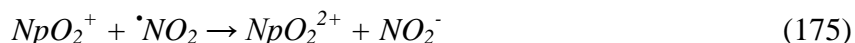
Regardless of the initial valence state of Np, a series of redox reactions leading to the generation of mixed valence solution occurs. The valence state of neptunium in aqueous nitric acid was reported to be a function of the concentration of nitrous acid, and according to equation (2) nitrous acid should reduce Np(VI), favoring production of Np(V) [49]:



Excess nitrite has been used to set the valence at Np(V) [17, 145]. On the other hand, HNO₂ appears to behave as a catalyst, promoting the rate of oxidation of higher relative abundances of Np(V) by nitric acid. With mixed success, this effect has been utilized industrially during separation of neptunium by the PUREX process [2]. An explanation of this behavior has been proposed by Tochiyama et al [55], who suggested that the catalytic effect of nitrous acid is facilitated by the $\cdot\text{NO}_2$ radical from N₂O₄, which is formed by interaction of nitric and nitrous acids:



The $\cdot\text{NO}_2$ radical then acts as the actual oxidizing agent:



and the oxidation of Np(VI) in the presence of low concentrations of HNO₂ may actually be due to reaction of Np(V) with the nitrogen dioxide radical ($\cdot\text{NO}_2$), rather than with HNO₂ itself [173].

Neptunium speciation thus clearly depends on the concentration of HNO₂ in a nitric acid solution. Nitrous acid is produced during processing of spent nuclear fuel by multiple sources, primarily from dissolution of the spent oxide fuel and from radiolysis of both aqueous and organic solutions of nitric acid [174]. HNO₂ is a weak acid with a low dissociation constant ($\text{pK}_a = 3.3$ at 25°C, [128]), which leads to almost complete protonation of nitrite anions in solutions with higher concentrations of nitric acid, which are relevant to reprocessing of spent nuclear fuel. Once in molecular form, nitrous acid is also easily extracted by tributylphosphate into the organic phase [175], where it also influences the chemistry of extracted neptunium [57].

This study was conducted to analyze the effect of gamma radiation on neptunium redox speciation in aqueous nitric acid solutions, primarily to identify the importance of the radiolytic production of nitrous acid.

11.3 Experimental

Acidic solutions of ²³⁷Np were prepared from on-hand stocks available at the Idaho National Laboratory (INL) and Oregon State University (OSU). Concentrations of nitric acid were confirmed by titration with NaOH, standardized by potassium biphthalate.

Concentration of ^{237}Np was confirmed spectroscopically and by gamma-spectrometry on a high-purity germanium detector. Prepared solutions were irradiated in sealable 1-cm pathlength cuvettes and 0.4cm width (supplied by Hellma USA for INL and by Starna Cells, Inc. for OSU) that have fused quartz optical windows that do not darken upon γ -irradiation.

The pre-irradiation oxidation state of Np was adjusted electrochemically using a BASi Epsilon E2 potentiostat and a PWR-3 current booster. The electrolysis was performed in a custom-built H-cell with the oxidizing and reducing compartments separated by a glass frit. The working electrode was a coiled platinum wire inserted into a constantly stirred Np solution, while the auxiliary compartment contained a wire platinum electrode and Ag/AgCl reference electrode. Hexavalent Np was prepared by application of +1250 mV potential to the working electrode while Np(V) was prepared at +700 mV [176].

Irradiation was performed using ^{60}Co -sources (Nordion Gammacell 220) available at both the Idaho National Laboratory (dose rate 7.0 kGy/h) and Oregon State University (dose rate 0.38 kGy/h). The dose rates for both irradiators were determined using standard Fricke dosimetry and the absorbed doses to the samples were calculated based on the duration of the irradiation.

The post-irradiation concentrations of HNO_2 , Np(V) and Np(VI) were determined by the UV/Vis/nIR absorption spectroscopy (Cary 6000i; OLIS RSM, OceanOptics QE6500).

The absorbance of Np(V) was measured using its sharp absorbance peak at 981 nm, while the Np(VI) concentration was determined at the maximum absorbance of the broad peak centered at 1225 nm. The molar extinction coefficients were determined independently for each instrument. The aqueous spectra of the nitrite anion and nitrous acid are well known [137]: the broad absorption band of the NO_2^- anion between 300-400 nm transforms into a distinct peak multiplet for molecular HNO_2 .

11.4 Results and Discussion

11.4.1 Effects of gamma radiation on neptunium(VI) in 4M HNO_3

A solution of pentavalent neptunium in 4M HNO_3 was first electrolytically oxidized to predominantly Np(VI), with a resulting molar fraction of Np(VI) up to 94% and 6% of Np(V) in 4M HNO_3 . Aliquots of this solution were then irradiated with a dose rate of 7.0

kGy/h; also an aliquot was saved as a reference. The results for the irradiation of such a solution with a total Np concentration 6 mM are shown in Figure 52. No tetravalent Np was detected in any post-irradiation spectrum, and a successful mass balance was always achieved as the sum of Np(V) and Np(VI). No changes in the distribution of neptunium species with time were observed in the non-irradiated reference solution.

Initially, at the lower radiation doses, these samples showed oxidation of the small amount of Np(V) to Np(VI). This effect is most likely explained by the effect of oxidizing $\bullet\text{NO}_3$ and $\bullet\text{NO}_2$ radicals produced from nitric acid radiolysis, combined with the oxidizing effects of $\bullet\text{OH}$ radical from water radiolysis. However, by ~ 1 kGy, the oxidation of Np(V) ended, and the reduction of Np(VI) to Np(V) by the radiolytically produced HNO_2 began to occur and continued to the end of the experiment, to a total dose of 18.5 kGy.

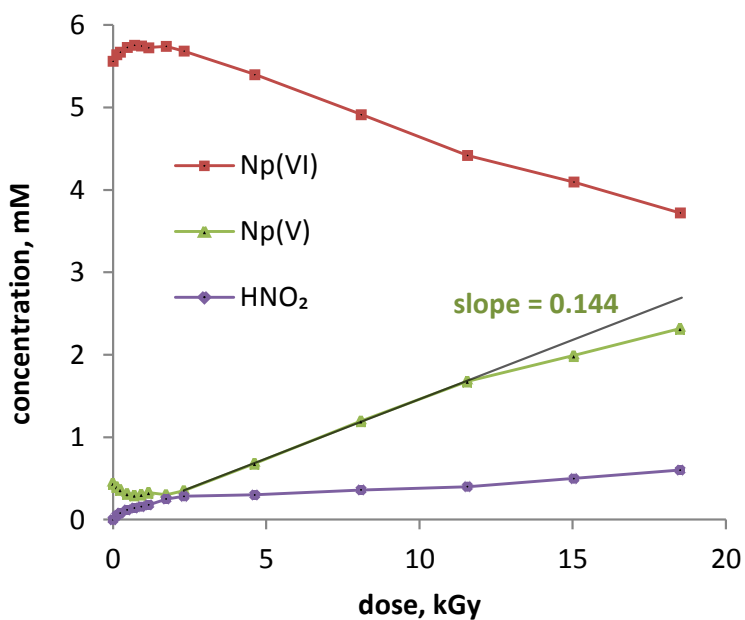


Figure 52 - The concentrations of Np(V), Np(VI) and HNO_2 versus absorbed dose for 6 mM initially $\sim 93\%$ Np(VI) in 4 M HNO_3 , dose rate 7.0 kGy/h

The linear portion of the obtained data for doses between 2.7 and 11.6 kGy (Figure 52) allows for the calculation of a radiolytic yield for Np(V) of $G_{\text{Np(V)}} = 0.144 \mu\text{mol/J}$. This value appears to be almost a double of the net radiolytic yield of HNO_2 of $0.076 \mu\text{mol/J}$ that could be predicted for 4M HNO_3 from data on HNO_2 yields determined previously

by Burger and Money [174]. As expected from the redox equilibrium (2):
$$Np(V) \approx 2 \times G_{HNO_2}$$

It can also be seen in Figure 52 that the concentration of radiolytically-produced HNO_2 grows continuously with increasing absorbed dose in the irradiated solutions; however, the initial rate slows after ~ 1 kGy when the concentration of HNO_2 reached 0.16M. This break in the HNO_2 -growth slope may be explained by the consumption of HNO_2 by $Np(VI)$ which results in lower effective yields of HNO_2 than in irradiated HNO_3 in absence of neptunium [174].

11.4.2 Influence of nitric acid concentration

Four different samples of 2.5 mM neptunium were prepared in sealable quartz semi-micro cuvettes (Starna Cells) with a 1cm pathlength. Three of these samples contained a $Np(VI):Np(V)$ ratio of 93:7 and were prepared in three concentrations of nitric acid (0.5, 1.0 and 4.0 M HNO_3). They were observed to have long-term stability, and the 4M HNO_3 sample was labeled as #1. Another 4M HNO_3 sample (#2) was prepared by reducing the initially 93% $Np(VI)$ with a substoichiometric amount of hydrogen peroxide to $Np(V):Np(VI)$ ratio close to 1:1 [76]. The redox reaction was complete within 2 hours. Irradiation of sealed vials was performed with a low dose rate of 0.38 kGy/h. The irradiation was practically continuous with 0.5 hour interruptions for measurement. The concentration of HNO_2 in the irradiated samples was determined by the deconvolution of the known nitrous acid spectrum from the absorption shoulder of neptunium-VI in the UV region 350-400nm. The error in the value of HNO_2 concentration was estimated as 0.05mM. The results of the experiment are summarized in Figure 53 and Figure 54:

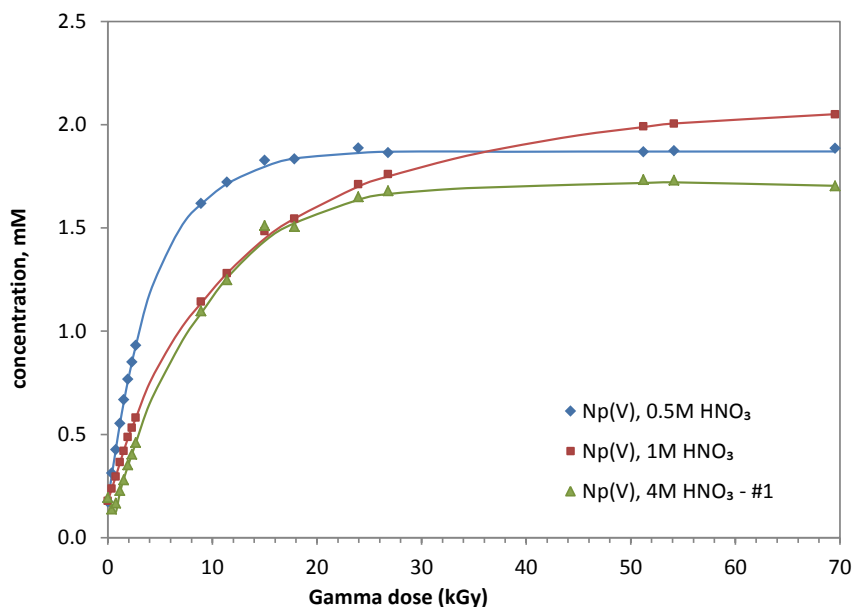


**Figure 53 - Irradiation at the 0.38 kGy/h dose rate:
Concentration profile of Np(V) versus absorbed dose in concentrations of HNO₃.
Np(VI) concentration (not plotted) should be assumed to be complementary to Np(V),
balancing the 2.5 mM of total Np**

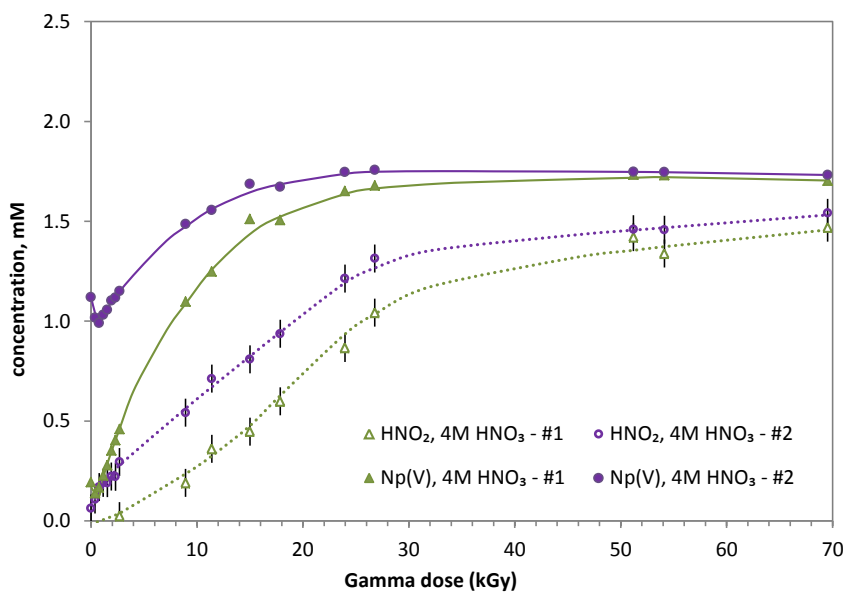


**Figure 54 - Irradiation at the 0.38 kGy/h dose rate:
Concentration profile of Np(V) and HNO₂ versus dose in two Np samples in 4M HNO₃.
The samples #1 and #2 differ in their initial fraction of Np(V)
in total Np: #1=7%, #2 =45%.**

The effect of radiation on neptunium oxidation state for all 3 different nitric acid concentrations (Figure 53) caused reduction of Np(VI) to Np(V), ultimately approaching

a predominantly pentavalent state. However, in the 4M HNO₃ samples (Figure 54), the initial Np(V) oxidation to Np(VI) was observed until 1 kGy of absorbed dose, similar to the effects observed for the higher dose rate in Figure 52. This initial oxidation of Np(V) and the production of HNO₂ was not observed at the lower nitric acid concentrations.

For the initial range of absorbed doses between 0.4 and 2.5 kGy, the observed radiolytic yield of Np(V) in 0.5, 1.0 and 4.0 M nitric acid with initial concentration of 93% Np(VI) was of 0.27, 0.151 and 0.146 $\mu\text{mol/J}$, respectively. The value of the Np(V) yield 0.146 $\mu\text{mol/J}$ in 4 M HNO₃ is in agreement with the radiolytic yield determined in the previous experiment with 18-fold higher dose rate (Figure 52).

The decrease in Np(V) yield with increasing HNO₃ concentration suggests that the reducing effect due to the radiolysis of aqueous nitric acid cannot be primarily attributed to the reaction with radiolytically produced HNO₂, at least not in lower concentrations of HNO₃. Reducing radiolytic species, such as H₂O₂, and H₂ are other possible candidates, since their yield increases with decreasing HNO₃ concentration [177].

Only the samples with 4M HNO₃ exhibited any concentrations of HNO₂ above 0.05 mM. Absolute differences in the HNO₂ concentration measured for the two 4M HNO₃ samples (dotted lines in Figure 54) can be explained by the effect of spontaneous oxidation of Np(V) by nitric acid (2), producing an excess of HNO₂ in the sample #2 (sample with the 45:55 initial ratio Np(V):Np(VI)).

During the course of the irradiation, both the 4M HNO₃ samples trended toward a common steady state redox speciation with an approximate ratio of Np(V):Np(VI) = 70:30, which was reached near 30 kGy of absorbed dose. At this point the increase in the HNO₂ concentration also slowed down, approaching a steady state concentration. The observed slope for initial growth of HNO₂ in both 4M HNO₃ samples was of ~ 0.04 mM HNO₂/kGy, which is approximately 50% lower than the yield that was observed in the absence of neptunium [174].

After 20 kGy dose, the fast increase in the Np(V) concentration slowed down, achieving a steady state concentration at about 30kGy. At that point also the linear increase of the HNO₂ concentration slowed to approach a steady state concentration. This may indicate the loss of HNO₂ to the gas phase, since only 0.6 mL of the 2.6 mL cuvette volume was

occupied by the liquid phase. Nitrous acid has been known to decompose into the headspace above the solution over longer periods of time [129].

It is interesting to note that the equilibrium yield of Np(V) in irradiated 1 M HNO₃ (Figure 53) is higher than in both 0.5 and 4M HNO₃. We suggest that the increase of steady-state concentration of Np(V) between 0.5 and 1M HNO₃ can be explained by the decreasing concentration of •OH radicals, primarily responsible for reoxidation of Np(V) back to Np(VI), by their reaction with molecular nitric acid. The rate constants for the reaction of •OH with molecular HNO₃ ($k = 1.4 \times 10^8 \text{ M}^{-1}\text{s}^{-1}$)[120] and with Np(V) ($k = 4.3 \times 10^8 \text{ M}^{-1}\text{s}^{-1}$)[116] are of comparable magnitude. Due to incomplete protonation of HNO₃ [178], the concentration of molecular HNO₃ in 0.5M and 1M nitric acid is approximately 4-fold higher, 7.4 and 27mM, respectively. Thus, the steady-state concentration of the •OH radical can be expected to decrease (by ~ 60%) as a result of increased scavenging of the hydroxyl radical by molecular HNO₃, and consequently, the absolute rate of oxidation of 2mM Np(V) by the •OH radical gets approximately 2.5-times slower. The •NO₃ radical also acts as an oxidizer of Np(V); however, the rate constant of this reaction ($k = 1 \times 10^5 \text{ M}^{-1}\text{s}^{-1}$)[173] is lower by three orders of magnitude compared to the rate of Np(V) oxidation by the •OH radical. Further increase in nitric acid concentration from 1 to 4 M leads to considerably greater yields of oxidizing •NO₃ and •NO₂ radicals (174) which decrease the Np(V) steady-state concentration.

11.5 Conclusion

During irradiation of neptunium solutions in nitric acid, nitrous acid represents an important radiolytically produced species. In 4 M HNO₃, the rise of HNO₂ concentration is followed by reduction of Np(VI) to mostly the pentavalent state; however, in the 1 and 0.5 M HNO₃ solutions of neptunium the reduction of Np(VI) has not been accompanied by a quantitative rise in HNO₂ concentrations. Eventually, a steady-state ratio was established between Np(V) and Np(VI) in the irradiated aqueous nitric acid solution, which occurred regardless of their initial relative concentrations.

The initial production of radical species during irradiation of 4M HNO₃ by different dose rates favored Np(V) oxidation; however, as the irradiation proceeds, the HNO₂ concentration increases and the Np(VI) reduction to Np(V) becomes predominant. A

lower degree of the Np(VI) reduction to Np(V) was favored in 4 M nitric acid, as opposed to 1 and 0.5 M HNO₃ solutions, which is related to the different yields of the radical species versus molecular radiolysis products in these matrices.

Comparison of two irradiation experiments of Np in 4M HNO₃ showed that the radiolytic yield of Np(V) was affected neither by the dose rate nor the total concentration of Np in these experiments.

12 RADIOLYTIC PRODUCTION OF NITROUS ACID IN THE HNO₃ - TBP EXTRACTION SYSTEM

Martin Precek, Bruce J. Mincher and Alena Paulenova

This manuscript was prepared for submission to Separation Science and Technology

12.1 Abstract

Analysis of radiolytic production of HNO_2 under the effect of gamma radiation in the HNO_3 /tributylphosphate (TBP) system has been performed. Radiolytic yields of HNO_2 in the 30% TBP in n-dodecane were found to increase from 0.26 to 0.48 $\mu\text{mol}/\text{J}$ with increasing the concentration of HNO_3 in the organic phase from 0.23 to 0.97 mol/L. This is significantly higher than from HNO_3 present in the aqueous phase that the organic phase was in contact with, most likely due to much smaller presence of nitrite-scavenging intermediate species produced by the radiolysis of water (such as is hydrogen peroxide).

12.2 Introduction

Nitrous acid (HNO_2) is an important redox-active compound that is produced during processing of spent nuclear fuel by multiple sources, primarily from dissolution of the spent oxide fuel and from radiolysis of both aqueous and organic solutions of nitric acid. [53] Presence of nitrous acid significantly influences speciation of neptunium and plutonium in aqueous solutions of nitric acid (HNO_3) and their behavior during separation processes. Distribution of these actinides between an organic phase based on tri-n-butylphosphate (TBP) in n-dodecane and aqueous nitric acid solutions is defined by their oxidation state [125]. A high nitrous acid content in the aqueous phase acts as a stabilizer of the extractable tetravalent plutonium [125] but also leads to reduction of a significant portion of neptunium to its inextractable pentavalent state [53, 126]. HNO_2 also influences the redox chemistry of actinides in the organic phase; a review on these reactions has been recently published by Marchenko et al. [57].

Nitrous acid is a weak acid with a small dissociation constant ($\text{pK}_a = 3.3$ at 25°C , [128]), which makes it almost entirely protonated under conditions of higher concentrations of nitric acid relevant to processing of spent nuclear fuel. Once in molecular form, nitrous acid is easily extracted by tributylphosphate into the organic phase [175]. The other important source of HNO_2 in organic phase is the direct radiolysis of the extracted nitric acid; however, only the radiolytic production of HNO_2 in aqueous nitrate solutions has been studied extensively in the past [155, 170, 174, 179, 180, 181, 182, 183, 184, 185]. Many studies were also devoted to investigation of the effect of gamma radiolysis of organic TBP solutions, but the focus was chiefly on the impact of radiolytic degradation

of TBP and the diluent on the efficiency of separation of elements [117, 186, 187, 188]. The 1959 Hanford report by Burger and Money [174] appears to be the only published work that studied the specific issue of nitrous acid radiolytic production in the organic TBP phase. However; it is important to note that investigations of photolytic [189] and sonolytic [190, 191] methods of artificial nitrous acid production have been performed too.

12.3 Experimental

12.3.1 Chemicals

Distilled deionized water (Barnstead Nanopure, 18 M Ω ·cm resistivity) was used in all experiments. Stock solutions of aqueous nitric acid were prepared from concentrated HNO₃ (68 w.%, EMD Chemicals GR ACS grade) and their concentration was determined to $\pm 0.3\%$ precision by potentiometric titration (Mettler-Toledo DL58 automatic titrator) using NaOH standardized by potassium hydrogen phthalate (Analytical Reagent, Mallinckrodt). Stock solutions of sodium nitrite were prepared by dissolution of NaNO₂ (Mallinckrodt, analytical reagent) in neutral distilled water and used as a source of nitrite anions, and, consequently, molecular nitrous acid when the acidity of solution was brought to pH < 3. The organic phase was prepared by dilution of tri-n-butylphosphate (TBP, Alfa Aesar) in n-dodecane (Alfa Aesar) to 30% by volume, and purified from possible tracers of dibutylphosphate by three-fold washing with 1 M sodium carbonate, and then pre-equilibrated with aqueous phase by five-fold agitation with solutions of desired concentration nitric acid. One minute vortexing time was used.

Distribution ratios of HNO₂ between 30% TBP and nitric acid solutions were determined by 1:1 volume ratio experiments, performed in duplicate. The decrease in aqueous HNO₂ concentration was determined spectrophotometrically. The concentration of nitric acid extracted into the equilibrated organic phase was determined by direct titration of 1 mL aliquot of organic phase by 0.1M NaOH in a large volume of aqueous solution (40 mL). According to [191], it can be assumed that a vigorous mixing leading to an emulsion ensured that all nitric acid was stripped from the organic phase and neutralized in the

aqueous phase by the additions of the basic titrant. The results on the HNO₃ extraction agree with data reported earlier [192].

12.3.2 Nitrous acid instability, sample preparation and irradiation

Nitrous acid disproportionates into NO_x gases (including nitric oxide, NO) which are volatile and reactive toward oxygen, and thus HNO₂ decomposes with a half-life of single hours in both aqueous and organic solutions if kept in vessels opened to air. The rate of decomposition is much increased if the contact with the gas phase is artificially promoted, e.g. by bubbling of inert gas through the solution [129, 130]. For this reason significant losses of HNO₂ have been observed in solvent extraction separation cascades, where vigorous mixing of the solutions under an inert gas blanket occurs [131]. Decomposition of HNO₂ can be prevented by using a hermetically sealed reaction vessel when nitric oxide (NO) vapors create a cover gas blanket; therefore, closed screw-cap vials almost completely filled with liquid (<5% headspace) were used in all experiments. A control test with irradiation of identical solutions enclosed in vials with the air:liquid ratio of 3:1 didn't lead to any measurable production of nitrous acid, which indicated that all nitric oxide produced was volatilized and possibly consumed by oxygen in the gas phase. Samples for irradiation were therefore sealed in nitrogen atmosphere inside a glove box. However, complete removal of dissolved oxygen by bubbling nitrogen through the samples was not attempted in order to prevent evaporation of water from the organic phase.

Samples were irradiated for different periods in a "GammaCell 220" ⁶⁰Co gamma-ray irradiator with a dose rate of 7.0-7.3 kGy/hour. Dose rate variation over the experimental period due to the radioactive decay of ⁶⁰Co (T_{1/2} = 5.3 y) was determined by Fricke dosimetry. To minimize loss of HNO₂ by volatilization, the irradiated vials were opened and transferred into quartz cuvettes for spectrophotometric analysis just prior to the measurements. For the single-phase experiment, the samples were sealed in 0.7 mL snap-cap polypropylene centrifuge vials (VWR), while the samples for irradiation of the biphasic system were prepared in a 1:1 aqueous-to-organic volume ratio in 2 mL screw-cap cryogenic vials (Thermo Scientific). Vials were shaken in between the individual dose increments. Kinetic extraction experiments confirmed a rapid distribution of HNO₂

into the organic phase even without mixing; hence, the measured concentrations of radiolytic HNO_2 in biphasic experiments are considered close to the extraction equilibrium of HNO_2 in organic and aqueous phases.

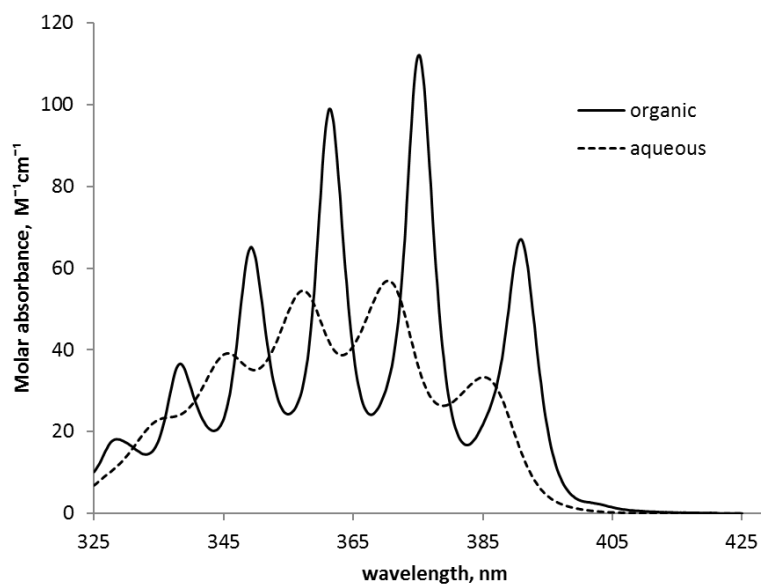


Figure 55 – Normalized absorption spectrum of HNO_2 in organic (0.23 M HNO_3 in 30% TBP) and aqueous (1 M HNO_3) phase

12.3.3 Spectrophotometry

Quantitative determination of HNO_2 concentration was performed using UV-VIS spectrophotometry with an OceanOptics QE65000 fiber-optic diode array spectrophotometer and with OLIS RSM 1000 double grating monochromator.

Absorption coefficients of organic HNO_2 were determined by contacting small aliquots of sodium nitrite solution with 40-fold excess of acidified 30% TBP solution in a magnetically stirred cuvette. Aqueous spectra of the nitrite anion and nitrous acid are well known [137]: the broad absorption band of the NO_2^- anion between 300 - 400 nm transforms into a distinct peak multiplet for molecular HNO_2 .

When HNO_2 is extracted into 30% TBP/n-dodecane solvent, the individual absorption peaks become better resolved and deeper, while also getting slightly red-shifted (bathochromic shift) compared to aqueous solutions (see Figure 55). This change increases the estimated limit for spectrophotometric detection of HNO_2 from 0.1 mM in aqueous phase to 0.05 mM in the organic phase. The 30% TBP/n-dodecane solvent

doesn't have any significant absorption in the UV-VIS spectrum. However, as a result of irradiation of the organic phase saturated with HNO_3 , other compounds besides HNO_2 are produced, some of them, identified as nitro-paraffins [117], have a smooth absorption shoulder starting from 450 nm and intensifying toward shorter wavelengths, adding a yellow color to the solvent. As a result of judicious evaluation of measured spectra, a 15% systematic error was estimated for the values determined for irradiated organic solutions as opposed to the < 5% systematic error associated with the analysis of aqueous samples.

12.4 Results and Discussion

12.4.1 Extraction of HNO_2 into 30% TBP/*n*-dodecane

The results of distribution studies indicate that HNO_2 is much better extracted from acidic solutions than HNO_3 (see Figure 56), in agreement with previously published values [72, 131, 174, 193]. It was discussed by Burger and Money [174] that the difference is primarily caused by nearly all nitrous acid being present in non-dissociated molecular form in the acidic solution (as opposed to nitric acid which is mostly dissociated). Compensating for the known magnitude of HNO_3 dissociation [158] reveals a similar magnitude of distribution values for both the molecular HNO_3 and HNO_2 . Fletcher et al. [175] spectroscopically determined that the extracted solvate complex can be attributed to the 1:1 adduct, TBP-HONO, which is a simpler case than distribution of HNO_3 where three adducts for TBP with HNO_3 (1:1, 1:2 and 2:1) were reported [192]. Although the hydrogen bond in the 1:1 complex of TBP with HNO_2 is weaker than in the same complex with HNO_3 [174], the molecular HNO_2 is more soluble in the non-polar organic phase, so tributylphosphate extracts nitrous acid almost quantitatively [175]. Competition of extracted water with HNO_2 and HNO_3 for the free TBP available for solvation [72] leads to reduced extraction of nitrous acid with increasing concentration of nitric acid in the aqueous phase. A similar trend was measured also for radiolytically produced HNO_2 (no initial HNO_2 added; see Figure 56).

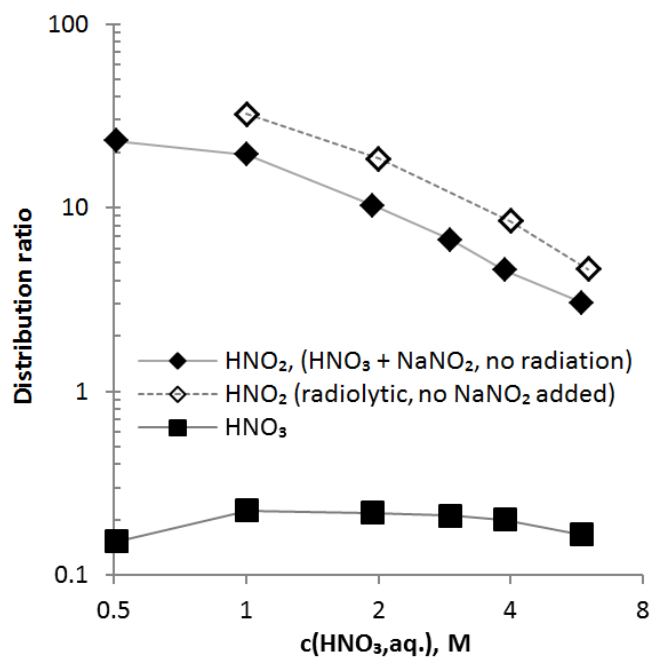


Figure 56 – Distribution ratios of HNO_3 and HNO_2 for the non-irradiated and irradiated (61kGy) system of the 30% TBP/n-dodecane and aqueous solutions of nitric acid

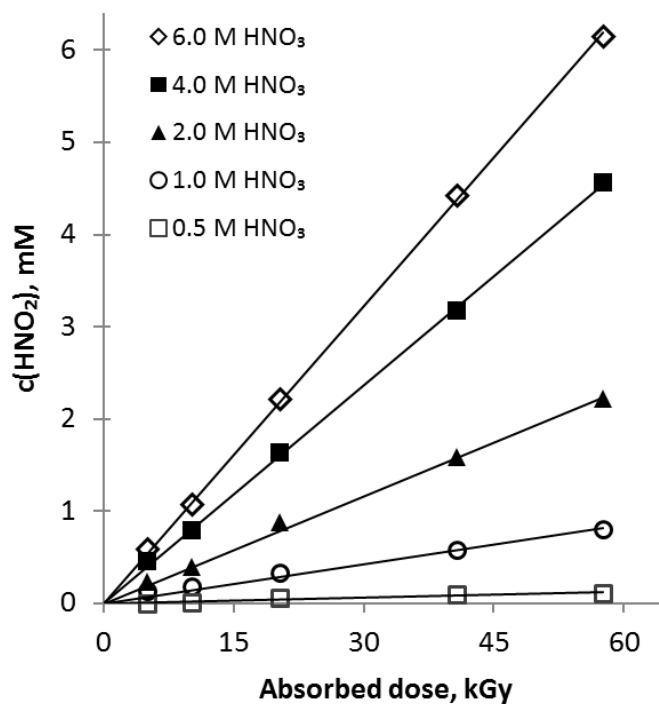


Figure 57 – Concentrations of nitrous acid ($\pm 5\%$ system. error), produced by irradiation different initial concentrations of HNO_3 in aqueous solutions.

12.4.2 Radiolytic production of HNO₂ in aqueous and organic solutions

12.4.2.1 Aqueous phase

Aqueous solutions containing different concentrations of nitric acid (0.5 – 6.2 M HNO₃) were irradiated up to a dose of 58 kGy. Post-irradiation analysis confirmed that production of HNO₂ increases with radiation dose (Figure 57) and with the initial concentration of HNO₃. Within the dose range studied, concentrations of produced HNO₂ were not observed to reach a plateau. Also, the aqueous yields of HNO₂ were found to be close to proportional to the concentration of nitric acid. Evidently, a significant amount of HNO₂ can be produced and affect the chemistry of neptunium and plutonium in separation systems [53, 125, 126].

Radiolytic production of HNO₂ in aqueous nitric acid solutions has been studied extensively in the past [155, 170, 174, 179, 180, 181, 182, 183, 184, 185]; however, many authors were mainly interested in the primary yields of HNO₂. These are substantially larger than the net yields due to rapid interactions of HNO₂ with other products of nitric acid radiolysis, primarily hydrogen peroxide (H₂O₂) [83]. Comparison of the results of the present study with past studies of net radiolytic yields of HNO₂ summarized in Table 1 indicate an approximate value of $G_{\text{HNO}_2, \text{aq}} \approx (0.02 \mu\text{mol J}^{-1}) \times C_{\text{HNO}_3, \text{aq}}$.

Table 12 - Overview of results of studies of radiolytic* yields of HNO₂ from aqueous HNO₃

Study	$G_{\text{HNO}_2}/C_{\text{HNO}_3}$ $\mu\text{mol J}^{-1} \text{M}^{-1}$	Conditions
1959 – Burger & Money [174]	0.019	3 M HNO ₃ , dose rate = 9 kGy/h
1963 – Vladimirova et al. [180]	0.019	(1-8) M HNO ₃ , dose rate = 0.006 - 5.9 kGy/h
1981 – Kulikov et al. [170]	0.018	(1-6) M HNO ₃ , dose rate = 1.9 -7.7 kGy/h
1984 – Andreichuk et al. [183]	0.019	6 M HNO ₃ , dose rate = 11.5 kGy/h *
2012 – Precek et al. [this study]	0.019	(0.5-6.2) M HNO ₃ , dose rate = 7.0 kGy/h

* Irradiation with ⁶⁰Co gamma-rays was used in all studies with the exception of the study Andreichuk et al. [183] in which internal 5.8 MeV alpha radiation from ²⁴⁴Cm (18.1 y half-life) was used (concentration of 4.7mM ²⁴⁴Cm can be inferred).

12.4.2.2 Organic phase

The radiolytic production of nitrous acid was measured for the solutions of 30 % of TBP in n-dodecane equilibrated with four different concentrations of aqueous nitric acid. The cumulative radiolytic yield of HNO_2 increased with absorbed dose and the concentration of nitric acid in the organic phase, but leveled off at concentrations higher than approximately 0.8 M org. HNO_3 , which is in equilibrium with aqueous 4 M HNO_3 . The non-zero intercepts of the cumulative yield of HNO_2 versus absorbed dose in Figure 58 indicate that nitrous acid production starts only after a certain dose is absorbed (~ 5 kGy) in the organic solvent. This threshold value could likely be a result of remaining dissolved oxygen in the solvent.

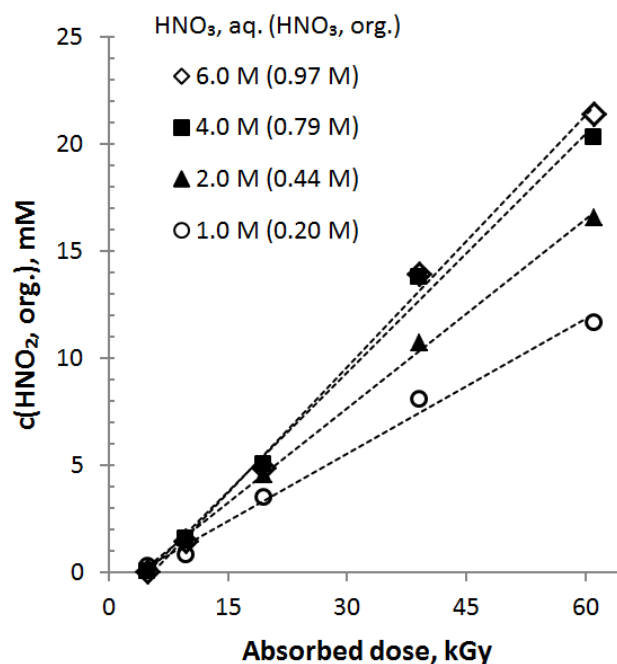


Figure 58 - Concentrations of nitrous acid in organic phase (± 15 % system. error), produced by irradiation of 30% TBP equilibrated with different initial aqueous concentrations of HNO_3 (concentrations of extracted HNO_3 are given in parentheses).

Burger and Money [174] reported yields of HNO_2 in 30% TBP in *Amsco 125-90W* diluent. At the 54 kGy dose level a final concentration of HNO_2 of 2.6 mM HNO_2 was measured in a solution of 0.3M HNO_3 concentration in the organic phase. This is significantly less than can be observed in our data presented in Figure 58.

The *Amsco* diluent is a mixture of aliphatic hydrocarbons very similar to n-dodecane; hence, the discrepancy in the yields of HNO_2 cannot be explained by diluent properties only. It can be speculated that the lower cumulative yield may have been a result of HNO_2 decomposition/volatilization. Although the authors acknowledged the issue of nitrite instability in acidic solutions, detailed experimental information on this point was not reported.

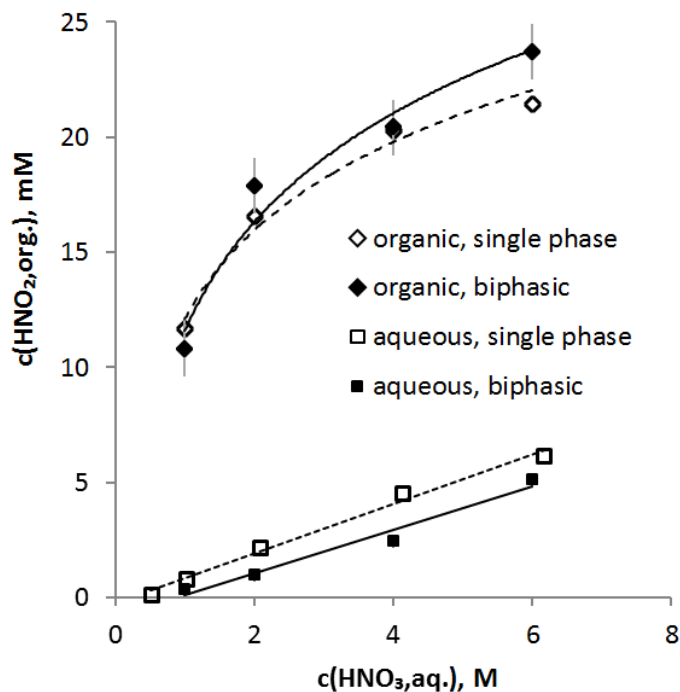


Figure 59 - Comparison of the aqueous ($\pm 5\%$ system. error) and organic ($\pm 15\%$ systematic error, error bars indicate random error) concentrations of HNO_2 produced by a 61 kGy dose in monophasic and biphasic experiments, plotted as a function of the nitric acid concentration in aqueous phase.

12.4.3 Combined organic and aqueous (biphasic system) system

The final concentration of HNO_2 in the biphasic system is a result of its radiolytic production and simultaneous partition between the two phases. Due to rapid extraction kinetics, it was assumed that the concentrations of HNO_2 measured in biphasic radiolytic experiments represent the true equilibrium concentrations of HNO_2 in the organic and aqueous phases.

In Figure 59, it is clear that in the irradiated biphasic systems the nitrous acid concentration was depleted in the aqueous phase and enriched in the organic phase

compared to the single phase system. This is a result of the expected extraction of HNO_2 from the aqueous to the organic phase. The distribution ratio calculated from the ratio of the determined concentrations of HNO_2 after irradiation has increased approximately by 70% compared to non-irradiated systems (Figure 56), which should be primarily attributed to the complex radiolytic changes of the organic phase [117].

12.4.4 Dependence of radiolytic yield of HNO_2 on HNO_3 concentration in aqueous and organic phases

Radiolytic yields of HNO_2 were calculated from the slopes of the total concentration of HNO_2 produced vs. absorbed dose in both aqueous and organic systems (Figure 57 and Figure 58). The low density of 30% TBP / n-dodecane (0.82 g/mL) was taken into account.

Table 13 - Comparison of radiolytic yields of HNO_2 in aqueous and organic solutions of HNO_3 in concentrations corresponding to extraction equilibrium

Aqueous solutions		Solutions of 30% TBP/dodecane	
c(HNO_3), aq. M	G ($\mu\text{mol}/\text{J}$) $\pm 5\%$ error	c(HNO_3), org. M	G ($\mu\text{mol}/\text{J}$) $\pm 15\%$ error
0.5	0.002	-	-
1.0	0.014	0.20	0.26
2.1	0.039	0.40	0.36
4.1	0.079	0.79	0.45
6.2	0.108	0.97	0.48

From the results summarized in Table 2 it is evident that the radiation yield of HNO_2 is about an order higher in the organic phase than in the corresponding aqueous phase. This should be attributed to practically inhibited reoxidation of HNO_2 back to HNO_3 caused by much lower concentration of H_2O molecules in the organic phase (100 to 300 times less than in the aqueous phase with the increase of HNO_3 concentration from 0.5 to 6 M) [33][194]). Both the hydroxyl radical [195] and hydrogen peroxide [83], typical products of radiolysis of water and strong oxidizers, are produced in much lower concentrations; hence, they cannot scavenge HNO_2 as efficiently as they do in the aqueous phase. The HNO_2 yields increase with the concentration of the extracted HNO_3 in the TBP phase

until ~0.8M HNO₃ (corresponding to 4 M HNO₃ in the aqueous phase) after which they level off. Elucidating this effect is presently difficult due to the low level understanding of the radiation chemistry of N-centered radical species in the organic phase [117] (compared to the area of their aqueous radiation chemistry [124]). We hypothesize that the generation of HNO₂ levels off down due to decreased availability of H₂O molecules for the reaction with the $\cdot\text{NO}_2$ radical, which is an important source of HNO₂ through a disproportionation reaction [196]:



The $\cdot\text{NO}_2$ radicals then instead increasingly contribute to the production of nitrated organic compounds by reacting with organic radicals resulting from the radiolysis of 30%TBP/n-dodecane, such as are the hydrocarbon radicals and radicals resulting from TBP radiolysis [117]:



It should be noted that the aqueous yield of HNO₂ is beginning to grow in a linear dependence on the nitric acid concentration just above 0.5M HNO₃. Nitric acid solutions of lower than 0.5 M concentrations have very low or zero nitrous acid yields. This is due the fact that the primary yield of H₂O₂ is related to the concentration of water and remains nearly unaffected with the increase in HNO₃ up to 8M HNO₃ [181, 182], while the primary yield of NO₂⁻/HNO₂ grows proportionally to the HNO₃ concentration and between 0.1 and 0.5 M HNO₃ the primary yield of HNO₂ surpasses the primary yield of hydrogen peroxide, so that net production of HNO₂ occurs [124].

12.5 Conclusion

The radiolytic production of nitrous acid from HNO₃ dissolved in the organic phase of 30% TBP-n-dodecane was found to be significantly higher than from HNO₃ in aqueous solutions. After a dose of 61 kGy, HNO₂ concentrations in excess of 10 mM were found in the organic phase containing 0.23 – 0.97 M HNO₃ (in extraction equilibrium with 1.0 – 6.0 M aqueous HNO₃). This means that during reprocessing conditions the organic phase is the most significant source of radiolytic nitrous acid in the separation system.

13 GENERAL CONCLUSION

13.1 Impact of work and summary of results

By the work described in this dissertation, the author has attempted to increase the existing knowledge on the issues related to the control of redox speciation of neptunium in nitric acid solutions, in particular with respect to application in Used Nuclear Fuel reprocessing. The most significant part of the work was devoted to the investigation of the kinetics of several important reactions of neptunium(V) and (VI) and of comparably important reactions of nitrous acid. This nitrogen compound has been confirmed to play an indisputably principal role in the redox chemistry of neptunium and in the chemistry of other actinide elements and compounds in nitric acid solutions. Although this fact has been recognized already more than half a century ago, certain areas related to the interactions of nitrous acid have received much smaller attention than they would deserve.

The studies of the reactions of neptunium(VI) and (V) were not the first to be made with these elements, but have been undertaken either to improve on older data – as in the case of the reactions of vanadium-V and of HNO_2 – or to elucidate discrepancies between the few recent studies – as was the case of the study of the reaction of Np-VI with acetohydroxamic acid. In the former two cases, the observations made by past researchers have been confirmed in general, while in the latter case a significant difference from the description of the previous study of the Np(VI) + AHA reaction system has been discovered (namely, the reaction was found to be significantly more rapid than reported by a previous study). Since this reaction fulfills the 2nd most important role of acetohydroxamic acid in several advanced reprocessing suites (reduction stripping of neptunium), the author is hopeful that his contribution in this area will provide designers of systems engineering models for these separation process one less issue to be concerned about.

The studies of the rapid reaction kinetics of nitrous acid with hydrogen peroxide and with acetohydroxamic acid had a with a very similar outcome, as the study of the rapid kinetics of AHA with Np(VI). Namely, in the case of the HNO_2 +AHA reaction, an

overwhelming body of evidence has been collected to completely reinterpret the findings of the only study published on the topic so far. In the case of the results of the study of the $\text{HNO}_2 + \text{H}_2\text{O}_2$ reaction, a completely new “territory” of conditions for the reaction has been investigated, and the results have already found practical application in modeling of the complicated radiation-chemical processes taking place in the radiolysis of nitric acid solutions of neptunium.

From another point of view, the combination of a modern stopped-flow spectrophotometer instrument with advanced numerical processing approaches that have been both made available in the recent two decades have significantly advanced the understanding on all the three rapid reaction kinetic problems that have been investigated.

In the studies concerned with radiation chemistry of neptunium and of nitrous acid, several new phenomena were discovered. Firstly, the effect of nitrous acid scavenger methylurea (MU) on the stabilization of neptunium in a hexavalent state has been exactly the opposite of the expectation. Not only was neptunium in the absence of HNO_2 reduced much faster with the absorbed radiation dose, but it has also progressed even further, leading to the formation of Np(IV) . Whether that is actually a positive outcome remains to be investigated in future. Secondly, the study was complemented with a more fundamental investigation of the role of nitrous acid in the radiolytic redox behavior of neptunium solutions in nitric acid. Both studies have confirmed the dual role nitrous acid plays in determining the redox behavior of neptunium – on one hand it is a reducing agent, but on the other hand it also facilitates the oxidizing effect of the otherwise kinetically stable nitrate. Without nitrous acid the radiation chemistry of the solution inevitably selects the inextractable pentavalent neptunium as the oxidation state of preference. Thirdly, the overall much greater radiolytic yields of nitrous acid were discovered from nitric acid solutions in the organic TBP phase compared to yields in aqueous nitric acid.

Against the initial expectations, the application of electrochemical methods during the work has been limited to a few specific applications, typically in a supportive role (but in these they usually performed very well). Despite being relatively inexpensive and easy to set up, electrochemical investigations demand a very high level of practical genius, prior

experience and deep thermodynamic insight into the studied processes to produce new and exciting data in an already very well discovered area, such as is the actinide electrochemistry. The research on the practicality of redox potential measurements in nitric acid system has also resulted in more opened questions than answers.

13.2 Future work

As is usual in scientific investigations, certain parts of the work have not been completed to the extent of the author's expectation. For instance, the study of the rapid kinetic reactions of HNO_2 using the stopped-flow system could be significantly extended by investigation of the effects of catalyzing and inhibiting substances (such as is iron, organic impurities and different inorganic anions) and by investigation into the nature of the intermediate and final products of the reactions of acetohydroxamic acid.

The radiolytic studies are by their nature even more enigmatic than classical reaction kinetics and the area of future possible research is considerably larger. E.g., despite many decades of research, a universally applicable model of all radiation-chemical reactions occurring in aqueous nitric acid solutions still does not exist; on the other hand, the author believes that marked progress in the area has been made recently due to widespread computerization of chemistry.

BIBLIOGRAPHY

1. Amaral, E; Brockman, K; Forsström, H G. International Perspectives on Spent Fuel Management. In: *Proceedings of the International Conference on Management of Spent Fuel from Nuclear Power Reactors, Vienna, Austria, 19–22 June 2006*. Vienna, Austria: International Atomic Energy Agency, 2007. URL: http://www-pub.iaea.org/MTCD/publications/PDF/Pub1295_web.pdf
2. Benedict, M; Pigford, TH; Levi, HW. *Nuclear Chemical Engineering*. 2nd ed. New York: McGraw-Hill Book Company; 1981. ISBN 978-0-07-004531-6
3. Vandegrift, George F; Regalbuto, Monica C; Aase, Scott; Bakel, Allen; Battisti, Terry J; Bowers, Delbert; Byrnes, James P; et al. Designing and Demonstration of the UREX+ Process Using Spent Nuclear Fuel. In: *ATALANTE 2004 - Advances for Future Nuclear Fuel Cycles International Conference, Nimes, France, June 21-24, 2004*. 2004. pp. 1–9.
4. Seaborg, Glenn T. *Transuranium Elements: A Half Century*. Berkeley, California: Lawrence Berkeley Laboratory Report LBL-29445; 1990. URL: http://www.osti.gov/energycitations/product.biblio.jsp?query_id=0&page=0&osti_id=6604648
5. McMillan, Edwin; Abelson, Philip. Radioactive Element 93. *Physical Review*, 1940, **57**(12), 1185–1186. DOI:10.1103/PhysRev.57.1185.2
6. Seaborg, Glenn T; McMillan, E. M.; Kennedy, J. W.; Wahl, A. C. Radioactive Element 94 from Deuterons on Uranium. *Physical Review*, 1946, **69**(7-8), 366–367. DOI:10.1103/PhysRev.69.366.2
7. Seaborg, Glenn T; Katz, Joseph J; Manning, Winston M. *The transuranium elements: research papers, Part I*. 1st ed. New York: McGraw-Hill; 1949.
8. Shulz, Wallace W; Benedict, Glen E. *Neptunium-237 Production and Recovery*. Atlantic Richfield Hanford Company, Richland, Washington: U. S. Atomic Energy Commission Report TID-25955; 1972. ISBN 0870790013
9. Singh, Balraj; Tuli, Jagdish K. Nuclear Data Sheets for A = 233. *Nuclear Data Sheets*, 2005, **105**(1), 109–222. DOI:10.1016/j.nds.2005.05.002
10. Ekström, L.P.; Firestone, R.B. WWW Table of Radioactive Isotopes, database version 2/28/99. 2004. Accessed: August 30, 2012. <http://ie.lbl.gov/toi/>
11. Garvey, Todd. *Closing Yucca Mountain : Litigation Associated with Attempts to Abandon the Planned Nuclear Waste Repository*. Congressional Research Service, Report R41675; 2012. URL: <http://www.fas.org/sgp/crs/misc/R41675.pdf>

12. Eckhardt, RC; Bish, DL; Bussod, GY; Fabryka-Martin, JT; Levy, SS; Reimus, PW; Robinson, BA; Runde, Wolfgang; Triay, Ines; Vaniman, DT. Yucca Mountain-Looking Ten Thousand Years into the Future. *Los Alamos Science*, 2000, (26), 464–489.
13. *Draft Nonproliferation Impact Assessment for the Global Nuclear Energy Partnership Programmatic Alternatives*. Washington, D. C.: National Nuclear Security Administration, Office of Nonproliferation and International Security; 2008.
14. Sanchez, RG; Loaiza, DJ; Kimpland, RH. Criticality of a ^{237}Np Sphere. In: *7th International Conference on Nuclear Criticality Safety (ICNC2003), Tokai-mura, Japan, October 2003*. 2003. pp. 107–109. URL: http://typhoon.jaea.go.jp/icnc2003/Proceeding/paper/2.14_107.pdf
15. Ng, Selena; Grenèche, Dominique; Guesdon, Bernard; Vinoche, Richard; Delpech, Marc; Dolci, Florence; Golfier, Hervé; Poinot-Salanon, Christine. Neptunium in the Fuel Cycle: Nonproliferation Benefits Versus Industrial Drawbacks. *Nuclear Technology*, 2008, **164**(1), 13–19.
16. Shiokawa, Yoshinobu; Yamana, Hajimu; Moriyama, Hirotake. An Application of Actinide Elements for a Redox Flow Battery. *Journal of Nuclear Science and Technology*, 2000, **37**(3), 253–256. DOI:10.1080/18811248.2000.9714891
17. Drake, V A. Extraction chemistry of neptunium. In: *Science and Technology of Tributyl Phosphate, Volume III*. Chapter 3, Ed. Wallace W. Schulz; L L Burger; James D Navratil; Karen P Bender Boca Raton, Florida: CRC Press Inc, 1990. pp. 123–145. ISBN 0-8493-6389-6.
18. Tompkins, J Andrew. *Engineering Evaluation of Nuclear Powered Pacemakers as Special Form Radioactive Material*. US DOE Los Alamos National Laboratory, Off-Site Source Recovery Project Report LAUR-01-6353; 2000. URL: http://osrp.lanl.gov/Documents/LAURS_Documents Page/LAUR-01-6353.pdf
19. Mallela, Venkateswara Sarma; Ilankumaran, V; Rao, N Srinivasa. Trends in cardiac pacemaker batteries. *Indian Pacing and Electrophysiology Journal*, 2004, **4**(4), 201–212.
20. Bennett, Gary L. Space Nuclear Power: Opening the Final Frontier. In: *4th International Energy Conversion Engineering Conference and Exhibit (IECEC) 26-29 June 2006, San Diego, California*. American Institute of Aeronautics and Astronautics, 2006. pp. 26–29. URL: <http://www.fas.org/nuke/space/bennett0706.pdf>
21. US DOE. *Start-up Plan for Plutonium-238 Production for Radioisotope Power Systems*. United States Department of Energy, Report to Congress; 2010.

22. Wham, Robert M; Caponiti, Alice K; Johnson, Stephen G. Future Production of ^{238}Pu for NASA Space Missions. *Transactions of the American Nuclear Society*, 2010, **103**, 200–201.
23. Todd, T; Herbst, R; Mincher, B; Frank, S; Law, J; Swanson, J. *Plutonium-238 Recovery From Irradiated Neptunium Targets Using Solvent Extraction*. Idaho National Laboratory paper preprint for 15th Pacific Basin Nuclear Conference, Report No. INL/CON-06-11850; 2006.
24. Edelstein, Norman M; Fuger, Jean; Katz, Joseph J; Morss, Lester R. Summary and Comparison of Properties of the Actinide and Transactinide Elements. In: *The Chemistry of the Actinide and Transactinide Elements*. 3rd ed. Chapter 15, Ed. Lester R. Morss; Norman M. Edelstein; Jean Fuger Dordrecht: Springer Netherlands, 2006. pp. 1753–1835. DOI:10.1007/1-4020-3598-5.
25. Bard, Allen J; Parsons, Roger; Jordan, Joseph. *Standard Potentials in Aqueous Solution*. New York: Marcel Dekker, Inc. / International Union of Pure and Applied Chemistry; 1985. ISBN 0-8247-7291-1
26. Schmets, J J. Reprocessing of Spent Nuclear Fuels by Fluoride Volatility Processes. *Atomic Energy Review*, 1970, **8**(1), 1–126.
27. Choppin, Gregory R; Jensen, Mark P. Actinides in Solution: Complexation and Kinetics. In: *The Chemistry of the Actinide and Transactinide Elements*. Chapter 23rd, Ed. Lester R Morss; Norman M Edelstein; Jean Fuger Dordrecht: Springer Netherlands, 2006. pp. 2524–2621. ISBN 978-1-4020-3598-2. DOI:10.1007/1-4020-3598-5_23.
28. Clark, David L; Hecker, Siegfried S; Jarvinen, Gordon D; Neu, Mary P. Plutonium. In: *The chemistry of the actinide and transactinide elements*. 3rd ed. Chapter 7, Ed. Lester R. Morss; Norman M. Edelstein; Jean Fuger Dordrecht: Springer Netherlands, 2006. pp. 813–1264. ISBN 978-1-4020-3598-2. DOI:10.1007/1-4020-3598-5_7.
29. Kihara, S; Yoshida, Z; Aoyagi, H. A critical evaluation of the redox properties of uranium, neptunium and plutonium ions in acidic aqueous solutions. *Pure and Applied Chemistry*, 1999, **71**(9), 1771–1807.
30. Runde, Wolfgang H; Schulz, Wallace W. Americium. In: *The chemistry of the actinide and transactinide elements*. 3rd ed. Chapter 8, Ed. Lester R. Morss; Norman M. Edelstein; Jean Fuger Dordrecht: Springer Netherlands, 2006. pp. 1265–1395. ISBN 978-1-4020-3598-2. DOI:10.1007/1-4020-3598-5_8.
31. Moulin, Jean-Paul. *Kinetics of redox reactions of neptunium in nitric acid: Oxidation of neptunium (IV) into neptunium (V) and oxidation of neptunium (V) into neptunium (VI) by nitric acid, catalyzed by nitrous acid*. Fontenay-aux-Roses:

L'Université Pierre et Marie Curie & Commissariat à l'Énergie Atomique, Report CEA-R-4912; 1978.

32. Laidler, Keith J. *Chemical Kinetics*. 2nd ed. New York: McGraw-Hill Book Company; 1965.
33. Burger, L L. Chapter 4 - Physical Properties. In: *Science and Technology of Tributyl Phosphate, Volume I - Synthesis, Properties, Reactions and Analysis*. Chapter 4, Ed. W W Schulz; J D Navratil; Andrea E Talbot Boca Raton: CRC Press Inc, 1984. pp. 25–68. ISBN 0-8493-6396-9.
34. Dinh, Binh; Moisy, Philippe; Baron, Pascal; Calor, Jean-noel; Espinoux, Denis; Lorrain, Brigitte; Benchikouhne-Ranchoux, Magali. Modified PUREX first-cycle extraction for neptunium recovery. In: *Proceedings of the International Solvent Extraction Conference (ISEC 2008), Tucson, Arizona, USA. 15-19 September 2008*. 2008. pp. 581–586.
35. Nash, Kenneth L; Madic, Charles; Mathur, Jagdish N; Lacquement, Jerome. Actinide separation science and technology. In: *The Chemistry of the Actinide and Transactinide Elements*. 3rd ed. Chapter 24, Ed. Lester R. Morss; Norman M. Edelstein; Jean Fuger Dordrecht: Springer Netherlands, 2006. pp. 2622–2798. DOI:10.1007/1-4020-3598-5_24.
36. Wilson, P D. *The Nuclear Fuel Cycle: from Ore to Wastes*. Oxford, UK: Oxford University Press; 1996. ISBN 9780198565406
37. Choppin, Gregory R.; Liljenzin, Jan-Olov; Rydberg, Jan. The Nuclear Fuel Cycle. In: *Radiochemistry and Nuclear Chemistry*. 3rd ed. Chapter 21, Butterworth-Heinemann, 2002. pp. 583–641.
38. Marchenko, V. I.; Polunin, A K; Zakharkin, B S; Rubisov, V N; Dzekun, E G; Starikov, V M; Ufimtsev, V P. Industrial tests on the electrochemical separation of uranium and plutonium in reprocessing spent fuel by aqueous methods. *Atomic Energy*, 1997, **82**(2), 152–155. DOI:10.1007/BF02413469
39. Koltunov, V S; Marchenko, V I. Stabilization of Pu and Np valences in Purex process : Problems and outlook. In: *RECOD 98: 5th International nuclear conference on recycling, conditioning and disposal (Nice, France, 25-28 October 1998)*. French Nuclear Energy Society (SFEN), Paris, FRANCE, 1998. pp. 425–431. URL: <http://cat.inist.fr/?aModele=afficheN&cpsid=1816508>
40. Birkett, J E; Carrott, M J; Fox, O D; Jones, C J; Maher, C J; Roubé, C V; Taylor, R J; Woodhead, D A. Recent developments in the purex process for nuclear fuel reprocessing: complexant based stripping for uranium-plutonium separation. *Chimia*, 2005, **59**, 898–904.

41. Leonard, Ralph A. Recent Advances in Centrifugal Contactors Design. In: *5th Symposium on Separation Science and Technology for Energy Application, Knoxville, TN, USA, 26-29 Oct 1987*. Argonne National Laboratory, Illinois, USA, Technical Report CONF-871038-11, 1987. URL: http://www.osti.gov/bridge/product.biblio.jsp?osti_id=5587676
42. Birkett, J. Eddie; Carrott, Michael J.; Fox, O. Danny; Jones, Chris J.; Maher, Chris J.; Roube, Cécile V.; Taylor, Robin J.; Woodhead, David a. Recent Developments in the Purex Process for Nuclear Fuel Reprocessing: Complexant Based Stripping for Uranium/Plutonium Separation. *Chimia*, 2005, **59**(12), 898–904. DOI:10.2533/000942905777675327
43. Tachimori, Shoichi; Morita, Y. Overview of Solvent Extraction Chemistry for Reprocessing. In: *Ion Exchange and Solvent Extraction: A Series of Advances, Volume 19*. Ed. Bruce A Moyer Boca Raton, Florida: CRC Press, Taylor & Francis Group, 2010. pp. 1–64. ISBN 978-1-4200-5970-0. DOI:10.1201/9781420059700-c1.
44. Madic, Charles. Overview of the Hydrometallurgical and Pyro-Metallurgical Processes Studied Worldwide for the Partitioning of High Active Nuclear Wastes. In: *6th Information Exchange Meeting on Actinide and Fission Product Partitioning and Transmutation, 11-13 December 2000, Madrid, Spain*. OECD Nuclear Energy Agency, Paris, France, 2000. pp. 53–64. URL: http://www.oecd-neo.org/pt/docs/iem/madrid00/booklet/Over_Madic.pdf
45. Pereira, Candido. UREX+ Process Overview. In: *Presentation for the Topical Seminar Series on Nuclear Fuel Separation Processes, March 26, 2008*. Argonne National Laboratory, Illinois, USA, 2008. URL: <http://www.ne.doe.gov/pdfFiles/DOENRCUREXSeminar.pdf>
46. Gelis, A. V.; Vandegrift, Georg F; Bakel, Allen; Bowers, Delbert L; Hebden, Andrew S; Pereira, Candido; Regalbuto, Monica. Extraction behaviour of actinides and lanthanides in TALSPEAK, TRUEX and NPEX processes of UREX+. *Radiochimica Acta*, 2009, **97**(4-5), 231–232. DOI:10.1524/ract.2009.1601
47. Escure, H; Gourisse, D; Lucas, J. Dismutation du neptunium pentavalent en solution nitrique - I, Etudes a l'équilibre. *Journal of Inorganic and Nuclear Chemistry*, 1971, **33**(6), 1871–1876. DOI:10.1016/0022-1902(71)80624-3
48. Koltunov, V S; Tikhonov, M F. Kinetics of the disproportionation of neptunium(V) in nitric acid solution. *Soviet Radiochemistry*, 1975, **17**(4), 538–541.
49. Siddal, T H; Dukes, E K. Kinetics of HNO₂ Catalyzed Oxidation of Neptunium(V) by Aqueous Solutions of Nitric Acid. *J. Am. Chem. Soc.*, 1959, **81**(4), 790–794. DOI:10.1021/ja01513a007

50. Swanson, J.L. *Oxidation of Neptunium (V) in Nitric Acid Solution: Laboratory Study of Rate Accelerating Materials (RAM)*. Richland, Washington: Battelle Memorial Institute - Pacific Northwest Laboratory, US AEC Research and Development Report BNWL-1017; 1969. URL: http://www.osti.gov/energycitations/product.biblio.jsp?osti_id=4805921
51. Gourisse, D. Oxydation du neptunium(V) par les solutions aqueuses d'acide nitrique en presence d'acide nitreux. *Journal of Inorganic and Nuclear Chemistry*, 1971, **33**(3), 831–837. DOI:10.1016/0022-1902(71)80484-0
52. Shilin, I V; Nazarov, V K. Determination of the thermodynamic equilibrium constant of the oxidation of pentavalent neptunium by nitric acid. *Soviet Radiochemistry*, 1972, **14**(2), 304–306.
53. Tochiyama, Osamu; Nakamura, Yoshinobu; Katayama, Yasushi; Inoue, Yasushi. Equilibrium of Nitrous Acid-Catalyzed Oxidation of Neptunium in Nitric Acid-TBP Extraction System. *Journal of Nuclear Science and Technology*, 1995, **32**(1), 50–59. DOI:10.3327/jnst.32.50
54. Koltunov, V S; Marchenko, V I. Kinetika okislitel'no-vosstanovitel'nykh reakcii' urana i transuranovykh elementov (Kinetics of Oxidative–Reductive Reactions of Uranium and Transuranium Elements). In: *Review of Science—Series: Chemistry—Inorganic Chemistry*. Industrial and Publishing Works of All-Russian Institute of Scientific and Technical Information, Moscow-Lyubertsy (publ. in Russian), 1969. pp. 75–210.
55. Tochiyama, Osamu; Nakamura, Yoshinobu; Hirota, M.; Inoue, Y. Kinetics of nitrous acid-catalyzed oxidation of neptunium in nitric acid-TBP extraction system. *Journal of Nuclear Science and Technology*, 1995, **32**(2), 118–124.
56. Marchenko, V. I.; Dvoeglazov, K. N.; Volk, V. I. Use of redox reagents for stabilization of Pu and Np valence forms in aqueous reprocessing of spent nuclear fuel: Chemical and technological aspects. *Radiochemistry*, 2009, **51**(4), 329–344. DOI:10.1134/S1066362209040018
57. Marchenko, V. I.; Koltunov, V. S.; Dvoeglazov, K. N. Kinetics and mechanisms of redox reactions of U, Pu, and Np in tributyl phosphate solutions. *Radiochemistry*, 2010, **52**(2), 111–126. DOI:10.1134/S1066362210020013
58. Koltunov, V. S.; Taylor, Robin J.; Marchenko, V. I.; Savilova, O. A.; Dvoeglazov, K. N. The oxidation of uranium(IV) ions by nitrous acid in 30% tri-butyl phosphate. *Radiochimica Acta*, 2004, **92**(7), 387–394. DOI:10.1524/ract.92.7.387.35750
59. Rance, P; Chesnay, B; Killeen, T; Murray, M; Nikkinen, M; Petoe, A; Plumb, J; Saukkonen, H. Neptunium Flow-Sheet Verification at Reprocessing Plants. In:

Proceedings of 7th International Conference on Advanced Nuclear Fuel Cycles and Systems GLOBAL 2007, Boise, Idaho, September 9-13, 2007. American Nuclear Society, 2007. pp. 346–352.

60. Sullivan, J. C.; Zielen, A J; Hindman, J C. Kinetics of the Reduction of Neptunium(VI) by Uranium(IV). *Journal of the American Chemical Society*, 1960, **82**(20), 5288–5292. DOI:10.1021/ja01505a004
61. Koltunov, V. S.; Taylor, Robin J.; Marchenko, V. I.; Zhuravleva, G.I.; Mezhev, E.A.; Koltunov, G. V.; Dvoeglazov, K. N. The kinetics and mechanism of the reduction of neptunium (VI) ions by uranium (IV) ions in nitric acid. *Radiochimica Acta*, 2002, **90**(5), 259–265. DOI:10.1524/ract.2002.90.5_2002.259
62. Newton, Thomas William. *The Kinetics of the Oxidation-Reduction Reactions of Uranium, Neptunium, Plutonium and Americium in Aqueous Solutions.* Oak Ridge, Tennessee: U. S. Energy Research and Development Administration, Technical Information Center, Report TID-26506; 1975. ISBN 0- 87079-020-9 DOI:10.2172/4188896
63. Bond, W.D.; Jao, Y.; Peterson, J.R. The oxidation-reduction kinetics involved in the $\text{Np(V)} + \text{Fe(II)} = \text{Np(IV)} + \text{Fe(III)}$ system in nitric acid solutions. *Journal of Inorganic and Nuclear Chemistry*, 1977, **39**(8), 1395–1402. DOI:10.1016/0022-1902(77)80305-9
64. Burney, G A; Harbour, R M. *Radiochemistry of Neptunium.* Oak Ridge, Tennessee: U. S. Atomic Energy Commission Technical Information Center / National Academy of Sciences - Report NAS-NS-3060; 1974. URL: <http://www.osti.gov/energycitations/servlets/purl/4242713-ARcu2Y/>
65. Crowder, Mark L; Thompson, Major C. *Studies with Ferrous Sulfamate and Alternate Reductants for 2nd Uranium Cycle.* US Department of Energy, Westinghouse Savannah River Company, Report WSRC-TR-2002-00389; 2002. DOI:10.2172/807667
66. Kessinger, G F; Kyser, E A; Almond, P M. *Literature Review: Reduction of Np(V) to Np(IV) - Alternatives to Ferrous Sulfamate.* US Department of Energy, Separations Campaign, Savannah River National Laboratory - Report SRNL-STI-2009-00610; 2009. URL: <http://dx.doi.org/10.2172/969037>
67. Fulton, Robert B.; Newton, Thomas W. Kinetics of the oxidation of plutonium(III) by neptunium(VI). *The Journal of Physical Chemistry*, 1970, **74**(8), 1661–1669. DOI:10.1021/j100703a002
68. Koltunov, V. S.; Marchenko, V. L.; Zhuravleva, G. I.; Tikhonov, M. F.; Shapovalov, M. P. Kinetics of the reactions of oxidation of Np(IV) by Pu(IV),

- Fe(III) and V(V) ions and the reduction of Np(V) by hydrazine. *Soviet Radiochemistry*, 1976, **18**, 59.
69. Koltunov, V. S.; Frolov, K. M.; Marchenko, V. L. Tikhonov, M. F. Zhuravleva, G. I.; Kulikov, I. A.; Ryabova, A. A. New investigations in the field of the kinetics and mechanism of reactions of neptunium and plutonium. *Soviet Radiochemistry*, 1982, **24**, 504.
70. Dissociation Constants of Inorganic Acids and Bases. In: *CRC Handbook of Chemistry and Physics, 92nd Edition (Internet Version 2012)*. Ed. W M Haynes Boca Raton, FL: CRC Press/Taylor and Francis, 2012. pp. 5/92–93.
71. Perron, John R.; Stedman, Geoffrey; Uysal, Nermin. Kinetic and product study of the reaction between nitrous acid and hydrazine. *Journal of the Chemical Society, Dalton Transactions*, 1976, **2**(20), 2058–2064. DOI:10.1039/dt9760002058
72. Uchiyama, Gunzo; Hotoku, Shinobu; Fujine, Sachio. Distribution of Nitrous Acid Between Tri-N-Butyl Phosphate/ N-Dodecane and Nitric Acid. *Solvent Extraction and Ion Exchange*, 1998, **16**(5), 1177–1190. DOI:10.1080/07360299808934575
73. Koltunov, V S; Baranov, S M. Organic Derivatives of Hydrazine and Hydroxylamine and Future Reprocessing of Irradiated Nuclear Fuel. *Radiochemistry*, 1993, **35**(6), 622–630.
74. Karraker, D.G. *Hydrazine reduction of Np(V) and Pu(IV)*. Du Pont de Nemours (E.I.) and Co., Aiken, SC (USA). Savannah River Laboratory, Report DP-1601; 1981. DOI: 10.2172/5642232.
75. El-Naggar, H A; Gourisse, D; Masoud, Mamdouh S. Neptunium Reduction by Hydrazine and Hydroxylamine. *Radiochimica Acta*, 1982, **31**, 51–55.
76. Zielen, AJ; Sullivan, JC; Cohen, D.; Hindman, JC. A Kinetic Study of the Reduction of Neptunium(VI) by Hydrogen Peroxide. *Journal of the American Chemical Society*, 1958, **80**(21), 5632–5635. DOI:10.1021/ja01554a012
77. Magnusson, L B; Hindman, J C; LaChapelle, T J. Chemistry of Neptunium. Kinetics and Mechanisms of Aqueous Oxidation-Reduction Reactions of Neptunium. In: *The Transuranium Elements: Research Papers, Part II*. Chapter 15.11, Ed. Glenn T Seaborg; Joseph J Katz; Winston M Manning New York: Division IV, Vol. 14B, National Nuclear Energy Series, McGraw-Hill Book Company, 1949. pp. 1134–1148.
78. Krot, N N; Shuiskaya, L G. Reaction of neptunium with hydrogen peroxide in concentrated nitric acid solutions. *Soviet Radiochemistry*, 1971, **13**(1), 73.

79. Bhattacharya, P K; Veeraraghavan, R. Reaction Between Nitrous Acid and Hydrogen Peroxide in Perchloric Acid Medium. *International Journal of Chemical Kinetics*, 1977, **9**, 629–640.
80. Haim, Albert; Wang, Nun-Yii; Bonner, Francis T. Comments on the Paper “Reaction Between Nitrous Acid and Hydrogen Peroxide in Perchloric Acid Medium.” *International Journal of Chemical Kinetics*, 1979, **11**, 339–341.
81. Lee, Yin-Nan; Lind, John a. Kinetics of Aqueous-Phase Oxidation of Nitrogen(III) by Hydrogen Peroxide. *Journal of Geophysical Research*, 1986, **91**(D2), 2793–2800. DOI:10.1029/JD091iD02p02793
82. Park, J.Y.; Choi, E.J.; Park, J.W. Effects of Added Anions on the Reaction of Nitrous Acid with Hydrogen Peroxide. *Bull. Korean Chem. Soc.*, 1992, **13**(1), 37.
83. Thomas, D; Vanderschuren, J; Barigand, M. Influence of acidity on the oxidation rate of nitrous acid by hydrogen peroxide. *J. Chim. Phys.*, 1998, **95**, 523–535.
84. Benton, DJ; Moore, P. Kinetics and mechanism of the formation and decay of peroxyntrous acid in perchloric acid solutions. *J. Chem. Soc. A*, 1970, 3179–3182.
85. Barney, G. Scott. A kinetic study of the reaction of plutonium(IV) with hydroxylamine. *Journal of Inorganic and Nuclear Chemistry*, 1976, **38**(9), 1677–1681. DOI:10.1016/0022-1902(76)80660-4
86. Koltunov, V S; Tikhonov, M F. Kinetics of the reaction of actinides by hydroxylamine. I. Reduction of neptunium(VI) in nitric acid solution. *Soviet Radiochemistry*, 1978, **19**(5), 502–509.
87. Koltunov, V S; Tikhonov, M F. Kinetics of the reaction of actinides by hydroxylamine. II. Reduction of neptunium(V) in nitric acid solution. *Soviet Radiochemistry*, 1978, **19**(5), 510–515.
88. Hughes, M. N.; Stedman, G. Kinetics and mechanism of the reaction between nitrous acid and hydroxylamine. Part I. *Journal of the Chemical Society (Resumed)*, 1963, (2), 2824–2830. DOI:10.1039/jr9630002824
89. Pembbridge, John R.; Stedman, Geoffrey. Kinetics, mechanism, and stoichiometry of the oxidation of hydroxylamine by nitric acid. *Journal of the Chemical Society, Dalton Transactions*, 1979, (11), 1657–1663. DOI:10.1039/dt9790001657
90. Gowland, Rory J.; Stedman, Geoffrey. Kinetic and product studies on the decomposition of hydroxylamine in nitric acid. *Journal of Inorganic and Nuclear Chemistry*, 1981, **43**(11), 2859–2862. DOI:10.1016/0022-1902(81)80631-8

91. Taylor, R J; May, I; Koltunov, V S; Baranov, S M; Marchenko, V I; Mezhev, E A; Pastuschak, V G; Zhuravleva, G I; Savilova, O A. Kinetic and Solvent Extraction Studies of the Selective Reduction of Np(VI) by New Salt-Free Reducing Agents. *Radiochimica Acta*, 1998, **81**, 149–156.
92. Taylor, R J; May, I; Wallwork, A L; Dennis, I S; Hill, N J; Galkin, B Y; Zilberman, B Y; Fedorov, Y S. The applications of formo- and aceto-hydroxamic acids in nuclear fuel reprocessing. *J. Alloys Comp*, 1998, 271–273534–537.
93. Taylor, R J; May, I. The reduction of actinide ions by hydroxamic acids. *Czechoslovak Journal of Physics*, 1999, **49**(S1), 617–621. DOI:10.1007/s10582-999-1041-0
94. Taylor, R J; Denniss, I S; May, I. Hydroxamic acids—novel reagents for Advanced Purex processes. In: *Proceedings of ATALANTE 2000 International Conference, Avignon, France, October 24-26, 2000*. Commissariat à l’Energie Atomique, paper P2-15, 2000. URL: <http://www-atalante2004.cea.fr/home/liblocal/docs/atalante2000/P2-15.pdf>
95. Chung, Dong Yong; Lee, Eil Hee. The Reduction of Np(VI) by Acetohydroxamic Acid in Nitric Acid Solution. *Bulletin of the Korean Chemical Society*, 2005, **26**(11), 1692–1694. DOI:10.5012/bkcs.2005.26.11.1692
96. Colston, Belinda J; Choppin, Gregory R; Taylor, Robin J. A preliminary study of the reduction of Np(VI) by formo-hydroxamic acid using stopped-flow near-infrared spectrophotometry. *Radiochimica acta*, 2000, **88**, 329–334.
97. Matteson, Brent S; Precek, Martin; Paulenova, Alena. A study of the kinetics of the reduction of neptunium(VI) by acetohydroxamic acid in perchloric acid. *IOP Conference Series: Materials Science and Engineering*, 2010, **9**, 012073. DOI:10.1088/1757-899X/9/1/012073
98. Alyapyshev, M; Paulenova, A; Cleveland, M A; Brusco, J E; Tkac, P. Hydrolysis of acetohydroxamic acid under UREX+ conditions. In: *Global 2007, Boise, Idaho, September 9-13, 2007*. ANS, ISBN 0-89448-055-3, 2007. pp. 1861–1864.
99. Zheng, Wei-fang; Yan, Tai-hong; Bian, Xiao-yan; Zhang, Yu. Reaction Kinetics of Nitrous Acid with Acetohydroxamic Acid in HClO₄ and HNO₃ Medium. *Journal of Nuclear and Radiochemistry*, 2007, **29**(3), 129–134 (in Chinese).
100. Hussain, M A; Stedman, G; Hughes, M. N. Kinetics and mechanism of the reaction between nitrous acid and hydroxylamine. Part III. The formation of hyponitrous acid. *Journal of the Chemical Society B: Physical Organic*, 1968, 597–603. DOI:10.1039/J29680000597

101. Morgan, T. D. B.; Stedman, G.; Hughes, M. N. Kinetics and mechanism of the reaction between nitrous acid and hydroxylamine. Part II. The alkyl hydroxylamines. *Journal of the Chemical Society B: Physical Organic*, 1968, 344–349. DOI:10.1039/J29680000344
102. Uchiyama, G; Asakura, T; Hotoku, S; Mineo, H; Kamei, K; Watanabe, M; Fujine, S. Solvent extraction behavior of minor nuclides in nuclear fuel reprocessing process. *Journal of Radioanalytical and Nuclear Chemistry*, 2000, **246**(3), 683–688. DOI:10.1023/A:1006756215590
103. Uchiyama, Gunzo; Fujine, Sachio; Hotoku, Shinobu; Maeda, Mitsuru. New separation process for neptunium, plutonium and uranium using butyraldehydes as reductants in reprocessing. *Nuclear Technology*, 1993, **102**(3), 341–352.
104. Uchiyama, Gunzo; Hotoku, Shinobu; Fujine, Sachio; Meada, Mitsuru. Reduction of Neptunium(VI) by Butyraldehyde Isomers in Nitric Acid Solution. *Nuclear Technology*, 1998, **122**(2), 222–227.
105. Jones, J. R.; Waters, William A. Oxidations of organic compounds by quinquivalent vanadium. Part XII. Oxidation of propionaldehyde, n-butyraldehyde, and isobutyraldehyde. *Journal of the Chemical Society (Resumed)*, 1963, 352. DOI:10.1039/jr9630000352
106. Dukes, Ernest K. *Oxidation of Neptunium(V) by Vanadium(V)*. Du Pont de Nemours (E.I.) & Co. Savannah River Lab., Aiken, S.C., US Atomic Energy Commission Report DP-434; 1959. DOI: 10.2172/4634036. URL: <http://sti.srs.gov/fulltext/DP-434N.PDF>
107. Arm, S T; Abrefah, J; Lumetta, Gregg J.; Sinkov, S. I. Neptunium – Uranium – Plutonium Co-Extraction in TBP-based Solvent Extraction Processes for Spent Nuclear Fuel Recycling. In: *Proceedings of 7th International Conference on Advanced Nuclear Fuel Cycles and Systems GLOBAL 2007, Boise, Idaho, September 9-13, 2007*. American Nuclear Society, ISBN 0-89448-055-3, 2007. pp. 700–706. URL: http://www.new.ans.org/store/i_700331
108. Srinivasan, N; Nadkarni, M N; Kumar, S V; Kartha, P K S; Sonavane, R R; Ramaniah, M V; Patil, S K. *Counter-Current Extraction Studies for the Recovery of Neptunium by the PUREX Process (Part I)*. Bombay, India: Government of India - Atomic Energy Commission, Bhabha Atomic Research Center - Report BARC-734; 1974.
109. Koltunov, V S; Frolov, K M; Tikhonov, M F. Interaction of actinides with vanadium ions. V. Kinetics of oxidation of Np(IV) by pentavalent vanadium. *Soviet Radiochemistry*, 1981, **23**(1), 76–83.

110. Koltunov, V S; Frolov, K M; Tikhonov, M F. Interaction of actinides with vanadium ions. II. Kinetics of the reduction of Np(VI) by vanadium(IV) in an HClO₄ solution in the presence of glyoxal. *Soviet Radiochemistry*, 1981, **22**(6), 633–637.
111. Koltunov, V S; Frolov, K M; Tikhonov, M F. Interaction of actinides with vanadium ions. III. Kinetics of the reduction of Np(VI) by V(IV) in an HNO₃ solution in the presence of glyoxal. *Soviet Radiochemistry*, 1980, **50**(1968), 638–643.
112. Koltunov, V S; Frolov, K M; Marchenko, V I. Interaction of actinides with vanadium ions. I. Equilibrium between Np(VI) and V(IV). *Soviet Radiochemistry*, 1981, **22**(6), 630–633.
113. Koltunov, V S; Frolov, K M; Marchenko, V I. Interaction of actinides with vanadium ions. IV. Kinetics of oxidation of Np(V) with vanadium(V) in HClO₄ solution. *Soviet Radiochemistry*, 1981, **23**(1), 70–76.
114. Choppin, Gregory R.; Liljenzin, Jan-Olov; Rydberg, Jan. Radiation Effects on Matter. In: *Radiochemistry and Nuclear Chemistry*. 3rd ed. Chapter 7, Butterworth-Heinemann, 2002. pp. 166–191. ISBN 978-0750674638. DOI:10.1016/B978-075067463-8/50007-8.
115. Loveland, W; Morrissey, D; Seaborg, G. *Modern Nuclear Chemistry*. Hoboken, New Jersey: John Wiley & Sons, Inc; 2006.
116. Pikaev, Alexei K; Shilov, Vladimir P; Gogolev, Andrei V. Radiation chemistry of aqueous solutions of actinides. *Russian Chemical Reviews*, 1997, **66**(9), 763–788. DOI:10.1070/RC1997v066n09ABEH000284
117. Mincher, Bruce J.; Modolo, Giuseppe; Mezyk, Stephen P. Review Article: The Effects of Radiation Chemistry on Solvent Extraction: 1. Conditions in Acidic Solution and a Review of TBP Radiolysis. *Solvent Extraction and Ion Exchange*, 2009, **27**(1), 1–25. DOI:10.1080/07366290802544767
118. Roth, Olivia; LaVerne, Jay A. Effect of pH on H₂O₂ production in the radiolysis of water. *The Journal of Physical Chemistry A*, 2011, **115**(5), 700–8. DOI:10.1021/jp1099927
119. Gogolev, A. V.; Shilov, V. P.; Fedoseev, A. M.; Pikaev, A. K. A pulse radiolysis study of the reactivity of neptunoyl ions relative to inorganic free radicals. *Bulletin of the Academy of Sciences of the USSR Division of Chemical Science*, 1986, **35**(2), 422–424. DOI:10.1007/BF00952941
120. Katsumura, Y; Jiang, P. Y.; Nagaishi, R; Oishi, T.; Ishigure, K.; Yoshida, Y. Pulse radiolysis study of aqueous nitric acid solutions: formation mechanism, yield, and

- reactivity of NO₃ radical. *The Journal of Physical Chemistry*, 1991, **95**(11), 4435–4439. DOI:10.1021/j100164a050
121. Mincher, Bruce J; Mezyk, Stephen P; Martin, Leigh R. A pulse radiolysis investigation of the reactions of tributyl phosphate with the radical products of aqueous nitric acid irradiation. *The Journal of Physical Chemistry A*, 2008, **112**(28), 6275–80. DOI:10.1021/jp802169v
 122. Heinglein, Arnim. Pulse Radiolysis and Polarography: Electrode Reactions of Short-lived Free Radicals. In: *Electroanalytical Chemistry: A Series of Advances, Vol. 9*. Ed. Allen J Bard New York: Marcel Dekker, Inc., 1976. pp. 163–265. ISBN 978-0824764289.
 123. Hiroki, Akihiro; Pimblott, Simon M.; LaVerne, Jay A. Hydrogen Peroxide Production in the Radiolysis of Water with High Radical Scavenger Concentrations. *The Journal of Physical Chemistry A*, 2002, **106**(40), 9352–9358. DOI:10.1021/jp0207578
 124. Katsumura, Yosuke. NO₂ and NO₃ Radicals in Radiolysis of Nitric Acid Solutions. In: *N-centered radicals*. Chapter 12, Ed. Zeev B. Alfassi Chichester: John Wiley & Sons, 1998. pp. 393–412. ISBN 978-0-471-96186-4.
 125. Dukes, E. K. Kinetics and Mechanisms for the Oxidation of Trivalent Plutonium by Nitrous Acid. *Journal of the American Chemical Society*, 1960, **82**(1), 9–13. DOI:10.1021/ja01486a003
 126. Precek, Martin; Paulenova, Alena. Kinetics of reduction of hexavalent neptunium by nitrous acid in solutions of nitric acid. *Journal of Radioanalytical and Nuclear Chemistry*, 2010, **286**(3), 771–776. DOI:10.1007/s10967-010-0724-0
 127. Reinschmiedt, Karen; Sullivan, J. C.; Woods, Mary. Kinetic study of the oxidation of p-hydroquinone and p-tolhydroquinone by neptunium(VI) in aqueous perchlorate media. *Inorganic Chemistry*, 1973, **12**(7), 1639–1641. DOI:10.1021/ic50125a032
 128. Stedman, G. Reaction mechanisms of inorganic nitrogen compounds. *Adv. Inorg. Chem. Radiochem*, 1979, **22**, 113–170.
 129. Taylor, Thomas Weston Johns; Wignall, Ernest William; Cowley, John Frederick. The decomposition of nitrous acid in aqueous solution. *Journal of the Chemical Society (Resumed)*, 1927, **1927**(2), 1923. DOI:10.1039/jr9270001923
 130. Park, Jong Yoon; Lee, Yin Nan. Solubility and decomposition kinetics of nitrous acid in aqueous solution. *The Journal of Physical Chemistry*, 1988, **92**(22), 6294–6302. DOI:10.1021/j100333a025

131. Gourisse, Daniel;; Gautier, A. Behavior of nitrous acid in tributyl phosphate extractions. *Journal of Inorganic and Nuclear Chemistry*, 1969, **31**(3), 839–850.
132. Cool, Raymond D.; Yoe, John H. Volumetric Methods of Estimating Nitrites. *Industrial & Engineering Chemistry Analytical Edition*, 1933, **5**(2), 112–114. DOI:10.1021/ac50082a019
133. Scholz, Fritz. *Electroanalytical Methods*. 1st ed. Berlin, Heidelberg: Springer Berlin Heidelberg; 2001. ISBN 3-540-42229-3
134. Ingle, James D; Crouch, Stanley R. *Spectrochemical Analysis*. Englewood Cliffs, New Jersey: Prentice-Hall, Inc.; 1988. ISBN 0138268762
135. Hindman, J. C.; Magnusson, L. B.; LaChapelle, T. J. Chemistry of Neptunium. Absorption spectrum studies of aqueous ions of neptunium. In: *The Transuranium Elements: Research Papers, Part II*. Chapter 15.2, Ed. Glenn T Seaborg; Joseph J Katz; Winston M Manning New York: Division IV, Vol. 14B, National Nuclear Energy Series, McGraw-Hill Book Company, 1949. pp. 1039–1058.
136. Friedman, HA; Toth, LM. Absorption spectra of Np (III),(IV),(V) and (VI) in nitric acid solution. *Journal of Inorganic and Nuclear Chemistry*, 1980, **42**, 1347–1349.
137. Chlistunoff, Jerzy; Ziegler, Kirk J.; Lasdon, Leon; Johnston, Keith P. Nitric/Nitrous Acid Equilibria in Supercritical Water. *The Journal of Physical Chemistry A*, 1999, **103**(11), 1678–1688. DOI:10.1021/jp983745o
138. Waggener, W. C. Absorbance of Liquid Water and Deuterium Oxide between 0.6 and 1.8 Microns. Comparison of Absorbance and Effect of Temperature. *Analytical Chemistry*, 1958, **30**(9), 1569–1570. DOI:10.1021/ac60141a039
139. Denning, Robert G. Electronic Structure and Bonding in Actinyl Ions. *Structure and Bonding*, 1992, **79**, 217–273. DOI:10.1007/BFb0036498
140. Denning, Robert G. Electronic structure and bonding in actinyl ions and their analogs. *The journal of physical chemistry. A*, 2007, **111**(20), 4125–43. DOI:10.1021/jp071061n
141. Matsika, Spiridoula; Pitzer, Russell M.; Reed, Donald T. Intensities in the Spectra of Actinyl Ions. *The Journal of Physical Chemistry A*, 2000, **104**(51), 11983–11992. DOI:10.1021/jp002580s
142. Matsika, Spiridoula; Pitzer, Russell M. Electronic Spectrum of the NpO²⁺ and NpO²⁺ + Ions. *The Journal of Physical Chemistry A*, 2000, **104**(17), 4064–4068. DOI:10.1021/jp993767q

143. Matsika, S.; Zhang, Z.; Brozell, S. R.; Blaudeau, J.-P.; Wang, Q.; Pitzer, R. M. Electronic Structure and Spectra of Actinyl Ions. *The Journal of Physical Chemistry A*, 2001, **105**(15), 3825–3828. DOI:10.1021/jp003085z
144. Infante, Ivan Antonio Carlo. *Computational Studies of Actinide Chemistry*. Vrije Universiteit Amsterdam, Doctoral Thesis; 2000. URL: <http://hdl.handle.net/1871/10227>
145. Yoshida, Zenko; Johnson, Stephen G; Kimura, Takaumi; Krsul, John R. Neptunium. In: *The chemistry of the actinide and transactinide elements*. 3rd ed. Chapter 6, Ed. Lester R. Morss; Norman M. Edelstein; Jean Fuger Dordrecht: Springer Netherlands, 2006. pp. 699–812. ISBN 978-1-4020-3598-2. DOI:10.1007/1-4020-3598-5_5.
146. Hagan, P.G.; Cleveland, J.M. The absorption spectra of neptunium ions in perchloric acid solution. *Journal of Inorganic and Nuclear Chemistry*, 1966, **28**(12), 2905–2909. DOI:10.1016/0022-1902(66)80016-7
147. Vasiliev, V.Ya.; Andreichuk, N.N.; Rykov, A.G. Spectrophotometric Study of Complex Formation and Solvation of Actinide Ions IX. Forms of Existence of Neptunium (VI) in Nitrate Solutions. *Soviet Radiochemistry*, 1975, **17**(1), 19–23.
148. Hughes, Gordon. *Radiation chemistry*. Oxford, UK: Oxford Chemistry Series, Oxford University Press; 1973.
149. *Specifications of the Gammacell 220 Irradiation Unit*. Ottawa, Canada: Atomic Energy of Canada Limited, Commercial Products, Specification No. JS-300; 1974. URL: <http://pbadupws.nrc.gov/docs/ML0216/ML021630456.pdf>
150. Press, W. H.; Teukolsky, S. A.; Vetterling, W. T.; Flannery, B. P. Integration of Ordinary Differential Equations - Runge Kutta Method. In: *Numerical Recipes: The Art of Scientific Computing*. 2nd ed. Chapter 16.1, Cambridge University Press, 1992. pp. 710–714. ISBN 0-521-43108-5.
151. *Ionic Strength Corrections using Specific Interaction Theory. Version 1.5*. Programmed and designed by: L.D.Pettit, Expert advice: Ignasi Puigdomenech, Hans Wanner, ©IUPAC 2003; 2003.
152. Ivakin, A A. Formation of quinquevalent vanadium complexes with nitrate, acetate, and oxalate ions. *Russian Journal of Applied Chemistry*, 1966, **39**(11), 2262–2265.
153. Lukachina, V V; Pilipenko, A T; Karpova, O I. Ion Exchange Study of the State of Vanadium(V) in Perchloric Acid Solutions. *Russian Journal of Inorganic Chemistry*, 1977, **22**(5), 694–696.

154. Weisberg, S. *Applied linear regression*. 3rd ed. Hoboken, New Jersey: John Wiley & Sons, Inc.; 2005. ISBN 0-471-66379-4
155. Kazanjian, AR; Miner, FJ; Brown, AK; Hagan, PG. Radiolysis of nitric acid solution: LET effects. *Transactions of the Faraday Society*, 1970, **66**(X), 2192–2198.
156. Koltunov, V S; Shilin, I V; Nazarov, P P; Zhuravleva, G I. *Materialy simpoziuma SEV: Issledovania v oblasti pererabotki obluchennogo topliva (Proceedings of CMEA Symposium: Research in the area of the reprocessing of spent nuclear fuel)*. Karlovy Vary, Czechoslovak Socialist Republic: 1968.
157. Woods, M; Montag, T A; Sullivan, J C. A kinetic study of the oxidation of nitrous acid by Np(VI) and Am(VI) in perchlorate media. *Journal of Inorganic and Nuclear Chemistry*, 1976, **38**(11), 2059–2061. DOI:10.1016/0022-1902(76)80468-X
158. Hood, G. C.; Reilly, C. A. Ionization of Strong Electrolytes. VIII. Temperature Coefficient of Dissociation of Strong Acids by Proton Magnetic Resonance. *The Journal of Chemical Physics*, 1960, **32**(1), 127. DOI:10.1063/1.1700885
159. Matteson, Brent S. *The Chemistry of Acetohydroxamic Acid Related to Nuclear Fuel Reprocessing*. Oregon State University; 2010. URL: <http://hdl.handle.net/1957/16389>
160. Senent, María L; Niño, Alfonso; Muñoz Caro, Camelia; Ibeas, Satunino; García, Begoña; Leal, José M; Secco, Fernando; Venturini, Marcella. Deprotonation sites of acetohydroxamic acid isomers. A theoretical and experimental study. *The Journal of organic chemistry*, 2003, **68**(17), 6535–42. DOI:10.1021/jo0341564
161. Bard, Allen J; Faulkner, Larry R. *Electrochemical Methods: Fundamentals and Applications*. 2nd ed. New York, USA: John Wiley & Sons, Inc; 2000. ISBN 9780471043720
162. Savel'ev, Y.I.; Ershova, ZV; Vladimirova, MV. Alpha Radiolysis of Aqueous Solutions of Nitric Acid. *Soviet Radiochemistry*, 1967, **9**(2), 221–225.
163. Mincher, Bruce J.; Precek, Martin; Mezyk, Stephen P.; Martin, Leigh R.; Paulenova, Alena. The role of oxidizing radicals in neptunium speciation in γ -irradiated nitric acid. *Journal of Radioanalytical and Nuclear Chemistry*, 2012, (3), 10967. DOI:10.1007/s10967-012-1937-1
164. Plimmer, Robert Henry Aders. The action of nitrous acid upon amides and other amino-compounds. *Journal of the Chemical Society, Transactions*, 1925, **127**, 2651–2659. DOI:10.1039/ct9252702651

165. Arndt, F.; Amstutz, E. D.; Myers, R. R. Nitrosomethylurea. *Organic Syntheses*, 1943, **2**, 461.
166. Williams, D L H. *Nitrosation Reactions and the Chemistry of Nitric Oxide*. Amsterdam, The Netherlands: Elsevier B.V.; 2004. ISBN 978-0-444-51721-0
167. Hughes, M. N.; Stedman, G. The mechanism of the deamination of acetamide. *Journal of the Chemical Society (Resumed)*, 1964, 5840.
DOI:10.1039/jr9640005840
168. Vladimirova, M V; Kulikov, A; Ryabova, A A. Radiation Chemical Behavior Of Ions Of The Transuranium Elements In Nitric Acid Solutions. *Radiokhimiya*, 1975, **17**(2), 327–331.
169. Tananaev, I. G.; Dzyubenko, V. I. Interaction of neptunium(V) with hydrogen peroxide in nitric acid solutions. *Radiokhimiya*, 1988, **30**(6), 842–845.
170. Kulikov, I A; Milovanova, A S; Vladimirova, M V. Oxidation of Np(IV) in HNO₃ During Gamma-Radiolysis. *Soviet Radiochemistry*, 1981, **23**(4), 479–484.
171. Rykov, A. G.; Timofeev, G. A.; Yakovlev, G. N. Oxidation-reduction reactions of the actinide elements. IX. Kinetics of the reactions between neptunium(IV) and plutonium(IV) in perchlorate media. *Soviet Radiochemistry*, 1969, **11**(4), 443.
172. Choppin, Gregory R.; Jensen, Mark P. Actinides in Solution: Complexation and Kinetics. In: *The Chemistry of the Actinide and Transactinide Elements*. 3rd ed. Chapter 23, Ed. Lester R. Morss; Norman M. Edelstein; Jean Fuger Dordrecht: Springer Netherlands, 2006. pp. 2524–2621. ISBN 978-1-4020-3555-5.
DOI:10.1007/1-4020-3598-5_23.
173. Vladimirova, MV. Mathematical Modeling of the Radiation-chemical Behavior of Neptunium in Nitric acid. Equilibrium States. *Radiochemistry*, 1995, **37**(5), 410–416.
174. Burger, L L; Money, M D. *Nitrous Acid Behavior in PUREX Systems*. General Electric Co. Hanford Atomic Products Operation, Richland, Wash.: Hanford Laboratories Operation, Report HW-60278; 1959. URL:
http://www.osti.gov/energycitations/product.biblio.jsp?osti_id=4837565
175. Fletcher, J. M.; Scargill, D; Woodhead, J. L. The Nitrous Acid-Tributyl Phosphate Complex. *Journal of the Chemical Society (Resumed)*, 1961, (4), 1705.
DOI:10.1039/jr9610001705
176. Cohen, Donald; Hindman, J C. Oxidation Potentials of the Neptunium(III)-(IV) and the Neptunium(V)-(VI) Couples in Perchloric Acid. *Journal of the American Chemical Society*, 1952, **74**(18), 4679–4682. DOI:10.1021/ja01138a068

177. Nagaishi, Ryuji; Jiang, Pei-yun; Katsumura, Yosuke; Ishigure, Kenkichi. Primary Yields of Water Radiolysis in Concentrated Nitric Acid Solutions. *Journal of the Chemical Society, Faraday Transactions*, 1994, **90**(4), 591–595. DOI:10.1039/FT9949000591
178. Davis, W; Bruin, H.J. De. New activity coefficients of 0–100 per cent aqueous nitric acid. *Journal of Inorganic and Nuclear Chemistry*, 1964, **26**(6), 1069–1083. DOI:10.1016/0022-1902(64)80268-2
179. Daniels, Malcolm. Radiolysis and Photolysis of the Aqueous Nitrate System. In: *Radiation Chemistry*. Chapter 10, Ed. Edwin J. Hart Washington, D.C.: American Chemical Society, 1968. pp. 153–163. ISBN 0-8412-0082-3. DOI:10.1021/ba-1968-0081.ch010.
180. Vladimirova, M V; Kulikov, I A; Savel'ev, Y.I. Steady-state Concentrations of Nitrous Acid in Gamma-Irradiated Nitric Acid Solutions. *High Energy Chemistry*, 1969, **3**(6), 477–478.
181. Faraggi, M; Zehavi, D; Anbar, M. Radiolysis of aqueous nitrate solutions. *Transactions of the Faraday Society*, 1971, **67**, 701–710. DOI:10.1039/ft9716700701
182. Bhattacharya, P; Saini, R. Radiolytic yields G(HNO₂) and G(H₂O₂) in the aqueous nitric acid system. *International Journal for Radiation Physics and Chemistry*, 1973, **5**(1), 91–99. DOI:10.1016/0020-7055(73)90031-4
183. Andreichuk, N. N.; Rotmanov, K. V.; Frolov, A. A.; Vasiliev, V. Ya. Effect of Alpha-Radiation on the Valence States of Actinides IV. Kinetics of HNO₂ Formation In Nitric Acid Solutions. *Soviet Radiochemistry*, 1984, **26**(6), 701–706.
184. Jiang, Pei-Yun; Nagaishi, Ryuji; Yotsuyanagi, Tadasu; Katsumura, Yosuke; Ishigure, Kenkichi. Gamma-radiolysis study of concentrated nitric acid solutions. *Journal of the Chemical Society, Faraday Transactions*, 1994, **90**(1), 93. DOI:10.1039/ft9949000093
185. Precek, Martin; Paulenova, Alena; Tkac, Peter; Knapp, Nathan. Effect of Gamma Irradiation on the Oxidation State of Neptunium in Nitric Acid in the Presence of Selected Scavengers. *Separation Science and Technology*, 2010, **45**(12-13), 1699–1705. DOI:10.1080/01496395.2010.493833
186. Mincher, Bruce J.; Modolo, Giuseppe; Mezyk, Stephen P. Review Article: The Effects of Radiation Chemistry on Solvent Extraction: 2. A Review of Fission-Product Extraction. *Solvent Extraction and Ion Exchange*, 2009, **27**(3), 331–353. DOI:10.1080/07366290902821263

187. Mincher, Bruce J.; Modolo, Giuseppe; Mezyk, Stephen P. Review Article: The Effects of Radiation Chemistry on Solvent Extraction 3: A Review of Actinide and Lanthanide Extraction. *Solvent Extraction and Ion Exchange*, 2009, **27**(5-6), 579–606. DOI:10.1080/07366290903114098
188. Mincher, Bruce J.; Modolo, Giuseppe; Mezyk, Stephen P. Review: The Effects of Radiation Chemistry on Solvent Extraction 4: Separation of the Trivalent Actinides and Considerations for Radiation-Resistant Solvent Systems. *Solvent Extraction and Ion Exchange*, 2010, **28**(4), 415–436. DOI:10.1080/07366299.2010.485548
189. Enokida, Youichi; Suzuki, Atsuyuki. Reduction stripping of low-concentration Np(VI) loaded on 30% tri-n-butyl phosphate through laser-induced reactions. *Nuclear Technology*, 1989, **88**(1), 47–54.
190. Nikitenko, S. I.; Moisy, Ph.; Venault, L.; Madic, C. Kinetics of nitrous acid formation in a two-phase tri-n-butylphosphate-diluent/aqueous nitric acid extraction system under the effect of power ultrasound. *Ultrasonics Sonochemistry*, 2000, **7**(3), 135–144.
191. Shimizu, Ryosuke; Sawada, Kayo; Enokida, Youichi; Yamamoto, Ichiro. Generation of Nitrous Acid by Ultrasound Irradiation in the Organic Solution Consisting of Tri-n-butylphosphate, Nitric Acid and Water. *Journal of Nuclear Science and Technology*, 2005, **42**(11), 979–983. DOI:10.3327/jnst.42.979
192. Chaiko, David J; Vandegrift, George F. A Thermodynamic Model of Nitric Acid Extraction by Tri-n-butyl Phosphate. *Nuclear Technology*, 1988, **82**, 52–59.
193. Marin, Bernard; Sellier, Jean-Yves; Gourisse, Daniel. Study of the competition between nitric acid and nitrous acid during extractions by tributylphosphate. *Journal of Inorganic and Nuclear Chemistry*, 1973, **35**(8), 2907–2915. DOI:10.1016/0022-1902(73)80522-6
194. Tedder, D. William. Chapter 3 - Water Extraction. In: *Science and Technology of Tributyl Phosphate, Volume IV - Extraction of Water and Acids*. Chapter 3, Ed. Wallace Shulz; James D Navratil; A. Steven Kertes Boca Raton: CRC Press, 1991. pp. 35–70. ISBN 0-8493-63934.
195. Vione, Davide; Maurino, Valter; Minero, Claudio; Borghesi, Daniele; Lucchiari, Mirco; Pelizzetti, Ezio. New processes in the environmental chemistry of nitrite. 2. The role of hydrogen peroxide. *Environmental science & technology*, 2003, **37**(20), 4635–41.
196. Grätzel, M; Henglein, A; Lilie, J; Beck, G. Pulsradiolytische Untersuchung einiger Elementarprozesse der Oxydation und Reduktion des Nitritions. *Berichte der*

Bunsengesellschaft für physikalische Chemie, 1969, **73**(7), 646–653.
DOI:10.1002/bbpc.19690730707

197. Colston, B J; Choppin, G R. Evaluating the performance of a stopped-flow near-infrared spectrophotometer for studying fast kinetics of actinide reactions. 2001, **250**(1), 21–26.
198. Tighezza, A.; Aldhayan, D.; Rezgui, Y.; Alarifi, A. A good alternative to Numerical Methods of Integration for the Simulation of Chemical Kinetics: The Monte Carlo Method. *Asian Journal of Chemistry*, 2005, **17**(2), 840–848.
199. Sandu, Adrian. Positive Numerical Integration Methods for Chemical Kinetic Systems. *Journal of Computational Physics*, 2001, **170**(2), 589–602.
DOI:10.1006/jcph.2001.6750
200. Olcese, Luis E.; Toselli, Beatriz M. Fast and reliable numerical methods to simulate complex chemical kinetic mechanisms. *International Journal of Chemical Kinetics*, 1998, **30**(5), 349–358. DOI:10.1002/(SICI)1097-4601(1998)30:5<349::AID-KIN5>3.3.CO;2-X
201. Jonnalagadda, S.B.; Parumasur, N.; Shezi, M.N. A user-friendly programme “SimKINE” for simulation of kinetics involving complex reaction mechanisms. *Computational Biology and Chemistry*, 2003, **27**(2), 147–152.
DOI:10.1016/S1476-9271(02)00084-1
202. Svir, I.B.; Klymenko, O.V.; Platz, M.S. “KINFITSIM”—a software to fit kinetic data to a user selected mechanism. *Computers & Chemistry*, 2002, **26**(4), 379–386.
DOI:10.1016/S0097-8485(02)00014-1
203. Edsberg, L. Implementation of programs for interactive simulation of chemical kinetics. *Studies in Physical and Theoretical Chemistry*, 1981, **16**, 79–87.
204. Absolute density of water. In: *31st edition of CRC Handbook of Chemistry and Physics*. Ed. C Hodgman Cleveland, Ohio: 1948. pp. 1720.
205. Newton, T W. Redox Reactions of Plutonium Ions in Aqueous Solutions. In: *Advances in Plutonium Chemistry 1967-2000*. Ed. Darleane Hoffman La Grange Park, Illinois: American Nuclear Society, 2002. ISBN 0-89448-039-1.
206. Koltunov, V S; Frolov, K M; Marchenko, V I; Tikhonov, M F; Shapovalov, M P. Interaction of actinides and vanadium. VI. Equilibrium and oxidation kinetics of Pu(III) with vanadium(V). *Soviet Radiochemistry*, 1981, **23**(1), 83–90.
207. Koltunov, V S; Frolov, K M; Marchenko, V I; Tikhonov, M F; Shapovalov, M P. Interaction of actinides and vanadium. VII. Kinetics of Pu(IV) reduction by V(IV). *Soviet Radiochemistry*, 1981, **23**(1), 91–94.

208. Burkhart, Mary J; Newton, T W. Kinetics of the reaction between vanadium(II) and neptunium(IV) in aqueous perchlorate solutions. *The Journal of Physical Chemistry*, 1969, **73**(6), 1741–1746. DOI:10.1021/j100726a018
209. Appelman, E H; Sullivan, J C. Kinetics of the Vanadium(III)-Neptunium(V) Reaction in Perchlorate Solutions. *Journal of Physical Chemistry*, 1962, **66**(3), 442–445. DOI:10.1021/j100809a016
210. Sheppard, J. C. The Kinetics of Reduction of Neptunium(VI) by Vanadium(III) in Perchloric Acid. *Journal of Physical Chemistry*, 1964, **68**(5), 1190–1193. DOI:10.1021/j100787a038
211. Watkins, Kay O.; Sullivan, J. C.; Deutsch, Edward. Kinetic study of the reaction neptunium(VII) + vanadium(IV) -- neptunium(VI) + vanadium(V) in aqueous perchloric acid media. *Inorganic Chemistry*, 1974, **13**(7), 1712–1715. DOI:10.1021/ic50137a035
212. Rabideau, S.W.; Kline, R.J. The kinetics of the reaction between plutonium(IV) and vanadium(III) in perchlorate solution. *Journal of Inorganic and Nuclear Chemistry*, 1960, **14**(1-2), 91–97. DOI:10.1016/0022-1902(60)80204-7
213. Rabideau, SW. Kinetics of Oxidation Reduction Reactions of Plutonium. The Reaction between Plutonium (VI) and Vanadium (III) in Perchlorate Solutions. *The Journal of Physical Chemistry*, 1958, **62**(4), 414–417. DOI:10.1021/j150562a008
214. Klotz, Irene; Gorman, Steve. Mars rover landing a miracle of engineering - scientists say. Reuters, August 6, 2012; 2012. Accessed: August 6, 2012. <http://www.reuters.com/article/2012/08/06/us-usa-mars-idUSBRE8721A920120806>
215. *Mars Science Laboratory Launch - Press Kit - November 2011*. National Aeronautics and Space Administration, Press Kit - November 2011; 2011. ISBN 0113462026 URL: <http://solarsystem.nasa.gov/docs/MSLLaunch.pdf>
216. Nordion Company website - Discontinued Gamma Sterilization Products. 2012. http://www.nordion.com/our_products/discontinued_products.asp

APPENDIX A.
ANALYSIS OF KINETIC DATA USING NUMERIC INTEGRATION

A.1 Background, rationale and significance

The analysis of chemical kinetics of actinides is very important in the process of identification of new redox agents and in their application to the development of modern nuclear fuel reprocessing technologies. These compounds sometimes react in relatively complex way and the identification of their reaction mechanism and its rate parameters is very important for prediction of its behavior in industrial process conditions. Classical instruments for study of chemical kinetics of systems with homogeneous (zero dimensional) isothermal reactions are developed only for reactions that can be easily solved using integrated forms of the rate laws. For the simplest reactions such as first order decay reactions (e.g. hydrolysis):



it is possible to integrate the differential rate equation and receive its integrated form predicting the dependency on time t of the immediate concentration of X and A (denoted $[X]$, $[A]$) on the basis of the value of the initial concentration $[A]_0$ and the rate constant k :

$$+\frac{d[X]}{dt} = k \cdot [A] \Rightarrow [X] = [A]_0 \cdot (1 - e^{-k \cdot t}) \quad , \quad [A] = [A]_0 \cdot e^{-k \cdot t} \quad (180)$$

Nonetheless, the reaction mechanisms can be quite complex and even a very simple second order reversible reaction



that has similarly comparatively simple differential rate equation

$$+\frac{d[X]}{dt} = k_1 \cdot ([A]_0 - [X])^2 - k_2 \cdot \left(\frac{[X]}{2} \right)^2 \quad (182)$$

is more challenging to integrate and yields a relatively complex integrated solution [32]:

$$\frac{[X]_e}{2[A]_0 ([A]_0 - [X]_e)} \cdot \ln \frac{[X]([A]_0 - 2[X]_e) + [A]_0[X]_e}{[A]_0 ([X]_e - [X])} = k_1 \cdot t \quad (183)$$

The solution (183) necessitates the introduction of a measurement of concentration of X at equilibrium $[X]_e$ and a simple analytical expression of the time dependency of $[A]$, $[X]$ and $[Y]$, as was the previous case (180), is not possible for (183).

Therefore, in systems where an unknown mechanism is composed of more than one kinetic reaction, the determination of the correct mechanism on the basis of the dependency of the concentration of one or several reactant or product species is a very laborious problem. For each proposed mechanism, which may involve several reactions between the reacting species, it is necessary to integrate the given set of differential rate equations. Sometimes these equations do not have an analytic solution. Even in case of successful integration, the resulting solution usually does not allow to express the individual concentrations as functions of time, initial concentrations and rate constants.

In experimental chemical kinetic research, kinetic equations of simpler reactions are usually integrated into forms similar to (183). For each point of time the measured time dependencies of concentrations of reactant and product species are used to calculate the left hand side of the equation and then plotted versus time. If the mechanism was correctly identified (and presuming that the experimental data were measured correctly), the slope of a linear fit through the data-points provides the rate constant of the studied reaction (for examples, see [113, 197]). In cases when the data cannot be fitted by a linear plot, a new mechanism has to be proposed, integrated and evaluated.

The process of testing proposed reaction mechanisms can be considerably easier by a chemical kinetic model that uses a numeric integration method (or in some cases a probability based calculation engine, such as a Monte-Carlo method [198]). The advantage of this approach is that it provides the researcher directly with the time dependencies of modeled concentrations that can be easily compared to the time dependencies of experimentally measured concentrations. Rate constants can then be calculated by a fitting procedure.

At present, numerical modeling of chemical kinetics is used for the purposes of research in chemical engineering. These tools are mainly dedicated to solving heterogeneous chemical kinetics in chemical reactors. The numerical problems are complicated by inclusion of differential equations of 3-dimensional mass-flow, phase-transport and heat-transfer. Tools for simplification of the routine study of complex reaction mechanisms in homogeneous chemical kinetics have been of a somewhat smaller interest.

Nevertheless, various numeric methods and programs for calculating homogeneous chemical kinetic models have been developed and used by many authors [198, 199, 200,

201, 202]. Particular interest areas were atmospheric chemistry and biochemistry. Although the robustness, resource efficiency and precision of some of these programs has become very high through gradual improvements (such as *SimKINE* [201], *KinFitSim*[®] [202]), these programs have usually the disadvantage of inconvenient interfacing with spreadsheet software – most notably *Microsoft*[®] *Office Excel*[®] (further on referred to as Excel) – that is nowadays predominantly used for data analysis by researchers with background in chemistry. In best cases these programs allow batch-wise direct input and output of data by the means of the operating system's clipboard, in the worst cases specially formatted data-files have to be created as input for the model and the output files then have to be imported back to the spreadsheet for further data-processing.

The spreadsheet software has become sufficiently robust and allows the coupling of three most important aspects in data analysis – data storage in an ordered cell structure, direct calculations using embedded functions and graphical display of data in charts, which can be modified to a high degree to user's desire. In addition, the modern Excel spreadsheet software (in its versions since 1990) includes the *Solver* add-in which makes possible to search for an optimal combination of rate constant values for a given mechanism. It is possible to build simple non-iterative numeric integrator method directly in the spreadsheet or in case of Excel use its interface with Visual Basic for Application[®] programming language environment to program more advanced algorithms as so called 'Macros'. Besides the simplicity of working in a single environment that is familiar to the researcher, the advantage of this approach lies within the possibility of real-time linking of the output data of a numeric model built inside the spreadsheet to post-processing operations in the spreadsheet that can be themselves the source of variables for the fitting procedure.

During the work on this project the author has developed a tool for analysis of chemical kinetics relevant to redox reactions of actinide elements by numeric modeling. The modeling engine is based on the Runge Kutta 4th order method (abbrev. RK4) [150] to integrate the problem set of ordinary differential equations in a *Microsoft*[®] *Office Excel*[®] spreadsheet environment. The model facilitates the use of its *Solver* add-in tool to fit

modeled concentration curves to concentrations calculated from measured spectrophotometric data by optimizing reaction rate constants.

A.2 Chemical kinetics as a set of differential equations

In order to understand the selected to the construction of a universally applicable numeric model that would enable fast evaluation of different reaction mechanisms, it is necessary to understand the unique form of the set of the differential equations of chemical kinetics. For a number of N species, the rate of change of the concentration of a particular chemical species A_i by a particular chemical reaction m is proportional to the rate of this reaction r_m and to the stoichiometric coefficient c_{im} .

$$\left(\frac{d[A_i]}{dt} \right)_m = c_{im} \cdot r_m \quad (184)$$

The coefficient expresses the production (if $c_{im} > 0$), consumption (if $c_{im} < 0$) or no change ($c_{im} = 0$) of the reactant A_i by the reaction m . The rate of the reaction m is proportional to a rate constant k_m and to the product of concentrations of all the N present species $A_1, A_2 \dots A_N$, each raised to a given power $\alpha_{m1}, \alpha_{m2} \dots \alpha_{mN}$.

$$r_m = k_m \cdot \prod_{j=1}^{j=N} [A_j]^{\alpha_{mj}} = k_m \cdot [A_1]^{\alpha_{m1}} \cdot [A_2]^{\alpha_{m2}} \dots [A_N]^{\alpha_{mN}} \quad (185)$$

In case a particular species A_j is not contributing to the rate of the reaction m , its power α_{mj} is equal to zero and the reaction order with respect to A_j is then zero. The overall reaction order of reaction m is equal to the sum of all the powers.

The effect of all the M reactions taking place in the studied system on the concentration of species A_i is a sum of the individual contributions:

$$\frac{d[A_i]}{dt} = \sum_{m=1}^{m=M} \left(\frac{d[A_i]}{dt} \right)_m \quad (186)$$

Combining (184), (185) and (186), it is possible to derive a general differential equation that describes the overall change the concentration of species A_i in the system:

$$\frac{d[A_i]}{dt} = \sum_{m=1}^{m=M} \left(c_{im} \cdot k_m \cdot \prod_{j=1}^{j=N} [A_j]^{\alpha_{mj}} \right) \quad (187)$$

As stated before, the model is based upon a numeric integration of a general set of these differential equations (120) using a single-step method, such as is the Runge-Kutta 4th

order method (RK4) [150]. The model calculates the concentrations of reacting species as a function of time. For a given set of c_{im} and α_{im} (usually integers or simple fractions of integer numbers selected manually) the optimized variables are the rate constants k_m of each assumed reaction m . Therefore, a mathematical solution is sought as a set of differential equations (120), where each reaction is proportional to concentrations of a reactants present in the system c_{im} , each of which is raised to a certain power α_{im} . A system of equations that is reasonably well capable of elucidating the mechanism of the reaction in each of the observed experiments is then expected to suggest an explanation of the mechanism of the studied reaction system.

A.3 Runge-Kutta 4th order (RK4) method

The RK4 is one of the most widely used numeric methods for integrating a set of differential equations because of its universality, ease of programming and robustness [150].

A step change in the value of the integrated function during a time step from point t_i to point $t_i + h$ calculated on the basis of 4 intermediate steps. The intermediate steps are predicting the dependence of the value of the derivative at the beginning, in the middle and at the end of this time interval.

For a differential equation of the form:

$$\frac{dy}{dt} = f(t, y) \quad (188)$$

the recursive prediction of the value y_{i+1} of the integrated function y at the end of the time-step h is based on the following formula:

$$y_{i+1} = y_i + \frac{1}{6} \cdot (q_1 + 2 \cdot q_2 + 2 \cdot q_3 + q_4) \cdot h \quad (189)$$

The co-efficients q_1 to q_4 are calculated on the basis of four recursive equations:

$$q_1 = f(t_i, y_i) \quad (190)$$

$$q_2 = f\left(t_i + \frac{h}{2}, y_i + q_1 \cdot \frac{h}{2}\right) \quad (191)$$

$$q_3 = f\left(t_i + \frac{h}{2}, y_i + q_2 \cdot \frac{h}{2}\right) \quad (192)$$

$$k_4 = f(t_i + h, y_i + q_3 \cdot h) \quad (193)$$

The main reason behind choosing the RK4 method over other single-step numeric methods is its ratio of its precision to the computing resource efficiency. This method is a significant improvement over the simpler Euler method that calculates the change only on the basis of the derivative at the beginning of the interval - for the differential equation defined as (188) the form of Euler's method is:

$$y_{i+1} = y_i + h \cdot f(t_i, y_i) \quad (194)$$

The equation (194) indicates that Euler's method needs 5-times smaller number of calculations per step. However, with reducing the step-size h the computation error with RK4 decreases with the order of h^4 , whereas for the Euler method it decreases only with the order of h^1 [150]. Halving the step-size thus increases the RK4 accuracy over the Euler method 8 times and thus fully compensates for the 5-times higher number of calculations per step. The high precision decreases the necessity for a large number of calculation steps in the kinetic model, reduces the necessary calculation time and reduces the number of cells necessary to reach sufficient precision when it would be implemented in a spreadsheet.

A.4 Solution of rate equations by the RK4 numeric method

As is described above, the solution of the set of rate equations in the environment of the Excel spreadsheet is based on calculating the four intermediate steps using regular in-cell calculations, no Visual Basic procedure or function ("Macro") is necessary to be activated. In the following text the description of the implementation of the RK4 method of numerical solution of a set of chemical kinetic equations (120) is described.

The input information for the calculation of the following step is the number of N immediate concentrations $[A_i]$ at time t , the appropriate reaction powers α_{im} , the reaction stoichiometric coefficients c_{im} and the rate constants k_{im} (of which the latter three remain constant during all calculations). Each intermediate step is based on two sub-calculations and provides an input for a successive intermediate step.

First – in the intermediate step no. 1, the reaction rates $(r_m)_1$ are calculated for all the M reactions present in the model (184) based on the concentrations of all N species at time t – denoted $([A_i])_t$. The reaction rates then are used in the second sub-step to calculate a

prediction of the concentrations of all A_i in the middle of the interval $([A_i J])_1$. Intermediate step no. 2 uses the predictions of concentrations of intermediate step no. 1 to calculate the values of the reaction rates at the mid-point $(r_m)_2$ and then use these to give a modified prediction of concentrations - $([A_i J])_2$. Intermediate step no. 3 and 4 work similarly, but they result in predictions of the concentrations at the end of the interval – as is summarized in the following proposal of all the intermediate calculations for each step.

$$\begin{array}{ll}
 (r_m)_1 = k_m \cdot \prod_{i=1}^{i=N} ([A_i J]^{a_{mi}})_t & ([A_i J])_1 = ([A_i J])_t + \frac{h}{2} \cdot \sum_{m=1}^{m=M} [c_{im} \cdot (r_m)_1] \\
 (r_m)_2 = k_m \cdot \prod_{i=1}^{i=N} ([A_i J]^{a_{mi}})_1 & ([A_i J])_2 = ([A_i J])_t + \frac{h}{2} \cdot \sum_{m=1}^{m=M} [c_{im} \cdot (r_m)_2] \\
 (r_m)_3 = k_m \cdot \prod_{i=1}^{i=N} ([A_i J]^{a_{mi}})_2 & ([A_i J])_3 = ([A_i J])_t + h \cdot \sum_{m=1}^{m=M} [c_{im} \cdot (r_m)_3] \\
 (r_m)_4 = k_m \cdot \prod_{i=1}^{i=N} ([A_i J]^{a_{mi}})_3 & ([A_i J])_4 = ([A_i J])_t + h \cdot \sum_{m=1}^{m=M} [c_{im} \cdot (r_m)_4]
 \end{array}
 \quad \begin{array}{l}
 (195 \text{ a-} \\
 \text{d)} \\
 \text{d)} \\
 \text{d)}
 \end{array}
 \quad \begin{array}{l}
 (196 \text{ a-} \\
 \text{d)} \\
 \text{d)} \\
 \text{d)}
 \end{array}$$

For each species A_i , the four predictions are used to calculate its concentration at the end of the interval by a formula stylized into the form of the recurrence relation:

$$([A_i J])_{t+h} = ([A_i J])_t + \frac{1}{6} \cdot \left\{ \begin{array}{l} 2 \cdot [(A_i J)_1 - (A_i J)_t] + 4 \cdot [(A_i J)_2 - (A_i J)_t] \\ + 2 \cdot [(A_i J)_3 - (A_i J)_t] + [(A_i J)_4 - (A_i J)_t] \end{array} \right\} \quad (197)$$

The second term of the formula on the right hand side represents a weighed change of the concentration of A_i over all the interval t to $t+h$ with two times higher relative weigh given to predictions no. 2 and 3 - these predictions utilize the rates calculated for the midpoint. Note that the concentration changes for predictions no. 1 and 2 calculated for the midpoint are additionally multiplied by two to extend them toward the end of the interval h so that they are comparable to concentration changes for predictions no. 3 and 4.

A.5 Implementation of the RK4 method in an Excel spreadsheet

Because the calculation scheme proposed above is not iterative, it is possible to implement it in an Excel spreadsheet with each calculated value stored in a specific cell. For one time-step of the length h represented by a row in the spreadsheet, a reaction needs 4 columns (195 a-d) and each species additional 5 columns (196 a-d) + (197). In the current implementation a matrix of 6 possible mutual reactions of 5 different species

is used, thus taking the space of 49 columns. Due to the flexibility of the Excel environment a potential future extension of the size of the model would be very easy (version 2003 of the Excel software supports up to 256 columns by 65 536 rows, version 2007 supports 16 384 columns by 1 048 576 rows).

Within the spreadsheets, the calculated values of concentrations are then compared to experimentally determined concentrations of several key species – e.g. concentrations calculated from spectrophotometric measurements of chemical reactions of actinides. For a selected number of species their sum of squares of differences S between experimentally measured and numerically modeled concentrations is calculated. For a given set of stoichiometric co-efficients c_{im} and reaction powers α_{im} the optimal rate constants k_m would be identified by using the *Solver* add-in to vary the rate constants to achieve a minimum sum of squares S .

The number of steps calculated in the current model is held constant and equal to around 32 in order to maintain precision and at the same time minimize the computation time. The length of each time-step is calculated on the basis of the experimental reaction time so that the 32 steps fill the whole length of the measured reaction interval, but the distribution of the time-points is altered by a user-controlled distribution function to give larger impact weight to a certain portion of the measured data which carries more information about the course of the reaction (e.g. in case of a reaction curve, where 90% of the data-points represent the last 10% of the conversion toward an equilibrium, it is possible to reassign 90% of the time-points to the group representing the first 90% of the reaction conversion).

The experimental data and model results is then plotted in charts to quickly display a result of a particular modeling run. Two groups of parameters of the model - stoichiometric co-efficients c_{im} and reaction powers α_{im} - have to be manually adjusted for each new proposed mechanism (this operation is the essential replacement of the laborious – if not impossible - integration of the set of rate equations in the classical approach). The optimal rate constants k_m are then in an ideal case acquired entirely automatically by running the *Solver* add-in; however, in practical applications a manual adjustment (a "guess") is necessary in certain cases when the solution of the constant is

considerably distant from the optimal solution and the *Solver* is not able to find the optimal solution.

Although the RK4 method is usually sufficient to explain the kinetic data from spectrophotometric measurements, it is not possible to use the method for modeling of concentration of ultra-low concentrations of short-lived intermediary products. Very large reaction rate constants in relation to the calculation time-step (when a reaction could convert all the reactants into products in one time-step) can force the model to exhibit non-realistic oscillation behavior. This so called "stiff system" problem [203] is caused by the inherent deficiency of the RK4 numeric method and prevents the calculation of e.g. fast reversible reactions of intermediate reaction products. These reactions – if their introduction into the system is necessary – have to be studied using quasi-equilibrium approach by an easy modification of the pattern of spreadsheet calculation.

Adaptation of more advanced numeric methods able to solve "stiff system" problems into the spreadsheet environment might be possible.

APPENDIX B.
ANALYSIS OF ERRORS OF PIPETTING USING
EPPENDORF VARIABLE VOLUME PIPETTES

B.1 Introduction

In the transuranic element radiochemical laboratory (TRUCLAB) of Dr. Alena Paulenova in the Radiation Center of Oregon State University, dispensing of small volumes is performed using a variety of pipettes. The error of a particular dispensation for a particular volume setting of pipet can be calibrated using the very accurate determination of weight of each dispensation on an analytical balance. At present, pipetting is routinely done with variable volume pipettors with disposable tip. During serial pipetting with large amounts of used pipet tips, it is impossible to perform calibrations for each particular tip. Moreover, tips from different manufacturers are being used in the laboratory. This study was performed to estimate the following errors:

- Errors when pipetting with the same pipette tip
- Errors between tips of the same type from the same manufacturer
- Errors between tips of different manufacturers

At a particular volume setting, the pipettor was designed by the manufacturer to deliver a nominal volume of fluid V_o . However, a pipette equipped with a particular individual tip will exhibit two kinds of errors making the actual volume dispensed V be different from the nominal volume ($V \neq V_o$). The first kind of error is a systematic error – otherwise referred to as inaccuracy or bias B_i . The second error is usually called imprecision and represents the random error of dispensation R . The random error fluctuates with successive aliquot deliveries, its distribution is assumed to be close to normal and the error can be characterized by a standard deviation SR . The mean value of the random error is assumed to be equal to zero. An individual dispensation is thus equal to the nominal value corrected for the sum of these one-time errors:

$$V = V_o + B_i + R \quad (198)$$

Exchanging the pipette tip for a different one introduces a different value of B_i . Since it can be assumed that the variable B_i behaves as a random variable itself, for a particular brand of pipette tip estimates of the average value of the bias B_{avg} and its standard deviation SB can be established. The combination of the random error of dispensation and

the random error of the tip bias gives rise to a combined random error E with a standard deviation SE , which can be theoretically calculated as a geometric average of SR and SE , according to the rules of error propagation:

$$SE = \sqrt{SR^2 + SB^2} \quad (199)$$

If we assume that the combined random error SE has a normal distribution, 68% of our dispersions with individually uncalibrated tips will then result in dispersions in the following range:

$$V = V_o + B_{avg} \pm SE \quad (200)$$

Even though the pipettor is not changing, tips from different manufacturers will have different values of their average bias value B_{avg} with different values of standard deviations SB and SR , due to their different construction and design and due to different level of manufacturing consistency between the tips.

By calibrating the pipet with one particular pipet tip, it is possible to determine an estimate of the individual tip bias B_i and thus eliminate the effect of the randomness due to differences between the biases of different tips of the same brand (which demonstrates itself as SB) from the overall random error SE . Thereafter, the remaining uncertainty comes from the random error of dispersion R of one particular tip, with standard deviation SR , which is fundamentally unavoidable.

Calibration of each tip is of course not always possible or practical and an estimate of the pipetting error needs to be done that includes the larger error SE caused by differences between the tips. Below, the relative values (as percentage of the nominal dispersion value) of average bias B_{avg} and the standard deviation of the combined error SE for different variable volume pipettors, brands of tips, and volume settings are reported in a graphical form.

B.2 Experimental

In order to avoid the introduction of pipetting technique error, the most recent appropriations of the lab - digital variable pipettors Xplorer from the German company Eppendorf - were used for the analysis. The motor-driven digitally controlled piston made sure that the individual aspirations and dispersions were reproducible, as opposed to manual pipettors (nonetheless, two manual pipettors were also tested in the end of the

experiments in order to compare the acquired results). The speed of dispensation and aspiration of the Xplorer digital pipettors can be varied in 8 steps. Plastic pipette tips from different manufacturers were used in the study.

De-ionized water with its well-known density dependence on temperature [204] (measured by a NIST-traceable digital thermistor thermometer from Cole-Palmer) was used as the working liquid. A Sartorius CP225D digital analytical balance was used for weighing the water dispersions, the standard deviation of weighing repeatability given by the manufacturer was below 0.02/0.05/0.1 mg for weighing below 40/80/220 g, respectively. Water evaporation error was attempted to be minimized by employing narrow-necked vessels. Different vessels appropriate for the size of the volumes were used, most of the measurements with dispersions bigger than 300 μL were done using a small 50 mL Erlenmeyer flask, smaller dispersions were collected into a 2 mL cryogenic vial stabilized in a tilted position in a small 10 mL glass beaker by paper wipes (this design allowed easier addition of the aliquot from the side door of the analytical balance). Water evaporation was spotted as an issue in stabilization of the balances, usually gradually decreasing the weight, while introducing an underestimation error of $\pm 0.05\text{mg}$. In experiments with 1-10 μL amounts, the evaporation rate was determined for the particular vessel (on the order of 0.01 mg/ 10s) and results were compensated for during the balance settling time. Attempts to prevent water evaporation by using vessels containing NaCl salt or dry silicagel particles were unsuccessful. Sodium chloride didn't prevent water vapor loss, while silicagel has exhibited an inverted effect – weight increase due to capturing of air humidity.

B.2.1 Dependence on the pipetting speed:

Only single experiment was performed on the influence of the aspirating and dispensing speed on the random error of dispensation. The same 1mL tip Eppendorf tip was used for a 1000 μL dispensation. Setting of the aspirating and dispensing speed is possible in eight one-step increments between “1” (slowest) and “8” (fastest). Four possible combinations of the extremes of setting were tried (8/8, 8/1, 1/8 and 1/1). Surprisingly, no excessive change in the random error of pipetting was observed, despite the rate of aspiration/dispensation at speed setting “8” being approximately one order of magnitude

faster than at speed “1”. The relatively small random error did increase approximately two-fold from ~0.08% to ~0.15% with change of the aspiration speed, no effect of change in the dispensation speed was observed.

Thus, it was concluded that the aspiration speed is more important than the dispensation speed on the random error behavior. During the experiments, the aspiration/dispensation speed was kept as low as reasonably attainable for achieving the experiments in a sufficiently fast fashion – speed settings between “2” and “4” were used.

B.2.2 Effect of Pipette Tip Pre-rinsing

During the pipetting a dynamic behavior was observed (see Figure 61). The average dispensation with a fresh unwetted tip was significantly different from dispensations made with a pipette tip that has already performed several initial pipettings. Therefore the results of the *accuracy* (as *average bias* of dispensation against the desired value) and *precision* (the standard deviation of the *random error* of dispensation around the average dispensed value of one particular tip) are reported separately for the fresh tip (as *SE*) and for the values recorded past the 3rd dispensation (as *SR*). Standard deviation of the average bias between pre-wetted tips *SB* is also reported.

For a specific brand of tips, the standard deviation of the random error of dispensation *SR* of one particular tip after the pre-wetting was usually smaller by 20-50% than the random error introduced by differences between the average values of dispensation between individual tips *SE* – this is summarized in Table 14 of all experimental results later in this appendix.

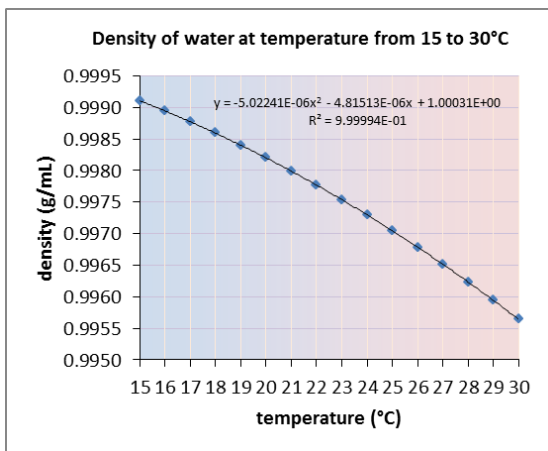


Figure 60 – Density of water (ref. [204])

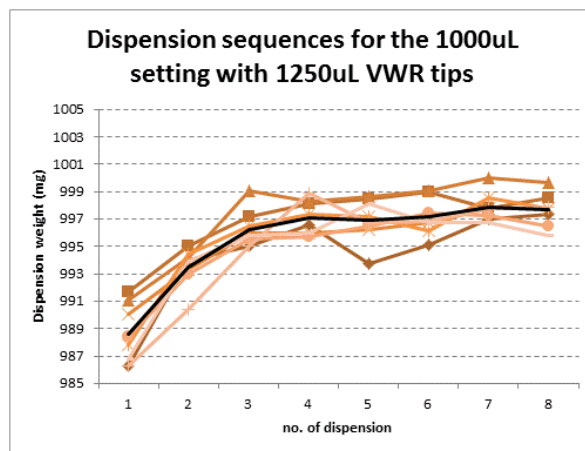


Figure 61 – Example of dispensation data

B.3 Results

B.3.1 1 mL digital pipettor

The pipetting characteristics for the 50, 300 and 1000 μL settings were tested (50 μL is the lowest possible setting for the 1mL Xplorer digital pipettor). Due to expected worsening of the accuracy, the manufacturer recommends to use the pipet only in the 30-100% capacity range. Three different types of pipet tips: the 1250 μL capacity “Ultrafine” tip from VWR International, and the 1000 μL tip and 1250 μL tips from Eppendorf. The construction of these tips differs primarily in their length, shape of the tip, size of the lower (for liquid displacement) opening and the design of the upper opening sleeve (for air displacement) where the pipettors are pressed into the tip to create a leak-tight seal. The VWR tip was the longest, followed closely by the 1250 μL Eppendorf tip, while the 1000 μL tip was somewhat shorter (see Figure 62). The 1250 μL tip featured a much wider liquid entrance (less fine tip) than the other two pipette tips.

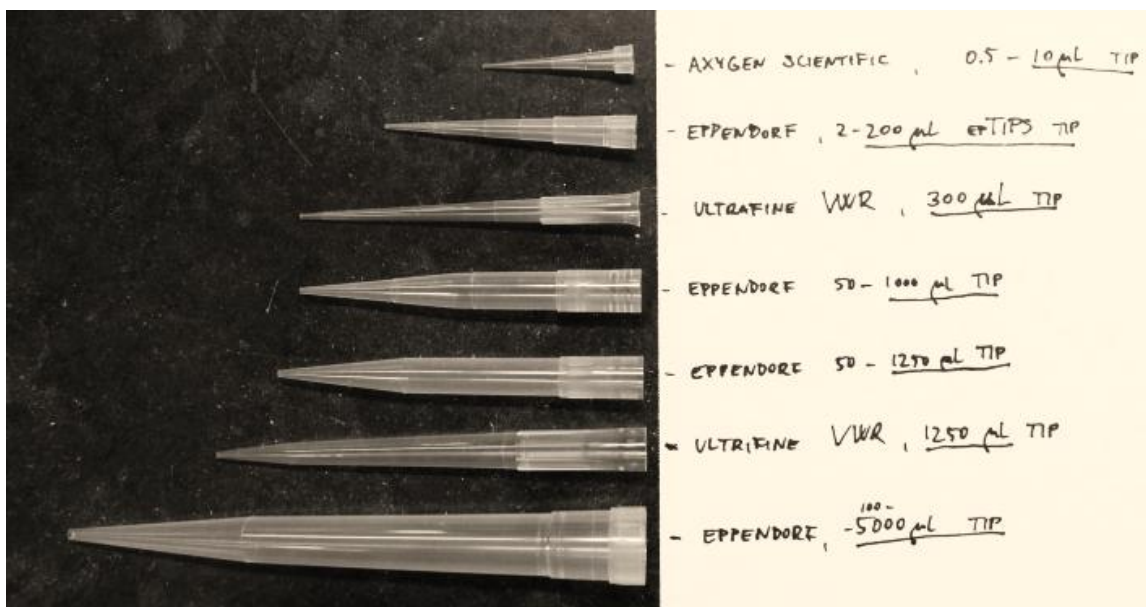


Figure 62- Photography of pipette tips employed during this study

The results seen below indicate that the 1250 μL (green) Eppendorf tips had the most significant problems with random error (in the lowest 50 μL setting, significant issue was random liquid implosion taking place during the blow-out phase, as a result of the implosion a small droplet of liquid stays inside the tip and cannot be removed, until

washed down by a new liquid aspiration). The random error of both 1250 μL VWR and the 1000 μL Eppendorf tips were comparable, with the accuracy of dispersions being significantly dependent on the pre-rinsing. The bias of most of the dispersions with all types of pre-rinsed tips was within the $\pm 1\%$ error range in the recommended 1/3-3/3 volume setting range.

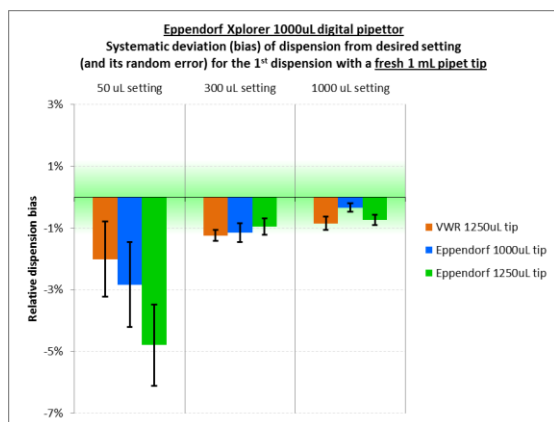


Figure 63 – Errors of the 1mL pipettor (fresh tips)

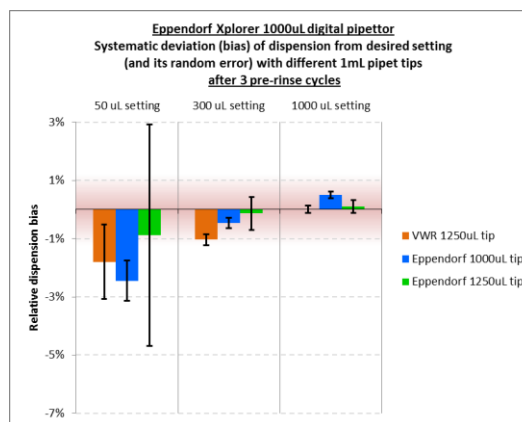


Figure 64 – Errors of the 1mL pipettor (rinsed tips)

B.3.2 300 μL digital pipettor

The pipetting characteristics for the 15.0 μL , 50.0 μL and 300.0 μL settings were tested for the 15 - 300 μL Xplorer digital pipettor. Two different types of pipet tips were evaluated: the 300 μL capacity “Ultrafine” tip from VWR International and the shorter 200 μL tip from Eppendorf. Surprisingly, it was quite possible to aspirate 300 μL of water into the nominally 200 μL capacity Eppendorf tips; however, this practice cannot be recommended because the liquid was separated by only 1 mm of air from the mouth of the pipettor, significantly increasing the risk of internal contamination of the pipettor.

Results of pipetting indicate that only the Eppendorf tips preserve the accuracy within the $\pm 1\%$ range. Some VWR tips have randomly exhibited unpleasant implosions when blowing out 50 μL water samples which resulted in a large random error.

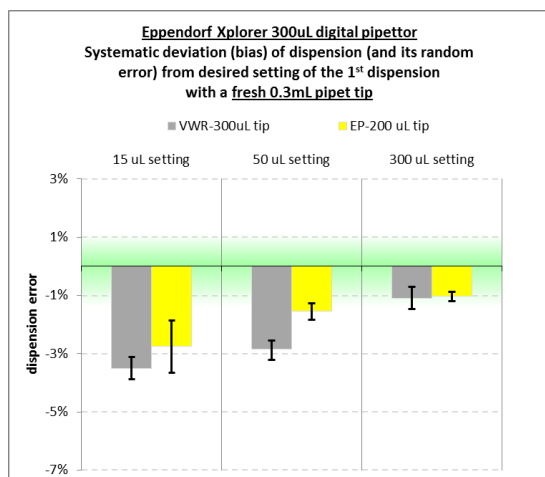


Figure 65 – Errors of the 300µL pipettor (fresh tips)

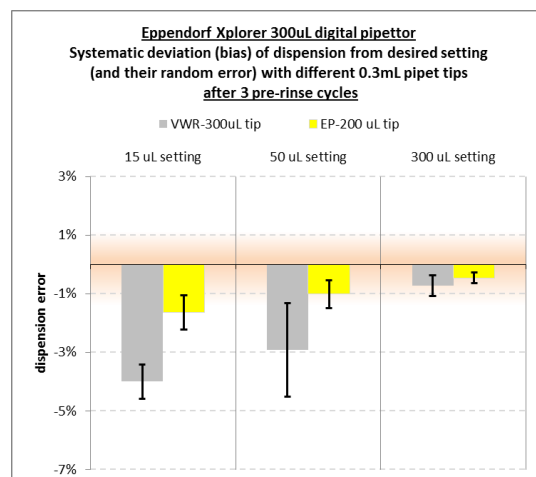


Figure 66 – Errors of the 300µL pipettor (rinsed tips)

B.3.3 5mL digital pipettor

Pipetting with the 5mL digital Eppendorf Xplorer pipettor while using the 5mL tips from the same manufacturer has proven to be very accurate and precise for the settings of 1000 and 5000 µL that are likely to be limiting the range of most commonly used settings for this large-volume pipettor, since smaller volumes than 1 mL are more precisely dispensed by pipettors of smaller nominal capacity. At the lowest possible setting of 250µL the dispersions exhibited significant bias and random error, but approximately only 3-times higher than for the 300 and 1000µL pipettor – therefore not ruling out its use in this range entirely.

At the highest 5000µL setting the differences in the bias of each individual tip proved to be the primary source of random error. A properly calibrated pipet with a 5mL could achieve an average random error well below $\pm 0.1\%$ (95% of dispersions would lie in an interval of $\pm 5\mu\text{L}$). At the 1000µL setting the results of bias and random error were quite comparable to the same setting for the 1mL pipettor.

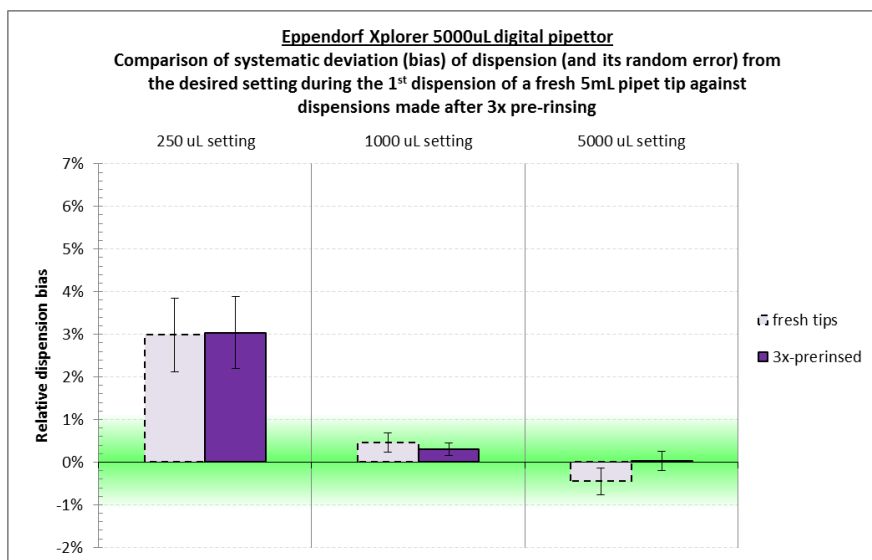


Figure 67 – Errors of the 5 mL pipettor

B.3.4 Dependence for the 10 μ L digital pipettor

The digital Xplorer micro-pipettor for dispensing of 10 μ L is naturally the device most likely to exhibit significant systematic and random errors due to the increasing effect of capillary forces and viscosity on the behavior of liquids at small linear dimensions and thus at small volumes too. Using the 10 μ L capacity tips from Axygen Scientific, two volumes were selected for dispensation: 1 and 10 μ L. While experimenting with the 1.0 μ L volume setting the evaporation errors arising as a result of the relatively long stabilization period of the analytical balance with purported precision of ± 0.01 mg (i.e. $\pm 1\%$ for the 1.0 μ L setting) were high enough that characterization of the pipettor lowest dispensing limit of 0.5 μ L was not attempted. At the 10 μ L level the pipettor was able to approach the 1% uncertainty level. The droplet was formed and was separated from the tip during the blown out phase relatively reliably by a small shaking motion with the pipettor. At the 1 μ L volume, however, the liquid droplet extruded from the capillary ending of the tip would not detach so the only possibility was direct immersion of the tip into a larger volume (droplet) of liquid. Visual observation didn't appear to suggest that some volume of water would stay in the tip, but the observed bias and random error was very high – the range of dispensation volumes spanned almost one fifth of the total pre-set volume for a pre-rinsed tip. This behavior was in a stark contrast to the values provided by the pipettor

manufacturer; however, it is important to note that the appropriate pipet tips were not used in this experiment.

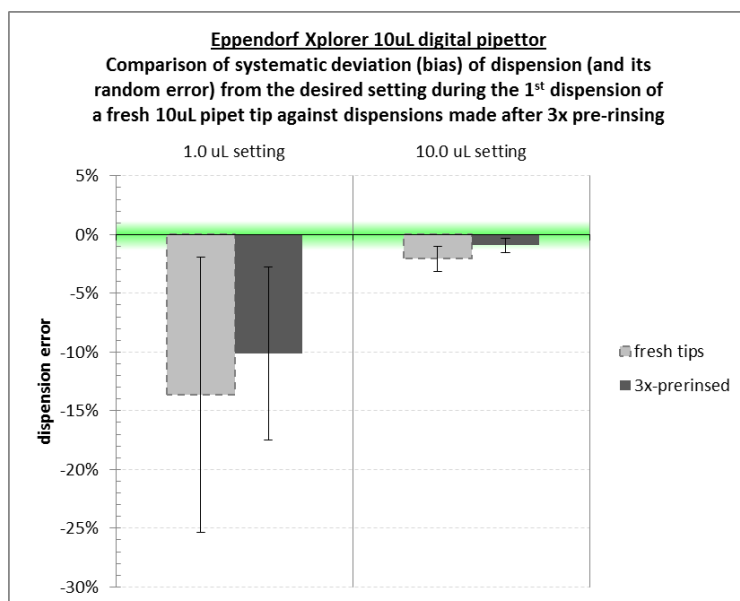


Figure 68 – Errors of the 10 μ L pipettor

B.3.5 Manual 100 μ L and 1000 μ L pipettors

In order to complement the performed study on the pipetting performance of manual pipettors, the Eppendorf Research pipettors for 100 μ L and 1000 μ L have been selected. The pipettors have been tested with the Eppendorf tips (200 μ L / 1000 μ L) and its alternative from the VWR International company (300 μ L / 1250 μ L) at one volume setting only – the nominal capacity volume of 100.0 μ L and 1000 μ L respectively. In the case of the 100 μ L pipettor, pre-wetting almost eliminated the bias with the Eppendorf 200 μ L tip, while significantly outperforming the VWR tip, which exhibited unpleasant implosion behavior after pre-rinsing, similar to the one seen for the 50 μ L dispensations with the digital pipettor. In case of the 1mL pipettor, no significant effect of pre-rinsing on the inaccuracy (bias) was observed, only a reduction in the random error. Besides the value of the bias, at this 1000 μ L setting the manual pipettor was quite comparable in its low random error to the digital Xplorer pipettor.

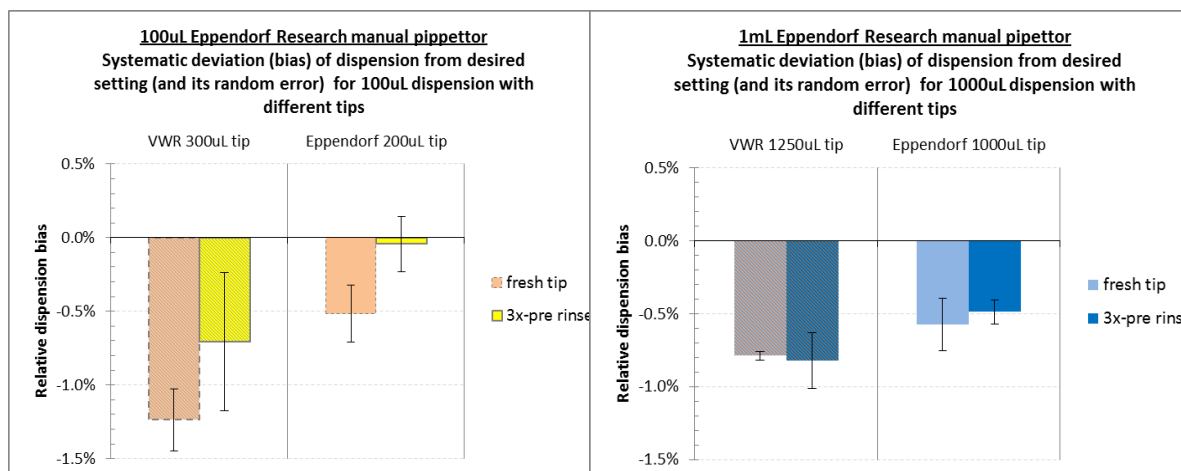


Figure 69 – Errors of the 100 µL manual pipettor

Figure 70 – Errors of the 1 mL manual pipettor

B.4 Concluding Recommendations

- Pre-rinsing the pipet tip 3 times significantly reduces overall dispensation error.
- Calibration of the pipette should be done with one particular brand of pipette tip to reduce systematic error.
- If possible – utilization of a single pipet tip allows complete elimination of the systematic pipetting error, leaving only the random pipetting error, which is usually very small for settings close to maximum capacity.
- Pipette tips provided by the pipette manufacturer appear to have usually better results than alternative brands from competitors.
- The errors determined in Table 14 below are relevant only for the pipetting of dilute water solutions – pipetting with different liquids (especially with organic solvents and with highly volatile solutions) will introduce much bigger systematic and random errors.

Table 14 – Summary of all experimental results

Pipettor type	Volume setting	Pipette tip type and brand	Fresh tip error		3x-pre-rinsed tip error		
			Average bias B_{avg}	Random error SE	Average bias B_{avg}	St. deviation of bias (tip-to-tip error) SB	Random error of one tip SR
10 μ L Eppendorf Xplorer (digital)	1.00 μ L	10 μ L Axygen Sci.	-13.64% \pm 11.68%	(-10.13% \pm 6.46%) \pm 4.28%			
	10.00 μ L		-2.07% \pm 1.08%	(-0.91% \pm 0.52%) \pm 0.37%			
300 μ L Eppendorf Xplorer (digital)	15.0 μ L	200 μ L Eppendorf	-2.76% \pm 0.90%	(-1.65% \pm 0.35%) \pm 0.50%			
		300 μ L VWR	-3.50% \pm 0.37%	(-4.01% \pm 0.21%) \pm 0.54%			
	50.0 μ L	200 μ L Eppendorf	-1.55% \pm 0.28%	(-1.02% \pm 0.36%) \pm 0.30%			
		300 μ L VWR	-2.84% \pm 0.30%	(-2.93% \pm 0.42%) \pm 1.15%			
	300.0 μ L	200 μ L Eppendorf	-1.04% \pm 0.17%	(-0.47% \pm 0.18%) \pm 0.08%			
		300 μ L VWR	-1.10% \pm 0.40%	(-0.73% \pm 0.38%) \pm 0.07%			
1000 μ L Eppendorf Xplorer (digital)	50 μ L	1250 μ L VWR	-2.01% \pm 1.22%	(-1.79% \pm 1.10%) \pm 0.70%			
		1000 μ L Eppendorf	-2.84% \pm 1.38%	(-2.44% \pm 0.23%) \pm 0.55%			
		1250 μ L Eppendorf	-4.79% \pm 1.32%	(-0.88% \pm 0.22%) \pm 3.29%			
	300 μ L	1250 μ L VWR	-1.24% \pm 0.18%	(-1.03% \pm 0.11%) \pm 0.16%			
		1000 μ L Eppendorf	-1.15% \pm 0.30%	(-0.46% \pm 0.14%) \pm 0.11%			
		1250 μ L Eppendorf	-0.96% \pm 0.26%	(-0.13% \pm 0.13%) \pm 0.45%			
	1000 μ L	1250 μ L VWR	-0.85% \pm 0.22%	(0.00% \pm 0.10%) \pm 0.09%			
		1000 μ L Eppendorf	-0.34% \pm 0.14%	(0.50% \pm 0.09%) \pm 0.08%			
		1250 μ L Eppendorf	-0.74% \pm 0.17%	(0.11% \pm 0.08%) \pm 0.20%			
5000 μ L Eppendorf Xplorer (digital)	250 μ L		2.99% \pm 0.87%	(3.04% \pm 0.65%) \pm 0.64%			
	1000 μ L	5000 μ L Eppendorf	0.46% \pm 0.23%	(0.30% \pm 0.12%) \pm 0.10%			
	5000 μ L		-0.45% \pm 0.31%	(0.03% \pm 0.24%) \pm 0.05%			
100 μ L Eppendorf Research (manual)	100.0 μ L	200 μ L Eppendorf	-0.51% \pm 0.19%	(-0.04% \pm 0.12%) \pm 0.14%			
		300 μ L VWR	-1.24% \pm 0.21%	(-0.71% \pm 0.16%) \pm 0.34%			
1000 μ L Eppendorf Research (manual)	1000 μ L	1250 μ L VWR	-0.79% \pm 0.03%	(-0.82% \pm 0.19%) \pm 0.07%			
		1000 μ L Eppendorf	-0.57% \pm 0.18%	(-0.48% \pm 0.08%) \pm 0.04%			

APPENDIX C.
**REVIEW OF REDOX REACTIONS OF VANADIUM IONS WITH NEPTUNIUM
 AND PLUTONIUM**

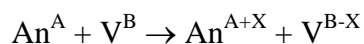
C.1 Introduction

The literature about different reducing and oxidizing agents that can be employed for changing the oxidation state of actinides has been collected and revised in tables especially by T.W. Newton in report *The Kinetics of the Oxidation-Reduction Reactions of Uranium, Neptunium, Plutonium, and Americium in Aqueous Solutions* [62] and a revised table of redox kinetics data in *Advances in Plutonium Chemistry, 1967-2000* [205].

Because of well-known redox properties of vanadium ions, their redox reactions with actinides were also studied and reported in these reviews. However; being somewhat older review [62] does not include all presently available scientific results, namely the most recent work on this issue reported by Prof. Valentin S. Koltunov and his co-workers in 1980s in the Russian *Radiokhimiya* (Radiochemistry) journal in a series of articles called *Interaction of Actinides With Vanadium Ions* [109, 110, 111, 112, 113, 206, 207].

The reason for performing this review was to identify possible applications of vanadium for the UREX/PUREX separation process with regard to the control of the redox state of each actinide in the plutonium – neptunium couple, specifically to find conditions that would enable their simultaneous extraction to the organic phase (in oxidation states Pu^{IV} or ^{VI} and Np^{IV} or ^{VI}) or re-extraction (in oxidation states Pu^{III} or ^V and Np^V or ^{VII}).

All the below-mentioned results were acquired while studying the following general summary redox reaction between appropriate redox forms of V (vanadium) and An (actinide = plutonium/ neptunium):



where A, B represent the oxidation states of the reactants (in this report the observed redox states were for vanadium: +II to +V, plutonium: +III to +VI, neptunium: +IV to +VII) and X represents the exchanged number of electrons (being positive if the reaction is an oxidation of neptunium-A and negative if it is a reduction of neptunium-A by vanadium-B).

Although the equilibrium of these redox reactions can be predicted by the knowledge of the appropriate redox potentials, the knowledge about the rate of the establishment of these equilibria is important to make assessment of their practical value for an industrial redox-state dependent extraction separation process, such as the UREX/PUREX.

Table 15 – Standard electrochemical potentials for vanadium redox reactions [25]

$V^{2+} + 2e = V^0$	$E_0 = - 1,13 \text{ V vs. SHE}$
$V^{3+} + e = V^{2+}$	$E_0 = - 0,255 \text{ V vs. SHE}$
$VO^{2+} + 2H^+ + e = V^{3+} + H_2O$	$E_0 = + 0,337 \text{ V vs. SHE}$
$VO_2^+ + 2H^+ + e = VO^{2+} + H_2O$	$E_0 = + 1,00 \text{ V vs. SHE}$

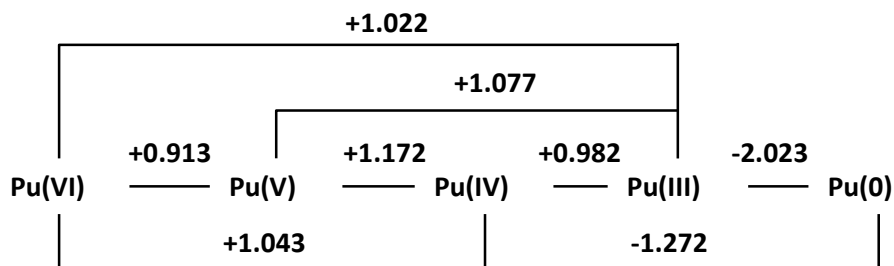
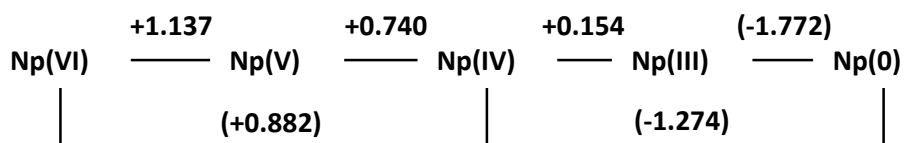


Figure 71 – Diagrams of formal redox potentials $E^{o'}$ for redox couples of Np and Pu in 1M HClO₄

data are in V vs. SHE and adopted from: Np - ref. [29], Pu – ref. [28]
(data in brackets are *standard* potentials E^o from ref. [25])

The thorough review of the source articles for Newton's publications [62] and [205] and Koltunov's articles [109, 110, 111, 112, 113, 206, 207] has shown that these process are truly behaving as of second order toward the concentrations of the reactants. The rate of the these chemical reactions (described in terms of concentration change of the reacting actinide in mol/L per second) were therefore usually described using a second order rate constant k'' that allowed to calculate the reaction rate when the analytical concentration

of reacting species changed while all other conditions (temperature, ionic strength, proton concentration, etc.) were kept constant^{§§}:

$$r \text{ (mol.L}^{-1}\text{/s)} = r\text{(M/s)} = -d[\text{An}^{\text{A}}]/dt = k'' \times [\text{An}^{\text{A}}] \times [\text{V}^{\text{B}}]$$

C.2 Review

The studied reactions have been summarized in tables with a brief description of acquired experimental results

Table 16 - Studied combinations of oxidation states of reactants in vanadium redox reactions with neptunium

	Np ^{IV}	Np ^V	Np ^{VI}	Np ^{VII}
V ^{II}	A) Reduction - Burkhardt & Newton			
V ^{III}		B) Reduction - Appelman & Sullivan	C) Reduction - Sheppard	
V ^{IV}			D) Reduction - Sheppard, Equilibrium and reduction - Koltunov	E) Reduction - Sheppard
V ^V	F) Oxidation - Koltunov	D) equilibrium - Koltunov G) Oxidation - Dukes, Koltunov		

A) Kinetics of reduction of Np^{IV} by V^{II} – studied by Burkhardt and Newton [208] in the environment of 2.0 M (H, Li)ClO₄, and the temperature range 0.9-36.7°C. The proton concentration dependent second order rate constant at 25°C is

$$k'' = (2.53 + 3.8 \times 10^{-2} \times [\text{H}^+]^{-1} + 6 \times 10^{-4} \times [\text{H}^+]^{-2}) \text{ M}^{-1}/\text{s}$$

The observation of reaction rate temperature dependence lead to (assuming Eyring activated-complex theory) $\Delta H^* = 40.7 \pm 0.2$ kJ/mol and $\Delta S^* = -100.4 \pm 0.8$ J/mol.K for the Np⁴⁺ + V²⁺ activated complex. The authors have also studied the influence of chloride ions on the process which generally increased the rate (from $k'' = 1.25 \text{ M}^{-1}/\text{s}$ at

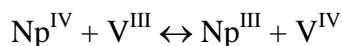
^{§§} The term “second order rate constant” is used in this text, although the k'' was often found to be composed of multiple additive terms, each of which was proportional to some power of proton concentration. The reason is that it is the actinide – vanadium couple that is interesting for studying the rate of these redox reactions.

[HCl] = 0.00 M to $k'' = 9.78 \text{ M}^{-1}/\text{s}$ in at [HCl] = 0.495 M, in solution of 2 M H(Cl,ClO₄) at 13.9°C and initial reactant concentrations of $3.6 \times 10^{-4} \text{ M Np}^{\text{IV}}$ and $1.57 \times 10^{-3} \text{ M V}^{\text{II}}$. The influence of raising the ionic strength also resulted in increased reaction rate (from $k'' = 0.453 \text{ M}^{-1}/\text{s}$ in $\mu = 0.275$ to $k'' = 5.93 \text{ M}^{-1}/\text{s}$ in $\mu = 3.73$, in solution of 0.25 M HClO₄ at 25.2°C and initial reactant concentrations of $3.6 \times 10^{-4} \text{ M Np}^{\text{IV}}$ and $2.35 \times 10^{-3} \text{ M V}^{\text{II}}$).

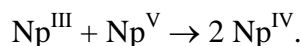
B) Kinetics of reduction of Np^V by V^{III} – were established by Appelman and Sullivan [209] in 3 M (H,Li)ClO₄ at 25°C. The observed reaction followed two paths for which empirical rate constant k'' for an apparent second rate process was formulated as

$$k'' = k_1 + k_2^0 [\text{Np}^{\text{IV}}][\text{V}^{\text{IV}}]^{-1} [\text{H}^+]^{-1.5},$$

where $k_1 = 0.30 \text{ M}^{-1}/\text{s}$ and $k_2^0 = 0.16 \text{ M}^{0.5}/\text{s}$. For the first reaction path with k_1 the temperature dependence observations yielded $\Delta H^* = 14.6 \pm 0.8 \text{ kcal/mol}$ and $\Delta S^* = -12.3 \pm 2.6 \text{ e.u.}$ The second term has been interpreted in terms of rapid equilibrium



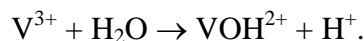
followed by the synproportionation of neptunium ion charge



C) Kinetics of reduction of Np^{VI} by V^{III} – were established by Sheppard [210] in 2 M (H,Na)ClO₄ at 25°C and then recalculated from original data by T.W. Newton [62]. The nature and reason of the recalculation is not clear from [62]. The data which were interfered by the further reduction of Np^{VI} by V^{IV} - the product of the studied reduction step and therefore the data had to be taken from only from the 20-30% of the reaction total conversion. The rate constant of the second rate process is equal to

$$k'' = (5.7 + 22.6 \times [\text{H}^+]^{-1}) \text{ M}^{-1}/\text{s}.$$

The rate constant is proton concentration dependent because of a side reaction of Np^{VI} by VOH²⁺ by the reaction, which is generated by hydrolysis of V³⁺:



For the proton-independent reaction the $\Delta H^* = 134 \pm 21 \text{ kJ/mol}$ and for the proton-dependent part it is $\Delta H^* = 54 \pm 8 \text{ kJ/mol}$ – the recalculated entropies were not published in [62].

D) Kinetics and equilibrium of reduction of Np^{VI} by V^{IV} – were first observed by Sheppard [210], but the reaction rate in 2M HClO₄ was established only as a preliminary result to help reduce the uncertainty of measurement in the Np^{VI} + V^{III} redox reaction (see c). The measured value was $k'' = 13.3 \text{ M}^{-1}/\text{s}$, which is 20% higher, but in accordance with later values given by Koltunov.

Koltunov's research group [112] has started the studies of the Np^{VI}-Np^V-V^{IV}-V^V system by determining its equilibrium in HClO₄ solution. The formal equilibrium constant

$$K = [\text{Np}^{\text{V}}] \cdot [\text{V}^{\text{V}}] \cdot [\text{H}^+]^2 / [\text{Np}^{\text{VI}}] \cdot [\text{V}^{\text{IV}}]$$

was found to be $K = 7.65 \pm 1.31 \text{ M}^2$ at 25.5°C at an ionic strength of $\mu = 4$. The enthalpy of the reaction was close to zero. Upon decreasing the ionic strength to $\mu = 2$ the K rose to $\sim 36 \text{ M}^2$.

Because the equilibrium is very close to 1, the Koltunov group chose a different approach to determine the reduction rate in perchloric [110] and nitrate [111] environment using a reducing agent glyoxal, which rapidly and completely reduces V^V to V^{IV} without reacting with the Np^{VI} ions. The vanadium ions thus served as a catalyzer for the reduction of Np^{VI} by glyoxal C₂H₂O₂, the rate of this reduction was however being limited by the V^{IV} facilitated reaction with Np^{VI}. During each experiment the concentration vanadium stood constantly in tetravalent form as all V^V ions were rapidly reduced back to the V^{IV} state by the glyoxal, which was used in 20-30-fold equivalent excess to total concentration of neptunium and vanadium - i.e. $[\text{C}_2\text{H}_2\text{O}_2] = 0.02 \text{ M}$ while $[\text{Np}^{\text{VI}}] \leq 1.25 \times 10^{-3} \text{ M}$, $[\text{V}^{\text{IV}}] \leq 8 \times 10^{-4} \text{ M}$. The observed reaction rate order with respect do glyoxal was thus zero.

In HClO₄ at $\mu=2$ and 25°C the second order rate constant with respect to concentrations of V^{IV} and Np^{VI} was found inversely proportional to the square root of proton concentration:

$$k''_{\mu=2} = (\{15.73 \pm 0.27\} \times [\text{H}^+]^{-0.5}) \text{ M}^{-1}/\text{s}.$$

With ionic strength increased to $\mu=4$ the power dependence of the rate constant on the proton concentration drops to -1 . At the temperature of 25°C the rate constant was observed to be:

$$k''_{\mu=4} = (\{27.22 \pm 1.07\} \times [\text{H}^+]^{-1}) \text{ M}^{-1}/\text{s}$$

From the temperature dependence it was established that the activation energies for the redox reaction are $E_{a,\mu=2}=56.8$ kJ/mol and $E_{a,\mu=4}=57.7$ kJ/mol.

In a later study of the reverse reaction (oxidation of neptunium-V by vanadium-V) in perchloric acid [113], Koltunov et al. re-determined the value of the 2nd order constant without the presence of glyoxal from at $\mu = 4$ M and found it to be somewhat slower:

$$k''_{\mu=4} = (\{18.5 \pm 1.8\} \times [H^+]^{-1}) M^{-1}/s^{-1},$$

while the rate constant temperature dependence between 25.5 and 45.8°C implicated that the activation energy was $E_{a,\mu=4} = 54 \pm 8$ kJ/mol. The latter value is probably more realistic, since it was determined in a system without the presence of glyoxal, which might have had a slight catalytic effect.

In HNO₃ a different ionic strength influenced behavior of proton concentration dependency of the rate constant was found than in HClO₄. At $\mu = 2$ and 25°C the second order rate constant with respect to concentrations of V^{IV} and Np^{VI} was found inversely proportional to the square root of proton concentration:

$$k''_{\mu=2} = (\{17.13 \pm 0.58\} \times [H^+]^{-0.5}) M^{-1}/s$$

With ionic strength increased to $\mu=4$ the power dependence of the rate constant on the proton concentration drops only slightly from -0.5 down to -0.6 , which is a change toward the behavior in HClO₄. At the temperature of 25°C the rate constant was observed to be:

$$k''_{\mu=4} = (\{22.43 \pm 1.02\} \times [H^+]^{-1}) M^{-1}/s$$

From the temperature dependence it was established that the activation energies for the redox reaction are $E_{a,\mu=2} = 54.9$ kJ/mol and $E_{a,\mu=4} = 55.7$ kJ/mol.

E) Kinetics of reduction of Np^{VII} by V^{IV} – were investigated by the stopped-flow spectrophotometry technique by Watkins, Sullivan and Deutsch [211] in (Li,H)ClO₄ media. The second order rate constant k'' had slight dependence on the proton concentration. The redox rate was very rapid, at $\mu = 1$, $[V^{IV}] = 9 \times 10^{-3}$ M, $[Np^{VII}] = 5 \times 10^{-4}$ M and 25°C the rate constant was found to be equal to:

$$k'' = (1.44 \times 10^3 \times [H^+]^{-0.1}) M^{-1}/s$$

The temperature dependence of k'' over the range 2.7 – 25°C showed that the Arrhenius activation energy is equal to 31 ± 4 kJ/mol.

F) Kinetics of Oxidation of Np^{IV} by V^{V} - were explored by Koltunov et. al. [109] in $(\text{H},\text{Na})\text{NO}_3$ and $(\text{Na},\text{H})\text{ClO}_4$ solutions at ionic strengths $\mu = 2 - 4$, concentrations . The second order rate constant was observed as directly proportional to the proton concentration, in $(\text{H},\text{Na})\text{NO}_3$ at $\mu = 2$ and 20.2°C it was equal to:

$$k'' = (\{1.33 \pm 0.02\} \times [\text{H}^+]^{-1}) \text{ M}^{-1}/\text{s}$$

and the activation energy was $E_a = 75.2$ kJ/mol. With raising the ionic strength to $\mu = 4$, the proton dependence remained constant, but the numeric factor has decreased to $0.957 \pm 0.033 \text{ M}^0/\text{s}$ and the activation energy to $E_a = 83.6$ kJ/mol

In $(\text{Na},\text{H})\text{ClO}_4$ at the same ionic strength of $\mu = 2$ and temperature reduced to 15°C the second order rate constant had a weaker inversely proportional dependency on proton concentration:

$$k'' = (\{0.635 \pm 0.012\} \times [\text{H}^+]^{-0.9}) \text{ M}^{-1}/\text{s}$$

at $\mu=4$ the proton concentration power dependence increased from -0.9 to -0.8 and the value of the numerical factor of the constant increased (as opposed to the behavior in nitric acid solutions) to $0,988 \pm 0,027 \text{ M}^{-0.2}/\text{s}$.

G) Kinetics of Oxidation of Np^{V} by V^{V} – were first explored in HNO_3 by Dukes [106] and then further examined by Koltunov et al. [113] in $(\text{Na},\text{H})\text{ClO}_4$.

In HNO_3 Dukes has employed a solvent extraction technique based on the difference in the distribution coefficients for Np^{V} and Np^{VI} . The measurements were made in only HNO_3 solution environment, however no treatment was made to keep the ionic strength at constant level (however, a side examination of the nitrate NO_3^- influence by addition of NaNO_3 at constant HNO_3 concentration was performed once without significant observational difference), therefore the second order rate constant measurements at 24°C and HNO_3 concentration range of 2.04 – 3.58 M yielded a value of relatively high error range:

$$k'' = (\{0.195 \pm 0.042\} \times [\text{H}^+]^2) \text{ M}^{-1}/\text{s}$$

Observation of the temperature measurement yielded activation energy $E_a = 48.9 \pm 1,7$ kJ/mol. Dukes has also made these experiments with plutonium and reached the conclusion that under the same oxidizing conditions Pu^{IV} was not oxidized to an appreciable extent (only 3% have been oxidized by 5×10^{-4} M VO_2^+ in 2.8 M HNO_3 to Pu^{VI} as opposed to 96% conversion of Np^{V} to the hexavalent form during 30 minute oxidation time).

In (Na,H)ClO₄ solutions at ionic strengths $\mu = 2 - 4$ Koltunov et. al. has studied equilibrium [112] (described in section **E**) and kinetics [113] by spectrophotometric observation of the time dependent establishment of equilibrium by reaction of Np^{V} produced from reverse reaction - reduction Np^{VI} and V^{IV} at the following various initial concentrations Np^{VI} (0.59 - 3.5 mM), V^{IV} (0.6 - 3.6 mM) and V^{V} (0.03 - 1.3 mM). The second order reaction constant was observed as directly proportional to the proton concentration, at $\mu = 4$ and 25.5°C it was equal to:

$$k'' = (\{1.97 \pm 0.17\} \times [\text{H}^+]) \text{ M}^{-1}/\text{s}$$

The enthalpy and entropy of activation were equal to $\Delta H^* = 56.4$ kJ/mol and $\Delta S^* = -59$ J/mol/K.

Table 17 - Studied combinations of oxidation states of reactants in vanadium redox reactions with neptunium

	Pu^{III}	Pu^{IV}	Pu^{V}	Pu^{VI}
V^{II}				
V^{III}		H) reduction, Rabideau	I) Reduction (slow), Rabideau	J) Reduction Rabideau 1958
V^{IV}		L) equilibrium, K) reduction kinetics, Koltunov		
V^{V}	L) Equilibrium, oxidation kin. Koltunov	M) Slow oxidation Dukes		

H) Reduction kinetics of Pu^{IV} by V^{III} – measured by Rabideau and Kline [212] at analytical concentration of 1.5×10^{-3} M V^{3+} in 2.0 M (H,Na)ClO₄ at 20°C the second order reaction rate in terms of $[\text{Pu}^{4+}]$ and $[\text{V}^{3+}]$ is

$$k' = 11.9 \times [\text{H}^+]^{-1} + 20.1 \times [\text{H}^+]^{-2} \text{ M}^{-1}/\text{sec}$$

while the activation energies are $E_a = 74 \pm 2$ and 92 ± 1.6 kJ/mol for the respective constants.

I) Kinetics of reduction of Pu^V by V^{III} – was not established directly, but only as a side observation during the study of Rabideau [213] of reduction of Pu^{VI} by the V^{III} reducing agent. It appeared that the formation of Pu^V by reduction of Pu^{VI} was much faster than its disappearing by its own reduction to Pu^{IV}. Therefore the second order reaction constant k'' has to be much lower than $0.24 \text{ M}^{-1}/\text{s}$ at 2.4°C in 1M HClO_4 at V^{3+} concentration approximately $3 \times 10^{-3} \text{ M}$.

J) Kinetics of reduction of Pu^{VI} by V^{III} – established by Rabideau [213] using spectrophotometric measurements in 2M (H,Na)ClO_4 at 25°C - the second order rate constant indicates two reaction paths and has a following form, depending on the proton concentration:

$$k'' = 2.12 \times [\text{H}^+]^{-1} + 0.228 \times [\text{H}^+]^{-2} \text{ M}^{-1}/\text{s}$$

while from the temperature dependence of the reaction rate the activation energy was found to be $E_a = 67 \pm 2$ kJ/mol in 1M HClO_4 . The reaction progress was followed by observing the diminishing absorption of PuO_2^{2+} and by another stoichiometry check by observing the rate of formation of VO^{2+} .

K) Kinetics of reduction of Pu^{IV} by V^{IV} – established in $(\text{H,Na})\text{ClO}_4$ by Koltunov [207] using also data from the establishment of equilibrium during the oxidation of Pu^{III} by V^V [206]. The second order rate constant is dependent on the proton concentration because of important influence of hydrolysis of VO^{2+} to VO(OH)_2 and it therefore contains two terms:

$$k'' = k_1 + k_2[\text{H}^+]^{-2},$$

the first constant was found to be equal $k_1 = 0.497 \pm 0.027 \text{ M}^{-1}/\text{s}$ at $\mu = 1.6$ and $k_1 = 1.90 \pm 0.03 \text{ M}^{-1}/\text{s}$ at $\mu = 3$, whereas the second constant did not show so strong dependence on ionic strength and equaled $k_2 = 0.482 \pm 0.03 \text{ M}/\text{s}$ at $\mu = 1.6$ and $k_2 = 0.610 \pm 0.138 \text{ M}/\text{s}$ at $\mu = 3$.

M) Equilibrium and kinetics of oxidation of Pu^{III} by V^V – established using spectrophotometry by Koltunov et. al. [206] – the formal equilibrium constant of the reaction:



in a solution of HClO₄ with ion strength $\mu = 1.6$ and at 25°C amounts to $7.2 \pm 0.7 \text{ M}^{-2}$.

The second order rate constant of the forward reaction was expressed as:

$$k'' = (k_1 + k_2[\text{H}^+]^2) / (1 + K_1[\text{H}^+] + K_2[\text{H}^+]^2)$$

where $k_1 = 3.38$ and $3.00 \text{ M}^{-1}/\text{s}$ and $k_2 = 3.73$ and $9.90 \text{ M}^{-3}/\text{s}$ at 25°C and $\mu = 1.6$ and 3, respectively, (K_1 and K_2 are the formal equilibrium constants of the protonization of VO_2^+ ions with respect to the first and second powers, the authors used values $K_1 = 0.18 \text{ M}^{-1}$ and $K_2 = 0.024 \text{ M}^{-2}$ for $\mu = 1.6$, and $K_1 = 0.33 \text{ M}^{-1}$ and $K_2 = 0.063 \text{ M}^{-2}$ for $\mu = 3$).

In HNO₃, the reactions were much more rapid, at ionic strength $\mu = 2$ and temperature of 25°C, $k_1 = 58.3 \text{ M}^{-1}/\text{min}$ and $k_2 = 270 \text{ M}^{-3}/\text{s}$. The authors concluded that the reaction proceeds along two paths in the slow stages in which ions of Pu^{3+} interact with VO_2^+ and VO^{3+} ions.

The authors also performed kinetic experiments in HNO₃ which were concluded by discovering that the above-mentioned equilibrium is shifted to the right and the oxidation proceeds 70-times more rapidly. The second-order rate constant was established only approximately as $k'' = 690 \pm 105 \text{ M}^{-1}/\text{s}$ at $[\text{H}^+] = 1.92 \text{ M}$ ($\mu = 2$).

N) Kinetics of Oxidation Pu^{IV} by V^V – were observed by extraction and radiometry as being slow by Dukes [106] in HNO₃ at temp 24°C under oxidation conditions used for oxidation of Np^V - at concentrations $10^{-5} \text{ M Pu}^{(\text{IV})}$ and $5 \times 10^{-4} \text{ M VO}_2^+$ in 2.8 M HNO₃. During 30 minutes of reaction only 3% have been oxidized to Pu^{VI} as opposed to 96% conversion of Np^V to the hexavalent form (see G).

C.3 Conclusion

The review of the reactions listed above discovered a possibility for the employment of vanadium as an extraction enabling agent. The rate of oxidation of non-extractable Np(V) form by V(V) into extractable Np(VI) in the work of Dukes [106] was much larger than the oxidation of extractable Pu(IV) into non-extractable Pu(V). This phenomenon can be

explained by the slow rate of forming Pu-O bonds in the process of creation of PuO_2^+ from water solvated Pu^{4+} . The possibility has to be verified by experiments containing UREX-process relevant concentration ratios of Pu : Np, also to verify that the mutual Pu-Np redox reactions do not prohibit this possibility.